



**TriDurLE**

---

**National Center for Transportation  
Infrastructure Durability & Life-Extension**

**Project ID:  
Grant #: 69A3551947137**

**Highway Pavement Condition Deterioration Modeling  
Considering Maintenance History**

**Final Report**

**By Hakan Yasarer and Rulian Barros**

**for**

National University Transportation Center TriDurLE  
Department of Civil & Environmental Engineering  
405 Spokane Street PO Box 642910  
Washington State University Pullman, WA 99164-2910

**Date**  
3/2/2022

## **ACKNOWLEDGEMENTS**

The authors of this report would like to express special thanks to Dr. Waheed Uddin, who led the majority of the research in this study on Highway Pavement Condition Deterioration Modeling, which helped discover significant knowledge to advance the pavement asset management systems.

## **DISCLAIMER**

The contents of this report reflect the views of the authors, who are responsible for the facts and the accuracy of the information presented. This document is disseminated under the sponsorship of the Department of Transportation, University Transportation Centers Program, in the interest of information exchange. The U.S. Government assumes no liability for the contents or use thereof.

# TABLE OF CONTENTS

Acknowledgements.....	2
Disclaimer.....	2
Table of Contents.....	3
List of Figures.....	4
List of Tables.....	6
Executive Summary.....	8
1. Introduction.....	10
1.1. Objectives.....	14
2. Literature Review.....	15
2.1. Literature Review of Mechanistic-Empirical Design of Asphalt Pavements.....	15
2.2. Roughness Modeling using MLR and ANN Methods.....	17
2.3. Literature Review of MEPDG Performance Modeling for Rutting Distress.....	25
2.4. Literature Review of MEPDG Cracking Distresses.....	27
2.5. Literature Review of Pavement Modulus Backcalculation Methods.....	34
2.6. Literature Review of 3D-FE Modeling of Uncracked Asphalt Pavements.....	41
2.7. Literature Review of 3D-FE Modeling of Cracked Pavements.....	42
3. Methodology.....	47
3.1. Methodology for Enhanced IRI Modeling.....	47
3.2. Methodology for Enhanced Rutting Modeling.....	52
3.3. Methodology for Enhanced Cracking Modeling.....	54
3.4. Methodology for Modulus Values Backcalculation Process.....	54
3.5. 3D-FE Modeling of Uncracked Asphalt Pavements.....	55
3.6. 3D-FE Modeling of Longitudinal Crack in Asphalt Layer.....	62
4. Results and Discussion.....	66
4.1. Pavement Condition Deterioration Modeling.....	66
4.2. Modulus Values Backcalculation.....	98
4.3. 3D-FE Modeling of Uncracked Asphalt Pavements.....	113
4.4. 3D-FE Modeling of Longitudinal Crack in Asphalt Pavements.....	124
5. Summary and Conclusions.....	140
5.1. Summary.....	140
5.2. Conclusions.....	141
5.3. Recommendation for Future Research.....	142
References.....	143
APPENDICES.....	148
Appendix A: Modeling of 3D-FE Cracked Asphalt Pavement Model.....	148
Appendix B: Prediction Model Equation for Condition Deterioration Progression.....	154
Appendix C: Full Factorial Design for Uncracked Asphalt Pavements.....	161

## LIST OF FIGURES

Figure 1. AASHTOWare Pavement ME Design software inputs.....	16
Figure 2. IRI based on reported miles of National Highway System in 2011 (FHWA 2016) .....	18
Figure 3. Example of ANN processing elements and interconnection network .....	23
Figure 4. Data transformation functions used in mathematical modeling as a function of time (x-axis) .....	24
Figure 5. Typical crack distress types observed on asphalt surfaced road network.....	31
Figure 6. Example of computational of CI (Paterson 1994b) .....	32
Figure 7. Point of interest to calculate vertical stress based on Boussinesq’s approach.....	35
Figure 8. Point of interest to calculate deflection value on Boussinesq’s approach (Ullidtz 1987) .....	36
Figure 9. Spatial Map of 2016 Average Pavement Condition Rating (PCR) by Counties in Mississippi.....	43
Figure 10. Rut depth per measurement year data.....	54
Figure 11. 3D-FE model of the pavement-subgrade system subjected to truck axle loading.....	55
Figure 12. Pavement-subgrade 3D-FE model of uncracked pavement developed .....	56
Figure 13. Undeformed 3D-FE model of uncracked asphalt pavement.....	57
Figure 14. Color codes assigned to pavement-subgrade 3D-FE model.....	57
Figure 15. Single unit truck rear axle compressive stress pulse .....	58
Figure 16. Single unit truck rear axle (P/Peak) stress ratio.....	58
Figure 17. Surface pressure (psi) used in the LS-DYNA analysis.....	58
Figure 18. Initial set up for truck wheel contact area for 3D-FE Half model .....	59
Figure 19. Final truck wheel contact area set up for 3D-FE half model.....	60
Figure 20. Boundary condition set up for the front and back sides of 3D-FE half model .....	60
Figure 21. Nodes used to set boundary conditions (front view of the 3D-FE half model) .....	61
Figure 22. Close-up view of asphalt layers (front view of the 3D-FE half model) .....	61
Figure 23. Nodes used to set boundary conditions (back view of the 3D-FE half model) .....	61
Figure 24. Plan views on top of the asphalt pavement for uncracked (a) and cracked pavement (b).....	62
Figure 25. Keyword input form for LS-DYNA software .....	63
Figure 26. Master segments defined on the vertical surfaces for left (a) and right (b) sides of the cracked area .....	64
Figure 27. Slave segments defined on both the left and right sides of vertical surfaces, and horizontal surfaces at the bottom of the cracked element .....	64
Figure 28. Truck tire contact area simulated in the 3D-FE analysis for cracked asphalt pavement .....	65
Figure 29. Sketch of an 18-kips single axle truck with 4 tires and contact areas developed in this research .....	65
Figure 30. Normality plots for the untransformed and transformed $Y_1$ data .....	67
Figure 31. Predicted vs measured plot for IRI multiple regression equation database .....	68
Figure 32. Predicted vs measured plot for IRI multiple regression verification database.....	69
Figure 33. Measured and predicted IRI using multiple regression .....	69
Figure 34. Predicted vs measured plot for IRI ANN model database.....	69
Figure 35. Predicted vs measured plot for IRI ANN verification database.....	70
Figure 36. Measured and predicted IRI using ANN model .....	70
Figure 37. Example of SPEC file set up for IRI model using ANN method .....	72
Figure 38. ANN model equation implementation to predict future IRI Section 40-4165 .....	72
Figure 39. Histogram plot of average rut depth per measurement year .....	74
Figure 40. Predicted vs measured plot for rut depth multiple regression equation database .....	82
Figure 41. Predicted vs measured plot for rut depth multiple regression verification database.....	82
Figure 42. Measured and predicted rut depth using multiple regression .....	83
Figure 43. Predicted vs measured plot for rut depth ANN model database.....	83
Figure 44. Predicted vs measured plot for rut depth ANN verification database.....	84
Figure 45. Measured and predicted rut depth using ANN model equation.....	84
Figure 46. Example of SPEC file set up for rutting model using ANN method .....	86
Figure 47. Distribution of the UCI per measurement year data according to sequential number .....	87
Figure 48. Normality plot for the combined UCI data transformed using $\text{Log}_{10}(Y_C+0.5)$ function.....	88
Figure 49. Two-tailed t-test probability distribution graph.....	89

Figure 50. Asphalt pavement age (years) at the most recent CN major M&R (CN <sub>m</sub> ) with crack data before and after major M&R treatment.....	90
Figure 51. UCI data plot for test section 47-3101 in Tennessee .....	91
Figure 52. Example of SPEC set up for combined all cracking distresses (UCI).....	95
Figure 53. Enhanced Pavement Asset Management (PAM) Framework (Uddin et al. 2013).....	96
Figure 54. Basic Concept of Life Cycle Cost (LCC) (Uddin et al. 2013).....	96
Figure 55. Comparison between the measured and calculated deflections in 1998.....	106
Figure 56. Backcalculated modulus values for asphalt surface layer.....	106
Figure 57. Backcalculated modulus values for asphalt treated base layer .....	107
Figure 58. Backcalculated modulus values for CTB layer.....	107
Figure 59. Backcalculated modulus values for the subgrade layer .....	108
Figure 60. Illustration of FWD load point and the locations of geophone sensors (not to scale) .....	109
Figure 61. Garza’s 3D-FE model was used to evaluate responses under the FWD load (Garza 2003).....	110
Figure 62. Deformed 3D-FE model subjected to FWD load .....	113
Figure 63. Example of GAMES software interface for initial set up before the structural analysis .....	115
Figure 64. Deformed 3D-FE model subjected to a single axle dual tire load .....	115
Figure 65. Treatment combination of the factorial design used for 3D-FE simulations.....	118
Figure 66. Front view of Model 000000 (Asphalt = 3 in, Base = 6 in, Subbase = 6 in, andSubgrade = 480 in).....	119
Figure 67. Front view of Model 010000 (Asphalt = 3 in, Base = 6 in, Subbase = 12 in, andSubgrade = 480 in) .....	119
Figure 68. Front view of Model 100000 (Asphalt = 9 in, Base = 6 in, Subbase = 6 in, andSubgrade = 480 in).....	119
Figure 69. Front view of Model 100000 (Asphalt = 9 in, Base = 6 in, Subbase = 12 in, andSubgrade = 480 in) .....	120
Figure 70. Critical asphalt pavement response locations .....	120
Figure 71. Asphalt surface deflections based on low and high modulus and thickness levels.....	124
Figure 72. Trial run with two spring elements on top and bottom of asphalt layer to simulate fulldepth cracked condition .....	125
Figure 73. Undeformed (a) and deformed (b) models for the top one-third cracked from overall asphalt thickness .....	127
Figure 74. Undeformed (a) and deformed (b) models for the middle one-third cracked from overall asphalt thickness.....	128
Figure 75. Undeformed (a) and deformed (b) models for the bottom one-third cracked from overall asphalt thickness.....	128
Figure 76. Undeformed (a) and deformed (b) models for the full cracked asphalt layer.....	128
Figure 77. Close up view of the elements close to the centerline of the loading area .....	129
Figure 78. Example of the deformed cracked model with dual tires on each side.....	129
Figure 79. Example of the LTPP manual distress survey manual sketch (Test date: 11/9/1995).....	131
Figure 80. Example of manual distress survey manual sketch (Test date: 03/07/2003) .....	132
Figure 81. Peak deflection ratios plot of uncracked and cracked pavement for the LTPP test section 28-3085 (deflections normalized to 9,000 lbs.).....	133
Figure 82. Surface deflections correspond to various cracked layer modulus.....	133
Figure 83. Peak deflection ratio for uncracked and cracked pavements: Surface deflections at the center of the loading area corresponding to various cracked layer modulus values .....	134

# LIST OF TABLES

Table 1. Independent variable used in the enhanced IRI MLR equation and MEPDG.....	19
Table 2. The parameters used to calculate rutting at the mid-depth of the asphalt layer .....	25
Table 3. The parameters used to calculate rutting at the mid-depth of all unbound sub-layers.....	26
Table 4. Parameters used in the MEPDG equations to calculate alligator and longitudinal cracks.....	28
Table 5. Parameters used in the MEPDG equations to calculate fatigue crack in the CTB layer.....	29
Table 6. Parameters used in the MEPDG equations to calculate fatigue crack in the CTB layer.....	30
Table 7. IRI data for LTPP test section 1-1011 in Lauderdale County, Alabama .....	49
Table 8. State-wise distribution of the $Y_1$ data .....	49
Table 9. Rut depth data sets for test section 1-1011 in Lauderdale County, Alabama .....	53
Table 10. Rut depth data sets based on LTPP regions, base type, major M&R.....	53
Table 11. Kolgomorov-Smirnov Test of Normality.....	66
Table 12. Accuracy measures for the untransformed and transformed $Y_1$ model database .....	67
Table 13. Accuracy measures for the untransformed and transformed $Y_1$ model verifications .....	68
Table 14. Lists of test sections in the LTPP database with zero rut depth values.....	72
Table 15. Test section 47-3101: Rut depth survey date and CN attributes .....	73
Table 16. Test of normality for average rut depth per measurement year datasets.....	73
Table 17. ANOVA test of between-subjects effects for average rut depth per measurement year.....	75
Table 18. List of independent variables for the rutting progression prediction model equation.....	75
Table 19. Descriptive statistics for independent variables used to develop rutting model equations .....	80
Table 20. UCI datasets based on climatic regions (Reg_Actual) and major M&R intervention (CND) .....	87
Table 21. Test of normality for combined UCI data sets .....	87
Table 22. ANOVA tests of between-subjects effects for combined UCI datasets.....	92
Table 23. Independent variables for enhanced cracking progression prediction model equation.....	93
Table 24. Descriptive statistics for independent variables used to develop enhanced cracking condition deterioration prediction equation .....	93
Table 25. Simplified M&R intervention criteria for pavement asset management.....	97
Table 26. Basic information for LTPP test section 28-2807 in Lafayette County, MS .....	99
Table 27. ESAL data for test section 28-2807 in Lafayette County, MS.....	99
Table 28. The FWD drop loads and peak deflections (Test section 28-2807, October 11, 1990) .....	100
Table 29. Default seed modulus values used in this research .....	101
Table 30. Modulus Values from Previous Study by Boriboonsin and Momm. (2002) .....	102
Table 31. Backcalculated modulus values for test section 28-2807 in Mississippi .....	103
Table 32. Summary of modulus values from UMPED for US45N North Project, Section 1, Station 461+05 (After (Garza 2003)).....	110
Table 33. Areas from measured deflection-time history for US45N, Cycle 3, Drop 2 (Garza 2003).....	111
Table 34. Comparison between UMPED and regression model using areas under deflection-time history data .....	112
Table 35. Linear elastic material properties for Highway US45N, North Project, Section 1, Station 461+05, Cycle 2, Drop 2 .....	113
Table 36. Degree of freedom, number of nodes, and elements for the US45N 3D-FE model.....	114
Table 37. Parameters for the 3D-FE half model with FWD load.....	114
Table 38. Parameters for the 3D-FE half model with 4,500 lbs truck wheel loads.....	115
Table 39. Measured and calculated peak surface deflections subjected to FWD load (normalized to 9,000 lbf) .....	116
Table 40. Comparison of the peak surface deflections calculated using 3D-FE and GAMES software subjected to truck wheel loads (4,500 lbf) .....	116
Table 41. Comparison of measured and calculated peak deflections from LS-DYNA finite element software and GAMES layered elastic static analysis software (FWD load) .....	117
Table 42. Treatment combinations for full factorial experiment design (six factors and two levels) (Connor and Zelen 1959; Uddin 1984).....	118
Table 43. Surface deflections, stresses, and strains for all treatment combinations of uncracked asphalt.....	122
Table 44. Surface deflection values for various treatment combinations .....	123

Table 45. Uncracked asphalt layer subjected to dynamic wheel load for models 000000 and 11111 without the spring element on top and bottom of the asphalt layer .....	126
Table 46. Uncracked asphalt layer subjected to dynamic wheel load for In Situ Condition and Model 000000 with spring element on top and bottom of the asphalt layer.....	126
Table 47. Pavement structures for in situ, low-level Model 000000, and high-level Model 111111 .....	127
Table 48. Summary of FWD data for the LTPP section 28-3085 and asphalt surface conditions in 1995.....	130
Table 49. FWD data for the LTPP test section 28-3085 and asphalt surface conditions in 2003.....	131
Table 50. Peak deflection ratios between uncracked and cracked pavement for the LTPP testsection 28-3085 (deflections normalized to 9,000 lbs.).....	132
Table 51. 3D-FE Cracked model: Surface deflections at the center of loading area with plus and minus 1 SD corresponding to various cracked asphalt layer modulus values .....	134
Table 52. Full factorial design for the 3D-FE cracked asphalt pavement model .....	135
Table 53. Layer thicknesses and modulus values for the 3D-FE analysis to study responses at different crack depth levels: Low-Level Modulus (Model 000000) .....	136
Table 54. Deflection, stress, and strain responses for cracked asphalt layer at various crack depth levels: Low-Level Modulus (Model 000000) .....	136
Table 55. Layer thicknesses and modulus values for uncracked and full depth cracked asphaltlayer at various treatment combinations.....	137
Table 56. Deflection, stress, and strain responses for uncracked and full depth cracked asphaltlayer at various treatment combinations.....	137
Table 57. Layer thicknesses and modulus values for various treatments for the 3D-FE models that simulate full-depth longitudinal cracks .....	138
Table 58. Comparisons of the effective asphalt pavement modulus values with uncracked pavements for seven different combination treatments .....	139

## EXECUTIVE SUMMARY

A nation's economy and prosperity depend on an efficient and safe transportation network for public mobility and freight transportation. A country's road network is recognized as one of the largest public infrastructure assets. About 93 percent of 2.6 million miles of paved roads and highways in the United States (U.S.) are surfaced with asphalt. Longitudinal roughness, pavement cracking, potholes, and rutting are the major reasons for the rehabilitation of asphalt roads. Billions of dollars are required annually for the maintenance and rehabilitation of road networks. If timely maintenance and rehabilitation are not performed, the pavement damages inflicted by heavy traffic repetitions and environmental impacts may lead to life-threatening conditions for road users. This report is focused on asphalt pavement condition deterioration progression modeling and computational simulations of uncracked and cracked asphalt pavement-subgrade models. The research objectives are to (1) evaluate and enhance asphalt pavement condition deterioration prediction models, (2) evaluate modulus backcalculation approaches for characterizing asphalt pavement layers of selected test sections, (3) develop three dimensional-finite elements (3D-FE) asphalt pavement models and study impacts of cracking on pavement structural responses, and (4) implement pavement condition deterioration models for improved structural design and asset management of asphalt highway pavements

The historical asphalt pavement database records of the Long-Term Pavement Performance (LTPP) research program were used to develop asphalt pavement condition deterioration progression models, considering LTPP regions and maintenance and rehabilitation history. The enhanced condition deterioration prediction equations of the International Roughness Index (IRI), rutting, and cracking distress were developed and evaluated in this research for LTPP datasets of 2,588 for IRI, 214 for rutting, and 2,240 for cracking. The LTPP regions and major maintenance intervention criteria were common factors considered in all multiple regression equations. The IRI prediction equation also considered the IRI measurement location factor. Additionally, the rutting prediction equation includes additional factors of in situ modulus of pavement layers and base layer type. In comparison, the U.S. national mechanistic-empirical pavement design guide (MEPDG) performance prediction models do not include maintenance and rehabilitation and climatic factors which present major limitations of the MEPDG method of pavement thickness design.

Both regression analysis and Artificial Neural Network (ANN) analysis methods were used, and the results were compared. The IRI multiple regression equation shows an R of 0.633, which is slightly lower compared to the ANN IRI model's R of 0.717. The IRI predictions using the enhanced multiple regression equation are comparable with the ANN results for verification data sets. The prediction equations from multiple regression modeling and ANN modeling of rutting distress show high R values above 0.93 and 0.94, respectively, and reasonably accurate results of the model database and verification section. These model equations have got higher R-value compared to the MEPDG's R-value.

A new cracking model namely Unified Cracking Index (UCI) was developed in this research by combining all crack types which is not available in the MEPDG. The overall UCI combines the densities (% crack area per total area) of the alligator, block, longitudinal, and transverse cracking types. This approach is practical and easy to implement with intervention criteria of maintenance and rehabilitation for life-cycle asset management of asphalt highway pavements. The UCI equations using multiple regression for log transformation and using sigmoidal transformation for the model database shows the



correlation, R, of 0.551 and 0.511 respectively, with 19.5 and 4.1 percent errors in predictions compared to the measured LTPP data. In comparison, the ANN model for UCI showed significant improvements in R-value (0.707) with a 14.6% error. It also showed a high R-value (0.861) and low error for the verification data sets.

The MEPDG method includes separate models of alligator crack, longitudinal crack (defined as a fatigue-induced crack in the MEPDG), and transverse crack. In comparison, this research developed prediction equations not only for alligator, longitudinal, and transverse cracks but for block cracks too. Individual ANN models of cracking (alligator, block, longitudinal, transverse) also showed reasonably accurate results.

In situ modulus values of existing pavements are other important material inputs for pavement structural response analysis of overlay thickness design. Several modulus backcalculation software, based on the layer elastic static analysis theory, were evaluated in this research for selected LTPP highway sections. The comparisons indicated that the backcalculated modulus values in the LTPP database were generally unreasonable using the EVERCALC 5.0 software. Overall, the backcalculated modulus values using BAKFAA 2.0 and PEDD/UMPED were generally reasonable for all pavement layers. It was also shown that the thickness design of longer-lasting pavement performance depends on seasonal layer modulus values considering extreme weather and climate attribute.

To create a structural response database for pavement-subgrade subjected to design truck axle load, the 3D-FE models of uncracked and cracked asphalt pavement layer were developed using the LS-DYNA finite element software. The structural responses such as surface deflections, stresses, and strains at different depths in the pavement-subgrade model were analyzed for critical locations. A full factorial experiment for six independent variables at two levels was designed, and the simulations for 64 treatment combinations were executed for the uncracked model. The results of the 3D-FE models showed comparable results with previous studies using the LS-DYNA software and the outputs of the GAMES linear elastic program. An extended analysis was conducted on the cracked model to study the effect of full-depth cracked on effective asphalt modulus values. Based on the full-depth cracked 3D-FE model results, low-level modulus of weak pavements showed a higher reduction of 81.0 % in the asphalt modulus compared to the asphalt modulus of the uncracked 3D-FE model, while the high-level modulus and thick pavement showed a low reduction of 13.5 % in the asphalt modulus of the uncracked pavement model.

The development of the enhanced pavement condition prediction equations provides significant improvements over the MEPDG method, such as consideration of maintenance and rehabilitation history and climatic regions, using a larger number of LTPP datasets, compared to model datasets used in the MEPDG. Therefore, the developed equations are more appropriate for the pavement structural design and asset management of asphalt highways. This implementation will contribute towards longer-lasting asphalt highway pavement assets to serve the public, improve safety, support efficient supply chain and economic growth.

# 1. INTRODUCTION

We live in a “global economy,” where the global supply chain interconnects a country’s transportation hubs through import/export demand of agriculture commodities, manufacturing goods, and fossil fuels. Ships, air cargo, and land transport are used as freight carriers for most goods. As discussed in a report of the National Academies (Plumeau et al. 2012), U.S. companies collectively spend a trillion dollars annually on freight logistics. This is nearly 10% of the nation’s gross domestic product (GDP). Considering about 80% of the population works and lives in cities and urban areas, 65% of goods originate or terminate in cities. The recent U.S. Department of Transportation (DOT) statistics based on a recent Commodity Flow Survey indicates that, on average, 54.7 tons of freight was shipped per person in the U.S. in 2016. The freight transportation system moved nearly 17.7 billion tons of goods valued at more than \$18.1 trillion in 2016 (U.S. Department of Transportation 2016). These statistics are indicative of the importance of the lifeline supply chain transportation infrastructure to support our society and everyday life. Understanding the risk of natural disaster catastrophes to highway infrastructure and impacts on disruptions of logistics and supply chain is a prerequisite for developing effective mitigation strategies and resilience management planning (Meyer et al. 2019).

Highways and roads represent the dominant mode of inland traffic in most countries and carry most of the passenger traffic and freight transport. The public highway network in the United States represents investments of 7.7 trillion dollars in 2016. It consists of about 6.56 million km (4.1 million miles), where 4.2 million km are paved roads, 2.36 million km are unpaved roads, and 615,000 bridges in 2016 (U.S. Department of Transportation 2016). About 93% of the 4.2 million kilometers of paved roads and highways are surfaced with asphalt (Uddin 2015a). This is the reason why this research focuses on the asphalt highway pavement. According to the U.S. Department of Transportation (USDOT), about 2,988.3 billion cumulative vehicle miles traveled (VMT) were observed in 2013 (NCHRP 2004a). Heavy commercial truck VMT increased about 10% of total VMT in the United States while trucks inventory was only 4% of total motor vehicle inventory for about 269 million motor vehicles in 2016. Trucks carried the largest share of goods shipped, 62.7 percent of the tonnage and 61.9 percent of the value in 2016 (U.S. Department of Transportation 2016). The average annual km driven by a truck is almost 2.24 times the distance traveled by car. These statistics show that road infrastructure is imperative to sustain a road user’s movement and ensure a nation’s economic competitiveness. Highway pavements are stressed by commercial trucks more than ever and any pavement design method and performance modeling must include accurate traffic volume and axle data and annual repetitions.

The Congressional Budget Office (CBO) (AASHTO 2020) reported that 146 billion USD was spent to build, operate, and maintain highway networks in the U.S. in 2007. This is the actual amount of money spent on maintaining a million miles of the nation’s aging highway networks. The real challenge that researchers face today is how to prevent asphalt pavements degradation over time as manifested by: longitudinal roughness, deformation distresses (rutting), cracking distresses (longitudinal and transverse cracking, fatigue cracking, low-temperature block cracking), and surface distresses (potholes, patching, etc.). These pavement condition attributes are monitored periodically by highway agencies as a part of the highway asset management system. The condition data are analyzed to identify candidate sections for the current year M&R intervention. However, it is hard to find a single mile of asphalt roads that

show no cracks. Regardless of how well a road material is mixed, the asphalt layer will eventually crack and degrade over time due to various factors including environmental conditions. Crack development is quick at the beginning, slows down after a certain time. If no timely maintenance and rehabilitation (M&R) treatments are applied, there are possibilities for the initial longitudinal and transverse cracks to interact and create block cracking. Under repetitive traffic loads, the block cracking deteriorates further to cause alligator cracking and end up with potholes spotted on the road surfaces. Therefore, pavement performance and condition deterioration progression models are needed to design pavement structure and to predict long-term major M&R interventions need by surface type.

A hairline crack starts it all. A small gap or discontinuity on the asphalt surface will allow water to seep through and accumulate beneath the pavement, which leads to the weaker underlying soil. Over time, rainwater flows through cracks surfaces and the moving traffic caused pumping, which eventually led to forming potholes and damaging the road surfaces. In colder regions, water from snow and ice seeps through an opening on the pavement surface. During cold weather, it freezes and expands which eventually leads to pavement and subbase break up. Once the ambient temperature increases, the melting ice leaves a gap inside the pavement. Over repetitive traffic loading, the asphalt eventually fails to support the weight of moving vehicles. Eventually, the asphalt layer disintegrates into smaller pieces, washed away and creating potholes. Potholes are not only among the top 20 causes of car accidents but also contribute to fatal motorcycle accidents in the U.S. (Plumeau et al. 2012).

According to the National Highway Traffic Safety Administration (NHTSA), the U.S. road and highway networks posed significant challenges over the last decade. In the U.S, the historical fatalities data revealed that a total of 1,658,458 fatalities occurred from 1975 to 2013 (U.S. Department of Transportation 2016). These statistics refer to passenger vehicle occupant, motorcyclist, and pedestrian deaths for a 1975 to 2013 analysis period. These fatalities are only 0.53 percent of the total population of 315,091,938 (2013) (Meyer et al. 2019). But, that small percentage means something important for those who experienced the loss of family members due to road fatalities. A recent study (AASHTO 1993) using datasets from 2004 to 2013 shows that, out of 340,879 deaths, about 76 percent are passenger vehicle occupants, 12 percent are a motorcyclist, and another 12 percent are road pedestrians. In 2013, a total of 32,719 deaths were reported, or ten deaths per 100,000 population, in the U.S. This is not the statistic to be proud of compared to only four deaths per 100,000 populations in Germany (Uddin 2015a).

Another major concern is the number of hours spent on the road due to traffic delays. The data sets from the USDOT Bureau of Transportation (FHWA 2019) showed in 2011, the annual person-hours of highway traffic delay per auto commuter were 52 hours for very large urban areas (> 3 million population), 37 hours for large urban areas (1 to 3 million population), 29 hours for medium urban areas (0.5 to one million population) and 23 hours for small urban areas (> 0.5 million population), respectively. These highway traffic delays caused annual congestion costs per auto commuter of \$16,243 for very large urban areas, \$23,305 for large urban areas, \$21,854 for medium urban areas, and \$10,173 for small urban areas (FHWA 2019). Additionally, highway traffic delays also contribute to higher carbon dioxide (CO<sub>2</sub>), harmful Particulate Matter (PM), and other emissions due to the trucks and cars burning more fossil fuel during highway traffic congestion. Eventually, the emission will cause health problems to an individual who lives in these areas with poor air quality index.

Therefore, there is a need to maintain acceptable road conditions over time. This goal is possible if

the enhanced predictions models are used in the pavement structural design. The literature review to date indicates that the lifetime M&R history was not considered in asphalt pavement condition deterioration progression modeling. In the historical asphalt pavement database records of the LTPP research program of the National Academy of Sciences, the M&R sequence is denoted by the construction number (CN). Thus, there is a need to consider the CN in pavement condition deterioration modeling.

In the U.S., the LTPP program was started in 1987 under the Strategic Highway Research Program (SHRP) to monitor the performance of more than 2,500 assigned test sections under the actual effect of continuous traffic applications in different climatic regions (FHWA 2019). In 1992, the LTPP program was transferred to the Federal Highway Administration (FHWA) to continue asphalt pavement performance monitoring for in-service state road and interstate highway networks. The LTPP database was established to store all essential information, including Falling Weight Deflectometer (FWD) data (FHWA 2019). Unfortunately, it was noted that before June 2015, Young's modulus values that describe the stiffness of the materials in different pavement layers were not included in the database. The modulus values are important for pavement layered elastic design of highway pavements.

There is also a need to backcalculate pavement layer modulus values for response analysis and numerical modeling purposes. Although the modulus values are provided in the LTPP database after June 2015, the initial evaluation to verify the modulus values from the LTPP database indicates unacceptable modulus values for test sections evaluated in this research. Therefore, the modulus values were backcalculated using several backcalculation software, and the results were compared.

The data sets from the LTPP database (FHWA 2019) were used to develop the asphalt pavement roughness, rutting, and cracking models. However, the research by Mohamed Jaafar et al. (Jaafar et al. 2015) on the development of the roughness deterioration prediction models for the LTPP Southern region in the U.S. showed large amounts of missing data from the database. Additionally, the literature review revealed that most of the research related to the development of condition deterioration prediction models show that the models did not consider lifetime M&R history. This includes the IRI roughness and rutting prediction models developed in the National Cooperative Highway Research Program (NCHRP) 1-37A study. The NCHRP 1-37A was conducted to establish a MEPDG (AASHTO 2008) to improve pavement structural design. This national project was completed in February 2004 with an approximately \$6.6 million research fund (NCHRP 2004a). However, the actual total cost of \$15 million spent on MEPDG was reported, and additional money was needed for calibration efforts (Uddin et al. 2013). The MEPDG was claimed to significantly improve pavement design as compared to the 1993 American Association of State Highway and Transportation Officials (AASHTO) guide (AASHTO 2008). Nonetheless, the design aspect alone is not enough to sustain long-lasting pavement but also requires timely M&R treatments (Uddin et al. 2013).

The AASHTOWare software was developed under the NCHRP1 1-37A project. This software did not provide any structural thickness values since it was designed to provide fail or pass criteria only. This software provides pass or fail criteria for terminal IRI, rut depth, fatigue cracking, combined reflective and alligator cracking, thermal cracking, and also longitudinal cracking (including top-down cracking (TDC)). The numerical models developed under the NCHRP1-37A study were calibrated with pavement performance data from the LTPP program (AASHTO 2008). However, the accuracy of the TDC numerical model is questionable since there is no TDC data available in the LTPP database. The

recent AASHTO MEPDG (AASHTO 2008) assumed that TDC was caused by repeatedly applied loads. It appears very doubtful that the appropriate regression models were used to predict the TDC. The previous study in Manitoba, Canada, showed that the longitudinal cracking or TDC prediction model in the MEPDG was found to be unreliable (Ahammed et al. 2013). In addition, through a class problem (Uddin 2015b) that simulates the U.S. Highway 45 Alternate, the predicted TDC contradicts the findings of visual observations that indicate no TDC distress occurred. Uddin (2013) reported an extensive literature review on TDC problems worldwide and field identification methods.

Further analysis is needed to enhance the understanding of the uncracked and cracked asphalt pavement responses using 3D-FE simulations. The latest AASHTO MEPDG assumed that TDC distress happened due to asphalt fatigue failure, which is unlikely. There are no proper models used to predict this distress type, most probably due to the limited amount of data sets related to TDC. Consequently, TDC was not properly considered for the pavement asset management system. This implies that the right M&R related to TDC can be applied, which will improve mechanistic-empirical design procedures. Additionally, the universal cracking prediction model is needed to consider different surface cracking types in M&R treatment intervention. This research topic needs urgent attention since surface cracking has become a common surface distress mode of failure in Hot Mix Asphalt (HMA).

In the future, further research is needed to highlight the TDC phenomena caused by the surface tensile stresses of wide truck tires, asphalt mix problems, and poor road construction processes (Uddin 2013). The advancement in nondestructive testing (NDT) technology may contribute to faster road surface condition monitoring. An extensive literature review was conducted to synthesize the potential of the ground penetration radar (GPR) remote sensing technology to map the TDC depth from the surface through asphalt layer thickness (Uddin 2013, 2014). However, based on the review of Uddin's GPR report (Uddin 2013), a nondestructive and noncontact technology operating at highway speed to evaluate TDC was not found in the literature (Uddin 2014, 2015b).

The use of the 3D-FE is important to study pavement responses for cracked pavement layers, considering that deflection tests are performed on existing pavements that may have cracked. The theory used to analyze deflection data in the commercial modulus backcalculation and pavement analysis software assume pavement layer without cracks or any other discontinuity, which is unlikely in the real world. Uddin et al. (1997) successfully evaluated the performance of jointed concrete pavement by analyzing 3D-FE pavement models created using the ABAQUS software and field condition data. The discontinuity in the concrete pavement was modeled using the unidirectional gap elements. In addition, a cracking model was also developed and applied beneath the concrete layer (Uddin et al. 1997).

Additionally, this research also investigates the development of a universal cracking progression model using the LTPP database (FHWA 2019). The concept of the universal cracking indicator (CI) was introduced by Paterson in 1994 (Paterson 1994a). The CI considers the extent, intensity, and crack width for transverse, longitudinal, and alligator cracking, respectively. The CI is the summation of the CI for each crack type. The concept of the proposed indicator of cracking was not well explored and reported in the literature review. The development of the enhanced condition deterioration progression model and the universal cracking progression model for a whole life analysis approach improves pavement design and asset management. The preservation of the road network over time demands condition monitoring and intensive financial considerations.

The pavement surface condition monitoring and structural integrity assessment periodically are

needed for timely M&R treatments. Application of the improved predictive models contributes toward a better pavement management decision support system for maintenance interventions.

## **1.1. Objectives**

The Year 1 research project objectives are, as follows:

1. Review the literature in detail for the evolution of asphalt pavement thickness design methods from the start of the Interstate highway construction program in the late 1950s to the post-2000 period, pavement performance models used for condition deterioration progression, and discuss the deficiencies.
2. Collect the LTPP pavement condition monitoring and FWD deflection data and process for developing innovative enhanced condition deterioration and performance models incorporating M&R history, climatic regions, and seasonal effects.
3. Verify and validate the developed models and conduct sensitivity analysis to understand the effect of variability of inputs (age, structure, materials, cumulative traffic, maintenance history, environment, and climate) on roughness and distress response variables.
4. Develop simplified predictive regression equations for structural response analysis using a database of response simulations from three dimensional-finite elements (3D-FE) models of pavement-subgrade structures to implement with the developed ME pavement performance models. The simulations will be conducted using a statistical sampling design.
5. Analyze the probability of intervention impacts of natural hazards and extreme weather and climate change events on the performance of constructed pavement structures. These interventions significantly influence pavement performance and result in catastrophic disasters but cannot be incorporated into the current design process. This will be a key step for developing disaster resilient design of highways.

## 2. LITERATURE REVIEW

### 2.1. Literature Review of Mechanistic-Empirical Design of Asphalt Pavements

The AASHTO 1993 empirical method of asphalt pavement structural design was developed based on the results of a series of experiments and experience of engineers involved in the AASHTO Road Test conducted in October 1958 and ended in November 1960 (AASHTO 1962). The AASHTO road test was carried out to assess serviceability-performance, load equivalency, create a performance database, and distress monitoring under periodical observations (Uddin 2015b). A total of \$27 million (1960 dollars) were invested by the U.S. government and industries to study the behavior of both concrete and asphalt highway pavement structures under moving trucks, driven on five out of six closed loops (two-lanes wide) developed for the study. One loop was evaluated under no traffic load repetitions and subjected to climate impacts for two years test period (AASHTO 1962).

There were 836 test sections of pavements, representing 200 various combinations of surface, base, and subbase layers with different thickness levels. This accelerated test was conducted at 18 hours per day and reached 1,114,000 axle load applications per loop during the two-year test. The longitudinal profile, roughness, cracking, patching, rut depth, and joint faulting were measured and extensively analyzed to develop the relationship between pavement performance, pavement design, and load variables (ENR 2006; Uddin 2015b). Uddin (2015c) summarized in detail the key lessons learned from the AASHTO Road Test. There are a few major limitations applied to the empirical equation used in the AASHTO 1993 design guide as follow (MDOT 2015; Uddin 2015c):

- Low truck traffic volumes (less than 1.8 million ESALs) and do not consider axle load spectra.
- Consider only climate condition and subgrade type at the AASHTO Road Test location in Ottawa, Illinois.
- Accelerated tests neglect the effects of climate and the aging of construction materials.
- A performance indicator is based only on the Present Serviceability Index (PSI).

However, truck-induced accelerated damage of highways in the 1980s steered to the introduction of the SHRP by Congress in 1987. The LTPP was one of the research programs that was successfully contributed towards the compilation and maintenance of the national LTPP pavement performance database at \$190 million from 1987 to 2007 (Uddin 2015c). In post-2000, advancements in computer and software technologies enabled the inclusion of theories of mechanics (MDOT 2015), which contributed to the development of mechanistic-empirical pavement design through NCHRP's Project 1-37 and Project 1-37A (NCHRP 2004a). The example of the AASHTO Ware Pavement ME Design software inputs is shown in Figure 1.

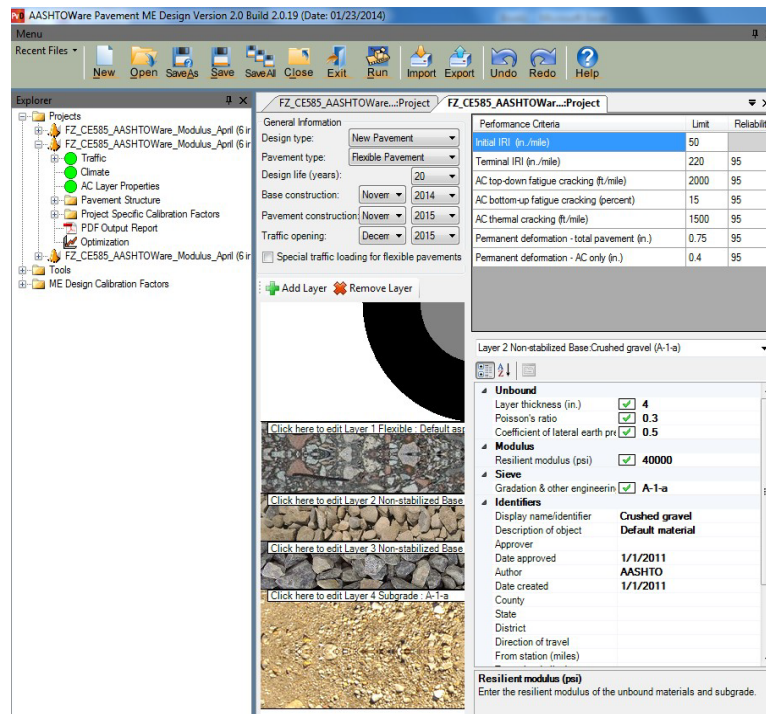


Figure 1. AASHTOWare Pavement ME Design software inputs

The mechanistic-empirical flexible pavement design approach has provided a huge step towards the betterment of the design by incorporating the following important input parameters through AASHTOWare pavement design software (AASHTO 2022; Uddin 2015c):

- Climate data from climate stations that are spatially distributed throughout the U.S. (more than 10 input data)
- Traffic inputs are normalized axle load spectra (NALS) for each truck class and axle group type, the number of axles of each type per vehicle class, percentile truck class volume distribution, truck volume, and truck growth (more than 120 input data).
- Variation of material properties (more than 100 input data) and layer properties (more than 20 input data)
- Six condition deterioration parameters of initial IRI (inches/mile), terminal IRI (inches/mile), rutting in asphalt layer only (inches), total rutting in asphalt and all unbound layers (inches), fatigue alligator cracking area (% surface area), transverse thermal cracking (feet/mile), and top-down cracking (feet/mile).

These six condition deterioration parameters were separately computed and compared with the threshold values to provide a pass or fail criteria over the design period. These criteria are a major improvement of only the PSI performance model used in the traditional method. However, there are also some limitations of the MEPDG methodology for asphalt pavements, which include no consideration of major maintenance and rehabilitation intervention as identified by CN in the LTPP database, in the design process. Other limitations are highlighted in detail by Uddin (Uddin 2015c) through his appraisal of the MEPDG in the U.S.



## 2.2. Roughness Modeling using MLR and ANN Methods

Historically, pavement longitudinal roughness has been an important component of the serviceability performance concept used in the development of the AASHTO pavement design procedures (AASHTO 1993). Pavement roughness describes the irregularities in the pavement surfaces that affect the ride quality experienced by daily road users. Consequently, rough road surfaces will adversely affect fuel consumption and maintenance costs. In 1986, an International Roughness Index concept was introduced by a group of researchers from the World Bank (Sayers et al. 1986).

The most recent MEPDG includes IRI as one of the criteria for any pavement section evaluations (AASHTO 2008). The IRI roughness (or smoothness called in the post-2000 MEPDG) is measured on an annual basis as part of the highway pavement asset management system (Uddin et al. 2013). Basic principles of pavement roughness evaluation are described by Plati (2011) in a study to establish pavement roughness evaluation criteria. An acceptable prediction of the future IRI value is closely related to a reasonable formulation of IRI roughness prediction models that consider all major factors such as initial IRI ( $IRI_0$ ), cumulative traffic ESAL (CESAL) applications, structural number (SN), and pavement age (year). The IRI prediction model is used for the life cycle assessment of pavement design alternatives and was selected as one of the important pavement condition attributes in this research.

In the U.S., the IRI for National Highway System (NHS) was measured by each state and the IRI data were compiled in FHWA's Table HM-47A (FHWA 2016). Figure 2 shows the NHS roughness conditions for all states in the U.S. A total of 157,426 miles of the NHS were surveyed in 2011. The IRI less than 1.5 m/km (95 in./mile) indicates a good ride quality. If the IRI is in between 1.5 m/km (95 in./mile) to 2.7 m/km (171 in./mile), the road surfaces are in medium condition. Additionally, the IRI of more than 2.7 m/km (171 in./mile) shows poor road conditions. The state of Texas recorded the highest NHS surveyed length for the IRI in 2011.

Ten out of 51 states reported more than 80% of the surveyed NHS with good ride quality (IRI less than 1.5 m/km) including Florida, Alabama, and Tennessee in the Southern LTPP region. On contrary, Washington D.C. surprisingly showed the worst road conditions with 86.3% of the surveyed NHS are in poor condition. In general, about 65.3% of the NHS in the U.S. are in good condition. About 28.8% of the NHS are in medium condition, and only 5.9% of the total NHS surveyed length are in poor condition. However, the statistics indicate that most of the NHS on the East Coast of the U.S. needs major M&R treatments. This implies that most of the surveyed NHS have higher percentages of medium and poor road networks, as compared to the NHS for the states in the Central and West Coast of the U.S.

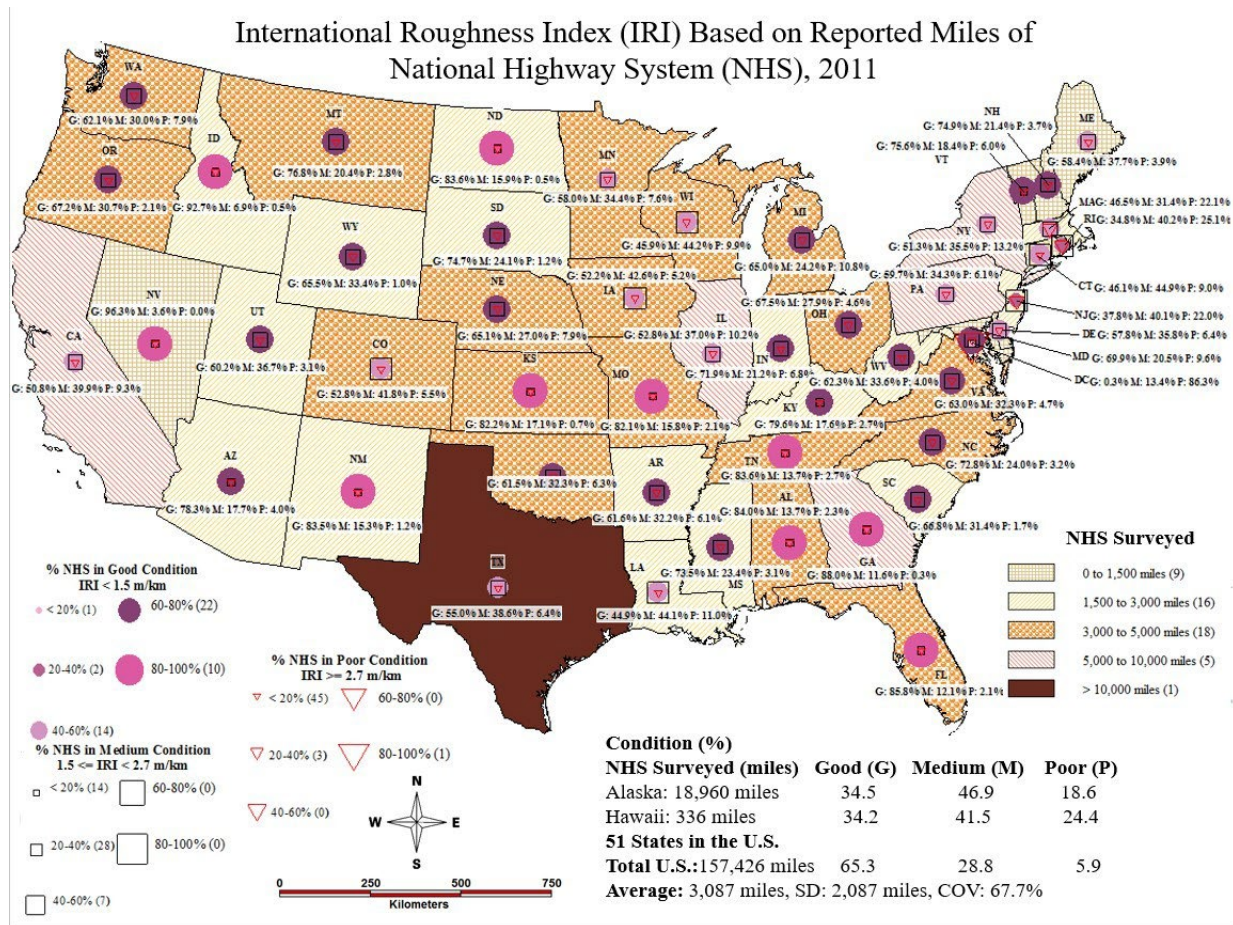


Figure 2. IRI based on reported miles of National Highway System in 2011 (FHWA 2016)

### 2.2.1. MEPDG Performance Modeling for Roughness

As mentioned earlier in this chapter, the IRI is one of the important performance criteria used in the design software. Equation 2.1 was developed using 1,926 data points from the LTPP database and was embedded in the MEPDG to predict the progression of the IRI over the design period for new and overlay of asphalt pavements (Johanneck and Khazanovich 2010). The reported Pearson's R-value is 0.75 ( $R^2 = 0.56$ ).

$$IRI = IRI_0 + 0.0150(SF) + 0.400(FC_{Total}) + 0.0080(TC) + 40.0(RD) \quad \text{Eq. 2.1}$$

The site factor (SF) was calculated using Equation 2.2.

$$SF = Age[0.02003(PI + 1) + 0.007947(Precip + 1) + 0.000636(FI + 1)] \quad \text{Eq. 2.2}$$

Table 1 summarizes the independent variables used in Equations 2.1 and 2.2. The independent variables used in the enhanced IRI multiple regression developed in this research were also shown for comparison purposes. The enhanced IRI multiple regression equations consider independent variables that are easier to use for future IRI value prediction without the need to use the data from the laboratory

tests. Additionally, the enhanced IRI multiple regression equation does not require the measurement of other asphalt surface distresses such as rut depth and area of fatigue cracking before the calculation of the future IRI values. Moreover, the enhanced IRI multiple regression equation also considers important factors such as maintenance and rehabilitation intervention factor, LTPP regions factor, and IRI roughness measurement locations.

The independent variables used in the enhanced IRI multiple regression developed in this research were also shown for comparison purposes and will be described later in this report. The enhanced IRI multiple regression equations consider independent variables that are easier to use for future IRI value prediction without the need to use the data from the laboratory tests.

Additionally, the enhanced IRI multiple regression equation does not require the measurement of other asphalt surface distresses such as rut depth and area of fatigue cracking before the calculation of the future IRI values. Moreover, the enhanced IRI multiple regression equation also considers important factors such as maintenance and rehabilitation intervention factor, LTPP regions factor, and IRI roughness measurement locations.

Table 1. Independent variable used in the enhanced IRI MLR equation and MEPDG

No.	Enhanced IRI multiple regression developed in this research		No.	MEPDG IRI Regression Equation	
1	IRI <sub>0</sub>	Initial IRI, m/km	1	IRI <sub>0</sub>	Initial IRI after construction, in./mi
2	Age	Pavement age, year	2	Age	Pavement age, year
3	PRECIP	Average monthly precipitation, mm	3	Precip	Average annual precipitation or rainfall, in.
4	SN	Structural number	4	PI	Plasticity Index (%)
5	CESAL	Cumulative ESAL	5	FI	Mean annual freezing index, °F days
6	TEMP <sub>AIR</sub>	Air Temperature, °C	6	TC <sub>Total</sub>	Length or transverse crack, ft./mi
7	Reg_D	Dummy variable for LTPP regions, assign 1 for Southern region and 0 for other regions	7	RD	Average rut depth, in.
8	CND	Dummy variable for major M&R, 0 for no major M&R; 1 if M&R has taken place	8	FC <sub>Total</sub>	FC <sub>Total</sub> is % area of fatigue cracking (combined alligator, longitudinal, and reflection cracking),
9	IRI_D	Dummy variable for roughness measurement locations, 0 for outside wheel path; 1 for inside wheel path			

### 2.2.2. Previous Studies on the Development of MLR Equations

Many researchers reported different approaches to model and predict IRI in future years. Paterson (1987) developed and implemented the performance models in the Highway Design and Maintenance Standards Model (HDM-III). The empirical data used to predict surface roughness were based on initial roughness IRI<sub>0</sub>, modified SN, cumulative ESAL traffic, and pavement age since construction,

rehabilitation, or reconstruction. The reported R-value is 0.866. In addition, a correlation between roughness and quarter-car index (QI) was developed, where IRI is equal to QI/13.

In 1989, a new model was developed to predict the progression of roughness overpavement life (Paterson 1989). It was developed based on field data in the Brazil-United Nations Development Program (UNDP) road cost study and includes structural, surface distresses, and combined environmental-age-condition factors, respectively. The new model predicted the increase of roughness over time and incorporated modified SN, the thickness of the crack layer, area of cracking in percent, and changes in ESAL per lane. In addition, an increase in rut depth, increase in the area of surface patching, pavement age, and road surface anomalies such as potholes were also considered as other contributing factors. The model had an R-value of 0.768. The researcher concluded that the development of road roughness involved a few stages which occurred through multiple mechanisms. The road surfaces degraded over time due to traffic loading, exaggerated by weak pavement strength and exposure to the environmental condition over the years (Paterson 1989).

Cardoso and Fortunato Marcon (1998) reported various pavement performance models as a function of the pavement age or the number of standard axle load applications. Data from the road network of the State of Santa Catarina in Brazil were used and the models were implemented in the Pavement Management System (PMS). Five different models were established including the models to predict QI based on age and cumulative ESAL, respectively. The model predicted QI for three different regions according to subgrade layer types and the R values ranged from 0.332 to 0.831. However, the prediction overestimated the results when compared to previous Brazilian studies by Queiroz (1981).

Soncim and Fernandes (2013) developed the IRI roughness prediction model, which includes pavement age, ESAL, and rainfall intensity (RFL). An ANOVA was performed from the data collected in 2009 from road roughness surveyed on a 650 km road network in the State of Bahia, Brazil. The model was verified using field data and compared to other IRI roughness prediction models. The results showed a reasonable correlation between the observed and predicted values with  $R^2$  equal to 0.91. Soncim and Fernandes's models are shown in Equations 2.3 through 2.6.

$$IRI = 4.55 + 0.57xP(AGE) + 0.86xP(EAL) + 0.38xP(RFL) + 0.25xP(EAL)xP(RFL) \text{ Eq. 2.3}$$

$$P(AGE) = \frac{AGE-22}{14} \text{ Eq. 2.4}$$

$$P(EAL) = \frac{EAL-1.1 \times 10^6}{1.6 \times 10^6} \text{ Eq. 2.5}$$

$$P(RFL) = \frac{RFL-505}{222} \text{ Eq. 2.6}$$

Where  $P(AGE)$  is the polynomial equation for the age factor;  $P(EAL)$  is the polynomial equation for the accumulated traffic factor;  $P(RFL)$  is the polynomial equation for the rainfall factor.

Meegoda and Gao (2014) investigated the time-sequence roughness data of the General Pavement Study (GPS) of the LTPP test sections and developed a model to predict the roughness progression over pavement age. The Meegoda and Gao (2014) final model is shown in Equation 2.7.

$$\ln IRI_{i+1} - \ln IRI_i = a_{i+1} \times t_{i+1}^{0.9715} - a_{i+1} \times t_i^{0.9715} \quad \text{Eq. 2.7}$$

Where, alpha is described in Equation 2.8 and freezing index (FI) is shown in Equation 2.9.

$$\alpha = \frac{CL^a}{SN^b} c + FI^d e + AP^f g \quad \text{Eq. 2.8}$$

$$FI = \sum_{i=1}^n 0 - T_i \quad \text{Eq. 2.9}$$

Where, the *CL* is cumulative traffic load kilo ESAL per year (KESAL/year); *SN* is structural number; *AP* is annual precipitation; *a*, *b*, *c*, *d*, *e*, *f*, *g* are model parameters; *FI* is freezing index (°C-days), and *T<sub>i</sub>* is average daily air temperature on a day *i*.

Madanat et al. (2005) developed a performance model to predict the progression of the asphalt pavement roughness. In this study, the MLR equation was developed to predict the incremental roughness progression ( $\Delta$ IRI) value using the Washington State's PMS database. Eight independent variables were included: (1) IRI in the previous year, (2) change in the ESAL in the year of observation, (3) cumulative ESAL, (4) base thickness, (5) total asphalt layer thickness, (6) time since last asphalt overlay or bituminous surface treatment (BST) overlay, (7) minimum air temperature, and (8) yearly precipitation. In addition, three dichotomous (dummy) variables for asphalt overlay, BST overlay, and maintenance application were also considered. The multiple linear regression with  $R^2$  of 0.526 was observed in this study.

Rahim et al. (2009) evaluated the IRI for asphalt pavement overlays over concrete slab treated with crack, seal, and overlay (CS&O) rehabilitation technique. The IRI prediction models were developed for wet-freeze and wet-no-freeze LTPP regions. An additional model was developed for pavement sections in California. The factors of asphalt overlay thickness and base type (bound or unbound) were evaluated in the study. The independent variables are pavement age, annual ESAL, cumulative ESAL, base type, asphalt, and concrete pavement thicknesses. The IRI models for wet-freeze (WF), wet-non-freeze (WNF), and California are shown in Equations 2.10 through 2.12. The observed  $R^2$  are 0.55 (WF), 0.50 (WNF), and 0.62 (California), respectively.

$$IRI_{freeze} = 1.097 + 0.0158(Age^{1.6747}) \left( \frac{KESAL^{0.0234}}{H_{ac}} \right) \times (1 + base)^{-1.103} \quad \text{Eq. 2.10}$$

$$IRI_{no-freeze} = 1.652 + 0.0751(Age) - 0.143H_{ac} + 0.57(base) \quad \text{Eq. 2.11}$$

$$IRI_{CA} = 0.754 + 0.0158(CESAL^{1.07}) \left( \frac{H_{ac}}{H_{pcc}} \right)^{-1.242} \quad \text{Eq. 2.12}$$

Where *age* is pavement age (year); *CESAL* is cumulative ESAL per year (million); *KESAL* is ESAL per year (millions); *H<sub>ac</sub>* is the depth of asphalt overlay; *H<sub>pcc</sub>* is the depth of the concrete slab; and *base* is the type of base (0 is bound; 1 is unbound).

Choi et al. (2004) established the roughness prediction model using the multiple linear regression method. The data sets for the LTPP GPS-1 test sections in the states of Texas, New Mexico, and Arizona were used and grouped according to the climatic zones (wet-no-freeze and dry-no-freeze), average daily truck traffic, construction number, and functional class. The multiple linear regression equation with the  $R^2$  of 0.714 is shown in Equation 2.13.

$$IRI = 4.08 - 0.616(SN) - 0.415(AC) + 7.79(P200) + 0.709(CESAL) - 0.48(Thick) \quad \text{Eq. 2.13}$$

Where the  $SN$  refers to the structural number,  $AC$  is asphalt content,  $P200$  is the percent passing no. 200 sieve, “*Thick*” represents the thickness of the top layer and  $CESAL$  is the cumulative ESAL in million.

### 2.2.3. Artificial Neural Network Models for IRI Roughness Prediction

A few studies related to the IRI roughness ANN modeling are reviewed and summarized in this research. Uddin et al. (2013) provide good explanations about the ANN modeling method. Attoh- Okine Attoh-Okine (1994) applied the ANN’s back-propagation method to evaluate the capabilities of the ANN to predict roughness progression in flexible pavement. Extensive research investigated structural deformation as the factors of modified SN, incremental traffic loadings, the extent of cracking and thickness of the cracked layer, and incremental variation of rut depth. In addition, the surface distresses (changes in cracking, patching, and potholing), environment, and other non-traffic-related mechanism were also investigated.

Choi et al. (2004) also developed the ANN model ( $ANN_{6-10-1}$ ) with the  $R^2$  of 0.723 to predict the IRI roughness value. The models were further evaluated using other data sets that are not included in the model development. The measured vs. predicted IRI plots showed the  $R^2$  of 0.212 and 0.757 for the MLR equation and the  $ANN_{6-10-1}$  model, respectively. Kargah-Ostadi et al. (2010) developed the changes in the IRI prediction model for rehabilitation recommendations using the ANN. The statistical analysis for 20 variables was conducted to determine any significant correlation with the IRI. Only eight variables were included in the final model. The  $R^2$  of 0.956 was observed between the predicted and measured IRI values which shows that it is feasible to use IRI as the prediction criteria.

In this research, the ANN analysis and modeling technique was also adopted for the development of asphalt pavement condition deterioration progression prediction models. The ANN is an advanced computing system established from several simple, highly interconnected elements that process information through dynamic responses to the external inputs (independent variables). The basic model for each neuron in a simple ANN is shown in Figure 3. The neural network gains its knowledge through a trained feed-forward network. During this process, a set of training data consisting of inputs (independent variable) and output (dependent variable) is presented to the network.

The resulted output is compared to the target values. Next, the backpropagation process adjusts the connection weight to reduce the error between actual and target values. Once trained, the networks provide an approximate functional mapping of any input pattern onto its corresponding output pattern. Subsequently, the validation process was carried out using data sets that are excluded from the model database (Uddin et al. 2013). The development of the ANN models was carried out using the TRSEQ1

computer program (Najjar 1999). Sigmoid activation function was embedded in the software for data generalization purposes. Figure 4 (i) shows the curve for the sigmoid function bounded between zero and one value together with the equation needed for data transformation using a sigmoid function.

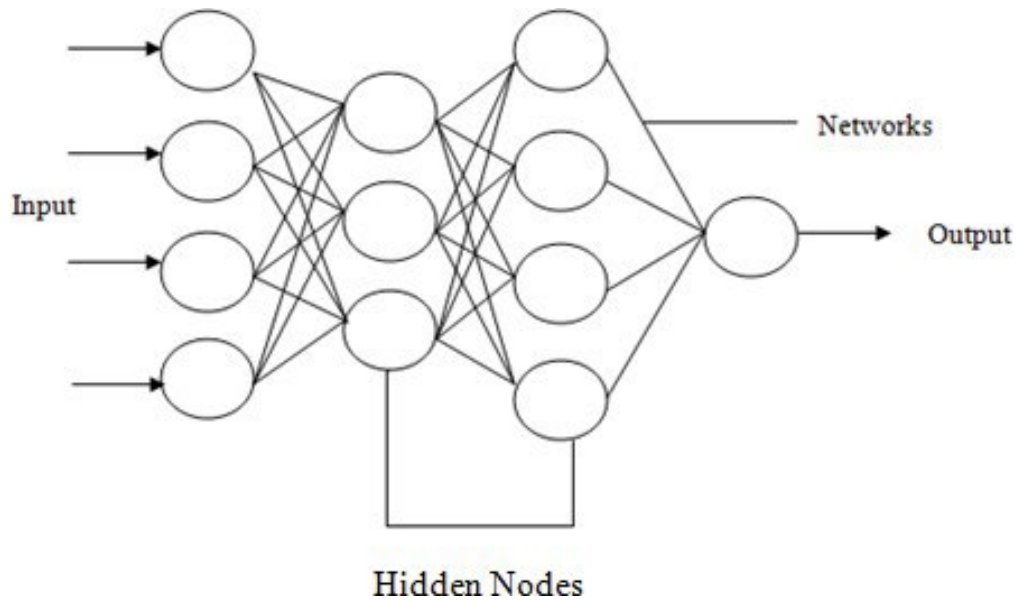


Figure 3. Example of ANN processing elements and interconnection network

This ANN model requires additional pre-processing of the model database prepared for multiple regression analysis, which are:

- Selecting the datasets for training, testing, and validation processes.
- Calculating the normalized minimum and maximum values for dependent and independent variables, respectively.
- Setting up the TRSEQ1 software SPEC and STP input files before the analysis.

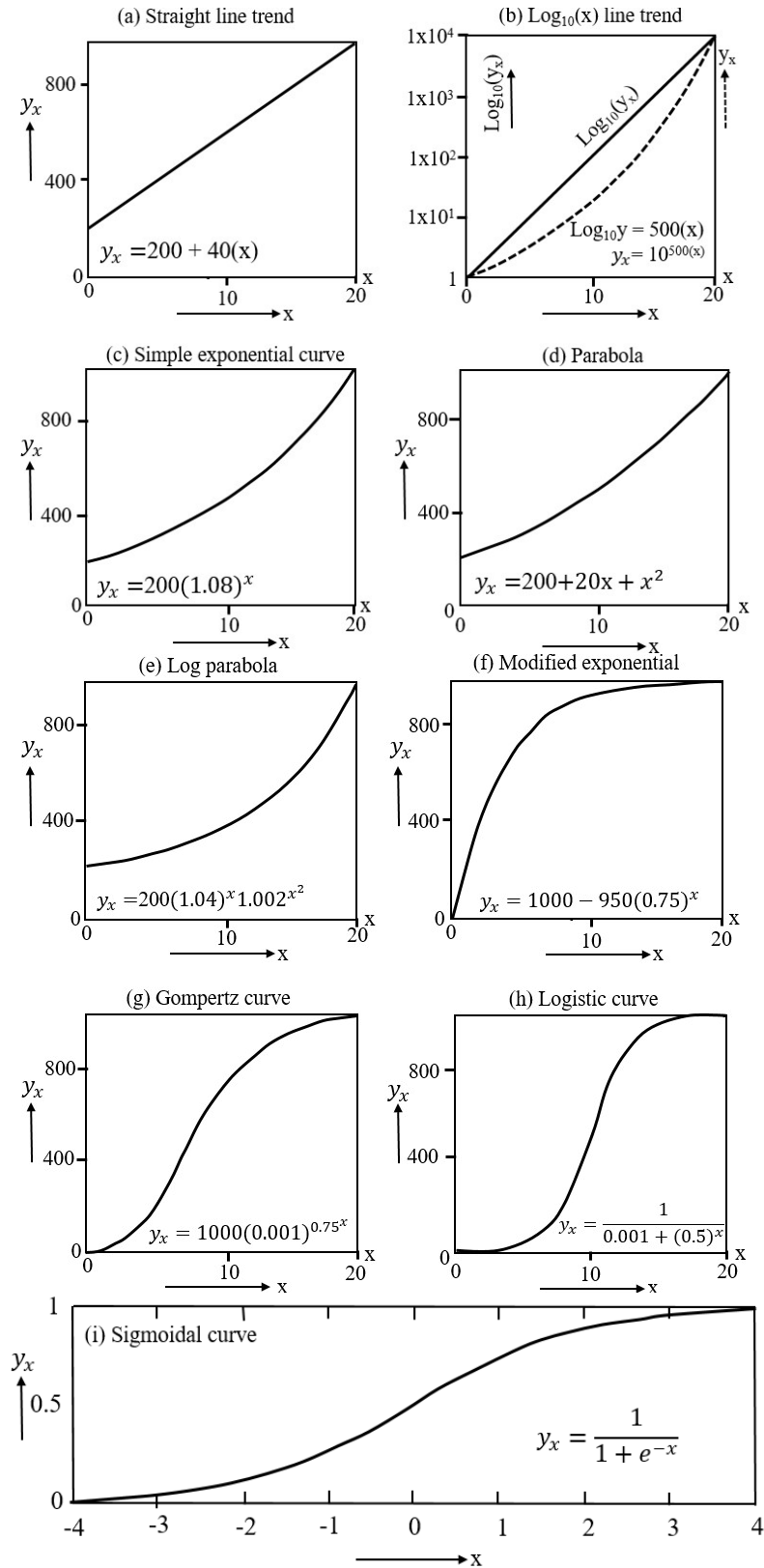


Figure 4. Data transformation functions used in mathematical modeling as a function of time (x-axis)



### 2.3.Literature Review of MEPDG Performance Modeling for Rutting Distress

Asphalt pavement rutting is known as one of the major pavement surfaces distresses that affect ride quality. The MEPDG defines rutting as distress that is caused by the permanent vertical deformation in the asphalt surface layer, unbound layers, and foundation soils (NCHRP 2004b). Equations 2.14 shows the MEPDG’s recalibrated model, including new model coefficients used to calculate total rutting in pavement layers (NCHRP 2004c). The Pearson’s R-value for the MEPDG rutting prediction model is 0.76 ( $R^2 = 0.58$ ), which was developed using 334 data sets.

$$TRUT = 0.51 \times ACRUT + 0.32 \times BASERUT + 0.33 \times SUBGRUT \quad \text{Eq. 2.14}$$

Where TRUT is total rutting, ACRUT is rutting in the asphalt layer, BASERUT is rutting in the base layer, and SUBGRUT is rutting in the subgrade layer.

The field calibrated mathematical equations to estimate incremental distortion or rutting at mid-depth of the asphalt layer are shown through Equations 2.15 to 2.18. Table 2 describes the parameters used in Equations 2.15 to 2.18, respectively.

$$\Delta_{p(HMA)} = \varepsilon_{p(HMA)} \times h_{(HMA)} = \beta_{1r} \times k_z \times \varepsilon_{r(HMA)} \times 10^{k_{1r}} \times n^{k_{2r}\beta_{2r}} \times T^{k_{3r}\beta_{3r}} \quad \text{Eq. 2.15}$$

$$k_z = (C_1 + C_2 D) \times 0.328196^D \quad \text{Eq. 2.16}$$

$$C_1 = -0.1039 \times (H_{HMA})^2 + 2.4868 \times H_{HMA} - 17.342 \quad \text{Eq. 2.17}$$

$$C_2 = 0.0172 \times (H_{HMA})^2 - 1.7331 \times H_{HMA} + 27.428 \quad \text{Eq. 2.18}$$

Table 2. The parameters used to calculate rutting at the mid-depth of the asphalt layer

Parameter	Explanations
$\Delta_{p(HMA)}$	Accumulated permanent or plastic vertical deformation in the HMA layer/sublayer, in
$s_{p(HMA)}$	Accumulated permanent or plastic axial strain in the HMA layer/sublayer, in./in
$h_{HMA}$	Thickness of the HMA layer/sublayer, in./in.
$n$	Number of axle-load repetitions
$T$	Mix or pavement temperature, F
$k_z$	Depth confinement factor
$k_{1r,2r,3r}$	Global field calibration parameters (from the NCHRP 1-40D recalibration; $k_{1r} = -3.35412$ , $k_{2r} = 0.4791$ , $k_{3r} = 1.5606$ )
$\beta_{1r}, \beta_{2r}, \beta_{3r}$	Local or mixture field calibration constants; for the global calibration, these constants were all set to 1.0
$D$	Depth below the surface, in
$H_{HMA}$	Total HMA thickness, in.

The field calibrated mathematical equations to calculate incremental distortion or rutting at mid-depth of all unbound sublayers are shown through Equations 2.19 to 2.22. Table 3 describes the parameters used in Equations 2.19 to 2.22, respectively.

$$\Delta_{p(soil)} = \beta_{s1} \times k_{s1} \times \varepsilon_v \times h_{soil} \times \left(\frac{\varepsilon_0}{\varepsilon_r}\right) \times \varepsilon^{-\left(\frac{p}{n}\right)\beta} \quad \text{Eq. 2.19}$$

$$\text{Log}\beta = -0.61119 - 0.017638 \times (W_c) \quad \text{Eq. 2.20}$$

$$p = 10^9 \times \left[\frac{C_o}{(1-(10^9)\beta)}\right]^{\frac{1}{\beta}} \quad \text{Eq. 2.21}$$

$$C_o = \ln \left[\frac{a_1 M_r^{b_1}}{a_9 M_r^{b_9}}\right] = 0.075 \quad \text{Eq. 2.22}$$

Table 3. The parameters used to calculate rutting at the mid-depth of all unbound sub-layers

Parameters	Explanations
$\Delta_{p(soil)}$	Permanent or plastic deformation for the layer or sublayer, in.,
$n$	Number of axle-load repetitions
$s_o$	Intercept determined from laboratory repeated load permanent deformation tests, in./in
$s_r$	Resilient strain imposed in laboratory test to obtain material properties $s_o$ , $s$ , and $\rho$ , in./in.,
$s_v$	Average vertical resilient or elastic strain in the layer or sublayer and calculated by the structural response model, in./in.
$h_{soil}$	Thickness of the unbound layer or sublayer, in.
$k_{s1}$	Global calibration coefficients; $k_{s1} = 1.673$ for granular materials and 1.35 for fine-grained materials
$s_{s1}$	Local calibration constant for the rutting in the unbound layers; the local calibration constant was set to 1.0 for the global calibration effort
$W_c$	Water content (%),
$M_r$	Resilient modulus of the unbound layer or sublayer, psi,
$a_{1,9}$	Regression constant; $a_1 = 0.15$ and $a_9 = 20.0$
$b_{1,9}$	Regression constants; $b_1 = 0.0$ and $b_9 = 0.0$
$W_c$	Water content (%)

About 20 input parameters are required to predict future rut depth using the MEPDG rutting prediction equation. The only load-related response parameter is  $s_v$ , which is the average vertical resilient or elastic strain in the asphalt layer or sublayers. The vertical strain was computed using the Jacob Uzan Layered Elastic Analysis (JULEA) multilayer elastic analysis computer program (NCHRP 2004b).

In general, the MEPDG rutting prediction model was developed to be used with the computer program, but not for manual calculation considering the complex input parameter that is based on the laboratory tests. In contrast, the enhanced rutting multiple regression equations developed in this research is easier to use for future rutting prediction considering reasonable input parameters such as initial rut depth value, cumulative traffic ESAL, layer modulus values, asphalt thickness, total layer

thicknesses, pavement age, SN, and air temperature. Moreover, the enhanced rutting multiple regression equation also considers important factors such as maintenance and rehabilitation intervention factor, LTPP regions factor, and base layer types.

## 2.4. Literature Review of MEPDG Cracking Distresses

In the MEPDG, asphalt surface cracking distresses are classified as load-related cracking (alligator cracking and longitudinal cracking), non-load-related cracking (transverse crack), and reflective cracking type. However, the latter is not one of the cracking distresses types that are in favor of this research. The following subchapters show the performance models for cracking distress predictions.

### 2.4.1. Load-Related Cracking (Alligator and Longitudinal Cracks)

The MEPDG describes alligator crack as load-related distress that initiates from the bottom of the asphalt layer and propagates upwards due to traffic load repetitions. In contrast, the longitudinal cracks are assumed to initiate from the asphalt surface (NCHRP 2004c). The incremental damage index approach was used to predict both alligator and longitudinal crack distresses. Equations 2.23 to 2.32 were used in the mechanistic-empirical design method of asphalt pavements.

$$N_{f-HMA} = k_{f1} \times (C) \times (C_H) \times \beta_{f1} \times (\varepsilon_t)^{k_{f2}\beta_{f2}} (E_{HMA})^{k_{f2}\beta_{f3}} \quad \text{Eq. 2.23}$$

$$C = 10^M \quad \text{Eq. 2.24}$$

$$M = 4.84 \times \left[ \frac{V_{be}}{V_a + V_{be}} - 0.69 \right] \quad \text{Eq. 2.25}$$

The MEPDG determines the thickness correction term,  $C_H$  for alligator crack and longitudinal crack based on Equation 2.26 and Equation 2.27, respectively.

$$C_H = \frac{1}{0.000398 + \frac{0.003602}{1 + e^{(11.02 - 3.49H_{HMA})}}} \quad \text{Eq. 2.26}$$

$$C_H = \frac{1}{0.01 + \frac{12.0}{1 + e^{(15.676 - 2.8186H_{HMA})}}} \quad \text{Eq. 2.27}$$

The incremental damage index ( $\Delta DI$ ) is calculated by dividing the actual number of axle loads by the allowable number of axles as described in Equation 2.28.

$$DI = \sum (\Delta DI)_{j,m,l,p,T} = \sum \left( \frac{n}{N_{f-HMA}} \right)_{j,m,l,p,T} \quad \text{Eq. 2.28}$$

Finally, the area of alligator cracking ( $FC_{BOTTOM}$ ) is predicted using Equation 2.29. Equation 2.32 is used to calculate the longitudinal fatigue cracks ( $FC_{TOP}$ ) (NCHRP 2004c).

$$FC_{Bottom} = \left(\frac{1}{60}\right) \left(\frac{C_4}{1+e^{(C_1 C_1^* + C_2 C_2^* \log(DI_{Bottom} \times 100))}}\right) \quad \text{Eq. 2.29}$$

$$C_1^* = -2C_2^* \quad \text{Eq. 2.30}$$

$$C_2^* = -240874 - 39.748(1 + H_{HMA})^{-2.856} \quad \text{Eq. 2.31}$$

$$FC_{TOP} = 10.56 \left(\frac{C_4}{1+e^{(C_1 - C_2 \log(DI_{TOP}))}}\right) \quad \text{Eq. 2.32}$$

Table 4 summarizes the explanations for each parameter used in the MEPDG equations to calculate the alligator and longitudinal cracks.

Table 4. Parameters used in the MEPDG equations to calculate alligator and longitudinal cracks

Parameters	Explanations
$N_{f-HMA}$	Allowable number of axle-load applications for a flexible pavement and HMA Overlays
$S_t$	Tensile strain at critical locations and calculated by the structural response model, in./in
$E_{HMA}$	Dynamic modulus of the HMA measured in compression (psi),
$k_{f1}, k_{f2}, k_{f3}$	Global field calibration parameters (from the NCHRP 1-40D re-calibration; $k_{f1} = 0.007566$ , $k_{f2} = -3.9492$ , $k_{f3} = -1.281$ )
$\beta_{f1}, \beta_{f2}, \beta_{f3}$	Local or mixture specific field calibration constants; for the global calibration effort, these constants were set to 1.0
$V_{be}$	Effective asphalt content by volume, %,
$V_a$	Percent air voids in the HMA mixture
$C_H$	Thickness correction term, dependent on the type of cracking
$H_{HMA}$	Total HMA thickness, in.,
$n$	Actual number of axle-load applications within a specific period
$j$	Axle-load interval
$m$	Axle-load type (single, tandem, tridem, quad, or special axle configuration)
$l$	Truck type using the truck classification groups included in the MEPDG
$\rho$	Month
$T$	Median temperature for the five temperature intervals or quintiles used to subdivide each month, °F
$FC_{Bottom}$	Area of alligator cracking that initiate at the bottom of the HMA layers, % of total lane area
$DI_{Bottom}$	Cumulative damage index at the bottom of the HMA layers
$C_{1,2,4}$	Transfer function regression constants; $C_4 = 6,000$ ; $C_1 = 1.00$ ; and $C_4 = 1.00$
$H_{HMA}$	Total HMA thickness, in
$FC_{Top}$	Length of longitudinal cracks that initiate at the top of the HMA layer, ft/mi
$DI_{Top}$	Cumulative damage index near the top of the HMA surface
$C_{1,2,4}$	Transfer function regression constants; $C_1 = 7.00$ ; $C_2 = 3.5$ ; $C_4 = 1,000$

The MEPDG also provides a specific equation to calculate fatigue crack in the Cement Treated Base (CTB) layer as shown in Equation 2.33 and Equation 2.34. Equation 2.33 is used to determine the number of load applications  $N_{f-CTB}$  for fatigue cracks in the CTB layers.

$$N_{f-CTB} = 10^{\left[ \frac{k_{C1}\beta_{C1}\left(\frac{\sigma_t}{M_R}\right)}{k_{C2}\beta_{C2}} \right]} \quad \text{Eq. 2.33}$$

$$FC_{CTB} = C_1 + \left( \frac{C_2}{1 + e^{(C_3 - C_4 \log(DI_{CTB}))}} \right) \quad \text{Eq. 2.34}$$

Equation 2.35 is used to calculate the damaged elastic modulus within each period for calculating critical pavement responses in the CTB and other pavement layers. Table 5 summarizes the explanations for each parameter used in the MEPDG equations to calculate fatigue crack in the CTB layer.

$$E_{CTB}^{D(T)} = E_{CTB}^{Min} + \left( \frac{E_{CTB}^{Max} - E_{CTB}^{Min}}{1 + e^{(-4 + 14(DI_{CTB}))}} \right) \quad \text{Eq. 2.35}$$

Table 5. Parameters used in the MEPDG equations to calculate fatigue crack in the CTB layer.

$N_{f-CTB}$	Allowable number of axle-load applications for a semi-rigid pavement
$\sigma_t$	Tensile stress at the bottom of the CTB layer (psi),
$M_R$	28-days modulus of rupture for the CTB layer, psi. The value used in the calculations are 650 psi
$\sigma_t$	Tensile stress at the bottom of the CTB layer (psi)
$DI_{CTB}$	Cumulative damage index of the CTB or cementitious layer determined in accordance with Equation 3e
$k_{c1}, k_{c2}$	MEPDG used 1.0 for these values
$\beta_{c1}, \beta_{c2}$	Local calibration constants; these values are set to 1.0 in the software
$FC_{CTB}$	Area of fatigue cracking, sq ft
$C_{1,2,3,4}$	Transfer function regression constants; $C_1 = C_2 = 1.0$ , $C_3 = 0$ , and $C_4 = 1,000$ (this value are not calibrated and may change once the transfer function has been Calibrated)
$E_{CTB}^{D(T)}$	Equivalent damaged elastic modulus at time t for the CTB layer (psi),
$E_{CTB}^{Min}$	Equivalent elastic modulus for the destruction of the CTB (psi),
$E_{CTB}^{Max}$	28-days elastic modulus of the intact CTB layer, no damage (psi)

#### 2.4.2. Non-Load Related Cracking – Thermal Cracking (Transverse Cracking)

The MEPDG describes transverse cracking as distress that is non-load related and predominantly perpendicular to the traffic direction. The low temperatures thermal cracking is the main reason for this type of cracking distress. The following Equations 2.36 to 2.40 are used to predict the thermal cracking.

$$\Delta C = A(\Delta K)^n \quad \text{Eq. 2.36}$$

$$A = 10^{k_t \beta_t (4.389 - 2.52 \log(E_{HMA} \sigma_m^n))} \quad \text{Eq. 2.37}$$

$$n = 0.8 \left[ 1 + \frac{1}{m} \right] \quad \text{Eq. 2.38}$$

$$K = \sigma_{tip} [0.45 + 1.99 C_o^{0.56}] \quad \text{Eq. 2.39}$$

$$TC = \beta_{t1} N \left[ \frac{1}{\sigma_d} \log \left( \frac{C_d}{H_{HMA}} \right) \right] \quad \text{Eq. 2.40}$$

Table 6 summarizes the explanations for each parameter used in the MEPDG equations to calculate fatigue crack in the CTB layer. Figure 5 shows typical crack distress types observed on asphalt surfaced road networks.

Table 6. Parameters used in the MEPDG equations to calculate fatigue crack in the CTB layer

$\Delta C$	Change in the crack depth due to a cooling cycle
$\Delta K$	Change in the stress intensity factor due to a cooling cycle
$A, n$	Fracture parameters for the HMA mixture
$k_t$	Coefficient determined through global calibration for each input level (Level 1 = 50; Level 2 = 1.5; and Level 3 = 3.0)
$E_{HMA}$	HMA indirect tensile modulus (psi),
$\sigma_m$	Mixture tensile strength (psi),
$m$	The m-value derived from the indirect tensile creep compliance curve measured in the laboratory
$\beta_t$	Local or mixture calibration factor
$\sigma_{tip}$	Far-fields stress from pavement response model at depth of crack tip (psi)
$C_o$	Current crack length, ft
$TC$	Observed amount of thermal cracking, ft/mi
$\beta_{t1}$	Regression coefficient determined through global calibration (400),
$N[z]$	Standard normal distribution evaluated [z],
$\sigma_d$	Standard deviation of the log of the depth of cracks in the pavement (0.769), in
$C_d$	Crack depth, in.,
$H_{HMA}$	Thickness of HMA layers, in

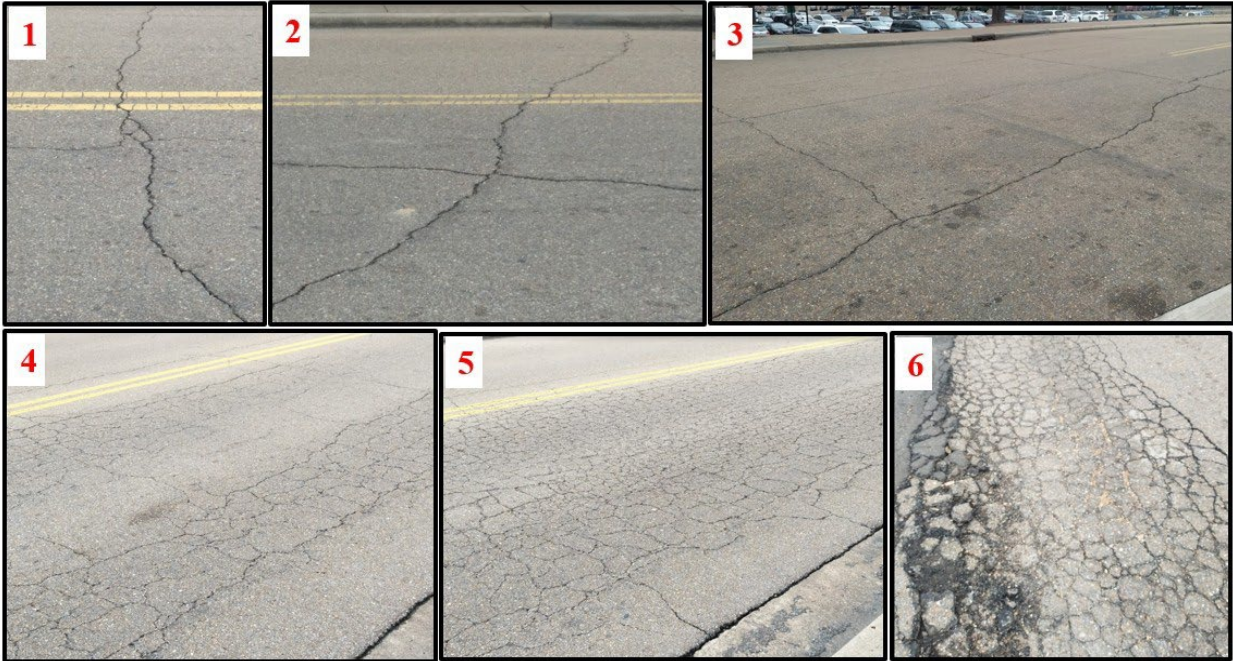


Figure 5. Typical crack distress types observed on asphalt surfaced road network

- Transverse crack: Initiation of block cracking, reflection cracking due to deterioration of cement or lime stabilized base or subbase (1)
- Longitudinal crack: Initiation of fatigue cracking, top-down cracking, poor longitudinal joint. (Fatigue is manifested as alligator cracking) (2)
- Block crack: Primarily due to low-temperature thermal cracking (3)
- Alligator crack: Primarily due to traffic load repetitions (4, 5, and 6)

### 2.4.3. UCI for Cracking Distress Indicator

In a road section, the severity levels of asphalt pavement surface distress of cracking and rutting are important factors for the M&R intervention. The most recent MEPDG method of pavement design for any road section requires passing six design distress criteria of TDC, fatigue cracking, low-temperature thermal cracking, rutting in total pavement system, and rutting only in asphalt layer (NCHRP 2004a). These criteria indicate the importance of considering cracking distress not only for pavement design but also for maintenance management and road infrastructure asset management. Therefore, it is imperative to consider reasonably accurate and reliable asphalt cracking deterioration initiation and progression prediction models for future prediction of distressed areas.

The mechanisms involved in developing different types of cracking distress include layer thickness, base material type, subgrade, traffic applications, and climate data. Eventually, all cracked distress areas are treated similarly for the M&R actions. Therefore, in this research, a new approach is proposed to rationally combine all cracking distresses into one parameter.

The Patterson concept of universal Cracking Indicator (CI) (Paterson 1994b) highlights the need for a distressing indicator that combined different cracking distress types as a unique indicator. The

proposed cracking indicator is the simple product of three primary physical dimensions of the amount of cracking (Equation 2.41). Figure 6 is used to describe the CI concept as proposed by the researcher.

$$CI = \text{extend} \times \text{intensity} \times \text{crack width} \quad \text{Eq. 2.41}$$

Where,

Extend = area of cracked pavement defined within a sample area, expressed as a percentage of total pavement area,

Intensity = total length of cracks within the area defining the extend, and Crack width = mean width of the crack opening at the surface of a set of cracks

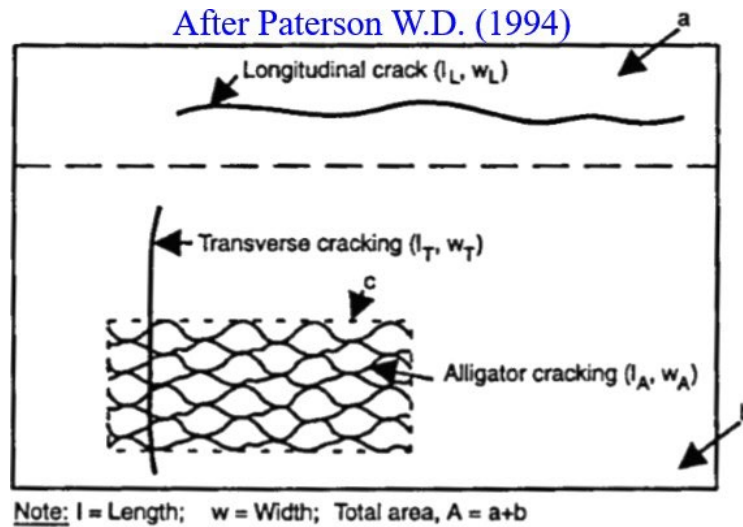


Figure 6. Example of computational of CI (Paterson 1994b)

Equations 2.42 and 2.43 are used to calculate CI for longitudinal cracks. Equations 2.44 and 2.45 are used to calculate CIs for alligator crack and transverse crack, respectively. The combined CI for all crack types is calculated using Equation 2.46.

### ***Longitudinal Cracking***

$$CI_L = 100 \left[ \frac{a}{A} \frac{l_L}{a} W_b + \frac{b}{A} \frac{0}{b} 0 \right] = \frac{100 l_L W_L}{A} \quad \text{Eq. 2.42}$$

Or calculating in the basis of the whole section

$$CI_L = 100 \left[ \frac{(a+b)}{A} \frac{l_L}{(a+b)} W_L \right] = \frac{100 l_A W_A}{A} \quad \text{Eq. 2.43}$$

### ***Alligator Cracking***

$$CI_A = 100 \left[ \frac{c}{A} \frac{l_A}{c} W_A \right] = \frac{100 l_A W_A}{A} \quad \text{Eq. 2.44}$$



### ***Transverse Cracking***

$$CI_T = 100 \left[ \frac{A}{A} \frac{l_T}{A} W_T \right] = \frac{100l_T W_T}{A} \quad \text{Eq. 2.45}$$

### ***Combined CI***

$$CI = \frac{100[l_L W_L + l_A W_A + l_T W_T]}{A} \quad \text{Eq. 2.46}$$

Important information on CI follows:

- CI is a cracking indicator (dimensionless)
- Extent is the area of cracked pavement (% of total pavement area)
- Intensity is the total length of crack within the area defining the extent (m/m<sup>2</sup>), and
- Crack width is crack opening (mm)
- Scaling factors: a) 100 (percentage area), b) 1,000 (mm/m)
- Range 0 – 10,000.
- Example CI of 3,200 may comprise of 2,000 alligator, 700 longitudinal, 500 irregular cracking.

However, adopting this concept in this research requires some alteration due to the following reasons:

- The intensity term requires the length of alligator cracking distress for low, medium, and high severity levels. Unfortunately, the length parameter of the alligator cracking distress type was not available in the LTPP database.
- No block cracking model, which is an important distress of low-temperature cracking.

Therefore, the development of the UCI that simplifies and considers the combination of various cracking distress types including block cracking was proposed in this research. In the MEPDG database, the alligator and block cracking distress are calculated as an area (square meter) for low, medium, and high severity levels, respectively. Longitudinal and transverse cracking distresses are reported based on the observed lengths (meter) for low, medium, and high severity levels, respectively. However, the crack width range for each severity level is small and not practical for the new UCI approach. The crack width for the low severity level was assumed as 0.05 meters, while the crack width of 0.1 meters was assumed for both medium and high severity levels of cracking distress. Equations 2.47 to 2.49 show the calculation of the combined UCI ( $Y_C$ ), which is the combination of the UCI for alligator crack ( $Y_{AC}$ ), block crack ( $Y_{BC}$ ), longitudinal crack ( $Y_{LC}$ ), and transverse crack ( $Y_{TC}$ ). There is no TDC data in the LTPP database. Therefore, the UCI equation does not account for the TDC distress. The UCI values are expressed in percentage of total LTPP test section area.

$$Y_C(\%) = \left[ \left( \frac{a_{AL} + a_{AM} + a_{AH}}{A_T} 100 \right) + \left( \frac{a_{BL} + a_{BM} + a_{BH}}{A_T} 100 \right) + \left( \frac{l_{LL}W_{LL} + l_{LM}W_{LM} + l_{LH}W_{LH}}{A_T} 100 \right) + \left( \frac{l_{TL}W_{TL} + l_{TM}W_{TM} + l_{TH}W_{TH}}{A_T} 100 \right) \right] \quad \text{Eq. 2.47}$$

$$Y_C(\%) = \left[ \left( \frac{a_{AL} + a_{AM} + a_{AH}}{A_T} 100 \right) + \left( \frac{a_{BL} + a_{BM} + a_{BH}}{A_T} 100 \right) + \left( \frac{a_{LL} + a_{LM} + a_{LH}}{A_T} 100 \right) + \left( \frac{a_{TL} + a_{TM} + a_{TH}}{A_T} 100 \right) \right] \quad \text{Eq. 2.48}$$

$$Y_C(\%) = Y_{AC} + Y_{BC} + Y_{LC} + Y_{TC} \quad \text{Eq. 2.49}$$

Where,

$a_{AL}$  = area of alligator crack for low severity level,

$a_{AM}$  = area of alligator crack for medium severity level,

$a_{AH}$  = area of alligator crack for high severity level,

$a_{BL}$  = area of block crack for low severity level,

$a_{BM}$  = area of block crack for medium severity level,

$a_{BH}$  = area of block crack for high severity level,

$a_{LL}$  = area of longitudinal crack for low severity level,

$a_{LM}$  = area of longitudinal crack for medium severity level,

$a_{LH}$  = area of longitudinal crack for high severity level,

$a_{TL}$  = area of transverse crack for low severity level,

$a_{TM}$  = area of transverse crack for medium severity level,

$a_{TH}$  = area of transverse crack for high severity level,

$l_{LL}$  = length of longitudinal crack for low severity level,

$l_{LM}$  = length of longitudinal crack for medium severity level,

$l_{LH}$  = length of longitudinal crack for high severity level,

$l_{TL}$  = length of transverse crack for low severity level,

$l_{TM}$  = length of transverse crack for medium severity level,

$l_{TH}$  = length of transverse crack for high severity level,

$A_T$  = total test section area in square meters (sq. m).

Note: All areas are in square meters and lengths are measured in meters.

## 2.5. Literature Review of Pavement Modulus Backcalculation Methods

### 2.5.1. Literature Review of Backcalculation Methods Based on Layered Elastic Theory

The basic pavement structural design is genuinely based on these two famous theories which are the one-layer linear elastic theory by Boussinesq reported in 1885, followed by Burmeister's two- and three-layers theory back in 1943 and 1945 (Haas et al. 1994; Huang 2004). These theories were explored as a result of great interest among scholars to understand the behavior of materials used to form a complete pavement system. Asphalt pavement systems composed of horizontal layers with different material types contributed to further research to study mechanistic responses (stress, strain, and

deflection) at critical locations to understand the mechanism of pavement deteriorations such as rutting and other distress types.

Boussinesq’s one-layer linear elastic theory was traditionally used for soil foundation design. The researcher assumed that the material is elastic, isotropic, and homogenous semi-infinite half-space. Half-space is defined as an infinite large horizontal plane area with semi-infinite depth. Another general assumption includes the load is point load, the stress imposed is bell-shaped whose amplitude decreases with depth, and maximum stress is near-surface and theoretically reduced to zero at an infinite depth. Equations 2.50 and 2.51 show a Boussinesq approach to calculate vertical stress ( $\sigma_z$ ) due to a point load at the surface (Figure 7). In general,  $\sigma_z$  is a function of P, z, and r, assuming no material properties, weightless, and no temperature effect.

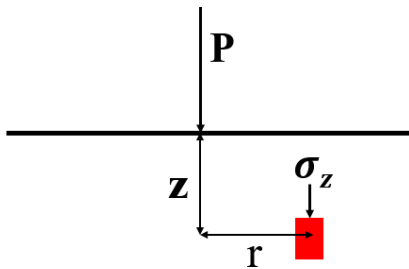


Figure 7. Point of interest to calculate vertical stress based on Boussinesq’s approach

$$\sigma_z = k \left( \frac{P}{z^2} \right) \tag{Eq. 2.50}$$

$$k = \left( \frac{3}{2\pi} \right) \left( \frac{1}{\left[ 1 + \left( \frac{r}{z} \right)^2 \right]^{\frac{5}{2}}} \right) \tag{Eq. 2.51}$$

Where  $\sigma_z$  is vertical stress, P is point load, Z is depth, and r is radial distance.

Furthermore, under an assumed circular loaded area, the modulus of elasticity (E) of the underlying soil can be determined if the applied pressure, the radius of loaded area, and the surface deflection are known (Figure 8). Equations 2.52 to 2.54 show the mathematical equations derived to determine the equation to determine modulus value and surface deflection for flexible plate (Equation 2.55) (Ullidtz 1987). Equations 2.56 and 2.57 were derived to determine modulus value and surface deflection for rigid plates (Equation 2.58) (Ullidtz 1987).

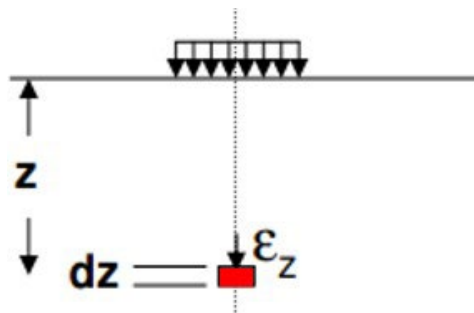


Figure 8. Point of interest to calculate deflection value on Boussinesq's approach (Ullidtz 1987)

$$\Delta_z = \int_0^z \varepsilon_z dz: \Delta_z = \frac{(1+\mu)p \times a}{E} \left[ \frac{a}{(a^2+z^2)^{0.5}} + \frac{1-2\mu}{a} [(a^2+z^2)^{0.5} - z] \right] \quad \text{Eq. 2.52}$$

$$\text{For } \mu = 0.5, \Delta_z = \frac{3pa^2}{2E(a^2+z^2)^{0.5}} \quad \text{Eq. 2.53}$$

$$\text{At } z = 0, \Delta_z = \frac{2(1-\mu^2)}{E} p \times a \quad \text{Eq. 2.54}$$

$$\text{At } z = 0 \text{ and } \mu = 0.5 \Delta_z = \frac{1.5pa}{E} \text{ or } E = \frac{1.5pa}{\Delta_z} \text{ (flexible plate)} \quad \text{Eq. 2.55}$$

Based on the research (Ullidtz 1987), the distribution of pressure under a rigid plate follows:

$$p(r) = \frac{pa}{2(a^2-r^2)^{0.5}} \quad \text{Eq. 2.56}$$

By integrating a point load over the contact area of the plate, it can be derived that:

$$\Delta_o = \frac{\pi(1-\mu^2)}{2E} p \times a \quad \text{Eq. 2.57}$$

$$\text{If } \mu = 0.5, \text{ then, } \Delta_o = \frac{1.18pa}{E} \text{ or } E = \frac{1.18pa}{\Delta_z} \text{ (rigid plate)} \quad \text{Eq. 2.58}$$

Where,

$\Delta$  = Deflection at the center of the loaded area associated with the surface pressure

E = Young's modulus of elasticity of the material

p = Unit pressure applied to the surface of the loaded area

a = radius of the loaded area

$\mu$  = Poisson's ratio of the material

However, the one-layer linear elastic theory has a few limitations as follow:

- The assumptions are suitable only for the pavement with a thin surface
- It is unreasonable to neglect the effects of stiffer and thicker pavements since it greatly affects the stress, strain, and deflection values
- Tensile stress and strain analysis were neglected. Unfortunately, stress and strain analyses were very important for fatigue failure analysis of concrete and asphalt pavements, respectively.

Therefore, in the early 1940s, Burmeister introduced more appropriate approaches to consider material stiffness and thicknesses through two layers and three-layer systems (Haas et al. 1994; Huang 2004; Uddin and Ricalde 2000; Ullidtz 1987). The approach is more reasonable for a pavement system

that has different layers with various material properties. Burmester's theory maintains the basic assumptions for one layer theory. Additional assumptions follow:

- The intermediate layer thickness is finite, while the bottom layer is assumed to be semi-infinite.
- Full friction between the layers.
- There is no shear stress at the surface.
- The material is assumed as linear elastic and the constitutive behavior of the material is defined by Young's elastic modulus and Poisson's ratio.
- The load is assumed to be static and uniformly distributed over a circular area.

Advancement through computer engineering contributed to the development of various computer programs based on multi-layer linear elastic theory to predict stress, strain, and deflection values for pavement structural design. Researchers (Haas et al. 1994; Huang 2004; Uddin and Ricalde 2000) describe the examples of that computer programs in detail.

### **2.5.2. Literature Review of Backcalculation Methods Based on Layered Elastic Analysis**

One of the most useful data available in the LTPP database is the deflection data sets obtained from the FWD non-destructive test to assess the structural integrity of the pavement system (FHWA 1993, 2017; Uddin 1984; Uddin and Garza 2003). The FWD test was conducted to measure asphalt pavement deflection using seismic sensors placed at different distances from the center point of the test load drop location (Schmalzer 2006). The deflection data sets extracted from the LTPP database are based on the computation of seven FWD geophone sensors located at 0, 8, 12, 18, 24, 36, and 60 inches from the center of the 5.91 inches loading plate. Typically, four different load weight levels are tested, four drops for each level which resulted in a total of 16 deflection basins. According to the FHWA (Schmalzer 2006), the FWD simulated the pavement surface deflection caused by a fast-moving truck.

The load pulse generated by dropping a specific weight was transmitted through the loading plate and caused the elastic deflections of pavement layers. The deflection basin corresponding to each drop load was determined from the sensor data. Uddin and Garza (Uddin and Garza 2003) provide detailed information related to the FWD test through their study on numerical simulation and dynamic response analysis of FWD impact test on asphalt pavement.

For years, Young's modulus values which describe the stiffness of the pavement layers were not reported for most of the test sections in the LTPP database. The modulus values are required for pavement evaluation and rehabilitation design (Stubstad et al. 2006), response analysis, and numerical studies of the pavement system for the specific test section. Therefore, the backcalculation using deflection data from the FWD test is essential to obtain modulus values for asphalt, base, subbase, and subgrade layers, respectively. The backcalculated modulus values are important to evaluate the structural integrity of the pavement system after a series of M&R treatments (Ameri et al. 2009).

The FHWA through SHRP carried out an extensive literature review and summarized important information for 17 different backcalculation programs (FHWA 1993). The review looked into program developers and forward calculation methods which used either multi-layer elastic theory, a method of equivalent thickness, finite element, or other closed-form solutions. In addition, the review also reported forward calculation subroutine approaches including BISAR, MET, FEACONS III, ELSYM5,

CHEVRON, and WESLEA. Moreover, nonlinear or linear methods, requirements of seed modulus values, and ranges of acceptable modulus values are among other criteria evaluated in the study. Six backcalculation programs were selected for detailed evaluations which are ELCON and ELI-BACK for rigid pavement, and ISSEM4, MODCOMP3, MODULUS, and WDEF for flexible pavements. The results were evaluated based on reasonableness, robustness and stability, the goodness of fit, and the suitability of SHRP purposes. The top three programs selected are MODCOMP3, MODULUS, and WESDEF. Further evaluations were conducted on these three programs. The user repeatability, reasonableness of results, deflection matching errors, ability to match the calculated modulus value from simulated deflection basins, and versatility are among the criteria assessed. Final evaluations revealed that the MODULUS backcalculation program was superior compared to the other two programs. The guideline for review and evaluation of backcalculation results are available in a report published in 2006 (Stubstad et al. 2006). However, the final LTPP deflection data analysis was conducted not using the reasonable backcalculation program, as discussed later.

According to Ameri et al. (Ameri et al. 2009), there are three modes of backcalculation available which include (1) radius of curvature, (2) deflection basin fit, and (3) Finite Element Method (FEM) or Linear Elastic Theory (LET) or Method of Equivalent Thickness (MET). All these modes are described in a comparative study for static and dynamic backcalculation approaches for asphalt, base, and subgrade layers. In this study, for static analysis, the MODULUS 6.0, ELMOD 5.0, and EVERCALC 5.0 were analyzed, while the Dynamic Backcalculation Procedure with Systems Identification Method (DBSID) program was employed for the dynamic backcalculation process. Ameri et al. (Ameri et al. 2009) concluded that MODULUS 6.0 was the most appropriate software to backcalculate modulus values. The comparison between the MODULUS 6.0 and DBSID indicated that the dynamic analysis approach showed a higher modulus for asphalt and subgrade layers compared to the static approach. In contrast, the backcalculated modulus value using a static approach showed a higher value for the base layer.

One of the widely used backcalculation software for military airports and roads is the Pavement-Transportation Computer Assisted Structural Engineering (PCASE) developed at Transportation Systems Center and Engineering Research and Development Center (ERDC) of the U.S. Army Corps of Engineers (U.S. Army Corps of Engineers 2021). This software was used as a tool for pavement design and repair alternatives for both airfield and road networks (flexible and rigid pavements). Users are prompted to choose either empirical or layered elastic design (LED) approaches. The empirical design requires California Bearing Ratio (CBR) or modulus of subgrade reaction (k) values. The LED requires Young's modulus values and Poisson's ratio for each layer. This software used the WESDEF layered linear elastic backcalculation routine to backcalculate modulus values. There is a limited number of research papers related to modulus backcalculation available for review using the PCASE 2.09 backcalculation software.

Priddy (2014) used the PCASE 2.09 software to determine the required thickness of the PCC slab for a 100-ft-length by 60-ft-wide test section construction. The study assumed the PCC airfield flexural strength of 650 psi, k equal to 15 pci, six inches aggregate base thickness, no drainage layer required, and a design life of 50,000 C-17 aircraft passes. The PCASE software proposed a 14 inches thick PCC slab with specific locations for the one-inch diameter of the rebar. The test section was constructed with

15 20-ft by 20-ft PCC slabs placed at 3x5 configurations. Three types of repair methods were evaluated. Repair one, two, and three explain the replacement of quarter, half, and full slab, respectively. Before the repair, the PCC slabs were sawed at a quarter, half, and full slab area at certain locations. A single 10-ft by a 10-ft concrete panel with dowel bars was used to replace the quarter slab. Additionally, the removed half slab was replaced with two concrete panels and four concrete panels replaced the removed full slab, respectively. A multi-wheel load cart simulating a C-17 aircraft landing gear was used to simulate aircraft passes, until 10,000 passes or until the PCC slab failed.

The heavyweight deflectometer (HWD) tests were conducted using the Dynatest model 8081 equipment. The HWD tests were conducted on a newly constructed test section (pre-repair) and post-traffic for both slabs and panels at different locations. Before the construction of the test section, the dynamic cone penetrometer (DCP) tests were carried out to determine the subgrade modulus value. Subsequently, the DCP estimated moduli in psi were determined by multiplying CBR values with 1500. The results showed no changes in pre-repair and post traffic PCC slabs modulus values. Less than three percent reductions for the backcalculated base and subbase modulus values were observed compared to pre-repair slabs conditions. This implies that no major loss in foundation support beneath the test section could lead to early deterioration of the repairs. For PCC panel cases, the post-traffic panels showed approximately 60 percent reductions in PCC modulus value. Additionally, about 40 percent reductions in the backcalculated modulus values were observed for the base layer and 53 percent reductions for the subgrade layer, compared to pre-repair panels. The significant reductions of the modulus values are not due to a reduction in foundation support but attributed to the deterioration of the panels during traffic simulation processes (Priddy 2014).

Priddy et al. (2015) evaluated procedures for backcalculation of airfield pavement modulus values and compared the backcalculated modulus values using the WESDEF, BAKFAA, and ELMOD6 backcalculation software. Both FWD and HWD deflection data sets from five army airports in the U.S and one in South Korea were used for backcalculation purposes. The backcalculated modulus values were evaluated to determine the number of allowable aircraft passes and allowable loads before the failure. The findings indicated that the analysis procedures for backcalculation and structural analysis vary between each software. Reasonable modulus can be obtained either using the WESDEF or BAKFAA although the users are inexperienced or have limited knowledge performing backcalculation using the software. The modulus values calculated from the BAKFAA and WESDEF software are more reasonable as compared to ELMOD6 software. The modulus values were calculated using ELMOD6 over predicted subgrade modulus for most of the sections analyzed.

Recently, the FHWA has updated the LTPP database with layers' modulus values backcalculated using the EVERCALC 5.0 (WSDOT 2005) backcalculation software. It is noted that this software ranked high in previous comparative studies (Ameri et al. 2009; FHWA 1993; Stubstad et al. 2006). The backcalculated modulus values are different for each CN for all test sections in the LTPP database InfoPave which includes test section 28-2807 located at Highway 6 East, Lafayette County, Mississippi.

#### **2.5.2.1. Previous Studies for Test Section 28-2807 in Mississippi**

The preliminary research for backcalculation of the modulus values was conducted for the LTPP test section 28-2807 on Highway 6 East, Lafayette County, MS. The pavement structure and

backcalculation of Young's modulus for similar test sections were initially analyzed in previous studies between 1998 to 2008 by Uddin (Uddin 2008), Uddin et al. (Uddin et al. 2003), and Boriboonsomsin and Momm (Boriboonsomsin and Momm. 2002). Uddin (Uddin 2008) backcalculated modulus values for pavement structure using the PEDD1 computer program. The nondestructive deflection data based on the FWD test and other data sets were used to determine the in situ backcalculated modulus values without making any correction for temperature. The modulus values were compared with the WESDEF and MODULUS5 backcalculation programs. The PEDD1 backcalculated modulus values of 473,000 psi for asphalt layer, 600,000 psi for asphalt base, 57,000 psi for CTB, and 43,600 psi for subgrade layer were more reasonable compared to other programs. These modulus values represented the pavement layer in a good condition without any crack and rutting in the test area. Further analysis using The 3D-FE analysis was conducted using the modulus values from the PEDD1 software to study surface deflection and pavement structural response subjected to the FWD dynamic load pulse.

Uddin et al. (Uddin et al. 2003) backcalculated modulus values for similar test sections using the UMPED static backcalculation program (Boriboonsomsin and Momm. 2002) which is a simplified version of the PEDD program. The PEDD is the Windows version of PEDD1, adjusted to adapt to the current changes in computer technologies. The PEDD and UMPED embedded a self-iterative equivalent linear elastic procedure to correct the backcalculated modulus values for unbound subbase and subgrade layers. The modulus values were corrected based on the normalized shear modulus versus shear strain curves implemented in earthquake engineering (Uddin 2008).

Uddin et al. (Uddin et al. 2003) used the FWD deflection data in 1993 and 1998 from the LTPP database for pavement structure with four layers and assigned different CNs. The FWD test in 1998 was conducted for one-inch thicker asphalt pavement layers and tested in 25.5°F higher air temperature compared to the 1993 FWD test condition. The deflection recorded by the first sensor placed closest to the drop location showed higher values for 1998 data sets due to a warmer temperature. Additionally, deflection data detected by this sensor showed the highest variability since the first sensor indicated traffic and environmental effects on the asphalt layer. On the other hand, sensor seven, placed at the longest distance from the load center point, recorded the lowest variability. In general, the backcalculated modulus values for asphalt pavement and asphalt base varies with temperatures and traffic applications. However, the backcalculated modulus values for subgrade soil showed no obvious changes. From 1993 FWD data sets, the in situ backcalculated modulus values were 623,300 psi for asphalt pavement, 623,600 psi for asphalt base, 90,500 psi for CTB, and 19,240 psi for subgrade layer. The calculated modulus values from 1998 FWD data sets were 264,600 psi for asphalt pavement, 236,400 psi for asphalt base, 91,400 psi for CTB, and 24,810 psi for subgrade layer.

Boriboonsomsin and Momm (2002) backcalculated the modulus values using the UMPED program using FWD deflection data sets collected in 1990, 1991, 1992, 1993, 1995, and 1998.

This study highlighted the importance of the CN, which is the intervention factor for maintenance and M&R on the backcalculated modulus values. The only major M&R for this test section was conducted on January 31, 1994, which involved milling of a 1.1-inch uppermost asphalt pavement layer and overlaid with 2.1 inches of new HMA. The asphalt layer is one inch thicker, while other layers remain the same. The FWD test data before (August 3, 1993) and after (December 1, 1995) the milling and resurface rehabilitation intervention were analyzed and the backcalculated modulus values were



compared. The results showed approximately 42 percent higher modulus values for the asphalt layer and 33 percent higher for the asphalt base layer, exaggerated by 26.8°F lower air temperature in 1995. Additionally, 29% and 39% higher modulus values were observed for the subbase and subgrade layers, respectively. The UMPED modulus values in 1998 were selected as the most reasonable modulus and used for preliminary finite element analysis (Uddin et al. 2003).

## **2.6.Literature Review of 3D-FE Modeling of Uncracked Asphalt Pavements**

The 3D-FE modeling allows the user to view the pavement system from multiple perspectives. Through observation, the 3D-FE helps to improve the visualization of the stress-strain and deflection behavior in the pavement layer subjected to dynamic loads. Furthermore, the 3D-FE allows the user to improve impact and sensitivity analysis and identify potential consequences of changing material properties and layer thicknesses on pavement response analysis. Once the final 3D-FE model is developed, it can be used to estimate modifications to implement any changes to the real pavement systems. According to Uddin et al. (1997), the FE numerical analysis helps users to realistically model pavement structure, evaluate, and visually check the integrity of the model. Most importantly, the 3D-FE analysis helps to reuse or reapply part of the existing information and knowledge from previous studies.

Uddin and Garza (2003) evaluated the dynamic effects such as damping, load pulse duration, and dynamic response analysis of FWD impact load tests on asphalt pavements. The study was conducted to quantify the needs of pavement response analysis considering the load-time history and related dynamic effects, which have been neglected in most of the modulus backcalculation programs. The traditional programs used only peak deflections, peak FWD load, and static linear response analysis to backcalculate Young's modulus value. A 3D-FE half model asphalt pavement section was modeled using LS-DYNA software to verify the in situ backcalculated modulus values for the U.S. Highway 45 North project, and compared with the UMPED backcalculated modulus values. Uddin and Garza (Uddin and Garza 2003) concluded that the effect of damping on the calculated dynamic FWD deflections and backcalculated modulus is very small and negligible. On the other hand, the load pulse duration of the FWD affected the backcalculated modulus values using dynamic analysis. A range of 40 to 100 milliseconds (msec) for the load pulse was found to generate a good dynamic response and provide a better simulation of moving highway traffic. Uddin and Garza (Uddin and Garza 2003) provide a thorough explanation of implicit and explicit analysis using ABAQUS, and only explicit analysis using LS-DYNA. The authors concluded that the explicit analysis is more accurate for pavements subjected to FWD dynamic loads (Uddin and Garza 2003).

Wang et al. (2008) studied the 3D-FE model of an asphalt pavement structure using the ABAQUS software. Instead of assuming an average tire pressure applied at only one position, Wang et al. simulated possible effects of changing load position due to wandering in the wheel path. Additionally, the stop, braking, and turning actions of a moving vehicle caused variations in applied direction and force due to wheel loads. To simulate different load pressures on the pavement surface, a reasonable wheel-load model was developed and used for the 3D-FE analysis. The wheel-load model consisted of a pair of the simulated longitudinal tire thread contours with simulated pressure values ranging from 460 to 870 kPa (66.7 to 126.2 psi). For details of the 3D-FE model, see Wang et al. (2008).

Wang et al. (2008) modeled asphalt, cement stabilized macadam, and lime stabilized layers with

the thicknesses of 15 in, 30 in, and 40 in, respectively. The modulus values ranged from 174,045 psi, 217,557 psi, 116,030 psi, and 5,802 psi, respectively from top to the bottom layers. The Poisson's ratios were 0.25 (asphalt), 0.25 (base), 0.30 (subbase) and 0.35 (subgrade), respectively. Asphalt pavement layer with different thicknesses was modeled and the maximum tensile stress and maximum shear stress at specific locations were computed. Wang et al. (2008) believed that the maximum shear stress on asphalt pavement surface has initiated the TDC. Maximum tensile stress at the bottom of the subbase was also believed to cause reflective cracking initiation. The research also showed pavement thicknesses have no obvious effects on the maximum shear stress. However, thicker asphalt pavement contributed to lower tensile stress and surface deflections (Wang et al. 2008).

The dimensions (length, width, thickness) of the 3D-FE model developed by Garza (2003) for the U.S Highway 45 North project subjected to FWD load were used as the reference for the new 3D-FE asphalt pavement models developed using the LS-DYNA software.

## **2.7. Literature Review of 3D-FE Modeling of Cracked Pavements**

The presence of asphalt surface discontinuity, such as surface crack, reduces the structural capacity of pavement systems. Continuous traffic load applications over the years caused surface crack distress on top of pavement surfaces. In the LTPP program, the selected test sections were evaluated for various crack types including alligator and block cracking that are measured as an area in a square meter. In contrast, transverse and longitudinal cracks are measured as a unit length in meters. In general, the LTPP data indicates more severe cracking distresses on asphalt surfaces due to repeated load cycles, for the test sections without any major M&R treatments over the years (FHWA 2019).

Figure 9 shows the spatial map of the average Pavement Condition Rating (PCR) in the state of Mississippi for 2016. The average PCR data for 82 counties indicated 70.7% are showing a fair condition of paved roads. Only two counties' road network is rated as in good condition, which are Greene (PCR = 81.6) and Harrison (PCR = 81.9) counties. The remaining counties (26.8%) recorded PCR of 71 or below, which indicated poor road conditions. The Lafayette County recorded a PCR of 80.2 over 100, which is under the fair condition group (PCR 72 to 81)(MDOT 2019). On the other hand, a statewide data summarized that out of 23,377 miles of MDOT state-maintained road network, 32.67% are in poor condition, 38.81% are in acceptable condition, while the remaining 28.52% of the inspected road network is in good condition (MDOT 2019).

These statistics show that it is needed to consider asphalt pavement surface discontinuity in the mechanistic-empirical pavement analysis. Most of the layered elastic software used to study pavement responses does not consider any discontinuity. The following statements highlight the limitations in static linear layer elastic assumptions (Uddin and Pan 1995):

- Inaccurate for pavements with cracking, discontinuities, and highly nonlinear material is used.
- The actual load is dynamic loading applications.

The only possible approach to study cracked pavement responses under the FWD and dynamic truck wheel loads are through the 3D-FE analysis. One of the advantages of the 3D-FE analysis is the capability to model discontinuity in asphalt pavement. The previous finite element studies reported that the INTERFACE element was used to simulate discontinuity in other structure materials (Burnett et al. 2007; Carol et al. 2007; Dias-Da-Costa et al. 2010; Muflahi et al. 2014; Nguyen 2014). Unfortunately,

this element type was not suitable for simulating pavement cracks, which always have some aggregate interlock. However, more reasonable approaches to simulate discontinuity in the asphalt surface layer were proposed and studied by Uddin and Pan (Uddin and Pan 1995) in 1995. The 3D-FE analysis of surface layer with discontinuity for concrete pavements was published by researchers in 1994, 1995, and 1997, respectively (Livermore 2022; Uddin et al. 1994, 1997). Previous research related to both concrete and asphalt pavement modeling was studied, however, only asphalt pavement is considered in the 3D-FE analysis of this research.

Uddin et al. (1994) studied the effects of pavement discontinuities on Portland cement concrete pavement. Before the 3D-FE analysis, the researchers optimized the pavement-subgrade structure of the model. Five important findings were reported, and two of them were used in this research. Those two findings follow:

- (1) A 12.2 meter (40 feet) of subgrade depth simulates a semi-infinite subgrade, and
- (2) The nodes at the bottom of the model were fixed, while rollers in the lateral sides of the model gave the best responses.

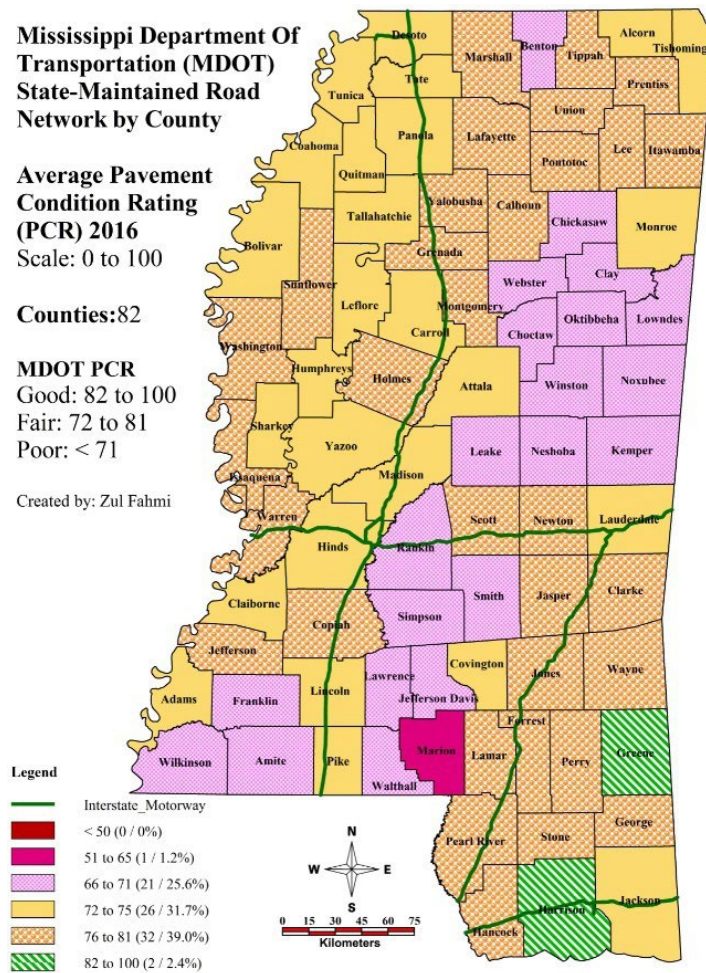


Figure 9. Spatial Map of 2016 Average Pavement Condition Rating (PCR) by Counties in Mississippi

The modulus values for the concrete, base and subgrade layers were backcalculated from the

deflection data using the FPEDD1 program. Later, the BISAR computer program was used to predict the surface deflection under layer elastic static analysis. Then the deflection value was compared with the results from static analysis using ABAQUS software. Only one percent difference in the deflection values suggests that the geometry, mesh, and boundary condition of the 3D-FE model are adequate for further analysis.

For dynamic analysis, Uddin et al. (1994) analyzed both implicit and explicit analysis approaches in the ABAQUS. It turns out that the deflection value based on the implicit approach shows an 18 percent lesser difference compared to static analysis. The explicit approach shows more error, therefore, only the implicit approach is considered for pavement discontinuity analysis.

The researchers (Uddin et al. 1994) also introduced an approach to simulate full-depth crack in the concrete layer using a special-purpose unidirectional gap element known as GAPUNI available in ABAQUS software. Gap elements allow a pair of continuous faces to be in contact (gap closure) or separation (gap opening) for directions and separation conditions. The gap elements control the interaction between the contact surfaces in such a way that these surfaces do not penetrate each other under contact pressure (Uddin and Pan 1995). The mechanism of GAPUNI element that requires a friction coefficient was described in detail by the researchers. Before simulating the crack condition, parametric studies were conducted to determine the crack gap width. It was discovered that the crack widths of 0.2, 0.1, 0.05, 0.02 inches were insignificant because the crack remains open throughout the analysis. Further studies conclude that the gap width of 0.01 inches is most reasonable. This implies that the effect of the friction coefficient of 0.5 on surface deflection is significant. The gap width of 0.01 inch (0.25 mm) and a friction coefficient of 0.5 were used between the two-contact surface of the gap elements. The friction coefficient of 0.5 was introduced to allow the contact surface to slide with a very minimal shear force developing during the simulation. These criteria were developed from a previous study conducted in 1994 by Uddin et al. (1995) for cracked asphalt pavement.

Further analysis was conducted to compare the deflection values between the uncracked and cracked pavement under dynamic loads. Transverse and longitudinal cracks were simulated using the GAPUNI element and the deflection under the FWD load was observed. It was discovered that the dynamic loading causes 17 to 22 percent higher deflection responses at the center of the loading area for cracked pavement, as compared to the uncracked pavement.

However, the difference becomes smaller as noticed from nodes farther away from the center of the loading area.

Uddin et al. (1995) conducted a few case studies to evaluate the effectiveness of the 3D-FE analysis to predict the modulus values for Portland concrete pavement with CTB layers. The deflection values from the FWD tests for the jointed concrete pavement with discontinuity were compared with the 3D-FE outputs. The 3D-FE model simulates the concrete pavement layer, CTB layer, and subgrade layer for U.S. Highway 78 in Marshall County, Mississippi. Both uncracked and cracked pavements were simulated incorporating layer modulus values backcalculated from PEDD1 backcalculation software.

As compared to the previous research (Uddin et al. 1994), Uddin et al. not only simulated crack using the GAPUNI element but also simulated a transverse joint with a dowel bar within the concrete slab. The dowel bars were modeled using beam elements. The Gap element in the ABAQUS was also used to simulate body-to-body contact to specify the interactions between the dowel bar and the

surrounding concrete medium. Like the previous study (Uddin et al. 1994), the gap width of 0.01 inch and a friction coefficient of 0.5 were used in the analysis. The modulus values for the following conditions were analyzed:

- 1) Uncracked concrete pavement and uncracked CTB layers,
- 2) Cracked concrete pavement and uncracked CTB layers,
- 3) Cracked concrete pavement and cracked CTB layers.

There are no changes applied to the subgrade layer with a 24,400-psi modulus value. The iterative procedures using the 3D-FE models using the ABAQUS software were considered. The ABAQUS dynamic deflections were compared, and the modulus values were adjusted until the smallest differences were observed between the predicted and measured deflection values. In general, it was noted that the 3D-FE predictions match reasonably well with the measured deflections. For both concrete and base layers, the modulus values for the cracked condition are less as compared to the uncracked layers.

In 1997, Uddin et al. (1997) enhanced the research on the concrete pavement with discontinuities using the ABAQUS software. This study not only simulates transverse joint with dowel bars but also simulates a void under the concrete slab. Like the previous study (Uddin et al. 1994, 1995) the gap width of 0.01 inch and a friction coefficient of 0.5 was adopted for simulating discontinuities using the Gap elements. The voids under the concrete pavement at certain pavement sections of US Highway 78 in Marshall County were detected using thermographic equipment.

The following conditions were evaluated in the study using the 3D-FE model simulations for the 80kN (18-kip) dual wheel single axle truck at the mid slab position, with a 100-psi tire pressure:

- 1) Uncracked pavement model
- 2) Crack only in concrete pavement layer
- 3) Cracked concrete pavement and cracked CTB layers
- 4) Cracked concrete and CTB with voids

In general, the researchers summarized that the surface deflection is the lowest for the uncracked model compared to models with the cracked condition. The comparison for the cracked condition follows:

- The deflection values are slightly higher for the pavement with concrete cracked only, compared to uncracked pavement.
- The deflection values for cracked concrete and cracked CTB layer are higher compared to concrete cracked only.
- The highest deflection values were observed for cracked concrete and cracked CTB with voids, as compared to all other simulations.

This research highlights the capability of the 3D-FE program to simulate the sophisticated conditions of discontinuities, which cannot be done using the multilayer linear elastic analysis and other finite element programs that do not consider crack modeling and dynamic analysis (NCHRP 2004c).

A comprehensive study on finite element analysis of flexible pavements with discontinuities was

conducted by Uddin and Pan (1995) in 1995. The researchers used ABAQUS software to simulate longitudinal cracks, transverse cracks, and alligator cracks in the asphalt surface layer. The details of pavement-subgrade model parameters were described in the paper. Two major requirements of the 3D-FE models follow:

- 1) To capture accurate responses results, the mesh size under the load must be smaller compared to other regions far from the loading area.
- 2) The size of the elements is gradually increased as it farther away from the simulated loading areas.

The seed modulus values for pavement layers were backcalculated using the PEDD1 computer program. The researchers stated that the backcalculated modulus values are reasonable and good estimates of the effective in situ modulus values for the selected test section. The modulus values were used in the 3D-FE analysis of cracked pavement. The deflections values from the 3D-FE models with continuities were compared with measured deflections.

Transverse and longitudinal cracks simulation procedures in ABAQUS were implemented by Uddin et al. (1994) for a full-depth cracked asphalt layer. High severity alligator cracks were modeled by using the gap elements in both longitudinal and transverse directions. The following observations were noted in this study based on the maximum deflection:

- The deflection values for asphalt pavement with transverse cracks are about 7% higher compared to uncracked pavements.
- The deflection values for asphalt pavement with longitudinal cracks are about 17% higher compared to uncracked pavements.
- The highest difference of 36% was observed for the asphalt layer with high severity of alligator cracks as compared to the uncracked pavements.

The studies showed that the ABAQUS software could simulate the pavement discontinuities including surface cracks. However, the literature review did not show any study that described the modeling of the cracked area in asphalt pavements using the LS-DYNA software. The previous studies reported that the INTERFACE element was used to simulate discontinuity on other structure materials (Burnett et al. 2007; Carol et al. 2007; Dias-Da-Costa et al. 2010; Muflahi et al. 2014; Nguyen 2014). This element was not suitable for simulating pavement cracks, which always have some aggregate interlock. For that reason, this research explores the potential of using LS-DYNA software to simulate the cracked asphalt layer and evaluate the responses under truck wheel loads.

### 3. METHODOLOGY

#### 3.1. Methodology for Enhanced IRI Modeling

The model development methodology for enhanced IRI modeling used in this study is described as follows:

- 1) Use the initial IRI condition deterioration prediction equation developed in a previous study (Jaafar et al. 2015) as shown in Equation 3.1.

$$IRI_y = 0.99 + 0.3637(IRI_0) - 0.074(SN) + 0.013(Age) - 1.734 \times 10^{-8}(CESAL) + 0.154(CND) \quad \text{Eq. 3.1}$$

- 2) Prepare an expanded database for the development of the enhanced multiple regression prediction equations. The expanded database considers the  $Y_I$  data sets from all four LTPP regions. A total of 2,588 data included in the analysis enabled further analysis using the ANN method as well.
- 3) Verify if the datasets used in the analysis complied with the assumptions required for multiple linear regression analysis. Those assumptions are:
  - The data are independent.
  - The data are normally distributed: The Kolmogorov-Smirnov test (K-S test) nonparametric test and the normality plot from the SPSS (IBM 2022) need to be performed to evaluate if the normality assumption is met.
  - The predicted and measured  $Y_I$  should show homogeneity of variance.
  - The residual plot must show normal distribution at a zero mean value.
- 4) Perform transformations of  $Y_I$  including  $\text{Log}_{10}Y_I$  and  $\text{Ln } Y_I$  (all IRI data were non-zero data).
- 5) Evaluate the autocorrelation value for the dataset.
- 6) Perform the normality test for  $Y_I$  and transformed  $Y_I$  data
- 7) Develop the enhanced IRI modeling equation
- 8) Evaluate the accuracy of the developed equations based on the following parameters:
  - The R and  $R^2$  values of the multiple regression equations
  - The predicted against measured data plots
  - The verifications of the multiple regression equations
  - The accuracy measures of the Mean Absolute Relative Error (MARE) and Root Mean Square Error (RMSE)

The MARE was calculated using Equation 3.2.

$$MARE = \frac{\sum_{i=1}^N \left| \frac{\hat{y}_i - y_i}{y_i} \right|}{N} \times 100 \quad \text{Eq. 3.2}$$

Where  $\hat{y}_i$  and  $y$  are the predicted and observed values of the IRI per measurement year. If the value of the MARE (%) is relatively small, close to zero, it means that the model performance is good. Equation 3.3 was used to calculate the RMSE accuracy measure.

$$RMSE = \sqrt{\frac{\sum_{i=1}^N (\hat{y}_i - y_i)^2}{N}} \quad \text{Eq. 3.3}$$

Where  $\hat{y}_i$  and  $y$  are the predicted and the observed value of the IRI per measurement year and the  $N$  is the total number of data sets.

- 9) Select the best enhanced IRI prediction model based on the most accurate statistical parameters.

### 3.1.1. LTPP Roughness Data Collection

The IRI roughness data for the test sections in 28 states in the U.S. were extracted from the LTPP database under the MON\_PROFILE\_MASTER section (FHWA 2019). The IRI per measurement year ( $Y_I$ ) for both inside and outside wheel paths was measured for every 500 feet (152.4 m) testsection. The measurements were repeated at least five times, and the average values for each runwere also recorded in the LTPP ACCESS database as shown in Table 7. Table 8 shows the counts and percentages of the  $Y_I$  data points for all 28 states in the U.S. that are included in the analysis. The  $Y_I$  data used in the model database ranged from 1990 to 2011. A total of 2,588 data points that are comprised of 1,294  $Y_I$  data the inside wheel path, and 1,294  $Y_I$  data outside the wheel path were used in the analysis.



Table 7. IRI data for LTPP test section 1-1011 in Lauderdale County, Alabama

STATE_CODE	SHRP_ID	PROFILE_DA	IRI_LEFT_WF	IRI_RIGHT_V	IRI_AVERAG	
1	1011	1	2/11/1992	0.844	0.817	0.831
1	1011	1	2/11/1992	0.86	0.856	0.858
1	1011	1	2/11/1992	0.844	0.854	0.849
1	1011	1	2/11/1992	0.838	0.82	0.829
1	1011	1	2/11/1992	0.841	0.837	0.839
1	1011	1	2/1/1994	0.776	0.827	0.802
1	1011	1	2/1/1994	0.756	0.842	0.799
1	1011	1	2/1/1994	0.74	0.843	0.792
1	1011	1	2/1/1994	0.73	0.813	0.772
1	1011	1	2/1/1994	0.767	0.848	0.807
1	1011	1	8/16/1995	0.814	1.124	0.969
1	1011	1	8/16/1995	0.826	1.093	0.959
1	1011	1	8/16/1995	0.805	1.144	0.974
1	1011	1	8/16/1995	0.851	1.053	0.952
1	1011	1	8/16/1995	0.797	1.1	0.949
1	1011	1	8/12/1998	0.865	1.075	0.97
1	1011	1	8/12/1998	0.849	1.027	0.938
1	1011	1	8/12/1998	0.836	0.983	0.909
1	1011	1	8/12/1998	0.848	1.102	0.975
1	1011	1	8/12/1998	0.867	1.09	0.978
1	1011	2	6/6/2002	1.107	1.391	1.249
1	1011	2	6/6/2002	1.092	1.399	1.245
1	1011	2	6/6/2002	1.172	1.375	1.273
1	1011	2	6/6/2002	1.123	1.386	1.254
1	1011	2	6/6/2002	1.185	1.377	1.281

Total distributions of Y<sub>I</sub> data points for each LTPP region follow:

- North Atlantic (716 data points, 27.7%)
- North Central (100 data points, 3.9%)
- Southern (1088 data points, 42%)
- Western (684 data points, 26.4%)

Table 8. State-wise distribution of the Y<sub>I</sub> data

State Code	State Name	LTPP Zone	N	%	State Code	State Name	LTPP Zone	N	%
1	Alabama	SR	62	2.4	32	Nevada	WR	36	1.4
4	Arizona	WR	46	1.8	34	New Jersey	NA	110	4.3
5	Arkansas	SR	64	2.5	35	New Mexico	SR	24	0.9
6	California	WR	328	12.7	36	New York	NA	68	2.6
8	Colorado	WR	34	1.3	37	North Carolina	NA	158	6.1
10	Delaware	NA	32	1.2	38	North Dakota	NC	14	0.5
12	Florida	SR	52	2.0	40	Oklahoma	SR	164	6.3
13	Georgia	SR	88	3.4	41	Oregon	WR	26	1.0
18	Indiana	NC	38	1.5	47	Tennessee	SR	208	8.0
22	Louisiana	SR	12	0.5	48	Texas	SR	162	6.3
24	Maryland	NA	128	4.9	50	Vermont	NA	54	2.1
28	Mississippi	SR	252	9.7	51	Virginia	NA	142	5.5
29	Missouri	NC	48	1.9	54	West Virginia	NA	24	0.9
30	Montana	WR	32	1.2	56	Wyoming	WR	182	7.0
Total number of IRI data points (N) = 2,588									

### 3.1.2. Dependent Variable

The dependent variable of the multiple regression equation is IRI per measurement Year ( $Y_I$ ) in meter per kilometer (m/km). Both  $Y_I$  measured inside and outside the wheel paths were considered in the analysis.

A dummy or dichotomous variable ( $IRI\_D$ ) with zero and one value was created to represent the IRI measurement locations. Zero value describes the IRI measured outside the wheel path, while one describes the IRI measured inside the wheel path.

### 3.1.3. Independent Variable

The following independent variables were considered to develop the enhanced IRI condition deterioration prediction equations

- The initial IRI per measurement year ( $Y_{10}$ ) is the IRI at the first measurement year from the LTPP database. As shown previously in Table 7, test section 1-1011 has the measured  $Y_I$  in 1992, 1994, 1995, 1998, and 2002. Therefore, the  $Y_{10}$  for this measurement year is the  $Y_I$  that are measured in 1992. It is important to include  $Y_{10}$  in the regression equation since this value describes the road surface condition at the beginning of the analysis period.
- The age (**Age**) attribute is chosen since it reflects the impacts of the season and the environment. The pavement age is calculated by subtracting the year when the test section was opened to the traffic from the IRI measurement year. The test section 1-1011 was opened to traffic on June 1<sup>st</sup>, 1985. Therefore, the corresponding age in 1992 is seven years (1992 to 1985), which explains that the pavement is exposed to traffic loads and the environmental condition for seven years.
- Another important input is the pavement structural number (**SN**) that is used in the 1993 AASHTO and earlier guides (AASHTO 1993). The SN represents the overall structure constructed to sustain the traffic loads. The SN considers structural layer coefficients, layer thicknesses, and base and subbase drainage coefficients. Higher SN exhibits stronger pavement and better load carrying capacity to ensure smooth road surfaces over the service life.
- The next variable selected is cumulative ESAL (**CESAL**) traffic application. The ESAL for certain years is not available in the LTPP database (Jaafar et al. 2015). Mohamed Jaafar et al. (Jaafar et al. 2015) show the example of interpolation for missing ESAL data. The missing ESALs are interpolated based on the average annual rate of growth (AARG). The missing values are estimated using the AARG that is determined by averaging growth rate before and after average years. The average year is 8.5, obtained by dividing 17 (number of years from 1990 to 2006) by two. The ESAL values for the missing data are estimated using Equation 3.4.

$$ESALs_y = ESALs_{y-1} \times (1 + AARG) \quad \text{Eq. 3.4}$$

Where  $y$  is the year of the measured or interpolated IRI. The latest ESAL depends on the ESAL of the preceding year multiplied with the AARG. The interpolated total ESAL for each year shows higher ESAL compared to the measured ESAL from the preceding year, corresponding to positive AARG. Some test sections are observed to have negative AARG values. Thus, smaller traffic ESAL values are

interpolated for those data points. A similar approach is applied to other test sections to predict missing traffic ESAL applications.

- The air temperature (**TEMP<sub>AIR</sub>**) attributes in degree Celsius (°C) are selected since the asphalt surface temperature data are not available in the LTPP IRI datasets. The changes in daily temperature affect the material properties of asphalt pavement. Therefore, the daily temperatures based on the IRI profile date are considered in the analysis.
- Precipitation (**PRECIP**) is another variable considered in the analysis. This attribute describes the amount of rainfall, snow, or sleet that each test section experienced, which affects the pavement layers. The engineering properties of bituminous mixtures, granular base course, and underlying subgrade soils are susceptible to both temperature and moisture variations. This research considers monthly average temperature based on the IRI measured date.
- Three dummy variables are also considered in the multiple regression equations. The explanations for each dummy variable follow:

a) Dummy variable for the LTPP regions (**Reg\_D**):

Where zero is for the North Atlantic, North Central, and Western regions (defined as other regions in this research), and one is for the Southern region.

Purpose: This dummy variable was used to differentiate IRI roughness data between the Southern region and other LTPP regions.

b) Dummy variable for the major M&R treatment applications intervention factor (**CND**): Where zero is for the test section without any major M&R treatment when  $Y_I$  is measured, and one is for the test section that has gone through major M&R treatment when the  $Y_I$  is measured.

The CND identifies changes in the pavement structure caused by major M&R treatment events. When the test section first entered the LTPP program, CN1 was assigned. The subsequent M&R changed the section's construction number to CN2, CN3, etc. Mohamed Jaafar et al. (Jaafar et al. 2015) described the importance of using the CND in the preliminary multiple regression equation developed for IRI prediction in the Southern region. Another study by Mohamed Jaafar and Uddin (Jaafar and Uddin 2016) highlighted the importance of using the CND in the development of the multiple regression prediction equations for asphalt pavement rutting distress in the Southern region. Both studies (Jaafar et al. 2015; Mohamed Jaafar et al. 2016) discovered that the use of the CND increased the R values of the condition deterioration prediction equations. There is a need to develop condition deterioration models using M&R history which were not considered in the National Pooled Fund Study Tpf-5(013) (FHWA 2006) and NCHRP 1-37 studies (NCHRP 2004a).

c) Dummy variable for the IRI measurement locations (**IRI\_D**):

Where zero represents the  $Y_I$  measured outside the wheel path, while one describes the IRI measured inside the wheel path. Detail descriptions related to the IRI\_D were already mentioned earlier in the report.

### **3.2.Methodology for Enhanced Rutting Modeling**

The following key steps are considered to develop a rutting progression prediction model equation:

- 1) Prepare the database for the development of the enhanced rutting multiple regression prediction equations.
- 2) Verify the database for test sections with zero average rut depth values to remove from the model development.
- 3) Before the development of the multiple regression model equation, evaluate if the data are (1) random, (2) independent of each other, and (3) normally distributed. Additionally, the variance between the measured and predicted average rut depth per measurement year data must be homogenous.
- 4) Perform transformations of  $Y_1$  using a  $\log_{10}$  function to obtain a linear relationship between two variables. Additionally, a dependent variable of  $\text{Log}_{10}(Y_R+0.5)$  was used to allow zero rut depth value to be considered in the development of the enhanced model equations.
- 5) Develop the enhanced rutting modeling equation using the same variables used in the IRI models
- 6) Introduce new variables of elastic modulus values for asphalt ( $E_1$ ), base ( $E_2$ ), subbase ( $E_3$ ), and subgrade ( $E_4$ ) layers using the equations developed by Uddin (1984).
- 7) Perform statistical tests to assess the effects of M&R history, LTPP climatic regions, and base type on the average rut depth per measurement year
- 10) Evaluate the accuracy of the developed equations based on the following parameters:
  - The R and  $R^2$  values of the multiple regression equations
  - The predicted against measured data plots
  - The verifications of the multiple regression equations
  - The accuracy measures of the MARE and RMSE
- 11) Select the best-enhanced rutting prediction model based on the most accurate statistical parameters.

#### **3.2.1. LTPP Rutting Data Collection**

The rutting data available for test sections in 24 states in the U.S. are extracted from the LTPP database under the MON\_RUT\_DEPTH\_POINT section (FHWA 2019). The rut depths are commonly measured at 11 equal intervals for both outside and inside wheel paths throughout 500 feet (152.4 m) test section. Table 9 shows the example of rut depth data sets for test section 1-1011 in Lauderdale County, Alabama. In this research, only the average rut depth per measurement year ( $Y_R$ ) is considered in the analysis. Total rut depth values from 11 points outside wheel path, and rut depth values from 11 points inside wheel path were divided by eleven to get the average values on both sides, respectively. Next, the average rut depth values on both sides were divided by two to obtain an average rut depth per measurement year, measured in millimeters (mm). For example, the average rut depth per measurement year for test section 1-1011 is 3.14 mm. A total of 214 data sets were used in the development of the

enhanced  $Y_R$  multiple regression and ANN model equations. The distribution of rut depth data sets based on LTPP regions (Reg\_Actual), base type (Base\_D), and major M&R intervention factor (CND) is shown in Table 10. Figure 10 shows the distribution of the rut depth per measurement year data used in this research.

Table 9. Rut depth data sets for test section 1-1011 in Lauderdale County, Alabama

SHRP_ID	STATE_COD	CONSTRUC	SURVEY_I	POINT_LO	LEFT_RUT	RIGHT_RUT
1011	1	1	3/30/1993	0	4	6
1011	1	1	3/30/1993	15.3	2	5
1011	1	1	3/30/1993	30.5	3	4
1011	1	1	3/30/1993	45.8	2	4
1011	1	1	3/30/1993	61	2	3
1011	1	1	3/30/1993	76.3	2	4
1011	1	1	3/30/1993	91.5	2	4
1011	1	1	3/30/1993	106.8	2	5
1011	1	1	3/30/1993	122	2	4
1011	1	1	3/30/1993	137.3	1	3
1011	1	1	3/30/1993	152.5	2	3

Table 10. Rut depth data sets based on LTPP regions, base type, major M&R

Between-Subjects Factors					
Group		Value Label	N	Percentage	
Reg_Actual	1	North Atlantic	7	3.3%	
	2	North Central	23	10.7%	
	3	Southern	175	81.8%	
	4	Western	9	4.2%	
Base_D	0	Stabilized Base	83	38.8%	
	1	Granular Base	131	61.2%	
CND	0	No Major M,R&R	159	74.3%	
	1	Major M, R&R Applied	55	25.7%	

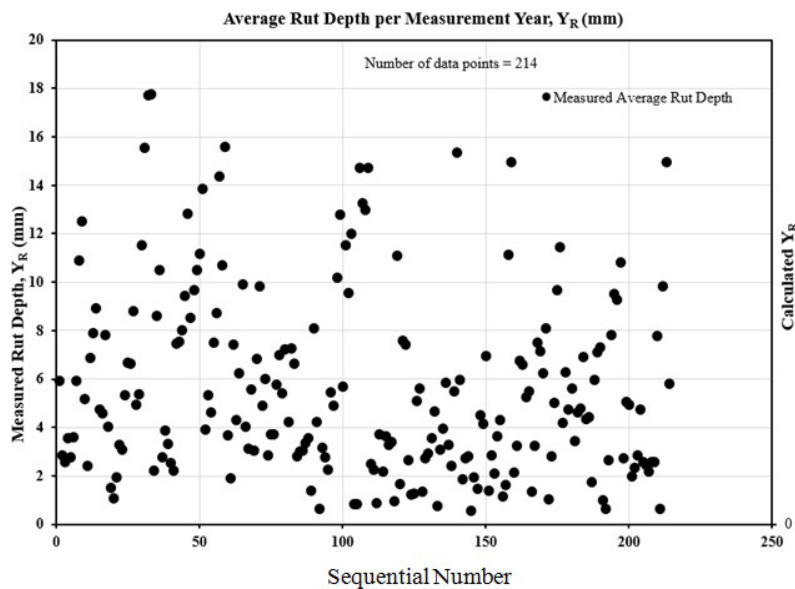


Figure 10. Rut depth per measurement year data

### 3.3. Methodology for Enhanced Cracking Modeling

The following key steps were implemented for the development of enhanced cracking models:

- 1) Extract cracking distress data from the LTPP database and convert it to the UCI for each cracking distress type (alligator, block, longitudinal, transverse). Add the individual UCI, which is the density of the crack area in % for each crack, to form a combined UCI.
- 2) Perform data transformations
- 3) Verify data normality using the K-S test and the normality plot from the SPSS (IBM 2022)
- 4) Select test sections to perform a t-test to analyze the effect of major M&R for CND factor on the UCI means.
- 5) Conduct t-tests for each section to observe the effect of major M&R on the UCI values.
- 6) Assign the correct construction number dichotomous variable value for each section.
- 7) Perform additional data transformations.
- 8) Conduct an ANOVA test to evaluate the effects of M&R history and LTPP climatic region factors on the combined UCI datasets.
- 9) Develop the enhanced cracking multiple regression equation and ANN model equation using selected input variables.
- 10) Evaluate the reasonableness of the multiple regression and ANN model equations based on the following parameters:
  - The R-value of the multiple regression equations.
  - The predicted against measured data plots.
  - The verifications of the multiple regression equations
  - The accuracy measures of the MARE and RMSE

### 3.4. Methodology for Modulus Values Backcalculation Process

The following key steps were implemented for the backcalculation of pavement layer modulus values:

- 1) Evaluate backcalculation method candidates using selected asphalt LTPP deflection data.
- 2) Select backcalculation software for the preliminary study.
- 3) Assign pavement layer configurations including layer thicknesses and Poisson's ratio referred to the previous study on test section 28-2807 by Uddin et al. (2003).
- 4) Extract FWD data conducted in 1990, 1991, 1992, 1993, 1995, and 1998 from the LTPP database.
- 5) Provide seed modulus values that are required by each backcalculation software used in this research.
- 6) Run backcalculation process using the PCASE 2.09, BAKFAA 2.0, EVERCALC 5.0, and UMPED software. Calculate the RMSE as shown in Equation 3.5.

$$RMS\ error\ (\%) = \sqrt{\frac{1}{n_d} \times \sum_{i=1} (d_{ci} - d_{mi})^2} \times 100 \quad \text{Eq. 3.5}$$

Where,

$d_{ci}$  = Calculated surface deflection at sensor  $i$ ,

$d_{mi}$  = Measured surface deflection at sensor  $i$ , and

$n_d$  = Number of deflection sensors used in the FWD test

- 7) Compare the modulus value with the backcalculated modulus values from the previous study by Boriboonsin and Momm (2002). The most acceptable modulus values were selected for further analysis using the 3D finite element software.

### 3.5. 3D-FE Modeling of Uncracked Asphalt Pavements

The step-by-step approaches for developing the 3D-FE model subjected to truck axle loading is presented, as follows:

- 1) Sketch the proposed asphalt pavement cross-section manually before creating the 3D-FE model using the LS-DYNA software. Take note of the important coordinates of nodes, sizes of the elements, pavement layer thicknesses, overall dimension of the 3D-FE model, and the proposed loading area subjected to truck wheel loads.
- 2) Create the cross-section of the pavement system in the LS-DYNA software from the asphalt pavement surface layer at the top to the underlying subgrade layer at the bottom. Figure 11 shows the completed 3D-FE model of the pavement-subgrade system developed in this research.

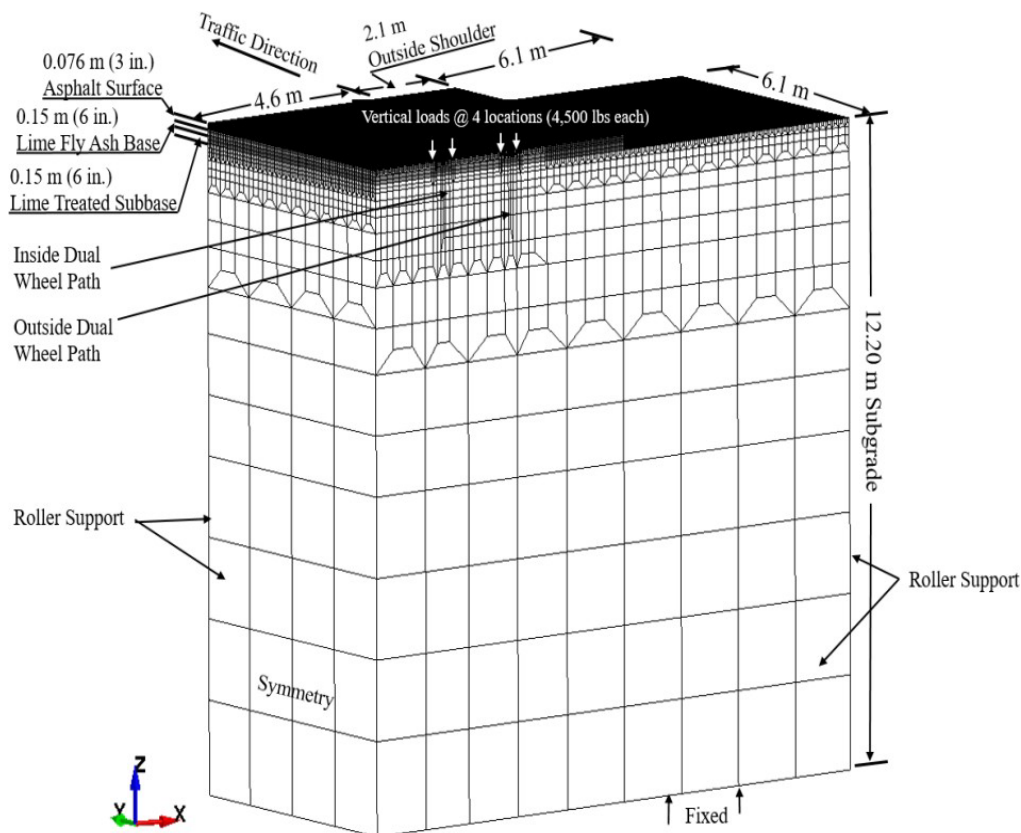


Figure 11. 3D-FE model of the pavement-subgrade system subjected to truck axle loading

3) Create each layer as a unique part. In this model a total of 26 parts are created to simulate the 3D-FE half model of uncracked asphalt pavement system (Figure 12):

- 6 parts of asphalt pavement layer (left side), 6 parts of asphalt pavement layer (right side).
- 4 parts of LFA base layer (left side), 4 parts of LFA base layer (right side).
- 2 parts of lime-treated subbase (left side), 2 parts of lime-treated subbase (right side).
- 1 part of subgrade, 1 part of outside shoulder.

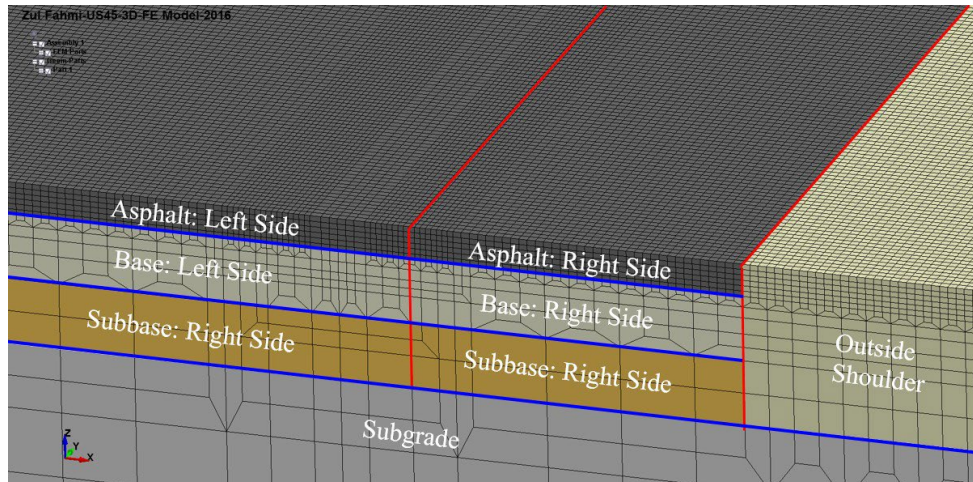


Figure 12. Pavement-subgrade 3D-FE model of uncracked pavement developed

Figure 12 shows the close-up view of asphalt, base, subbase, subgrade layers, and outside shoulder parts from the final 3D-FE half model. The following description of the 3D-FE model under in situ conditions applies:

- Asphalt, base, and subbase layers were developed not as a single layer, but as a combination of a few thinner layers. The thinner layer was developed as a unique part with a specific part identification number.
- The asphalt layer was developed with six thinner layers of asphalt pavement (six parts). The thickness for each asphalt layer is 12.7 mm (0.5 in.), therefore the total thickness is 76.2 mm (3 inches).
- The base layer consists of four different parts. The total base layer thickness of 152.4 mm (6 inches) is the combination of four thinner layers of 25.4 mm (1 in.), 25.4 mm (1 in.), 38.1 mm (1.5 inches), and 63.5 mm (2.5 inches), respectively, from the first to the fourth layers.
- The subbase layer consists of two different parts. This layer was divided into two different parts with 76.2 mm (3 inches) thick, respectively.
- The subgrade layer consists of only one part, with a total thickness of 12,192 mm (480 inches).
- A total of 26 parts were used to develop the model including one part of the outside shoulder section. The undeformed 3D-FE model of uncracked asphalt pavement is shown in Figure 13.



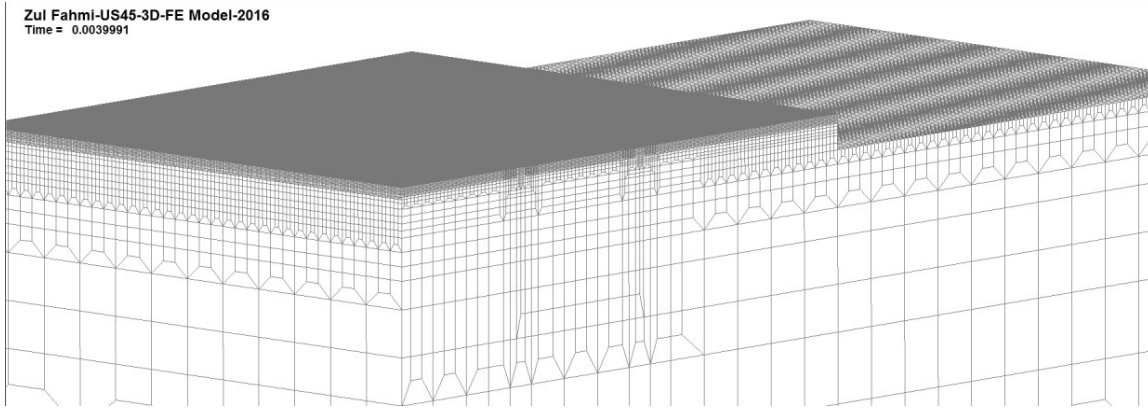


Figure 13. Undeformed 3D-FE model of uncracked asphalt pavement

4) Each layer was assigned with a proper color code as shown in Figure 14.

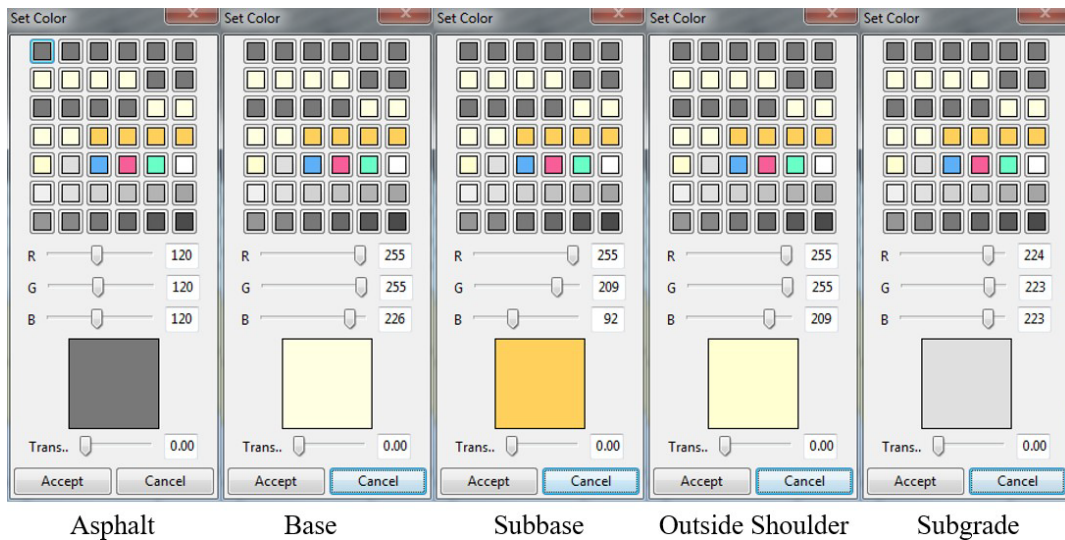


Figure 14. Color codes assigned to pavement-subgrade 3D-FE model

5) The truck rear axle load-time history curve was created based on a previous study by Hajj et al. (2012). The researchers studied the influence of tire-pavement stress distribution, shape, and braking performance predictions for asphalt pavement. The comprehensive stress curve for the rear axle was traced on a piece of transparent paper. More than 150 points of time (x-axis) and compressive stress (y-axis) coordinates were noted, as shown in Figure 15. Next, the peak stress ratios were calculated by dividing each compressive stress value with the maximum compressive stress of 42.5 kPa. Figure 16 shows the stress ratios bounded between zero to one ratio. The stress ratios were then converted to simulate maximum tire pressure of 100 psi with 200 milliseconds time-history curve as shown in Figure 17.

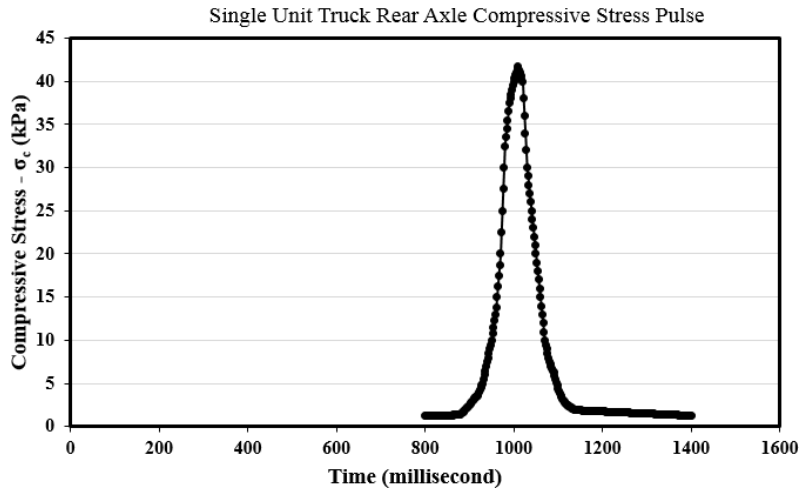


Figure 15. Single unit truck rear axle compressive stress pulse

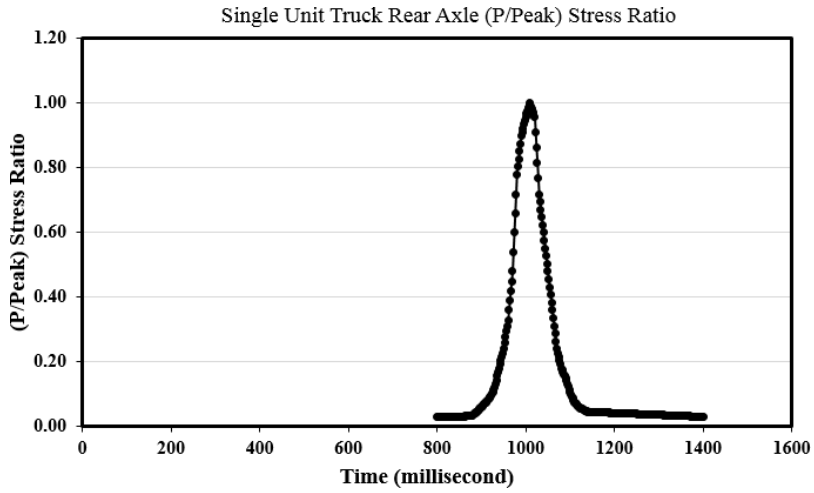


Figure 16. Single unit truck rear axle (P/Peak) stress ratio

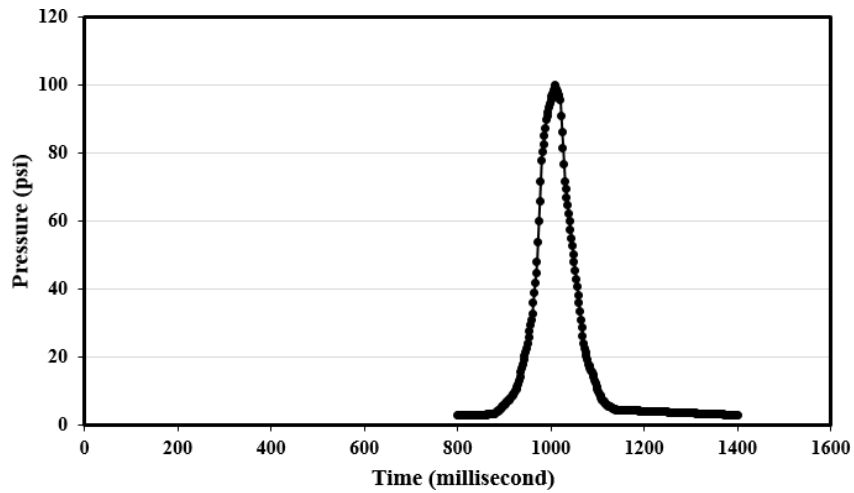


Figure 17. Surface pressure (psi) used in the LS-DYNA analysis

- 6) In the 3D-FE dynamic analysis, the nodal force association with mass, damping, and stiffness attributes is explained through Equation 3.6 (Garza 2003).

$$M\ddot{U} + C\dot{U} + KU = F(t) \tag{Eq. 3.6}$$

Where M is the mass matrix, C is the damping matrix, K is the stiffness matrix,  $\ddot{U}$  is the vector of acceleration,  $\dot{U}$  is the vector of velocity, and U is the vector of displacement. F(t) is the vector of nodal forces. In this research, the effect of damping is ignored because the duration of the truck axle load pulse is short (less than one second) and does not affect the results of the analysis.

- 7) Next, a truck wheel contact area was assigned on top of the asphalt pavement surface. The initial setup was discarded due to the elongated oval shape as shown in Figure 18. The final truck wheel contact area set up (Figure 19) shows a more reasonable footprint of the truck wheel contact area. The calculated contact area in the 3D-FE half model is 22.5 in<sup>2</sup>.
- 8) The 3D-FE model was subjected to 18,000 lbs (18-kips) single axle truck wheel loads with four tires. This research simulates 4,500 lbs of truck wheel load on each tire as shown previously in Figure 11. For the 3D-FE half model, the required load is 2,250 lbs (4,500 lbs divide by two) and the tire pressure is 100 psi. By dividing the required load with the tire pressure (2,250 lbs / 100 psi), the calculated truck wheel contact area under one tire is 22.5 in<sup>2</sup>. Therefore, the applied peak load was 4,500 lbs. The LS-DYNA calculated peak deflections are normalized to 4,500 lbs by multiplying the calculated peak deflections with 1.0 (4,500 lbs / 4,500 lbs).

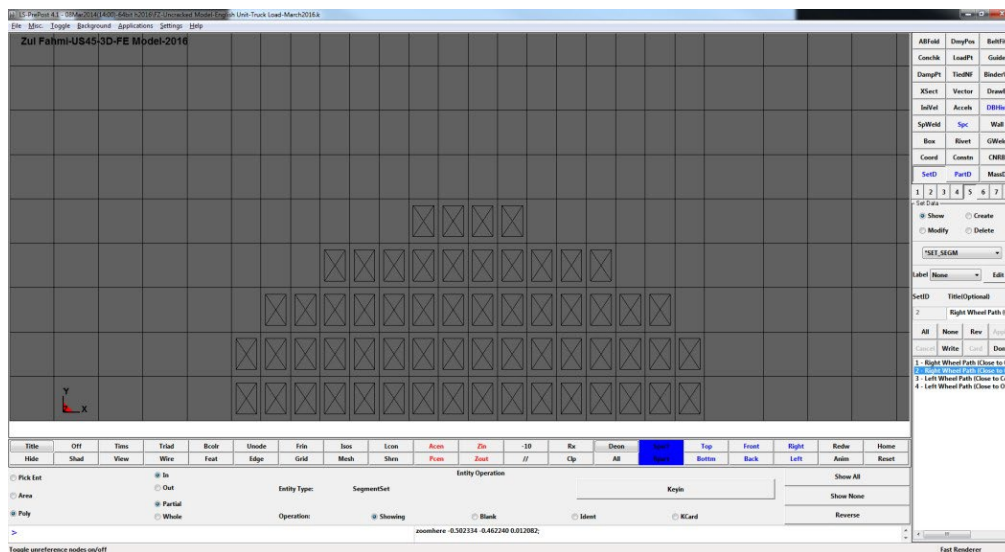


Figure 18. Initial set up for truck wheel contact area for 3D-FE Half model



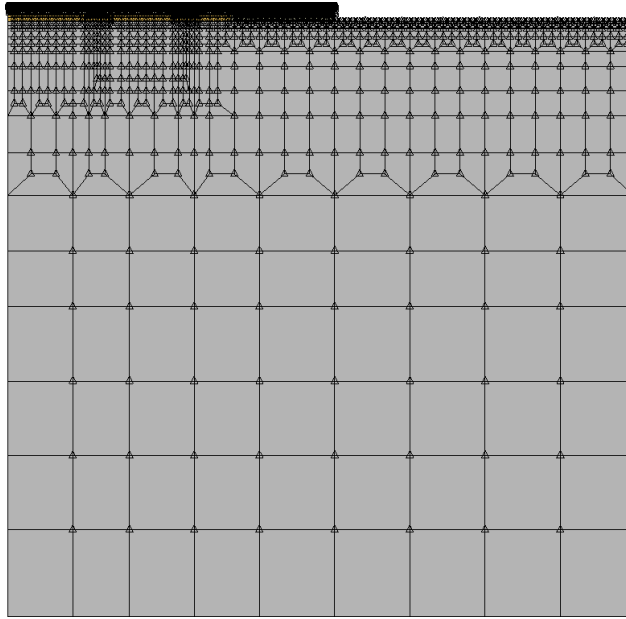


Figure 21. Nodes used to set boundary conditions (front view of the 3D-FE half model)

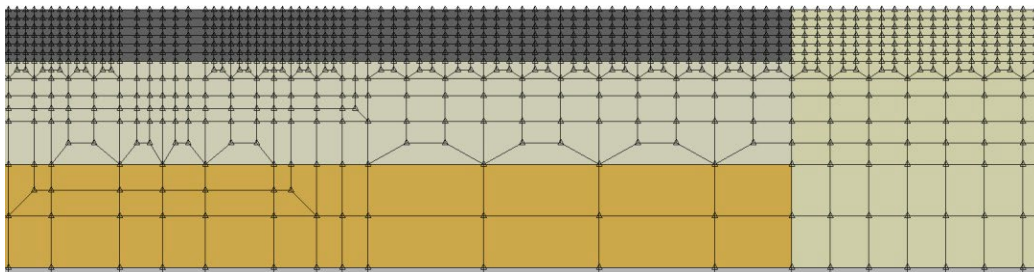


Figure 22. Close-up view of asphalt layers (front view of the 3D-FE half model)

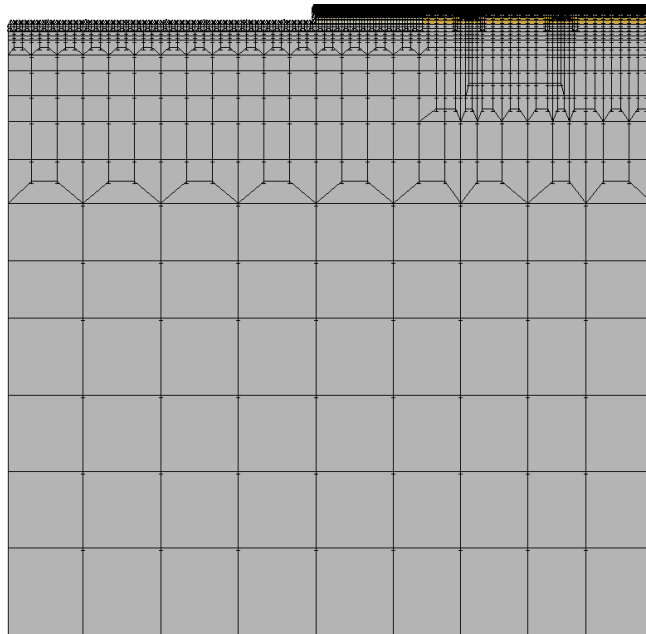


Figure 23. Nodes used to set boundary conditions (back view of the 3D-FE half model)

10) Once the 3D-FE model is ready, make a few trials runs to ensure the model is functional and reliable for further analysis. Run the simulations based on the proposed full factorial experiment design. Connor and Zelen (1959) provide the guideline for the partial factorial design that considers a subset of a full factorial design to reduce the number of simulations, if necessary.

### 3.6. 3D-FE Modeling of Longitudinal Crack in Asphalt Layer

In this research, the following key steps were used to develop the 3D-FE model and simulate longitudinal crack in the surface layer.

1. The 3D-FE for the cracked asphalt model was created like the dimensions of the uncracked 3D-FE pavement-subgrade model using the LS-DYNA software. However, the cracked pavement was set up with finer meshes to simulate a 0.1-inch width of the cracked area.

This crack area was set up in the traffic direction to the other ends of the 3D-FE model, for the outside wheel path close to the shoulder. The middle of the crack area is 30.25 inches (about 2.52 feet) from the road shoulder. Figure 24 compares the surface views on top of the asphalt pavement layer for uncracked pavement (a) and cracked pavement (b).

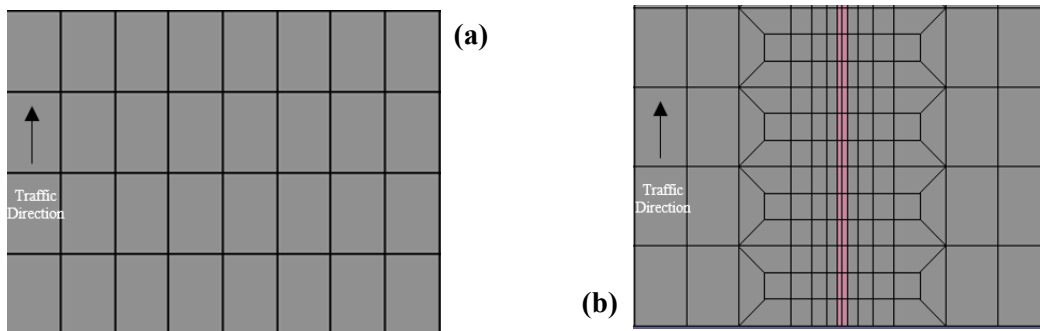


Figure 24. Plan views on top of the asphalt pavement for uncracked (a) and cracked pavement (b)

2. This research proposed the simulation of the longitudinal crack in asphalt pavement using the CONTACT SURFACE TO SURFACE definition in the LS-DYNA software (Livermore 2022). Figure 25 shows the parameters required to set the CONTACT definition.

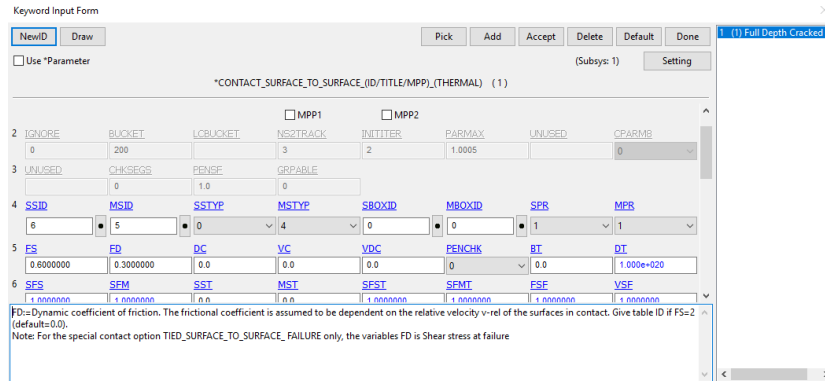


Figure 25. Keyword input form for LS-DYNA software

There are two most important parameters, which are the definitions of the master segment (MSID) and slave segment (SSID), and static friction (FS) and dynamic friction (FD) of coefficient values. In this research, the FS of 0.6 and FD of 0.3 were used in the analysis. These friction coefficients are used to simulate the pavement cracks which always have some aggregate interlock. Details on part of the parameters are described in Appendix A (Figure A1).

Parametric studies were conducted earlier in this research to determine the effects of coefficient of friction values on the deflections. In the LS-DYNA software, the deflection value was determined from the nodes' output. The analysis evaluates the deflection values for the nodes on the asphalt surface layer, at the middle of the asphalt layer, and the bottom of the asphalt layer. The following parametric studies were conducted to evaluate the effects of friction coefficients on the surface deflections.

- Parametric Study 1: Fix the FS at 0.7, and change the FD values from 0.1, 0.2, 0.3, 0.4, 0.5, 0.6, and 0.7, respectively.
- Parametric Study 2: Change FS values from 0.1, 0.2, 0.3, 0.4, 0.5, and 0.6, and fix the FD at 0.3 for each run.

These two case studies were conducted for the nodes at the asphalt surface layer, at the middle of the asphalt layer, and the bottom of the asphalt layer, respectively. The results are summarized in Appendix A (Table A1). It was discovered that the friction coefficient values did not affect the deflections, regardless of the node locations. Therefore, based on certain engineering justification and experience, the final FS and FD used in this research are 0.6 and 0.3, respectively.

3. The FS and FD are used in between the master and slave segments of the 3D-FE cracked model. The master and slave segments are required as part of the surface CONTACT definition in the 3D-FE analysis. The master segment is the asphalt vertical surfaces, and base layer horizontal surfaces surrounding the cracked areas. Figure 26 shows the master segment defined on the vertical surfaces of a wider asphalt layer on the left side of the cracked area (a), and the master segment defined on the vertical surfaces of the asphalt layer on the right side (b), which is closer to the shoulder. Both pictures also show the master segments set on the surfaces of the base layer.

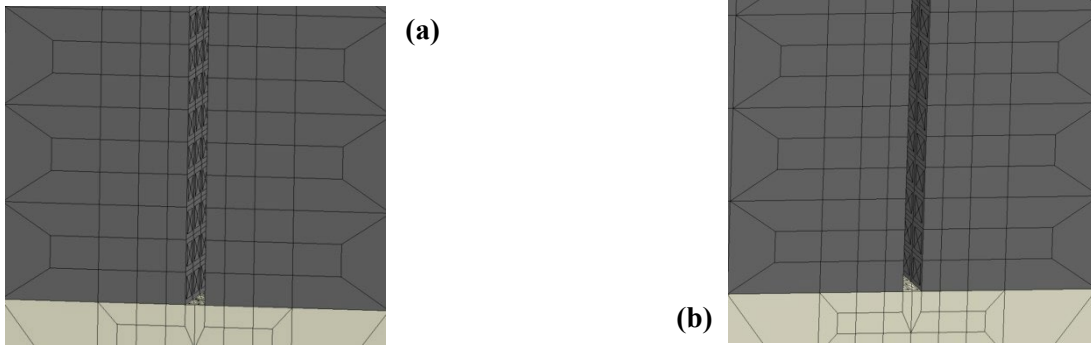


Figure 26. Master segments defined on the vertical surfaces for left (a) and right (b) sides of the cracked area

4. In contrast, the slave segment was set on the horizontal and vertical surfaces of the cracked layer as shown in Figure 27. The SEGMENT SET command was used to define both master and slave segments.

Further analysis will be conducted to study the structural responses of uncracked and cracked asphalt pavements under the FWD and wheel loads by simulating cracks at the surface and several different depth levels.

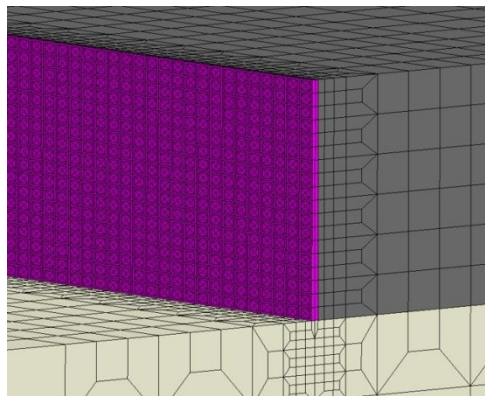


Figure 27. Slave segments defined on both the left and right sides of vertical surfaces, and horizontal surfaces at the bottom of the cracked element

5. Next, set the boundary conditions for the cracked 3D-FE models. Use roller-type boundary conditions on all sides to unconstraint lateral motion. In the LS-DYNA, the translational and rotational constraints in the local x-axis, y-axis, or z-axis are controlled by using binary logic zero and one value. Choosing zero will restrain translation or rotation at the local axis. In contrast, the translation and rotation at the local axis are permitted if the binary logic of one is selected in the keyword input form. Appendix A (Figure A2 to A5) shows the screenshots of the keyword input form for boundary conditions set up for the cracked 3D-FE model.
6. Subsequently, the SEGMENT SET command was used to define the loading areas on top of the asphalt layer. Figure 28 shows the segments set to simulate the contact area between the truck tire and road surface on top of the cracked areas. This research modeled a standard 18-kips single axle truck with four tires, and the truck load of 4,500 lbs on each tire at 100 psi tire pressure (Uddin



1984). However, the longitudinal crack in the asphalt layer was simulated only for the outside wheel path at about 2.5 feet from the road shoulder. Figure 29 shows the original sketch of the 18-kips single axle truck (Uddin 1984), and the dimension of the tire contact area developed in this research. The LS-DYNA peak deflections for this analysis were calculated using a pressure value of 100 psi over an area of 22.5 in<sup>2</sup>, therefore the applied peak load was 4,500 lbf. The LS-DYNA calculated peak deflections were normalized to 4,500 lbf, multiplying the calculated peak deflections by the factor 1.00 (4,500 lbs / 4,500 lbf).

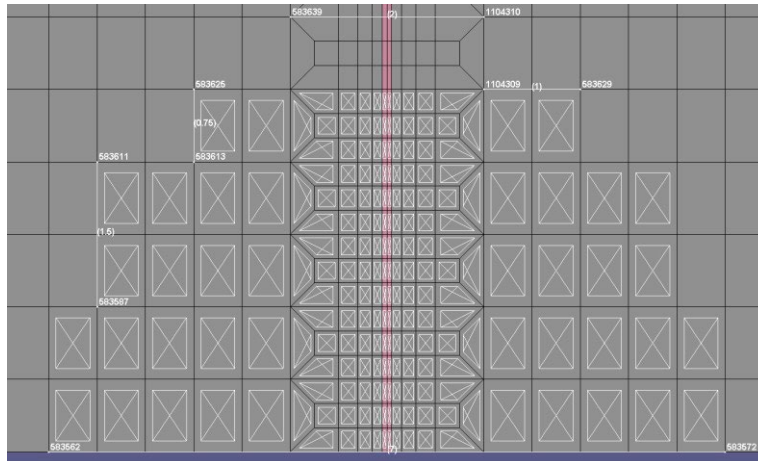


Figure 28 Truck tire contact area simulated in the 3D-FE analysis for cracked asphalt pavement

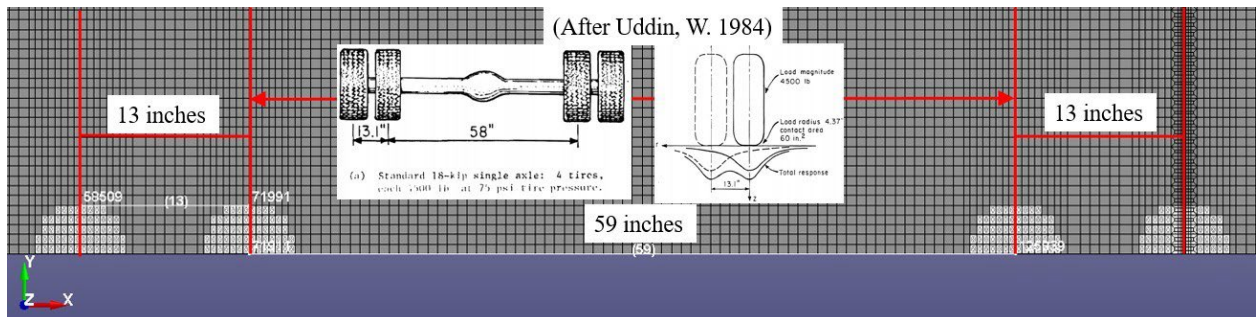


Figure 29. Sketch of an 18-kips single axle truck with 4 tires and contact areas developed in this research

7. Once all the requirements in step one to step seven are fulfilled, the 3D-FE model is ready for simulations based on the factorial design. Finally, the deflection values for specific nodes are available through the NODOUT option under the ASCII output command. Additionally, the stress and strains results are available in the ELOUT option under the ASCII output command. The deflection, stress, and strain values are plotted, and the findings are compared between both uncracked and cracked asphalt pavement conditions.

## 4. RESULTS AND DISCUSSION

### 4.1. Pavement Condition Deterioration Modeling

#### 4.1.1. Enhanced IRI Modeling

An expanded database using a total of 2,588 data points was used for the development of the enhanced multiple regression prediction equations and ANN modeling. Many transformations of  $Y_I$  were tried including  $\text{Log}_{10} Y_I$  and  $\text{Ln } Y_I$  (all IRI data were non-zero data). The regression equations for  $Y_I$ ,  $\text{Log}_{10} Y_I$ , and  $\text{Ln } Y_I$  are shown in Equations 4.1 to 4.3, respectively.

$$Y_I = 0.642 + 0.726 (Y_{I0}) + 0.006 (Age) - 0.045 (SN) - 1.542 \times 10^{-8} (CESAL) + 0.002 (TEMP_{AIR}) - 0.000349 (PRECIP) + 0.08 (Reg\_D) - 0.105 (CND) - 0.061 (IRI\_D)$$

Eq. 4.1

$$\text{Log}_{10} (Y_I) = 0.119 + 0.626 (\text{Log}_{10} Y_{I0}) + 0.002 (Age) - 0.014 (SN) - 6.34 \times 10^{-8} (CESAL) + 0.000377 (TEMP_{AIR}) - 0.000112 (PRECIP) + 0.023 (Reg\_D) - 0.037 (CND) - 0.016 (IRI\_D)$$

Eq. 4.2

$$\ln (Y_I) = 0.274 + 0.626 (\ln Y_{I0}) + 0.005 (Age) - 0.032 (SN) - 1.46 \times 10^{-8} (CESAL) + 0.001 (TEMP_{AIR}) - 0.000258 (PRECIP) + 0.054 (Reg\_D) - 0.086 (CND) - 0.038 (IRI\_D)$$

Eq. 4.3

To verify if the data complied with the assumptions required for multiple linear regression analysis, several tests were performed, as follows:

- Data independence: the autocorrelation of the  $Y_I$  datasets was assessed using the CORREL function in the Microsoft Excel datasheet. The autocorrelation value is less than 0.4 showing that the data are independent of each other.
- Data normality: a Kolmogorov-Smirnov nonparametric test (K-S test) and a normality plot from the SPSS (IBM 2022) were performed to verify if the data were normally distributed

The normality test results for  $Y_I$  and transformed  $Y_I$  data are shown in Table 11. Normality test results for  $Y_I$  and transformed  $Y_I$  data

Table 11. Kolmogorov-Smirnov Test of Normality

Tests of Normality			
Kolmogorov-Smirnov <sup>a</sup>			
	Statistic	df	Sig.
$Y_I$	.119	2,588	< 0.001
$\text{Log}_{10} Y_I$	0.054	2,588	< 0.001
$\text{Ln } Y_I$	.054	2,588	< 0.001
a. Lilliefors Significance Correction			

Kolmogorov-Smirnov is a nonparametric (distribution-free) test that is used to test the normality of the data. The test hypotheses for the probability of type I error alpha ( $\alpha$ ) = 0.05 are described, as follow:

- Null hypothesis,  $H_0$ : The distribution of the  $Y_I$  data is normal
- Alternative hypothesis,  $H_A$ : The distribution of the  $Y_I$  data is not normal

The normality test of  $Y_I$  data in the LTPP database shows that the probability of significance, the p-value is less than the  $\alpha$  0.05 probability of chance error, which is statistically significant. Therefore, the null hypothesis is rejected, and the  $Y_I$  data is not normally distributed. Figure 30 shows the normality plots for the untransformed and transformed  $Y_I$ .

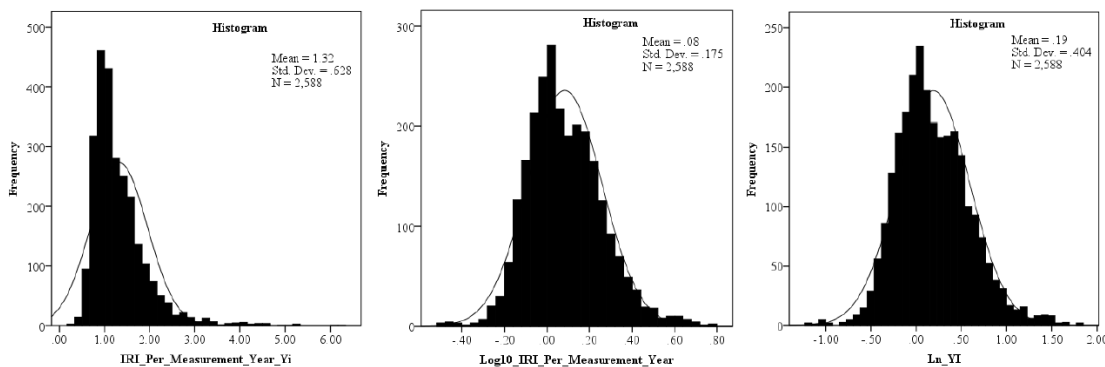


Figure 30. Normality plots for the untransformed and transformed  $Y_I$  data

The distributions of the  $Y_I$  data do not exactly follow the bell curve of normal distribution. Part of the histogram data is way out of the distribution curve. These histograms indicate that the  $Y_I$  data are not normally distributed. The results of the normality test reveal that multiple linear regression modeling may be problematic if residuals are not normally distributed with zero mean value. An alternative method for condition deterioration progression modeling is the ANN method.

Table 12 summarizes the number of data sets (N), coefficient of correlation (R), coefficient of determination ( $R^2$ ), the average measured  $Y_I$ , average predicted  $Y_I$ , RMSE, and MARE(%) for the untransformed and transformed  $Y_I$  model database. The verification results for Equations 4.1 to 4.3 are shown in Table 13.

Table 12. Accuracy measures for the untransformed and transformed  $Y_I$  model database

Regression Equations (SPSS)				Database (Predicted vs Measured)					
Dependent Variable	N	R	$R^2$	Measured $Y_I$ (m/km)	Predicted $Y_I$ (m/km)	% Difference (Average)	R	RMSE	MARE (%)
$Y_I$	2,588	0.633	0.401	1.32	1.32	0.0	0.633	0.484	26.8
$\text{Log}_{10}(Y_I)$	2,588	0.622	0.387	1.32	1.25	-5.3	0.633	0.494	24.5
$\text{Ln}(Y_I)$	2,588	0.622	0.387	1.32	1.25	-5.3	0.633	0.494	24.5

Table 13. Accuracy measures for the untransformed and transformed  $Y_I$  model verifications

Verification of IRI Multiple Regression Equations							
(Predicted vs Measured)	Measured $Y_I$ (m/km)	Predicted $Y_I$ (m/km)	% Difference (Average)	N	R	RMSE	MARE (%)
$Y_I$	2.25	1.74	-22.7	18	0.99	0.21	9.6
$\text{Log}_{10}(Y_I)$	2.25	1.61	-28.4	18	0.96	0.38	11.6
$\text{Ln}(Y_I)$	2.25	4.23	88.0	18	0.98	3.22	122.2

For model databases, the untransformed  $Y_I$  gives the most accurate regression results as shown by the listed accuracy measures. The measured R values are similar for all three equations. However, the average predicted  $Y_I$  using equation 4.1 shows no difference as compared to the measured value. The other two equations underpredicted the  $Y_I$  (1.25 m/km). The untransformed  $Y_I$  has the least RMSE despite a slightly higher MARE of 26.8%. The verification results show that the untransformed  $Y_I$  outperformed the other equations based on the average percent difference, RMSE, and MARE. Therefore, Equation 4.1 was selected as the best enhanced IRI prediction equation. The final results are shown in Figure 31 to Figure 33. Figure 31 shows the measured and predicted values using the enhanced multiple regression prediction equations with respect to data sequential numbers on the x-axis.

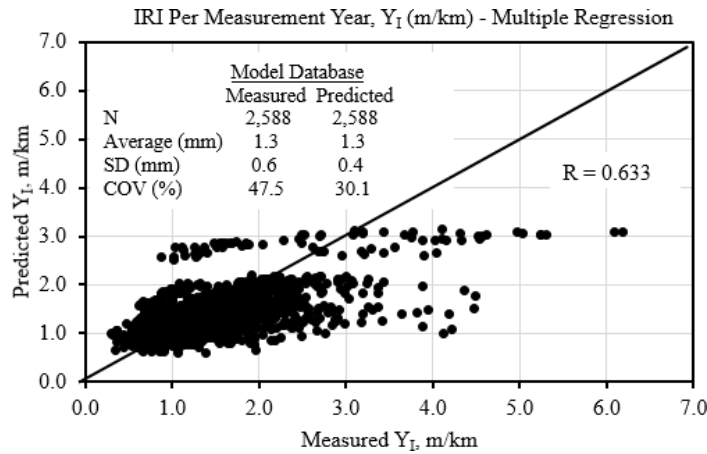


Figure 31. Predicted vs measured plot for IRI multiple regression equation database

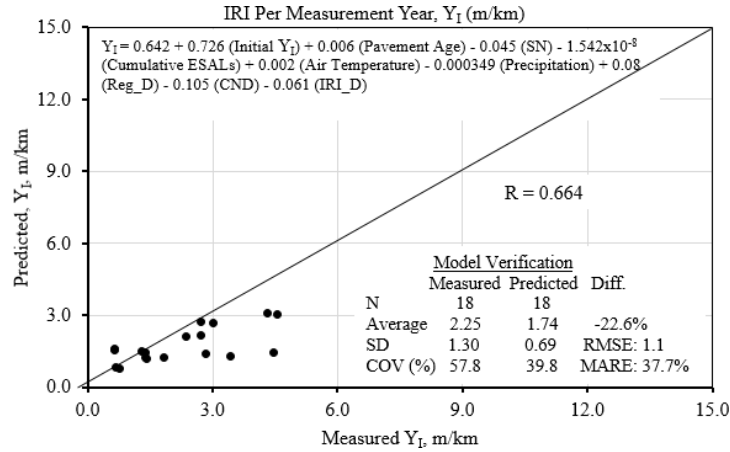


Figure 32. Predicted vs measured plot for IRI multiple regression verification database

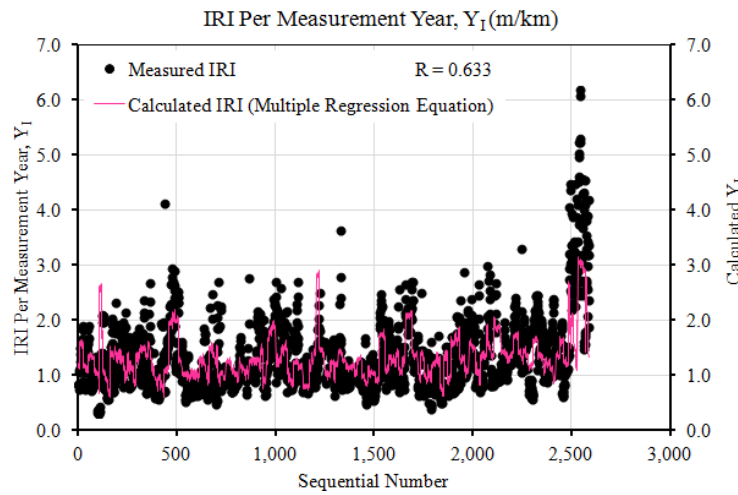


Figure 33. Measured and predicted IRI using multiple regression

The ANN model results are shown in Figure 34, Figure 35, and Figure 36, respectively.

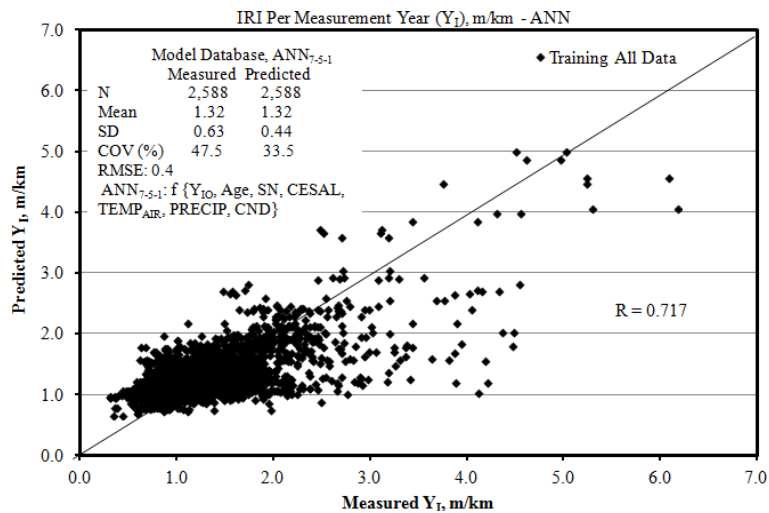


Figure 34. Predicted vs measured plot for IRI ANN model database

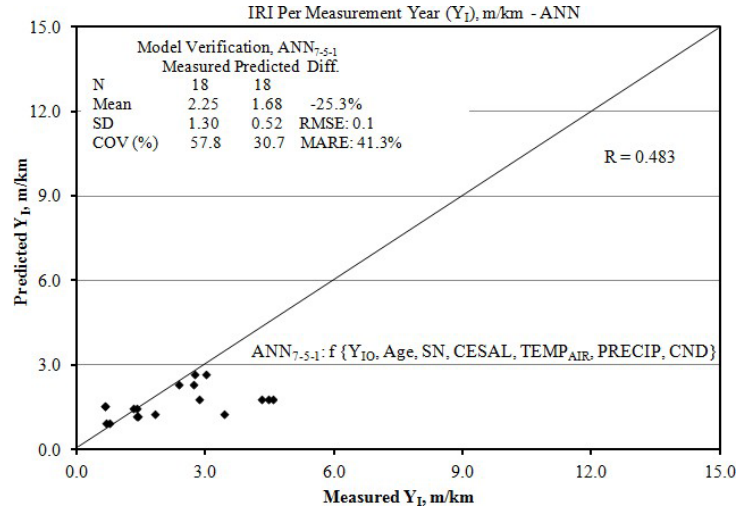


Figure 35. Predicted vs measured plot for IRI ANN verification database

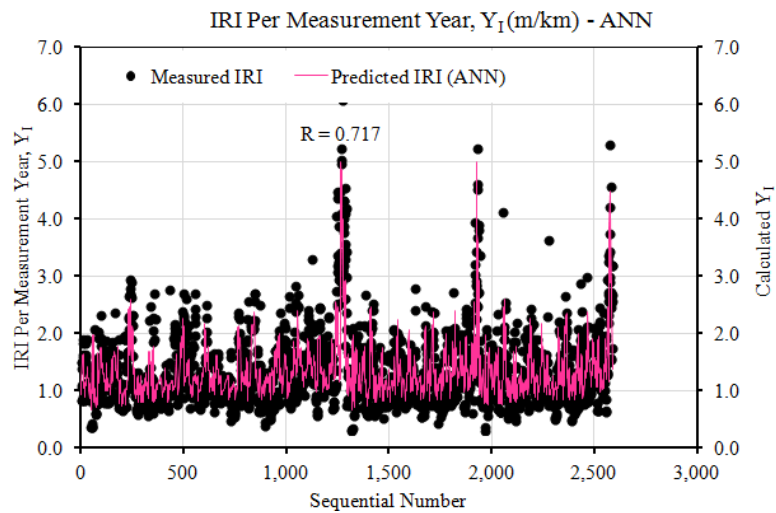


Figure 36. Measured and predicted IRI using ANN model

The verification results are better predicted using the enhanced multiple regression model equation for untransformed IRI values. However, both the ANN model and the enhanced IRI multiple regression equations are recommended for implementation.

#### 4.1.1.1. Application of IRI Performance Condition Deterioration Model Equations

Both enhanced IRI multiple regression equation and ANN IRI models were proposed for asphalt pavement design purposes. The final multiple regression equation for IRI condition deterioration prediction is shown in Equation 4.4. It is important to point out that Equation 4.4 applies only to high-quality road networks with the IRI equal to or less than 3 m/km. This includes the national highway system that is maintained periodically.

$$Y_I = 0.642 + 0.726(Y_{I0}) + 0.006(Age) - 0.045(SN) - 1.542 \times 10^{-8}(CESAL) + 0.002(TEMP_{Air}) - 0.000349(PRECIP) + 0.08(Reg_D) - 0.105(CND) - 0.061(IRI_D) \quad \text{Eq. 4.4}$$

The necessary keys steps required in the implementation of the enhanced IRI multiple regression equations for pavement design follow:

- Set the initial IRI to 0.5 m/km for the newly paved road network. For older road networks, the most recent IRI data must be known to use the proposed multiple regression equation. The initial IRI value must be between 0.53 m/km to 3.55 m/km.
- Pavement age (year) is calculated from the last year since the major maintenance and rehabilitation has taken place. If there is no major maintenance and rehabilitation history recorded, the pavement age is calculated from the initial year when the road was opened to the traffic. If the pavement age in 2019 is 10 years, and the predicted IRI in 2029 is required, then the pavement age of 20 years will be used in the equation. The pavement age must be between 0 to 48 years.
- Estimate the CESAL for the projected years based on a known traffic growth factor. If the recent CESAL is 500,000 in 2019, and the annual traffic growth factor is 0.01, the estimated CESAL in 2029 is 552,311 and will be used in the equation. The maximum CESAL is 36,669,857 and the minimum CESAL is 3,000.
- Calculate the SN based on the layer coefficients, layer thicknesses, and drainage coefficients for asphalt, base, and subbase layers, respectively. The minimum and maximum SN values are 1.4 to 10.8, respectively.
- Assume an average monthly air temperature ( $^{\circ}\text{C}$ ) based on the most recent year data that are available in the national database. The minimum and maximum air temperatures ranged from  $-8.3^{\circ}\text{C}$  to  $46^{\circ}\text{C}$ , respectively.
- Assume average monthly precipitation (mm) based on the most recent year data that are available in the national database. The average monthly precipitation ranged from 0 to 645mm.
- For the LTPP climatic region factor (Reg\_D), assign zero for the Southern region. In contrast, assign one for other regions.
- For the major maintenance and rehabilitation intervention (CND) variable, assign zero if there is no major maintenance and rehabilitation has taken place. Assign one if the old pavement layer has been removed and resurfaced.
- For the IRI measurement location factor (IRI\_D), assign zero for the outside wheel path, and one for the inside wheel path.

The ANN<sub>7-5-1</sub> provides the most optimum network for future IRI prediction. The ANN<sub>7-5-1</sub> refers to a total of seven inputs ( $Y_{10}$ , Age, SN, CESAL,  $\text{TEMP}_{\text{AIR}}$ , PRECIP, and CND), five hidden nodes, and one output. Figure 37 shows the setup for the optimum network used in the analysis using the TRSEQ1 ANN computer program (Najjar 1999).

Figure 38 shows an example of the implementation of the ANN model for future IRI prediction. This extended analysis intends to predict the remaining duration (years) before the surface roughness of in-service asphalt pavement located at LTPP test section 40-4165 in the Southern region reaches the terminal IRI of 2.71m/km as outlined by the MEPDG. The prediction was carried out by changing only pavement age and traffic data at 3% annual CESAL growth in the ANN model. The initial IRI, SN, air

temperature and CND data are assumed like the final measured data in 2005. Based on Figure 38, asphalt surface roughness for test section 40-4165 will reach a terminal IRI of 2.71 m/km in 2020.

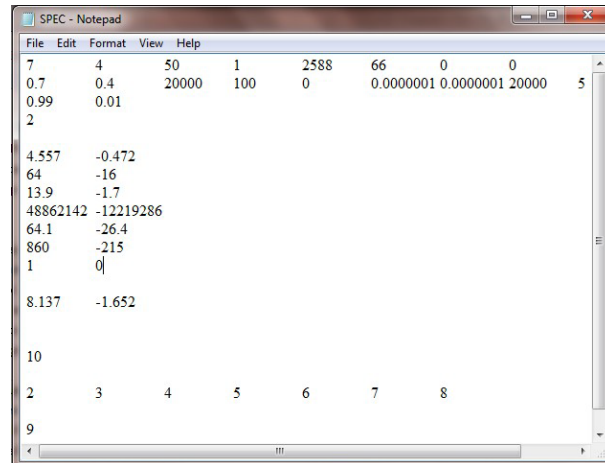


Figure 37. Example of SPEC file set up for IRI model using ANN method

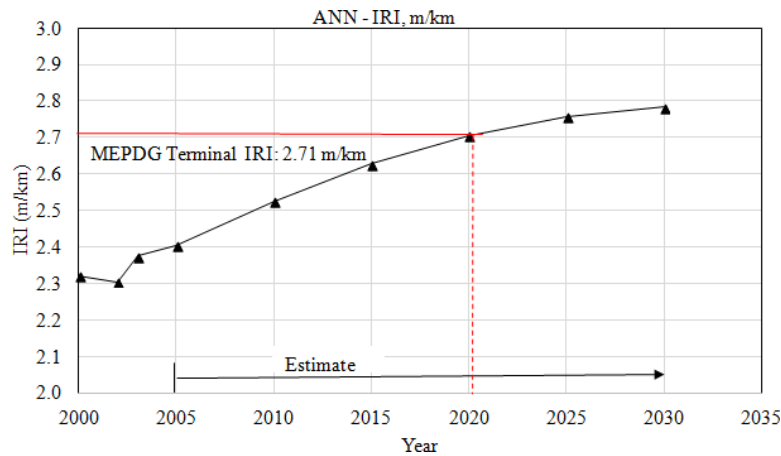


Figure 38. ANN model equation implementation to predict future IRI Section 40-4165

#### 4.1.2. Enhanced Rutting Modeling

Data screening indicated a few test sections with zero average rut depth values (Table 14) and therefore, the data were removed from the database.

Table 14. Lists of test sections in the LTPP database with zero rut depth values

No.	Test Sections	Survey Date for Rut Depth	Reasons
1	28-3083	11/8/1995	Zero average rut depth values
2	28-3085	11/9/1995	
3	28-3091	9/1/1978	
4	36-1644	5/4/1992	
5	48-1048	5/20/1991	
6	48-3835	12/9/1991	
7	47-9024	4/18/1995	



Further observations showed the average rut depth data for test section 47-3101 were suspected of error. This test section had rut depth data sets for 1990, 1991, and 1995, and was assigned as CN one to CN three as shown in Table 15. The rut depth data surveyed on 4/20/1995 were not supposed to have zero value since the road was opened to traffic on 1/1/1980, and there was no major maintenance and rehabilitation treatment taking place. In 1995 the major maintenance of road milling and overlay with asphalt pavement (LTPP code: 51) only happened about 50 weeks after the measurement of the rut depth on 4/20/1995. Therefore, the zero values of rut depth were ambiguous and questionable, which resulted in the termination of the data set from the model database.

Table 15. Test section 47-3101: Rut depth survey date and CN attributes

SHRP ID	CN	CN Assigned Date	CN Change Reason	Rut Depth Survey Date	Rut Depth Data
47-3101	1	1/1/1987		11/16/1990	Available
	2	9/1/1995	51	18/14/1991	Available
	3	5/15/1998	25	4/20/1995	<b>Zero Values</b>

After several iterations, it was noticed that the average rut depth per measurement year data need transformation using a log<sub>10</sub> function to obtain a linear relationship between two variables. Additionally, a dependent variable of Log<sub>10</sub> (Y<sub>R</sub>+0.5) was used to allow zero rut depth value to be considered in the development of the enhanced model equations. This variance stabilizing transformation was in this research and it appears that the data were more compressed and less scattered as compared to the rut depth data without log base 10 functions. A total of 214 normally distributed data sets were considered in the database for the development of the enhanced rutting prediction equation.

Before the development of the multiple regression model equation, the data were evaluated to ensure that the data are (1) random, (2) independent of each other, and (3) normally distributed. Additionally, the variance between the measured and predicted average rut depth per measurement year data must be homogenous. The results follow:

- The data were random because the average rut depth data are measured for different test sections in different states throughout the U.S.
- The data were independent of each other since the average measured rut depth data are for different years. The autocorrelation test shows a low value of 0.42, which suggests that the data were independent of each other.
- The normality test has proved that the data are normally distributed with a mean of 0.70 mm and a standard deviation of 0.28 mm. Table 16 shows the result of Kolmogorov-Smirnov normality test.

Table 16. Test of normality for average rut depth per measurement year datasets

	Kolmogorov-Smirnov <sup>a</sup>		
	Statistic	df	Sig.
Log <sub>10</sub> (Y <sub>R</sub> +0.5)	.040	214	0.200*
*This is the lower bound of the true significance			

### a. Lilliefors Significance Correction

The test hypotheses for the probability of type I error  $\alpha$  equal to 0.05 follows:

- Null hypothesis,  $H_0$ : The distribution of the average rut depth data per measurement year data is normal
- Alternative hypothesis,  $H_A$ : The distribution of the average rut depth data per measurement year data is not normal

The normality test for average rut depth data per measurement year data in the LTPP database showed that the probability of significance, p-value (Sig.) was more than the  $\alpha$  0.05 probability of chance error, which is not statistically significant for Kolmogorov-Smirnov normality test. Therefore, the test failed to reject the null hypothesis, and the average rut depth data per measurement year data are normally distributed. Figure 39 shows a histogram plot of average rut depth per measurement year with descriptive statistics and a normal distribution plot for the data used in this research.

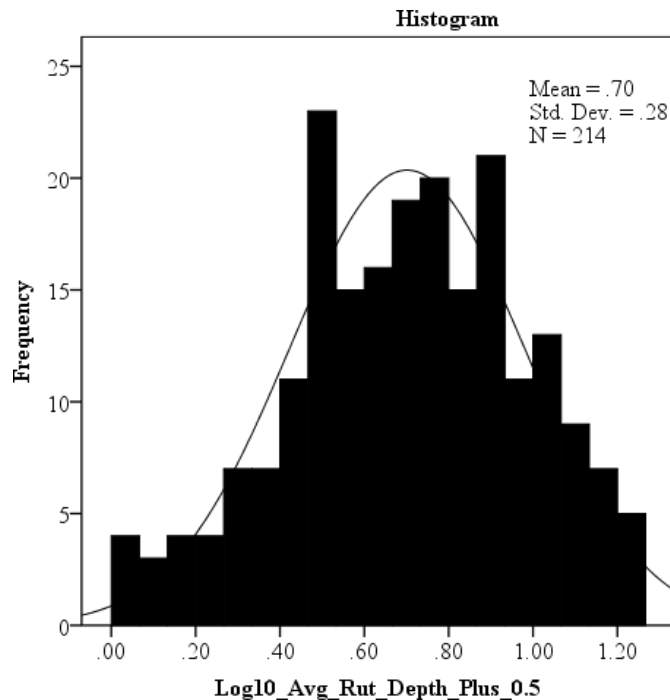


Figure 39. Histogram plot of average rut depth per measurement year

The distribution of the data follows the bell curve of normal distribution. This histogram supports the results from the normality test, which indicates that the average rut depth data per measurement year are normally distributed.

An ANOVA test was used to assess the effects of M&R history, LTPP climatic regions, and base type (stabilized and granular) on the average rut depth per measurement year data, and the results are shown in Table 17. For the CND factor, there is a statistically significant difference in the average rut depth per measurement year before and after major M&R treatments. The main effects of the base type (Base\_D) factor and LTPP climatic region (Reg\_D) alone are not showing statistically significant

differences in the means of the average rut depth per measurement year. However, the interactions of *CND* with base type and *CND* with LTPP climatic region show a statistically significant difference in the means of the average rut depth per measurement year. Therefore, the *CND*, *Base\_D*, and *Reg\_D* factors are used as the dummy variables in both multiple regression and ANN modeling of rutting prediction equations.

Table 17. ANOVA test of between-subjects effects for average rut depth per measurement year

Source	Type III Sum of Squares	df	Mean Square	F	Sig.
Corrected Model	389.703 <sup>a</sup>	13	29.977	2.250	.009
Intercept	1169.695	1	1169.695	87.792	.000
Reg_Actual	35.386	3	11.795	.885	.450
Base_D	6.625	1	6.625	.497	.482
CND	63.208	1	63.208	4.744	.031
Reg_Actual * Base_D	25.093	2	12.546	.942	.392
Reg_Actual * CND	110.183	3	36.728	2.757	.044
Base_D * CND	58.478	1	58.478	4.389	.037
Reg_Actual * Base_D * CND	41.711	2	20.856	1.565	.212
Error	2664.706	200	13.324		
Total	9771.050	214			
Corrected Total	3054.409	213			

a. R Squared = .128 (Adjusted R Squared = .071)

Table 18 shows the independent variables used to develop the enhanced rutting multiple regression equation and ANN model equation. The age, SN, CESAL,  $TEMP_{AIR}$ , PRECIP, *Reg\_D*, and *CND* variables are already described in the previous sub-chapter (IRI roughness modeling).

Table 18. List of independent variables for the rutting progression prediction model equation

No.	Independent Variable	Notes	Unit
1	$\log_{10} Y_{R0}$	$\log_{10}$ Initial average rut depth per measurement Year	-
2	Age	Pavement age	Year
3	CESAL	Annual cumulative ESALs	Year
4	$TEMP_{AIR}$	Air temperature during rut depth measurement	°C
5	$E_1$	Asphalt modulus	psi
6	$E_2$	Base modulus	psi
7	$E_3$	Subbase modulus	psi
8	$E_4$	Subgrade modulus	psi
9	$T_1$	Asphalt thickness	inch
10	$T_T$	Total thicknesses ( $T_T$ ), Asphalt thickness ( $T_1$ ), base layer thickness ( $T_2$ ), and subbase layer thickness ( $T_3$ ): $T_T = T_1 + T_2 + T_3$	inch
11	SN	Structural Number	-

12	CND	Dummy variable for CN (0 if no major M&R treatment history, 1 if major M&R treatment has taken place)	-
13	Reg_D	Dummy variable for LTPP climatic regions (zero for Southern region, one for other regions)	-
14	Base_D	Dummy variable for base layer type (zero for stabilize base, one for granular base)	-

Since rutting is a structural-related problem, additional independent variables that are related to the structural integrity of pavement layers (layer thicknesses and modulus values) are introduced in the enhanced rutting multiple regression equation and ANN model equation. The modulus values for asphalt ( $E_1$ ), base ( $E_2$ ), subbase ( $E_3$ ), and subgrade ( $E_4$ ) layers are calculated using the equations developed by Uddin (Uddin 1984). If the calculated layer modulus values are less than or more than the minimum and maximum modulus values, respectively, change the modulus values based on the ranges proposed by Uddin (Uddin 1984). However, best judgments are required to decide whether to keep or discard the modulus values that are slightly above or below the proposed ranges.

Initially, the modulus value for the subgrade layer is calculated, followed by the asphalt layer modulus value. Then the modulus values for the base layer and subbase layers are calculated, respectively. Uddin (Uddin 1984) developed separate multiple regression equations for the stabilized and granular base, respectively, to calculate modulus values for all layers as described in the following paragraph.

- **Subgrade Layer** (Modulus values typically between 10,000 to 50,000 psi)

Subgrade layer modulus value ( $E_4$ ) for pavement system with stabilized base layer is calculated using Equation 2.30. Meanwhile, subgrade layer modulus for pavement system with granular base layer is calculated using Equation 2.31.

$$E_4 = 10^y; y = 5.42783 + 0.00894 (X_7) - 0.14851 (X_9) - 0.86213(X_{13}) \quad \text{Eq. 4.5}$$

Where,

$X_7 = \text{Log}_{10} (1+T_3)$ ;  $T_3$  is the thickness of the subbase layer (inches)

$X_9 = \text{Log}_{10} (R_2 \times W_2)$ ;  $R_2$  is the radial distance of FWD sensor number two from the center of loading area (12 inches),  $W_2$  is peak deflection under sensor number two (mils) for FWD load normalized to 1,000 lbs.

$X_{13} = \text{Log}_{10} (R_6 \times W_6)$ ;  $R_6$  is the radial distance of FWD sensor number six from the center of loading area (60 inches),  $W_6$  is peak deflection under sensor number six (mils) for FWD load normalized to 1,000 lbs.

$$E_4 = 10^y; y = 5.43813 - 0.15369 (X_9) + 0.04114 (X_{10}) - 0.90072(X_{12}) \quad \text{Eq. 4.6}$$

Where,

$X_9 = \text{Log}_{10} (R_2 \times W_2)$ ;  $R_2$  is the radial distance of FWD sensor number two from the center of

loading area (12 inches),  $W_2$  is peak deflection under sensor number two (mils) for FWD load normalized to 1,000 lbs.

$X_{10} = \text{Log}_{10} (R_3 \times W_3)$ ;  $R_3$  is the radial distance of FWD sensor number three from the center of loading area (24 inches),  $W_3$  is peak deflection under sensor number three (mils) for FWD load normalized to 1,000 lbs.

$X_{12} = \text{Log}_{10} (R_5 \times W_5)$ ;  $R_5$  is the radial distance of FWD sensor number five from the center of loading area (48 inches),  $W_5$  is peak deflection under sensor number five (mils) for FWD load normalized to 1,000 lbs.

- **Asphalt Layer** (Modulus values typically between 100,000 to 1,000,000 psi)

Asphalt layer modulus value ( $E_1$ ) for pavement system with stabilized base layer is calculated using Equation 4.7. Meanwhile, the asphalt layer modulus value for pavement system with granular base layer is calculated using Equation 4.8

$$E_1 = \frac{10^y}{(T_1)^3} \quad \text{Eq. 4.7}$$

Where,

$$y = 2.91794 + 3.51615 (X_5) - 3.28093 (X_8) + 5.97415 (X_9) - 4.76039 (X_{10}) + 1.49939 (X_{13})$$

$X_5 = \text{Log}_{10} (1+T_1)$ ;  $T_1$  is the thickness of the asphalt layer (inches)

$X_8 = \text{Log}_{10} (R_1 \times W_1)$ ;  $R_1$  is the radial distance of FWD sensor number one from the center of loading area (0 inches),  $W_1$  is peak deflection under sensor number one (mils) for FWD load normalized to 1,000 lbs. Set  $R_1 \times W_1$  to zero value due to zero  $R_1$ .

$X_9 = \text{Log}_{10} (R_2 \times W_2)$ ;  $R_2$  is the radial distance of FWD sensor number two from the center of loading area (12 inches),  $W_2$  is peak deflection under sensor number two (mils) for FWD load normalized to 1,000 lbs.

$X_{10} = \text{Log}_{10} (R_3 \times W_3)$ ;  $R_3$  is the radial distance of FWD sensor number three from the center of loading area (24 inches),  $W_3$  is peak deflection under sensor number three (mils) for FWD load normalized to 1,000 lbs.

$X_{13} = \text{Log}_{10} (R_6 \times W_6)$ ;  $R_6$  is the radial distance of FWD sensor number six from the center of loading area (60 inches),  $W_6$  is peak deflection under sensor number six (mils) for FWD load normalized to 1,000 lbs.

$$E_1 = \frac{10^y}{(T_1)^3} \quad \text{Eq. 4.8}$$

Where,

$$y = -22.82457 + 2.35850 (X_5) - 4.37037 (X_8) + 6.60322 (X_9) - 3.21414 (X_{10}) + 4.83214 (X_{16})$$

$X_5 = \text{Log}_{10} (1+T_1)$ ;  $T_1$  is the thickness of the asphalt layer (inches)

$X_8 = \text{Log}_{10} (R_1 \times W_1)$ ;  $R_1$  is the radial distance of FWD sensor number one from the center of loading area (0 inches),  $W_1$  is peak deflection under sensor number one (mils) for FWD load normalized to 1,000

lbs. Set  $R_1 \times W_1$  to zero value due to zero  $R_1$ .

$X_9 = \text{Log}_{10} (R_2 \times W_2)$ ;  $R_2$  is the radial distance of FWD sensor number two from the center of loading area (12 inches),  $W_2$  is peak deflection under sensor number two (mils) for FWD load normalized to 1,000 lbs.

$X_{10} = \text{Log}_{10} (R_3 \times W_3)$ ;  $R_3$  is the radial distance of FWD sensor number three from the center of loading area (24 inches),  $W_3$  is peak deflection under sensor number three (mils) for FWD load normalized to 1,000 lbs.

$$X_{16} = \text{Log}_{10} (X_{15})$$

Where,  $X_{15} = (R_6 \times W_6 \times E_4)$ ;  $R_6$  is the radial distance of FWD sensor number six from the center of loading area (60 inches),  $W_6$  is peak deflection under sensor number six (mils) for FWD load normalized to 1,000 lbs,  $E_4$  is modulus value for subgrade layer.

- **Base Layer** (Modulus values typically between 22,500 to 80,000 psi for granular base layer, and 25,000 to 600,000 psi for stabilized base layer)

Base layer modulus value ( $E_2$ ) for pavement system with stabilized base layer is calculated using Equation 4.9. Meanwhile, the base layer modulus value for pavement system with granular base layer is calculated using Equation 4.10.

$$E_2 = \frac{10^y}{(1+T_2)^3} \quad \text{Eq. 4.9}$$

Where,

$$y = 31.99946 - 1.20607 (X_5) + 2.40370 (X_6) - 1.22023 (X_8) - 3.19149 (X_9) + 2.84323(X_{12}) - 4.68852 (X_{16})$$

$X_5 = \text{Log}_{10} (1+T_1)$ ;  $T_1$  is thickness of asphalt layer (inches),  $X_6 = \text{Log}_{10} (1+T_2)$ ;  $T_2$  is thickness of base layer (inches),

$X_8 = \text{Log}_{10} (R_1 \times W_1)$ ;  $R_1$  is the radial distance of FWD sensor number one from the center of loading area (0 inches),  $W_1$  is peak deflection under sensor number one (mils) for FWD load normalized to 1,000 lbs. Set  $R_1 \times W_1$  to zero value due to zero  $R_1$ .

$X_9 = \text{Log}_{10} (R_2 \times W_2)$ ;  $R_2$  is the radial distance of FWD sensor number two from the center of loading area (12 inches),  $W_2$  is peak deflection under sensor number two (mils) for FWD load normalized to 1,000 lbs,

$X_{12} = \text{Log}_{10} (R_5 \times W_5)$ ;  $R_5$  is the radial distance of FWD sensor number five from the center of loading area (48 inches),  $W_5$  is peak deflection under sensor number five (mils) for FWD load normalized to 1,000 lbs,

$$X_{16} = \text{Log}_{10} (X_{15})$$

Where;  $X_{15} = (R_6 \times W_6 \times E_4)$ ;  $R_6$  is the radial distance of FWD sensor number six from the center of loading area (60 inches),  $W_6$  is peak deflection under sensor number six (mils) for FWD load normalized to 1,000 lbs,  $E_4$  is modulus value for subgrade layer.

$$E_2 = \frac{10^y}{(1+T_2)^3} \quad \text{Eq. 4.10}$$

Where,

$$y = 27.17619 - 1.23502 (X_4) - 0.50339 (X_5) + 3.38241(X_6) - 0.59163(X_8) - 1.32598(X_9) - 2.9170 (X_{16})$$

$X_4 = \text{Log}_{10} (E_4)$ ;  $E_4$  is modulus value for subgrade layer,  $X_5 = \text{Log}_{10} (1+T_1)$ ;  $T_1$  is thickness of asphalt layer (inches),  $X_6 = \text{Log}_{10} (1+T_2)$ ;  $T_2$  is thickness of base layer (inches),

$X_8 = \text{Log}_{10} (R_1 \times W_1)$ ;  $R_1$  is the radial distance of FWD sensor number one from the center of loading area (0 inches),  $W_1$  is peak deflection under sensor number one (mils) for FWD load normalized to 1,000 lbs. Set  $R_1 \times W_1$  to zero value due to zero  $R_1$ ,

$X_9 = \text{Log}_{10} (R_2 \times W_2)$ ;  $R_2$  is the radial distance of FWD sensor number two from the center of loading area (12 inches),  $W_2$  is peak deflection under sensor number two (mils) for FWD load normalized to 1,000 lbs,

$$X_{16} = \text{Log}_{10} (X_{15})$$

Where;  $X_{15} = (R_6 \times W_6 \times E_4)$ ;  $R_6$  is the radial distance of FWD sensor number six from the center of loading area (60 inches),  $W_6$  is peak deflection under sensor number six (mils) for FWD load normalized to 1,000 lbs,  $E_4$  is modulus value for subgrade layer.

- **Subbase Layer** (Modulus values typically between 10,000 to 50,000 psi)

Subbase layer modulus value ( $E_3$ ) for pavement system with stabilized base layer is calculated using Equation 4.11. Meanwhile, the subbase layer modulus value for pavement system with granular base layer is calculated using Equation 4.12.

$$E_3 = \frac{10^y}{(T_3)^3} \tag{Eq. 4.11}$$

Where,

$$y = 4.55483 - 0.17133 (X_5) - 0.27774 (X_6) + 3.44927 (X_7) - 1.81765 (X_{10}) + 1.52304(X_{13})$$

$X_5 = \text{Log}_{10} (1+T_1)$ ;  $T_1$  is thickness of asphalt layer (inches),  $X_6 = \text{Log}_{10} (1+T_2)$ ;  $T_2$  is thickness of base layer (inches),

$X_7 = \text{Log}_{10} (1+T_3)$ ;  $T_3$  is the thickness of the subbase layer (inches),

$X_{13} = \text{Log}_{10} (R_6 \times W_6)$ ;  $R_6$  is the radial distance of FWD sensor number six from the center of loading area (60 inches),  $W_6$  is peak deflection under sensor number six (mils) for FWD load normalized to 1,000 lbs,

$X_{10} = \text{Log}_{10} (R_3 \times W_3)$ ;  $R_3$  is the radial distance of FWD sensor number three from the center of loading area (24 inches),  $W_3$  is peak deflection under sensor number three (mils) for FWD load normalized to 1,000 lbs.

$$E_3 = \frac{10^y}{(T_3)^3} \tag{Eq. 4.12}$$

Where,

$$y = -9.14746 - 0.37575 (X_5) - 0.23825(X_6) + 3.42105(X_7) - 1.05695(X_9) - 0.93991(X_{10}) + 1.36417(X_{13}) + 2.61730(X_{16})$$

$X_5 = \text{Log}_{10} (1+T_1)$ ;  $T_1$  is thickness of asphalt layer (inches),  $X_6 = \text{Log}_{10} (1+T_2)$ ;  $T_2$  is thickness of base layer (inches),

$X_7 = \text{Log}_{10} (1+T_3)$ ;  $T_3$  is the thickness of the subbase layer (inches),

$X_9 = \text{Log}_{10} (R_2 \times W_2)$ ;  $R_2$  is the radial distance of FWD sensor number two from the center of loading area (12 inches),  $W_2$  is peak deflection under sensor number two (mils) for FWD load normalized to 1,000 lbs,

$X_{10} = \text{Log}_{10} (R_3 \times W_3)$ ;  $R_3$  is the radial distance of FWD sensor number three from the center of loading area (24 inches),  $W_3$  is peak deflection under sensor number three (mils) for FWD load normalized to 1,000 lbs,

$X_{13} = \text{Log}_{10} (R_6 \times W_6)$ ;  $R_6$  is radial distance of FWD sensor number six from the center of loading area (60 inches),  $W_6$  is peak deflection under sensor number six (mils) for FWD load normalized to 1,000 lbs,  $X_{16} = \text{Log}_{10} (X_{15})$

Where;  $X_{15} = (R_6 \times W_6 \times E_4)$ ;  $R_6$  is the radial distance of FWD sensor number six from the center of loading area (60 inches),  $W_6$  is peak deflection under sensor number six (mils) for FWD load normalized to 1,000 lbs,  $E_4$  is modulus value for subgrade layer.

Table 19 shows the maximum, minimum, average, SD, and COV (%) for the data sets used in the development of the enhanced rutting condition deterioration prediction equations.

Table 19. Descriptive statistics for independent variables used to develop rutting model equations

Descriptive Statistics	Rut depth per measurement year, $Y_R$ (mm)	Initial rut depth per measurement year, $Y_{R0}$ (mm)	Age (Year)	Cumulative ESAL, CESAL	Air Temperature, $TEMP_{AIR}$ (°C)	Asphalt Modulus, $E_1$ (psi)
Maximum	17.8	15.4	28.0	7,612,665	31.1	1,183,987
Minimum	0.5	0.5	0.0	3,000	-3.0	100,000
Average	5.6	5.1	13.2	491,616	19.7	553,611
SD	3.8	3.2	6.3	928,150	7.7	398,513
COV (%)	67.7	63.6	47.7	189	39.2	72

Descriptive Statistics	Base Modulus, $E_2$ (psi)	Subbase Modulus, $E_3$ (psi)	Subgrade Modulus, $E_4$ (psi)	Asphalt Thickness, $T_1$ (inches)	Total Thickness, $T_T$ (inches)	SN
Maximum	862,470	129,359	53,270	14.6	34.7	8.8
Minimum	0	0	9,034	0.9	7.2	1.0
Average	198,122	18,726	19,128	4.9	18.7	4.0
SD	218,557	25,293	9,970	3.2	6.5	1.5
COV (%)	110	135	52	65.3	34.8	38.5

The enhanced rutting multiple regression equation and ANN model equation were developed, and



the reasonableness of the multiple regression and ANN model equations were evaluated based on the following parameters:

- The R-value of the multiple regression equations
- The predicted against measured data plots
- The verifications of the multiple regression equations
- The accuracy measures of the MARE and RMSE

Initially, two enhanced rutting multiple regression equations were developed as shown in Equations 4.13 and 4.14, respectively. Equation 4.13 contains an additional variable of peak deflection values under sensor one ( $DEF_{W1}$ ) normalized to 1,000 lbs. FWD load and measured in mils. Due to difficulty to predict the future value for  $DEF_{W1}$ , this independent variable was not selected in the final multiple regression equation. Therefore Equation 4.14 without the  $DEF_{W1}$  variable was proposed as the final enhanced rutting multiple regression equation.

$$\begin{aligned} \text{Log}_{10} (Y_{R+0.5}) = & 0.032 + 0.952 (\text{Log}_{10} (Y_{R0} + 0.5)) - 0.000447 (\text{Age}) + 2.607 \times 10^{-9} (\text{CESAL}) + \\ & 0.023 (\text{SN}) + 1.843 \times 10^{-8} (E_1) - 1.158 \times 10^{-7} (E_2) - 3.465 \times 10^{-8} (E_3) + 4.855 \times 10^{-7} (E_4) - 0.000173 \\ & (\text{TEMP}_{\text{AIR}}) + 0.013 (DEF_{W1}) + 0.003 (\text{Reg\_D}) + 0.006 (\text{CND}) - 0.037 (\text{Base\_D}) + 8.145 \times 10^{-6} (T_T) - \\ & 0.01 (T_1) \end{aligned} \quad \text{Eq. 4.13}$$

$$\begin{aligned} \text{Log}_{10} (Y_{R+0.5}) = & 0.058 + 0.952 (\text{Log}_{10} (Y_{R0+0.5})) - 0.000481 (\text{Age}) + 2.962 \times 10^{-9} (\text{CESAL}) + \\ & 0.021 (\text{SN}) + 2.562 \times 10^{-8} (E_1) - 1.356 \times 10^{-7} (E_2) - 1.171 \times 10^{-7} (E_3) + 2.348 \times 10^{-7} (E_4) - 0.000141 \\ & (\text{TEMP}_{\text{AIR}}) + 0.010 (\text{Reg\_D}) + 0.006 (\text{CND}) - 0.041 (\text{Base\_D}) + 0.000259 (T_T) - 0.011 (T_1) \end{aligned} \quad \text{Eq. 4.14}$$

Subsequently, the ANN<sub>15-3-1</sub> was observed to give the optimum network for the prediction of future rutting value using the ANN model equation. The ANN<sub>15-3-1</sub> refers to a total of 15 inputs ( $\text{Log}_{10} (Y_{R0+0.5})$ , Age, CESAL, SN,  $E_1$ ,  $E_2$ ,  $E_3$ ,  $E_4$ ,  $\text{TEMP}_{\text{AIR}}$ , Reg\_D, CND, Base\_D,  $T_T$ ,  $T_1$ ,  $DEF_{W1}$ ), three hidden nodes, and one output ( $\text{Log}_{10} (Y_{R+0.5})$ ).

The final results are shown in Figure 40 and Figure 41. Figure 42 shows the measured and predicted values using the enhanced multiple regression prediction equations with respect to data sequential numbers on the x-axis.

The average rut depth per measurement year data that was transformed using  $\log_{10}$  form, showed lesser variances in the measured and predicted values as shown in Figure 40. This is the best transformation model to reduce the variance of the average rut depth per measurement year data. The data are less scattered and aligned closely to the equity line with a higher R of 0.932. This implies that the variances are more uniform between the measured and predicted values, with only -8% difference compared to the measured average rut depth per measurement year. Therefore, the assumption of the homogeneity of the variance is met.

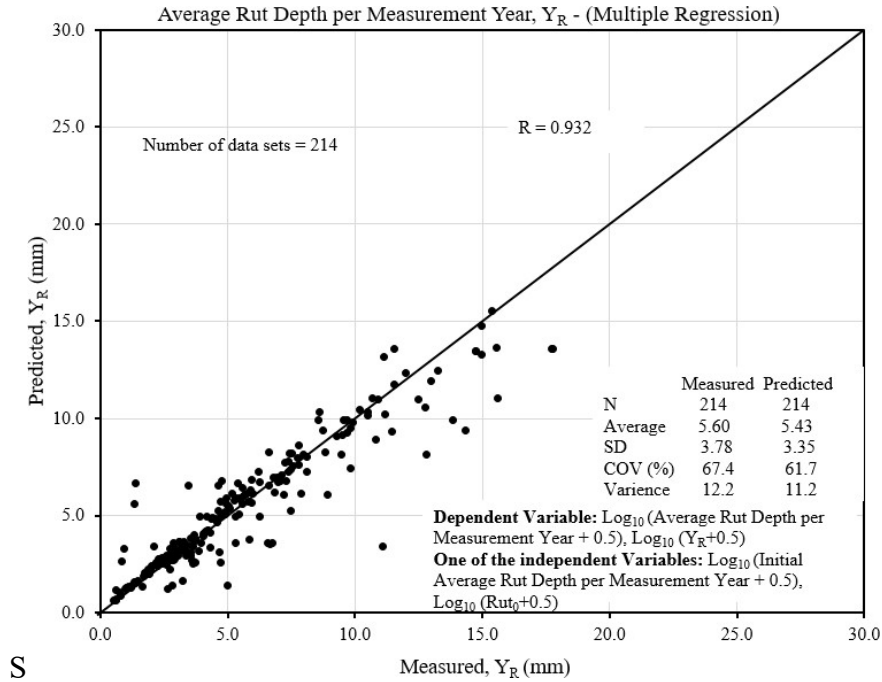


Figure 40. Predicted vs measured plot for rut depth multiple regression equation database

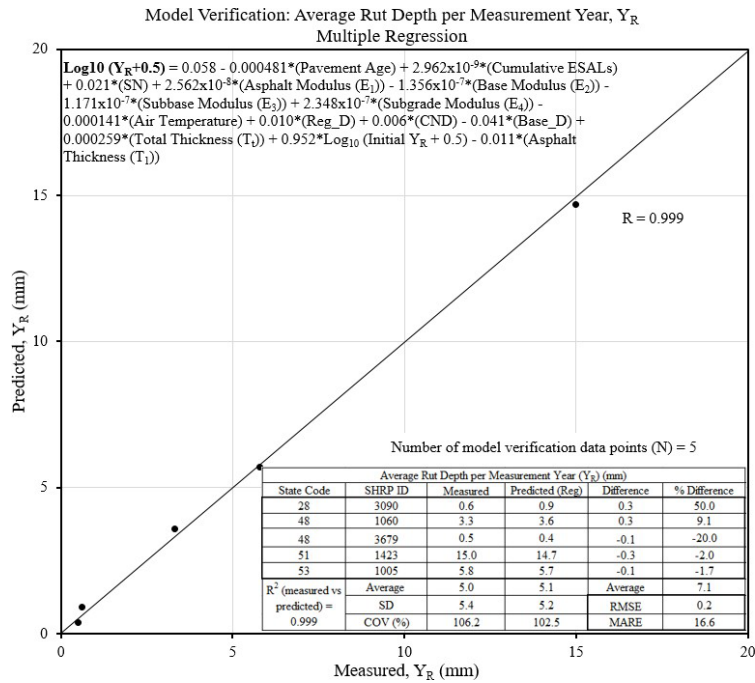


Figure 41. Predicted vs measured plot for rut depth multiple regression verification database

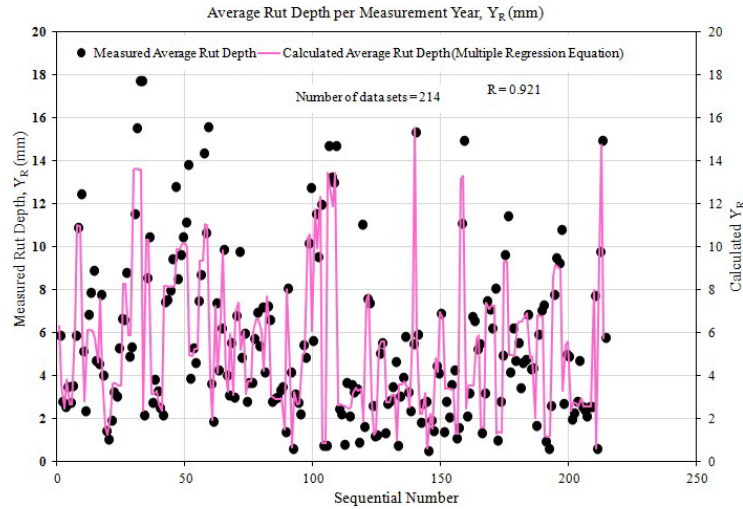


Figure 42. Measured and predicted rut depth using multiple regression

The ANN model results are shown in Figure 43 to Figure 45. The model database and verification results are outstanding for both the enhanced multiple regression model equation and the ANN model equation. Therefore, both enhanced rutting IRI multiple regression equations and ANN model equations are recommended for implementation.

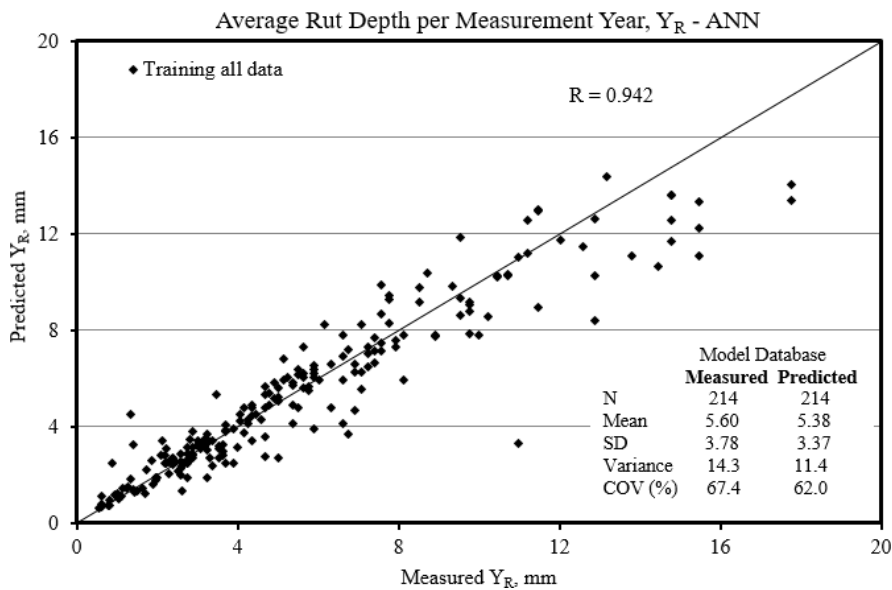


Figure 43. Predicted vs measured plot for rut depth ANN model database

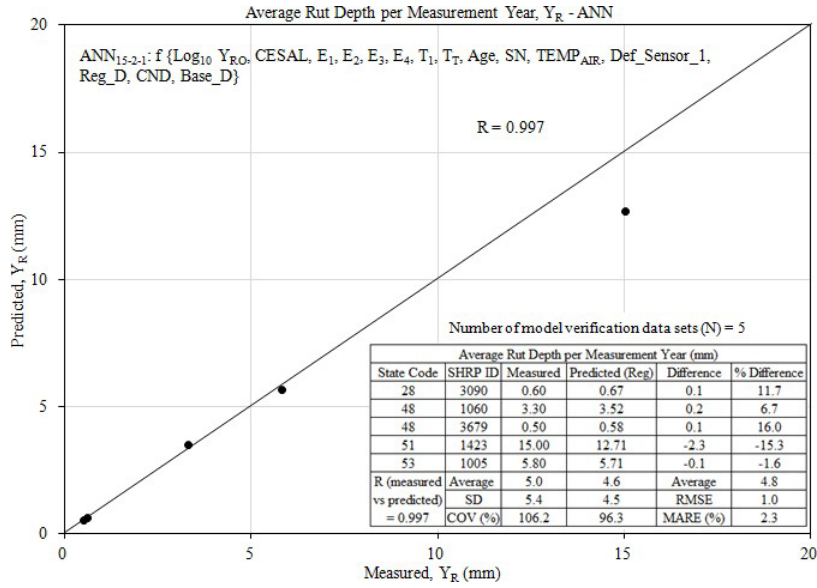


Figure 44. Predicted vs measured plot for rut depth ANN verification database

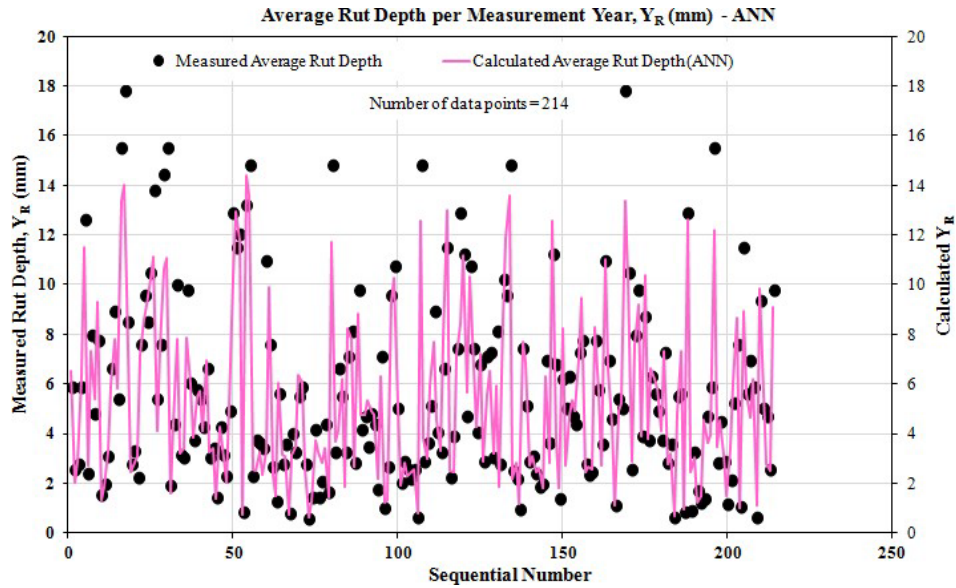


Figure 45. Measured and predicted rut depth using ANN model equation

The enhanced rutting multiple regression equations developed in this research are easier to use for future rutting prediction considering reasonable input parameters such as initial rut depth value, cumulative traffic ESAL, layer modulus values, asphalt thickness, total layer thicknesses, pavement age, SN, and air temperature. Moreover, the enhanced rutting multiple regression equations also consider important factors such as maintenance and rehabilitation intervention factor, LTPP climatic region factor, and base layer types.

#### 4.1.1.2. Application of Rutting Performance Condition Deterioration Model Equations

Both enhanced rutting multiple regression equation and ANN rutting model were proposed for asphalt pavement design purposes. The final enhanced multiple regression equation for rutting condition deterioration prediction is shown in Equation 4.15.

$$\begin{aligned} \log_{10}(Y_R + 0.5) = & 0.058 + 0.952(\log_{10}(Y_{RO} + 0.5)) - 0.000481(Age) + 2.962 \times \\ & 10^{-9}(CESAL) + 0.021(SN) + 2.562 \times 10^{-8}(E_1) - 1.356 \times 10^{-7}(E_2) - 1.171 \times 10^{-7}(E_3) + \\ & 2.348 \times 10^{-7}(E_4) - 0.000141(TEMP_{AIR}) + 0.010(Reg_D) + 0.006(CND) - 0.041(Base_D) + \\ & 0.000259(T_T) - 0.011(T_1) \end{aligned} \quad \text{Eq. 4.15}$$

The necessary keys steps required in the implementation of the enhanced rutting multiple regression equation for pavement design follow:

- Set the initial IRI to zero mm for the newly paved road network. For older road networks, the rut depth data must be known to use the proposed multiple regression equation. The initial IRI value must be between 0 to 15 mm. Transform the rut depth value to  $\log_{10}(Y_{RO}+0.5)$  for implementation in the enhanced rutting prediction equation.
- Pavement age (year) is calculated from the last year since the major maintenance and rehabilitation has taken place. If there is no major maintenance and rehabilitation history recorded, the pavement age is calculated from the initial year when the road was opened to the traffic. The pavement age must be between zero to 28 years.
- Estimate the CESAL for the projected years based on a known traffic growth factor. The maximum CESAL is 7,612,665 and the minimum CESAL is 3,000.
- Calculate the SN based on the layer coefficients, layer thicknesses, and drainage coefficients for asphalt, base, and subbase layers, respectively. The minimum and maximum SN values are 1.0 to 9.0, respectively.
- Asphalt layer modulus ( $E_1$ ) value must be known and must be between 100,000 psi to 1,183,987 psi.
- Base layer modulus value ( $E_2$ ) must be known and must be between zero (no base layer) to 1,346,116 psi.
- Subbase layer modulus value ( $E_3$ ) must be known and must be between zero (no subbase layer) to 129,359 psi.
- Subgrade layer modulus value ( $E_4$ ) must be known and must be between 9,034 psi to 53,270 psi.
- Assume an average monthly air temperature ( $^{\circ}\text{C}$ ) based on the most recent year data that are available in the national database. The minimum and maximum air temperatures ranged from  $-3.0^{\circ}\text{C}$  to  $31.1^{\circ}\text{C}$ , respectively.
- Total pavement layers thicknesses ( $T_T$ ) must be known and range from 7.2 to 34.7 inches.
- Asphalt layer thickness ( $T_1$ ) must be known and range from 0.9 to 14.6 inches.
- For the LTPP climatic region factor ( $Reg\_D$ ), assign zero for the Southern region. In contrast, assign one for other regions.

- For the major maintenance and rehabilitation intervention (CND) variable, assign zero if there is no major maintenance and rehabilitation has taken place. Assign one if the old pavement layer has been removed and resurfaced.
- For the base layer type factor (Base\_D), assign zero for the stabilized base, one for the granular base.

The ANN<sub>15-3-1</sub> provides the most optimum network for future rutting prediction. The ANN<sub>15-3-1</sub> refers to a total of 15 inputs ( $\log_{10}(Y_{R0}+0.5)$ , Age, CESAL, SN, E<sub>1</sub>, E<sub>2</sub>, E<sub>3</sub>, E<sub>4</sub>, TEMP<sub>AIR</sub>, Reg\_D, CND, Base\_D, T<sub>T</sub>, T<sub>1</sub>, DEF<sub>W1</sub>), three hidden nodes, and one output ( $\log_{10}(Y_R+0.5)$ ). Figure 46 shows the setup for the optimum network used in the analysis using the TRSEQ1 ANN computer program (Najjar 1999).

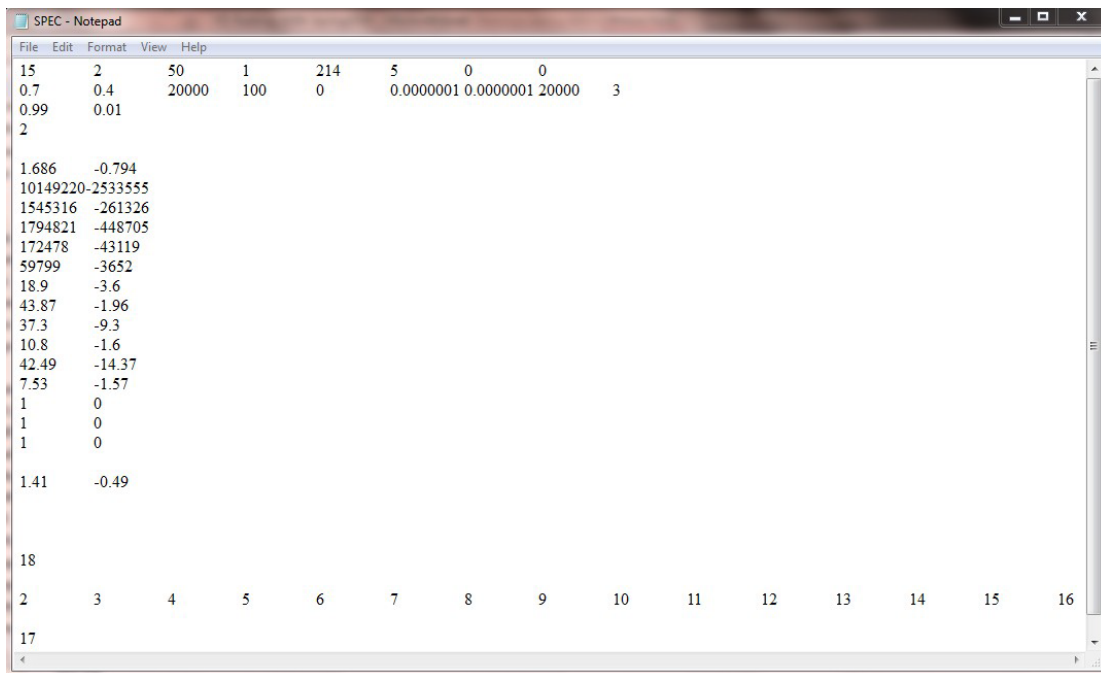


Figure 46. Example of SPEC file set up for rutting model using ANN method

### 4.1.3. Enhanced Cracking Modeling

The cracking data available for test sections in 47 states in the U.S. are extracted from the LTPP database under the MON\_DIS\_AC\_REV section. The cracking distresses were observed for the whole 500 feet test section and were observed on the same day when the FWD test was carried out for the structural assessment of pavement layers. A total of 2,240 data sets were used in the development of the enhanced UCI multiple regression and ANN model equation. The distribution of combined UCI data sets based on LTPP climatic regions (Reg\_Actual) and major M&R intervention factor, CND is shown in Table 20. Figure 47 shows the distribution of the UCI datasets per measurement year used in this research.

Table 20. UCI datasets based on climatic regions (Reg\_Actual) and major M&R intervention (CND)

Between-Subjects Factors				
Group		Value Label	N	Percentage
Reg_Actual	1	North Atlantic	386	17.2%
	2	North Central	230	10.3%
	3	Southern	976	43.6%
	4	Western	648	28.9%
CND	0	No Major M,R&R	1,316	58.8%
	1	Major M, R&R Applied	924	41.2%

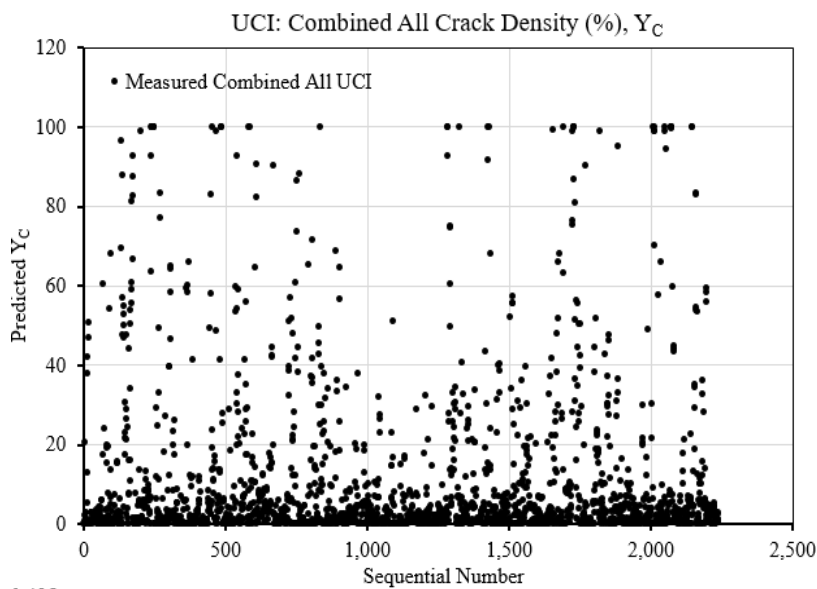


Figure 47. Distribution of the UCI per measurement year data according to sequential number

The combined UCI data were transformed using a few transformation functions including  $\text{Log}_{10}(Y_C+0.5)$ , which works well for rutting data as explained in the previous sub-chapter. Table 21 shows the normality test result for the combined UCI data transformed using  $\text{Log}_{10}(Y_R+0.5)$  function.

Table 21. Test of normality for combined UCI data sets

	Kolmogorov-Smirnov <sup>a</sup>		
	Statistic	df	Sig.
$\text{Log}_{10}(Y_R+0.5)$	.113	2,240	< 0.001*
*This is the lower bound of the true significance a. Lilliefors Significance Correction			

The test hypothesis for the probability of type I error  $\alpha$  equal to 0.05 follows:

- Null hypothesis,  $H_0$ : The distribution of the combined UCI data is normal
- Alternative hypothesis,  $H_A$ : The distribution of the combined UCI data is not normal

The normality test for the combined UCI showed that the probability of significance, p-value (Sig.) was less than the  $\alpha$  0.05 probability of chance error, which is statistically significant. Therefore, the null hypothesis is rejected, and the combined UCI data is not normally distributed. Figure 48 shows a histogram plot for combined UCI with descriptive statistics and a normal distribution curve.

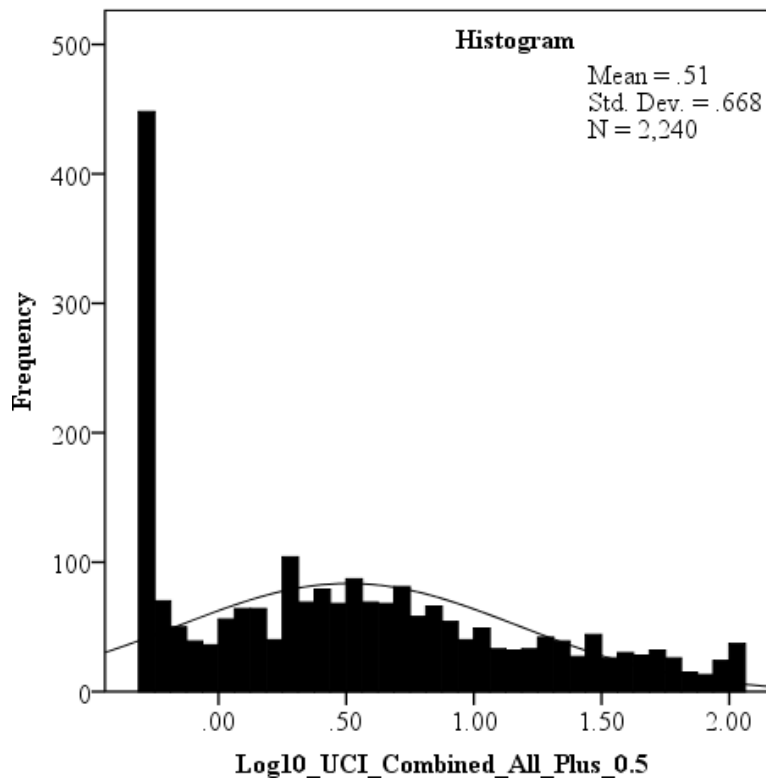


Figure 48. Normality plot for the combined UCI data transformed using  $\text{Log}_{10}(Y_C+0.5)$  function

The effect of major M&R was further analyzed by selecting 25 test sections and tested for the CND factor on the UCI means. The hypothesis testing using t-test for UCI data before and after major M&R for all 25 test sections follow:

- Step 1: Setup null hypothesis and alternative hypothesis.
  - Null Hypothesis:  $H_0: \mu_1 = \mu_2$   
The UCI means before and after major M&R treatments are equal.
  - Alternative Hypothesis:  $H_A: \mu_1 \neq \mu_2$   
The UCI means before and after major M&R treatments are not equal.
- Step 2: Select  $\alpha$  probability of Type 1 chance error for  $\alpha$  level of statistical significance.
  - $\alpha = 0.05$
  - $\alpha/2 = 0.025$  (for two-tailed test)

Figure 49 shows the two-tailed t-test probability distribution.



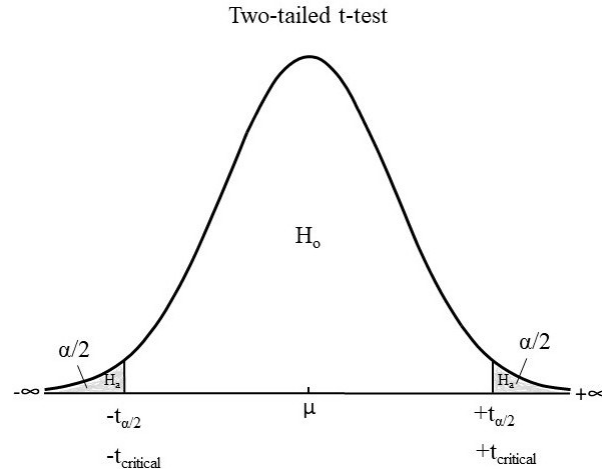


Figure 49. Two-tailed t-test probability distribution graph

- Step 3: Define test criteria and the decision rule for rejecting  $H_0$ .
  - Test criteria:  $t_{critical} = 1.96$  for degree of freedom (dof) = 185 and  $\alpha/2 = 0.025$
  - Decision Rule: Reject  $H_0$  if t-test statistics  $t_{test}$  exceeds the absolute value of  $t_{critical}$  ( $t_{test} > t_{critical}$ ) and probability of significance value,  $p \leq$  Probability of Type-1 chance error,  $\alpha/2$ .
- Step 4: Calculate t-test statistics,  $t_{test}$ , and p-significance value.
  - $t_{test} = 4.93$
  - Probability of significance, p-value  $< 0.001$
- Step 5: Interpret the results.
  - $t_{test} (4.93) > t_{critical} (1.96)$  and  $p (< 0.001) < \alpha/2 (0.025)$

Therefore, the test rejected the null hypothesis. The results show that the difference in the means of the UCI values before and after major M&R treatments for all 25 test sections are statistically significant at  $\alpha/2$ , 0.025 level probability of chance error. The t-test was conducted to give a good estimate of the population's UCI data.

A t-test was also conducted for each test section to observe the effect of major M&R on the UCI values. As can be seen, Figure 50 shows eight out of 25 sections t-test showed that there is a statistically significant difference in the means of the UCI values before and after the most recent major M&R treatments

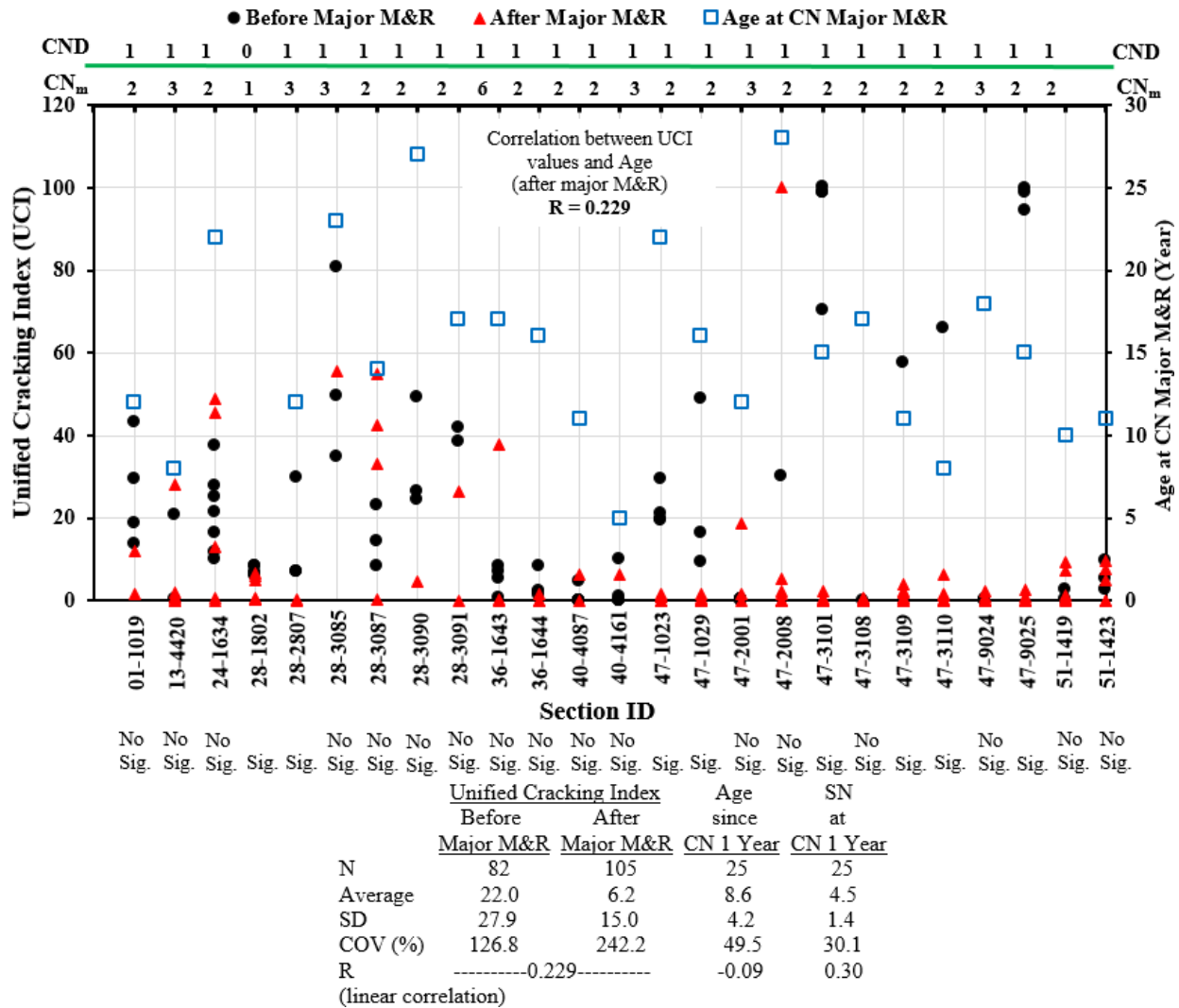


Figure 50. Asphalt pavement age (years) at the most recent CN major M&R (CN<sub>m</sub>) with crack data before and after major M&R treatment

Therefore, based on these results of 25 samples, the most recent CN for major M&R on an entire asphalt surface is considered as a candidate dichotomous or dummy variable for multiple regression modeling together with other independent variables. It is important to use a dummy variable to consider the effect of M&R in the equation.

Figure 51 shows the UCI plot for LTPP test section 47-3101 in Tennessee. There is a significant decrease in the UCI values after major M&R of milling of the existing asphalt layer and overlay with the new hot mix asphalt layer. Therefore, CN 1 was assigned as CND 0, while CN 2 and CN 3 were assigned as CND 1 in the model database.

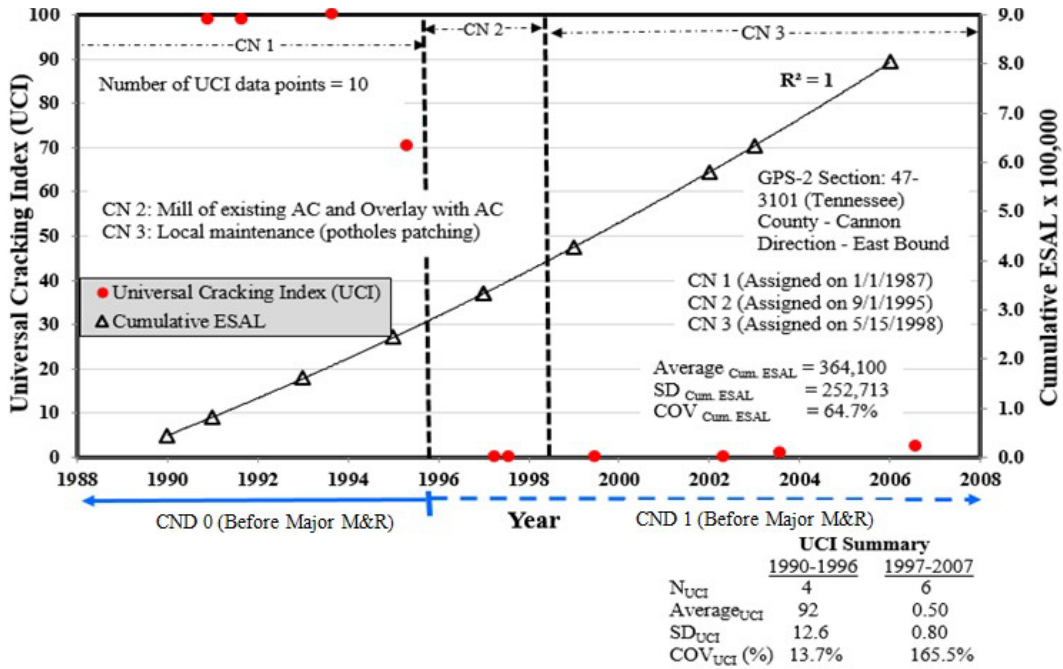


Figure 51. UCI data plot for test section 47-3101 in Tennessee

- Step 1: Setup null hypothesis and alternative hypothesis.
  - Null Hypothesis:  $H_0: \mu_1 = \mu_2$   
The UCI means before and after major M&R treatments are equal.
  - Alternative Hypothesis:  $H_A: \mu_1 \neq \mu_2$   
The UCI means before and after major M&R treatments are not equal.
- Step 2: Select  $\alpha$  probability of Type 1 chance error for  $\alpha$  level of statistical significance.
  - $\alpha = 0.05$
  - $\alpha/2 = 0.025$  (for two-tailed test)
- Step 3: Define test criteria and the decision rule for rejecting  $H_0$ .
  - Test criteria:  $t_{critical} = 2.306$  for degree of freedom (dof) = 8 and  $\alpha/2 = 0.025$
  - Decision Rule: Reject  $H_0$  if t-test statistics  $t_{test}$  exceeds the absolute value of  $t_{critical}$  ( $t_{test} > t_{critical}$ ) and probability of significance value,  $p \leq$  Probability of Type-1 chance error,  $\alpha/2$ .
- Step 4: Calculate t test statistics,  $t_{test}$ , and p-significance value.
  - $t_{test} = 15.8$
  - Probability of significance, p-value  $< 0.001$
- Step 5: Interpret the results.
  - $t_{test} (15.8) > t_{critical} (2.306)$  and  $p (< 0.001) < \alpha/2 (0.025)$

Therefore, the test does not reject the null hypothesis. The results show that the difference in the

means of the UCI values before and after major M&R treatments for test section 47-3101 is statistically significant at  $\alpha/2$  0.025 level probability of chance error. This implies that there is a need to consider dummy construction number CND 0 (before major M&R treatments) and CND 1 (after major M&R treatments) in the multiple linear regression prediction equations.

Further transformation using  $Y_{Beta}$  and Sigmoid functions were also tested in this research. Equations 4.16 and 4.17 were used to transform combined UCI data (dependent variable) into  $Y_{Beta}$ , and sigmoidal function ( $Y_{CS}$ ), respectively. However, the normality tests for these data sets ( $Y_{Beta}$  and  $Y_{CS}$ ) also showed that data were not normally distributed. Therefore, an alternative method for condition deterioration progression modeling is the ANN method.

$$Y_{Beta} = \frac{1}{3.1429 \times \sqrt{Y} \times \sqrt{1-Y}} \tag{Eq. 4.16}$$

$$Y_{CS} = \frac{1}{[1+e^{-Y_{CP}}]}; Y_{CP} = \frac{Y_C}{100} \tag{Eq. 4.17}$$

An ANOVA test was conducted to evaluate the effects of M&R history and LTPP climatic region factors on the combined UCI data sets and the results are shown in Table 22.

Table 22. ANOVA tests of between-subjects effects for combined UCI datasets

Source	Type III Sum of Squares	df	Mean Square	F	Sig.
Corrected Model	30080.818 <sup>a</sup>	7	4297.260	10.768	.000
Intercept	187354.202	1	187354.202	465.539	.000
LTPP_Region	10603.508	3	3534.503	8.783	.000
CND	13333.051	1	13333.051	33.130	.000
LTPP_Region * CND	4089.964	3	1363.321	3.388	.017
Error	898258.999	2232	402.446		
Total	1173237.740	2240			
Corrected Total	928339.817	2239			

a. R Squared = .032 (Adjusted R Squared = .029)

For the CND factor, there are statistically significant differences in the means of combined UCI values before and after major M&R treatments. Additionally, the LTPP climatic region factor also showed a statistically significant difference in the means of the combined UCI values. Therefore, both CND and Reg\_D factors are used as the dummy variables in both multiple regression and ANN modeling of cracking distress prediction equations.

The independent variables used to develop the enhanced cracking multiple regression equation and ANN model equation are shown in Table 23. The modulus values for pavement layers were calculated using the same procedures applied for rutting distress modeling. The interaction terms between two variables that showed significant correlation was also considered as one of the independent variables. For example,  $T_1 \times E_1$  explains the interaction between the thickness of the asphalt layer with the modulus value of the asphalt layer, which has significant interaction and is considered in the model database.

Table 23. Independent variables for enhanced cracking progression prediction model equation

No.	Independent Variable	Notes	Unit
1	$\text{Log}_{10} Y_{C0}$	$\text{Log}_{10}$ Initial UCI value per measurement year	-
2	Age	Pavement age	Year
3	CESAL	Annual cumulative ESALs	Year
4	$\text{TEMP}_{\text{PAVE}}$	Pavement temperature measured during the assessment of cracking distress	°C
5	$E_1$	Asphalt modulus	psi
6	$E_2$	Base modulus	psi
7	$E_3$	Subbase modulus	psi
8	$E_4$	Subgrade modulus	psi
9	$T_1$	Asphalt thickness	inch
10	$T_T$	Total thicknesses ( $T_T$ ), Asphalt thickness ( $T_1$ ), base layer thickness ( $T_2$ ), and subbase layer thickness ( $T_3$ ): $T_T = T_1 + T_2 + T_3$	inch
11	SN	Structural Number	-
12	PRECIP	Average monthly precipitation	mm
13	CND	Dummy variable for CN (0 if no major M&R treatment history, 1 if major M&R treatment has taken place)	-
14	Reg_D	Dummy variable for LTPP climatic regions (zero for Southern region, one for other regions)	-
15	$T_1 \times E_1$	Interaction between asphalt thickness and asphalt modulus	-
16	$\text{TEMP}_{\text{PAVE}} \times E_1$	Interaction between pavement temperature and asphalt modulus	-
17	$\text{SN} \times \text{CESAL}$	Interaction between SN and cumulative ESAL	-
18	$T_T \times \text{CND}$	Interaction between total thickness and CND	-
19	$\text{TEMP}_{\text{PAVE}} \times \text{PRECIP}$	Interaction between pavement temperature and precipitation	-
20	$\text{Age} \times \text{Log}_{10}(Y_{C0}+0.5)$	Interaction between age and $\text{Log}_{10}(Y_{C0}+0.5)$	-
21	$\text{CESAL} \times \text{Log}_{10}(Y_{C0}+0.5)$	Interaction between CESAL and $\text{Log}_{10}(Y_{C0}+0.5)$	-

The descriptive statistics are shown in Table 24 for the datasets used in the development of the enhanced cracking condition deterioration prediction equations.

Table 24. Descriptive statistics for independent variables used to develop enhanced cracking condition deterioration prediction equation

Descriptive Statistics	Combined UCI, $Y_c$ (%)	Initial Combined UCI, $Y_{C0}$	Asphalt Modulus, $E_1$ (psi)	Base Modulus, $E_2$ (psi)	Subbase Modulus, $E_3$ (psi)	Subgrade Modulus, $E_4$ (psi)	Asphalt Thickness, $T_1$ (inch)
Minimum	0	0	93,859	0	0	9,003	0
Maximum	104	100	1,238,563	1,351,856	604,293	53,655	25
Mean	10	9	445,043	210,162	16,545	17,697	7
SD	20	19	373,055	245,297	24,032	8,535	4
COV (%)	194.7	222.9	83.8	116.7	145.3	48.2	54.2

Descriptive Statistics	Total Thickness, $T_T$ (inch)	Age (Year)	SN	Cumulative ESAL, CESAL	Pavement Temperature, $TEMP_{PAVE}$ (°C)	Precipitation, PRECIP (mm)
Minimum	6	0	1	2,000	(12)	0
Maximum	58	48	10	56,568,503	68	381
Mean	21	19	5	2,364,607	24	76
SD	8	8	2	4,605,857	12	63
COV (%)	40.7	42.8	34.1	194.8	49.3	81.9

The development of a new cracking model using UCI combines all crack types (alligator, block, longitudinal, and transverse) and is beneficial for pavement asset management purposes. The UCI is practical and applicable for a decision support system for the maintenance and rehabilitation programs. However, this research also developed the enhanced multiple regression equations and ANN models for alligator crack, block crack, longitudinal crack, and transverse crack, respectively. These individual enhanced multiple regression and ANN model equations are practical and applicable for pavement structural design purposes. The independent variables used in the development of multiple regression equations and ANN model equations for each crack type are like the independent variables used in the equations for combined all crack types.

Initial approaches to develop ANN model equations using only 50% training data sets showed less promising outputs for both combined and individual crack model equations. Therefore, additional analysis using 100% training data sets was conducted and the results showed significant improvement for both model database and verification data sets.

#### 4.1.3.1. Final Enhanced UCI Multiple Regression and ANN Model Equations

This sub-chapter discusses the results from the analysis using enhanced multiple regression equations and ANN model equations. For the model database, the following criteria were evaluated to decide the best-performing model equation.

- Average predicted values (%)
- Average % difference,
- R and  $R^2$  values
- RMSE

Additional accuracy measure of MARE was used to decide the best performing model for model verifications. The MARE was not calculated for the model database due to zero values of certain cracking distress data sets. The analysis was conducted using SPSS software and the outputs that showed the coefficients for all multiple regression equations developed in this research were described in Appendix B.

### 4.1.3.2. Application of Cracking Performance Condition Prediction Model Equations

The ANN models for combined cracking distress types and individual cracking types are better predictors for asphalt layer cracking distresses. Figure 52 shows the setup for the optimum network used in the analysis using the TRSEQ1 ANN computer program (Najjar 1999). The optimum ANN cracking models follow:

- Combined UCI: ANN<sub>21-9-1</sub>
- UCI for alligator crack: ANN<sub>21-9-1</sub>
- UCI for block crack: ANN<sub>21-9-1</sub>
- UCI for longitudinal crack: ANN<sub>21-9-1</sub>
- UCI for transverse crack: ANN<sub>21-8-1</sub>

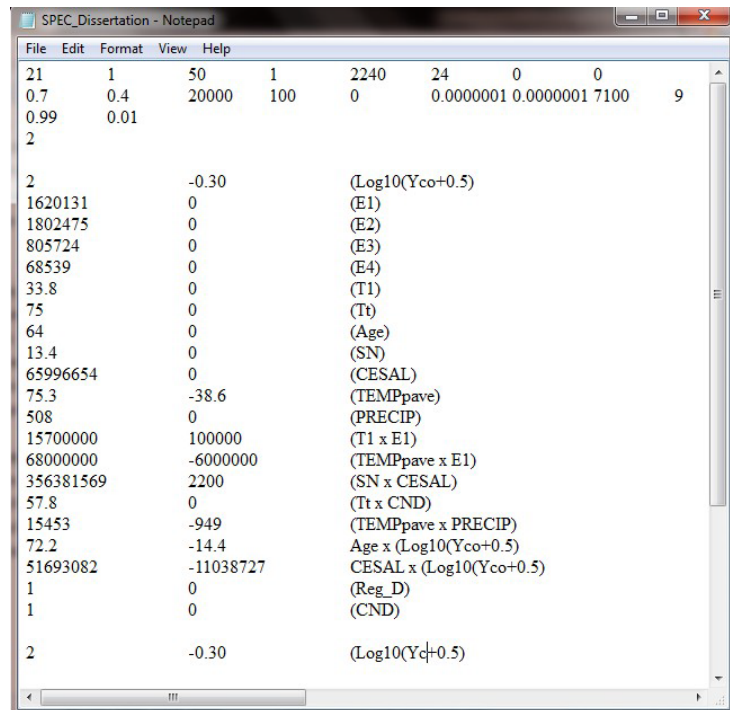


Figure 52. Example of SPEC set up for combined all cracking distresses (UCI)

### 4.1.4. Application of Condition Deterioration Predictive Equations for Asphalt Pavement Asset Management

Figure 53 shows an enhanced Pavement Asset Management (PAM) framework (Uddin et al. 2013), which was developed based on the U.S. Governmental Accounting Standards Board (GASB) Statement 34 framework (GASB 2000). The influence of life-cycle M&R is significant for longer-performing highway conditions, as shown in Figure 54. It is recommended to implement the enhanced pavement deterioration model equations developed in this research for life-cycle assetmanagement and M&R

programs. A simplified M&R intervention criterion for PAM is shown in Table 25.

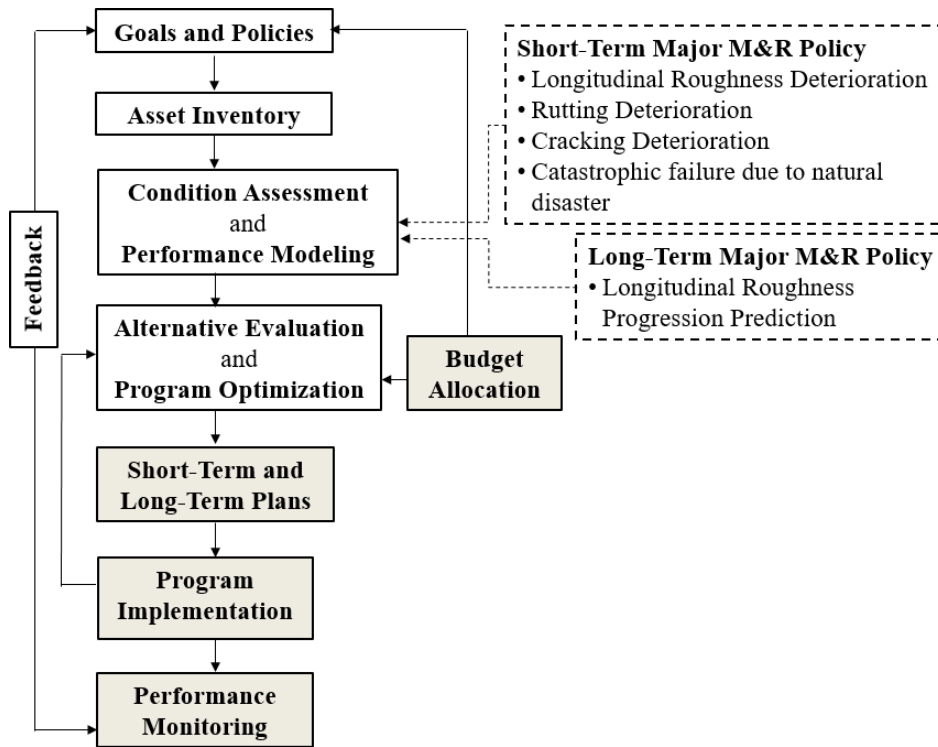


Figure 53. Enhanced Pavement Asset Management (PAM) Framework (Uddin et al. 2013)

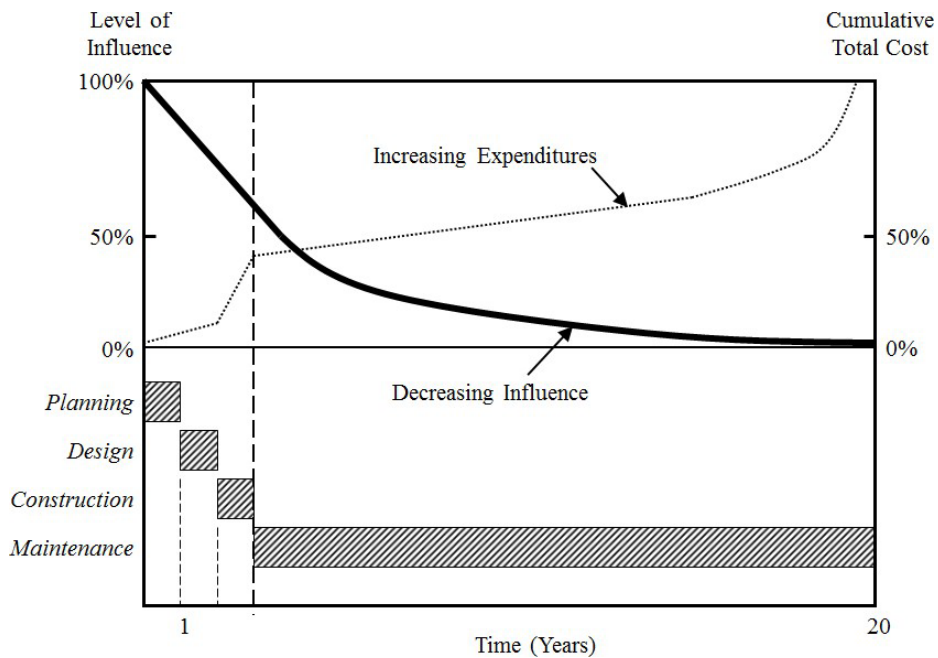


Figure 54. Basic Concept of Life Cycle Cost (LCC) (Uddin et al. 2013)



Table 25. Simplified M&R intervention criteria for pavement asset management

<b>1. Short Term or Single Year M, R&amp;R Intervention Policy</b>			
	Asphalt Pavement M, R&R	Intervention Criteria	M, R&R Treatment
(a)	Total Distress Area Low (L), Medium (M), High (H)	(L, M, H Severity) > 60%	<b>Asphalt Pavement:</b> M1 for freeway and highway; M2 for other roads <b>Concrete Pavement:</b> M1P for freeway and highway; M2P (extensive) for other roads
(b)	Cracking Area	< 60% H - Severity $\geq$ 20%	<b>Asphalt Pavement:</b> M3 (Minor, seal coat) <b>Concrete Pavement:</b> M2P (extensive)
(c)	Rutting Area	< 60% H - Severity $\geq$ 20%	<b>Asphalt Pavement:</b> M2 (Milling and inlay)
(d)	Total Distress Area	< 60% H - Severity < 20%	<b>Asphalt Pavement:</b> M4 (Local minor maintenance) <b>Concrete Pavement:</b> M4P (Local)
(e)	Longitudinal Roughness	IRI exceeds 5.2 m/km (Rough & Unsafe)	<b>Asphalt Pavement:</b> M3 (Minor, seal coat) <b>Concrete Pavement:</b> M2P (Extensive)
			(Only if distress repairs are not being applied)
(f)	Catastrophic Failure Policy (Flood due to rain, hurricane, river overflow), Others: Earthquake	Rapid Condition Assessment to Identify: (1) Local Failure (> 60% area)	<b>Asphalt Pavement:</b> M3 <b>Concrete Pavement:</b> M2P
		(2) Mitigation by Major Maintenance & Rehabilitation	Reconstruction as needed
<b>Asphalt Pavement Treatment Codes</b>		<b>Unit Cost, US \$</b>	
M1	Major maintenance, rehabilitation	1.5-inch milling, 4 inches asphalt overlay on freeways and highways, \$6.0/sq. yard on 100% area	
M2	Major, Milling, and inlay	1.5-inch milling and asphalt inlay, \$3.0/sq. yard on 100% area	
M3	Minor, seal coat	Asphalt slurry seal or micro-surfacing, \$1.5/sq. yard on 100% area	
M4	Local, minor for H - severity	Asphalt patching \$2.5/sq. yard for the rutted area; Crack sealing \$1.5/sq. yard for cracked area	
(If both M2 and M3 are selected then use <b>only</b> M2 for freeways and highways and use <b>only</b> M3 for other types of roads)			
<b>Concrete Pavement M, R&amp;R Treatment Codes</b>		<b>Unit Cost, US \$</b>	
M1P	Major maintenance, rehabilitation	4 inches asphalt overlay on freeway and highway; \$8.0/sq. yard on 100% area	
M2P	Concrete pavement restoration	Extensive; \$7.0/sq. yard on distressed area	
M4P	Concrete pavement restoration	Local; \$6.0/sq. yard on distressed area	
<b>2. Long Term or Multi-Year M, R&amp;R Intervention Policy</b>			
Asphalt Pavement Intervention Criteria Based on Longitudinal Roughness		M2 if IRI equals or exceeds 5.2 m/km	
Concrete Pavement Intervention Criteria		M1P if PSR equals or < 2.0	
If PCR model is available (not in this dissertation), PCI $\leq$ 30 (Maintenance intervention level)			

#### **4.1.5. Concluding Remarks**

The developed enhanced condition deterioration model equations for asphalt highway pavement present a significant improvement on the models currently used in the mechanistic-empirical pavement design method. It is recommended to calibrate the regression prediction model using condition and traffic data for selected pavement sections if desired to implement in other geographic and different climatic regions.

#### **4.1.6. Recommendations for Implementation of Condition Deterioration Progression Model Equations**

The recommendations for implementation of the enhanced condition deterioration progression model equations follow:

- **IRI Roughness:** Both enhanced multiple regression and ANN model equations are recommended for asphalt pavement IRI roughness modeling and prediction for future IRI values.
- **Rutting:** Both enhanced multiple regression and ANN model equations are recommended for asphalt pavement rutting modeling and prediction for future rut depth values.
- **Cracking:** ANN model equations are better predictors for future UCI values and are recommended for implementation in both asphalt pavement structural design and asphalt pavement asset management. However, it is also recommended to calibrate the enhanced regression prediction equations using condition and traffic data for selected pavement sections, if desired to implement in other geographic and different climatic regions.

### **4.2. Modulus Values Backcalculation**

#### **4.2.1. Evaluation of Candidate Backcalculation Methods using Selected Asphalt LTPP Deflection Data**

The LTPP test section 28-2807 located at Highway 6 East in Lafayette County, MS, was opened to traffic on January 1, 1982. This test section was assigned the CN value of one when the LTPP program started in 1987. The test section comprises four layers of asphalt, asphalt base, CTB, and subgrade layers. The subgrade soil type is sandy lean (low plasticity) clay with a CBR value of eight. For analysis purposes, the Poisson's ratio for asphalt pavement and asphalt base is set to 0.35. Ali GA et al. (1970) studied the influence of Poisson's ratio on the surface deflection of layered systems. The deflection factors obtained from laboratory evaluation were compared with the theoretical values. A Poisson's ratio of 0.35 is the ideal value for asphalt material. The use of a higher value of 0.5 for asphalt material resulted in an increased deviation between the calculated modulus using theoretical and experimental approaches. The Poisson's ratio of 0.25 and 0.45 was set for the CTB and subgrade layers, respectively. Since 1987, the test section was subjected to six series of FWD tests from 1990 to 1998 as shown in Table 26.

Table 26. Basic information for LTPP test section 28-2807 in Lafayette County, MS

State Code	SHRP ID	Construction Number, CN	CN Assigned Date	CN Change Reason Code	FWD Test Date
(MS)	2807	1	1 <sup>st</sup> Jan. 1987		11 <sup>th</sup> Oct 1990
					19 <sup>th</sup> July 1991
		2	15 <sup>th</sup> May 1992	25	24 <sup>th</sup> June 1992
					3 <sup>rd</sup> August 1993
		3	31 <sup>st</sup> Jan. 1994	51	1 <sup>st</sup> Dec. 1995
		4	15 <sup>th</sup> May 1997	24	9 <sup>th</sup> July 1998

**Where CN Change Reason Code**

- 25: Patch potholes-hand spread, compacted with the truck
- 51: Mill of asphalt concrete and overlay with asphalt concrete
- 24: Full-depth patch of AC pavement (removing damaged material, repairing supporting layer)

Four different CNs were assigned to this test section. The CN is an intervention factor that describes any M&R event that has been applied to the pavement section. The local maintenance to patch potholes has changed the CN to CN two. The FWD tests were conducted annually from October 11, 1990, until August 3, 1993. The thickness of asphalt, base, and subbase layers under CN one and two are 5.5, 5.1, and 6.6 inches, respectively and the subgrade layer is semi-infinite in depth. The major M&R treatment was conducted on January 31, 1994, and the test section was assigned the CN three. About 1.1 inches of asphalt top layer was milled and resurfaced with 2.1 inches of HMA. Therefore, asphalt layer thickness increased to 6.5 inches and the thicknesses for the base and subbase layers remain unchanged. The FWD tests were continued in 1995 and 1998 to assess the structural integrity of the pavement structure under continuous traffic ESAL applications and environmental factors. Table 27 shows annual and cumulative ESAL from 1982 until 2001. The annual ESALs show a steady increase in vehicles from 1982 until 1989.

Table 27. ESAL data for test section 28-2807 in Lafayette County, MS

State Code	SHRP ID	Age (Year)	Traffic Year	Annual ESAL	Cumulative ESAL
28	2807	1	1982	53,000	53,000
		2	1983	55,000	108,000
		3	1984	57,000	165,000
		4	1985	51,000	216,000
		5	1986	61,000	277,000
		6	1987	65,000	342,000
		7	1988	69,000	411,000
		8	1989	85,000	496,000
		9	1990	72,000	568,000
		10	1991	74,000	642,000
		11	1992	91,000	733,000
		12	1993	94,000	827,000

	13	1994	97,000	924,000
	14	1995	100,000	1,024,000
	15	1996	103,000	1,127,000
	16	1997	106,000	1,233,000
	17	1998	109,000	1,342,000
	18	1999	135,000	1,477,000
	19	2000	140,866	1,617,866
	20	2001	146,986	1,764,852

In 1990 the recorded annual ESAL reduced by 15.3% compared to the previous year's data (1989). Then the traffic count gradually increases until 1998, but a rapid increase in ESAL was observed in 1999. In the LTPP database, traffic data for 2000 and 2001 are missing, so the number is estimated based on the formula proposed in this study. Therefore, the calculated average annual rate of growth is 4.3%. In this case, the estimated annual ESAL for the years 2000 and 2001 are 140,866 and 146,986, respectively. The cumulative ESAL for 20 years is calculated and shown in Table 27.

Table 28 shows the applied loads and corresponding deflections in mils for test section 28-2807. The FWD test was conducted on October 11, 1990.

Table 28. The FWD drop loads and peak deflections (Test section 28-2807, October 11, 1990)

28-2807 Drop No.	Drop Load (lbs.)	Area sq. in., Radius = 5.9 in.	Peak Deflections (mils) Test date: October 11, 1990						
			Sensor 1	Sensor 2	Sensor 3	Sensor 4	Sensor 5	Sensor 6	Sensor 7
1	6,207	109.4 sq.in.	3.56	3.00	2.71	2.36	2.10	1.65	1.05
2	6,203		3.54	3.00	2.71	2.35	2.11	1.65	1.05
3	6,218		3.55	3.00	2.71	2.35	2.11	1.66	1.06
4	6,216		3.53	2.99	2.70	2.34	2.10	1.65	1.05
5	9,109		5.17	4.50	4.07	3.53	3.17	2.50	1.60
6	9,163		5.19	4.52	4.10	3.55	3.18	2.52	1.61
7	9,157		5.20	4.52	4.10	3.55	3.18	2.50	1.61
8	9,155		5.19	4.51	4.09	3.54	3.18	2.51	1.60
9	12,534		7.20	6.17	5.59	4.86	4.35	3.43	2.18
10	12,566		7.24	6.20	5.61	4.88	4.37	3.45	2.19
11	12,563		7.24	6.20	5.62	4.88	4.37	3.45	2.19
12	12,560		7.25	6.21	5.62	4.89	4.38	3.45	2.20
13	17,682		9.91	8.54	7.75	6.72	6.03	4.75	3.01
14	17,689		9.96	8.58	7.78	6.75	6.05	4.77	3.00
15	17,690		9.96	8.60	7.79	6.77	6.06	4.78	3.01
16	17,671		9.95	8.59	7.78	6.75	6.05	4.77	3.02
Mean	11,399		6.5	5.6	5.0	4.4	3.9	3.1	2.0
SD	4,407		2.5	2.1	1.9	1.7	1.5	1.2	0.7
COV	38.7%		38.1%	38.4%	38.5%	38.5%	38.5%	38.6%	38.1

For comparison purposes, each software was analyzed using deflections measured at loadlevels closest to the standard 9,000 lbs. level of load. Typically, the pavement structural design is based on a loaded axle of 18,000 lbs. (9,000 lbs. per one-half of the axle). In this research, only the deflection data for drop number eight is used to backcalculate modulus values.

#### 4.2.2. Backcalculation Software Evaluated for Preliminary Study in This Research

The FWD data for test section 28-2807 was extracted from the LTPP database and used as an input in the PCASE 2.09, BAKFAA 2.0, and EVERCALC 5.0 backcalculation software. The PCASE 2.09 software was developed under collaboration between the Transportation System Center and ERDC of the U.S. Army Corps of Engineers (U.S. Army Corps of Engineers 2021). The PCASE 2.09 software allows the user to backcalculate pavement layers modulus values and evaluates response analysis for both asphalt and concrete pavements. Users are required to provide traffic data, pavement layers with specific thicknesses, seed modulus values, Poisson’s ratio, interface parameter for each layer, monthly air temperatures, and FWD data. A maximum of ten iterations for each drop is allowed for evaluation of the backcalculated modulus.

The BAKFAA 2.0 software was developed by the Federal Aviation Administration (FAA) and is more straightforward as compared to the PCASE 2.09 software. This software used FAA Layered Elastic Analysis (LEAF) backcalculation subroutine (FAA 2011). The required inputs for analysis are pavement layers (up to 10 layers), seed modulus values, Poisson’s ratio, interface parameter for each layer, FWD sensor location, and deflection data. A maximum number of 5,000 iterations was reported (Priddy et al. 2015). The EVERCALC 5.0 software was developed by Mahoney et al. (1993) and included as one of the EVERSERIES software packs developed by the Washington Department of Transportation (WSDOT 2005). The software adopted CHEVRON forwarded subroutine and an iterative subroutine for the backcalculation process. The required inputs for analysis are pavement layers which are limited to four layers including stiff layer, seed modulus values, Poisson’s ratio, interface parameter for each layer, pavement temperature, and FWD data. A maximum of 10 iterations are set for analysis and the deflection tolerance is based on percent RMSE. The LTPP database InfoPave is now populated with the backcalculated modulus values using this software (WSDOT 2005).

##### 4.2.2.1. Seed Modulus Values Required by each Backcalculation Software

The default seed modulus values for BAKFAA 2.0 and PCASE 2.09 (Priddy et al. 2015), and EVERCALC 5.0 (WSDOT 2005) are shown in Table 29. On the other hand, no seed modulus values are used by the UMPED software.

Table 29. Default seed modulus values used in this research

Default seed modulus values used in this research (psi)			
*Default, **Automatically generated from UMPED			
Layer	*BAKFAA (2.0)	*EVERCALC (5.0)	*PCASE (2.09)
Asphalt	500,000	150,000	350,000
Asphalt Treated Base (ATB)	500,000	50,000	300,000
Cement Treated Base (CTB)	750,000	400,000	300,000
Subgrade	7,000	10,000	15,000

For the asphalt layer, the seed modulus value for BAKFAA 2.0 is the highest compared to other software. The modulus of 150,000 psi which is in the proposed ranges of 100,000 to 200,000 psi was used for EVERCALC 5.0 software. The asphalt modulus value for the PCASE 2.09 is 350,000 psi. For the base layer, BAKFAA 2.0 specified 500,000 psi for a stabilized baselayer. The PCASE 2.09 software

used 300,000 psi for asphalt base layers. In EVERCALC 5.0 manual, only lime stabilized, and cement stabilized modulus values are specified (WSDOT 2005). Therefore, a similar modulus value of 50,000 psi was used for the asphalt base layer. For the CTB layer, the modulus values vary from 300,000 to 750,000 psi. The proposed values are significantly higher compared to the modulus value backcalculated by Uddin et al. (Uddin et al. 2003). The subgrade modulus values are 7,000 psi for BAKFAA 2.0, 10,000 psi for the EVERCALC 5.0, and 15,000 psi for the PCASE 2.09 software, respectively.

**4.2.2.2. Backcalculated Modulus Values from The Previous Study By Boriboonsin And Momm (2002)**

Table 30 presents the backcalculated modulus values from a previous study by Boriboonsin and Momm. (2002) for comparison with the backcalculated values from other software.

Table 30. Modulus Values from Previous Study by Boriboonsin and Momm. (2002)

FWD Date Test	Air Temp. (° F)	CN	Backcalculated Young’s Modulus Summary Results (psi)				
			Statistics	Layer 1 Asphalt	Layer 2 Asphalt Base	Layer 3 CTB	Layer 4 Nonlinear (Subgrade)
Oct. 11, 1990	43.3	1	Mean COV (%)	989,900 50	1,093,300 57	119,100 41	24,160 15
July 19, 1991	77.7	1	Mean COV (%)	536,200 32	655,600 40	102,800 35	20,160 19
June 24, 1992	85.5	2	Mean COV (%)	403,500 32	367,800 29	74,600 25	17,720 18
Aug. 3, 1993	77.6	2	Mean COV (%)	623,300 32	623,600 40	90,500 41	19,240 16
Dec 1, 1995	50.8	3	Mean COV (%)	884,00 49	826,800 63	116,800 45	26,700 16
July 9, 1998	96.3	4	Mean COV (%)	264,600 44	236,400 54	91,400 45	18,010 18
Average				616,917	633,917	99,200	20,998
Standard Deviation (SD)				253,863	282,150	15,601	3,316
Coefficient of Variation (%)				41.2	44.5	15.7	15.8

The backcalculated modulus values for the subgrade layer are corrected for the nonlinear behavior corresponding to the effect of the design wheel load (Boriboonsin and Momm. 2002). On the other hand, no correction to the modulus values of the asphalt base and the CTB layers are applied since these are the stabilized layers. The important findings from the study (Boriboonsin and Momm. 2002) follow:

- The modulus values for asphalt pavement and asphalt base layers increase caused by the lower air temperature during the FWD tests due to the viscoelastic properties of the asphalt layer. This implies that the backcalculated temperature-dependent modulus values for asphalt pavement and asphalt base layers for higher temperature (1991, 1992, 1993, and 1998) are smaller compared to the modulus values at lower temperatures for 1990 and 1995.

- The modulus values for the CTB layer show a decreasing trend over time. Under constant temperature, the modulus value for the CTB in 1991 is about 12 percent lower compared to the modulus in 1993. This implies that under continuous traffic loads application, the CTB is prone to crack-related degradation and age-related degradation (Uddin et al. 2003).

The modulus values for the subgrade layer show no obvious changes with only less than 20% in COV. The relatively small variation indicates an almost homogenous soil layer, and most importantly, the subgrade layer is not affected by the seasonal changes. According to Uddin et al. (2003), the modulus value for the subgrade layer is usually four to six times less than the CTB layer. Additionally, the increase in subgrade modulus values is closely related to the variations in moisture content in the subgrade layer. Lower subgrade modulus values are observed during the summer months due to frequent rainfall compared to the modulus values in the winter months.

#### 4.2.3. In Situ Material Characterization of Selected Asphalt Pavement Structures

This sub-chapter compares the stiffness of asphalt pavement, asphalt treated base, cement-treated base, and subgrade layers based on the modulus values calculated using different computer programs. In general, material characterization focuses on two main parameters, which are Young’s modulus, and Poisson’s ratio.

The reasonableness of the backcalculated modulus values is evaluated by comparing modulus values from different software as shown in Table 31.

Table 31. Backcalculated modulus values for test section 28-2807 in Mississippi

SHRP ID 28(MS)-2807	Layer (thickness)	Backcalculation Method	Backcalculated Moduli (psi)				# of Iterations	RMSE (%)
			Asphalt Surface	Asphalt Base	Cement TreatedBase	Subgrade		
FWD Test Date: 10/11/1990	Asphalt (5.5 in.)	BAKFAA 2.0	943,693	899,389	126,802	28,096	408	1.3%
Construction Number: 1	Asphalt Treated Base (5.1 in.)	EVERCALC 5.0 (From	170,569	27,011	3,599	4,241	-	1.3%
Temperature: Air: 43.3°F, Surface: 32.7°F	Cement Treated Base (6.6 in.)	EVERCALC 5.0 (Calculated)	446,740	847,440	35,000	43,600	10	21.1%
	Subgrade	PCASE 2.09	2,195,236	115,301	1,029,395	17,105	3	0.8%
		UMPED	1,200,000	90,000	70,000	36,650	1	78.6%

SHRP ID 28(MS)-2807	Layer (thickness)	Backcalculation Method	Backcalculated Moduli (psi)				# of Iterations	RMSE (%)
			Asphalt Surface	Asphalt Base	Cement Treated Base	Subgrade		
FWD Test Date: 07/19/1991	Asphalt (5.5 in.)	BAKFAA 2.0	1,083,350	66,789	862,736	22,155	192	4.4%
Construction Number: 1	Asphalt Treated Base (5.1 in.)	EVERCALC 5.0 (From	170,569	27,011	3,599	4,241	-	1.3%
Temperature: Air: 77.7°F, Surface: 103.1°F	Cement Treated Base (6.6 in.)	EVERCALC 5.0 (Calculated)	1,687,500	35,000	35,000	43,600	10	26.0%
	Subgrade	PCASE 2.09	598,751	180,249	463,786	16,626	2	0.8%
		UMPED	1,029,300	89,300	70,000	29,760	1	42.1%

SHRP ID 28(MS)-2807	Layer (thickness)	Backcalculation Method	Backcalculated Moduli (psi)				# of Iterations	RMSE (%)
			Asphalt Surface	Asphalt Base	Cement Treated Base	Subgrade		
FWD Test Date: 06/24/1992	Asphalt (5.5 in.)	BAKFAA 2.0	501,588	107,923	191,511	21,894	365	3.2%
Construction Number: 2	Asphalt Treated Base (5.1 in.)	EVERCALC 5.0 (From	75,547	22,063	3,320	3,696	-	1.3%
Temperature: Air: 85.5°F, Surface: 122.0°F	Cement Treated Base (6.6 in.)	EVERCALC 5.0 (Calculated)	828,100	35,000	35,000	43,600	10	31.1%
	Subgrade	PCASE 2.09	377,683	128,154	281,308	15,290	4	2.6%
		UMPED	789,800	90,000	60,000	20,060	1	14.9%

SHRP ID 28(MS)-2807	Layer (thickness)	Backcalculation Method	Backcalculated Moduli (psi)				# of Iterations	RMSE (%)
			Asphalt Surface	Asphalt Base	Cement Treated Base	Subgrade		
FWD Test Date: 08/03/1993	Asphalt (5.5 in.)	BAKFAA 2.0	1,125,212	206,918	127,573	23,359	288	1.3%
Construction Number: 2	Asphalt Treated Base (5.1 in.)	EVERCALC 5.0 (From	75,547	22,063	3,320	3,696	-	1.3%
Temperature: Air: 77.6°F, Surface: 95.5°F	Cement Treated Base (6.6 in.)	EVERCALC 5.0 (Calculated)	1,538,460	35,000	35,000	43,600	10	27.8%
	Subgrade	PCASE 2.09	1,033,789	142,985	340,384	15,880	2	0.8%
		UMPED	1,091,100	85,600	70,000	28,530	1	40.5%

SHRP ID 28(MS)-2807	Layer (thickness)	Backcalculation Method	Backcalculated Moduli (psi)				# of Iterations	RMSE (%)
			Asphalt Surface	Asphalt Base	Cement Treated Base	Subgrade		
FWD Test Date: 12/01/1995	Asphalt (5.5 in.)	BAKFAA 2.0	1,761,351	96,012	307,207	27,436	455	1.2%
Construction Number: 3	Asphalt Treated Base (5.1 in.)	EVERCALC 5.0 (From	167,557	29,613	3,961	4,371	-	1.4%
Temperature: Air: 50.8°F, Surface: 44.7°F	Cement Treated Base (6.6 in.)	EVERCALC 5.0 (Calculated)	2,295,000	35,000	35,000	43,600	10	18.2%
	Subgrade	PCASE 2.09	1,652,768	54,809	1,195,041	18,157	10	5.5%
		UMPED	1,200,000	90,000	70,000	36,900	1	68.5%

SHRP ID 28(MS)-2807	Layer (thickness)	Backcalculation Method	Backcalculated Moduli (psi)				# of Iterations	RMSE (%)
			Asphalt Surface	Asphalt Base	Cement Treated Base	Subgrade		
FWD Test Date: 07/09/1998	Asphalt (5.5 in.)	BAKFAA 2.0	146,430	738,211	66,901	24,480	295	1.6%
Construction Number: 4	Asphalt Treated Base (5.1 in.)	EVERCALC 5.0 (From	35,517	32,432	2,841	3,991	-	1.3%
Temperature: Air: 96.3°F, Surface: 117.5°F	Cement Treated Base (6.6 in.)	EVERCALC 5.0 (Calculated)	433,100	35,000	35,000	43,600	10	29.6%
	Subgrade	PCASE 2.09	215,763	76,104	800,768	16,096	3	0.6%
		UMPED	559,900	90,000	63,300	21,110	1	11.2%



The FWD test date, CN, air and surface temperatures, layer thicknesses, and RMSE in percent for test section 28-2807 are included in the table. The reasonableness of the backcalculated modulus is assessed based on sensitivity to temperature changes for the first two layers, changes of the CTB layer modulus values over time, acceptable changes of the modulus values for the subgrade layer for different years and must be within the specified modulus ranges.

In general, although the same deflection data sets are used, the backcalculated modulus values from each software are greatly different. This implies that the analysis subroutine for each software is different. The BAKFAA 2.0 used LEAF (Priddy et al. 2015) subroutine, a layered elastic computational program. The EVERCALC iteration is based on the CHEVRON subroutine (Priddy et al. 2015). The PCASE 2.09 adopted the WES5 subroutine (Priddy et al. 2015), and the UMPED used the BASIN backcalculation analysis subprogram incorporated in the PEDD software (George and Uddin 2000; Uddin et al. 1986). Comparison with the previous study (Boriboonsin and Momm. 2002) shows the inconsistency of the backcalculated modulus values using BAKFAA 2.0 and PCASE 2.09 which are noted through the unexpected increase in the modulus values for the CTB layer. The BAKFAA 2.0 software also shows an unreasonable asphalt base modulus value that in most cases was excessively higher than the asphalt layer modulus value.

For data sets in 1990, the EVERCALC 5.0 software over-predicted asphalt base modulus value, almost double the modulus value for asphalt pavement. Additionally, for all other cases, the EVERCALC 5.0 software shows excessively low modulus values for the asphalt base and the CTB layers. For test section 28-2807 in MS, the backcalculated modulus values from the LTPP database are unreasonable due to very low values compared to the Boriboonsin and Momm (2002) study. Only the UMPED software shows reasonable modulus values for all cases. In general, the modulus values relatively decrease as the distances of the underlying layers are farther from the asphalt surface. The comparison between the measured and calculated surface deflection values for each backcalculation software is shown in Figure 55.

The RMSE in percent depends on the deviation between the calculated and measured deflections. The BAKFAA 2.0, EVERCALC 5.0 from the LTPP database, and the PCASE 2.09 software show the least error compared to the measured deflection values. This implies that the differences between the measured and final calculated deflections are relatively small. However, it is noted that the backcalculation subroutine used in that software tries to minimize the RMSE by repeating the iteration processes but compromise the reasonableness of the backcalculated modulus values. The deflection values calculated using the EVERCALC 5.0 software are very poor compared to other software. Both PCASE 2.09 and EVERCALC have been set to a maximum of 10 iterations. The maximum number of iterations is 455 for the BAKFAA2.0 software in this research.

For the UMPED software, after a single iteration for each layer, the calculated deflections at sensors one, six, and seven show very small differences compared to the measured deflection values. Generally, the deviation between the measured and calculated deflections at sensor one reflects the asphalt layer modulus values. On the other hand, the differences between the measured and calculated deflection for sensors six and seven affect the modulus value for the subgrade layer.

The UMPED backcalculation subroutine calculates seed modulus values as a function of the peak test load, measured deflections, and pavement layer thicknesses. Then it starts the iteration initially for the subgrade layer. Once the modulus value for the subgrade layer is determined, the iteration process

continues for the asphalt layer and other intermediate layers (Uddin et al. 1986). Although the RMSE is higher compared to other software, the UMPED is more efficient in predicting reasonable modulus values since those values are computed only after one iteration. The modulus values from Table 31 were plotted as shown in Figure 56 through Figure 59 for asphalt, asphalt base, CTB, and subgrade layers, respectively. For the asphalt layer (Figure 56), only the modulus values determined using the PCASE 2.09 and UMPED software show higher modulus values as the temperatures decrease. The calculated modulus using the EVERCALC 5.0 gave an unacceptable modulus of more than 2.2 million psi at 50.8°F air temperature, which is too high for asphalt pavement.

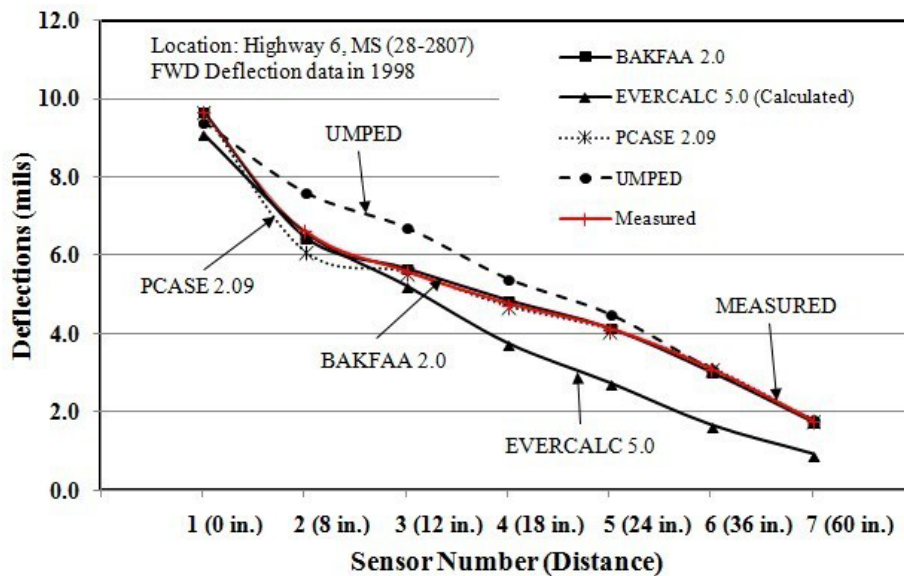


Figure 55. Comparison between the measured and calculated deflections in 1998

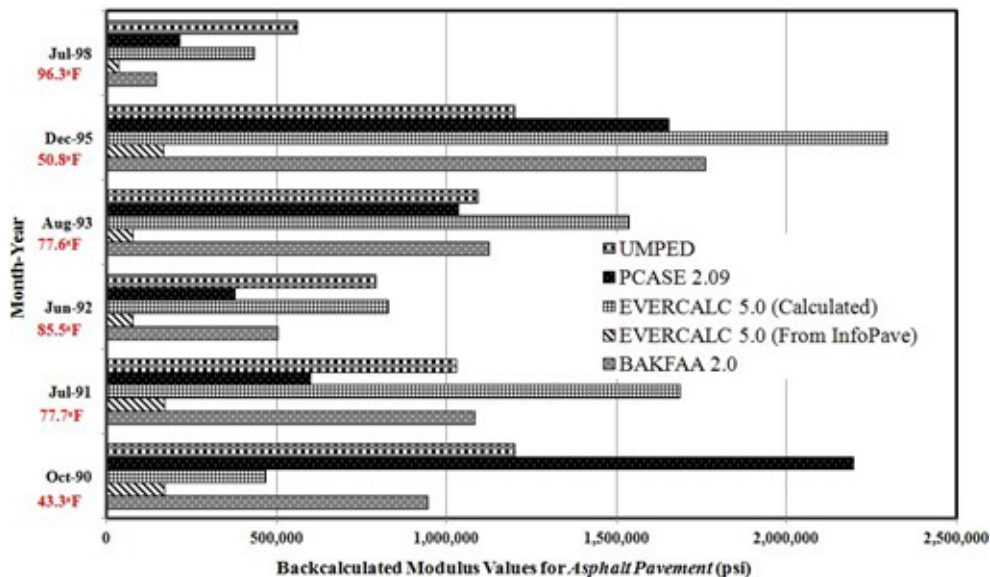


Figure 56. Backcalculated modulus values for asphalt surface layer

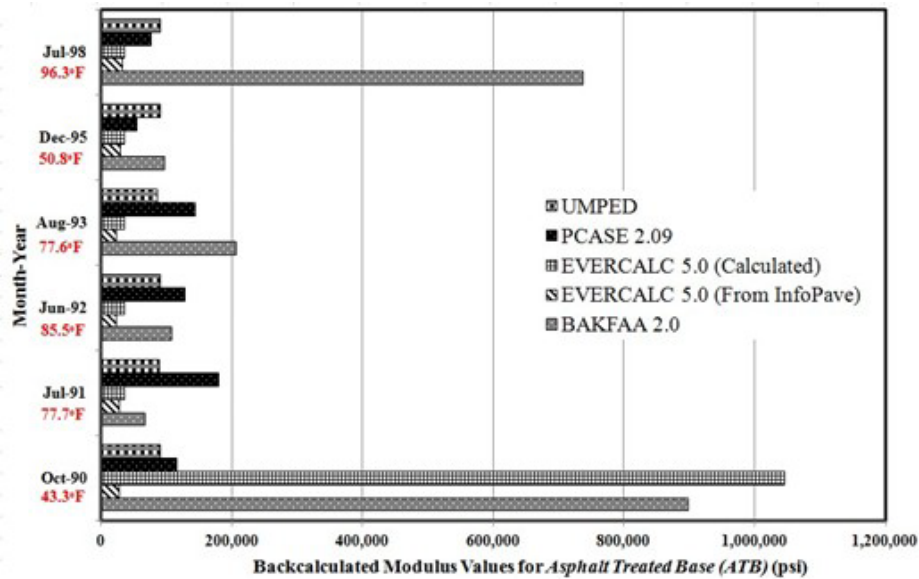


Figure 57. Backcalculated modulus values for asphalt treated base layer

The modulus values from the LTPP InfoPave database are very low for all years. In general, the modulus values are higher than the backcalculated values from the previous study (Boriboonsin and Momm. 2002). However, according to Priddy et al. (2015), the acceptable ranges are between 70,000 to 3,625,000 psi for the asphalt layer.

For the asphalt treated base layer (Figure 57), the modulus values are relatively low for all cases compared to Boriboonsin and Momm. (2002) predictions. The modulus value of 899,389 psi (1990) determined using the BAKFAA 2.0 software is reasonable for the FWD deflection data measured during a near-freezing condition. Additionally, this value is slightly lower than the asphalt pavement modulus and higher than the modulus values for the CTB (Figure 58) and subgrade layers, respectively. The proposed range for asphalt base is 100,000 to 3,625,000 psi (Priddy et al. 2015).

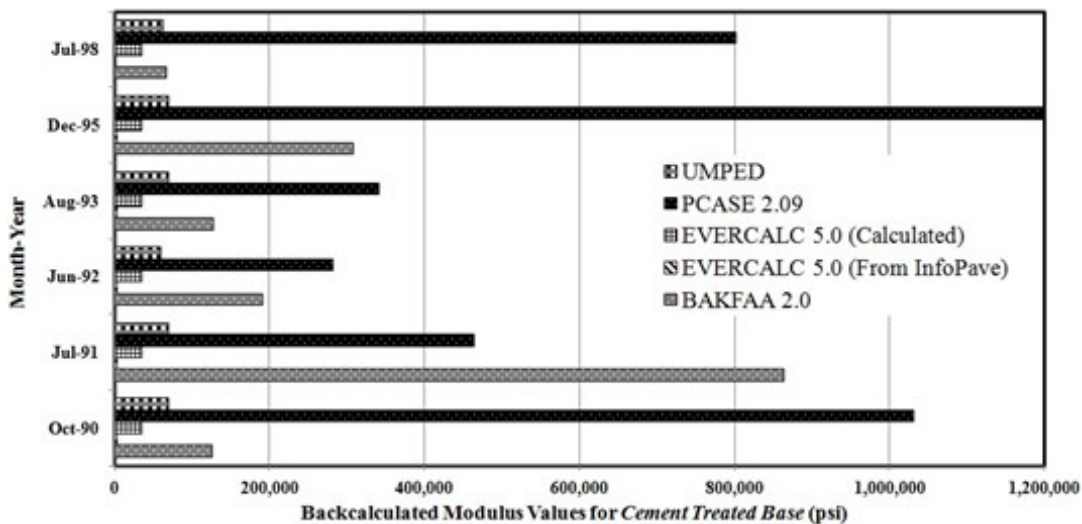


Figure 58. Backcalculated modulus values for CTB layer

For the CTB, only the UMPED and PCASE 2.09 software indicate decreasing values over time from 1990 to 1992 due to possible cracks in the CTB layer under continuous traffic application. The reasonable modulus values are between 10,000 to 1,000,000 psi for the stabilized base (Priddy et al. 2015). The backcalculated modulus values using the EVERCALC 5.0 from the LTPP InfoPave database are very low and unreasonable.

The backcalculated modulus values for the subgrade layer are compared and shown in Figure 59. A reasonable range for subgrade modulus is from 1,000 to 30,000 psi (Priddy et al. 2015). Only the PCASE 2.09 software shows the least variation in subgrade modulus values from 1990 to 1998. In contrast, the UMPED and BAKFAA 2.0 have more than 25% difference between the lowest and the highest modulus values. The variation is expected as moisture content changes throughout the year and over the life of the pavement. The subgrade modulus values calculated using the EVERCALC 5.0 software are very low for all cases. Overall, the 1998 FWD test data analyzed by the BAKFAA 2.0 software and the UMPED backcalculation software provide reasonable in situ modulus values for all pavement layers.

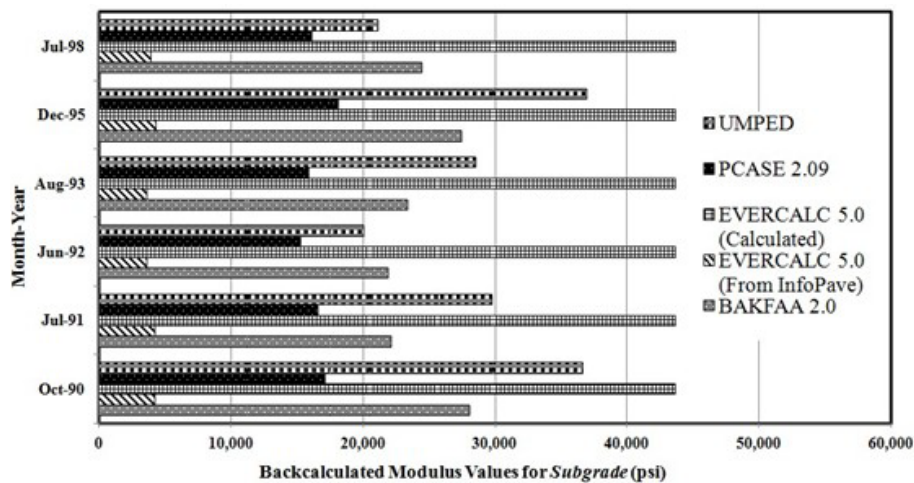


Figure 59. Backcalculated modulus values for the subgrade layer

Based on the research, it can be concluded that the UMPED software shows a consistent reasonable set of backcalculated modulus values for FWD data collected over the years for all layers. The next-reasonable modulus values were backcalculated using the BAKFAA 2.0 software using the FWD deflection data collected in 1998 (Table 31). It is observed that the modulus values of both asphalt layers are higher than expected. The output for 1998 data shows 295 iterations and an RMSE of 1.6 percent, respectively. On the other hand, the most reasonable modulus values backcalculated using the UMPED software for 1998 data are 559,900 psi (asphalt surface layer), 90,000 psi (asphalt treated base), 63,300 psi (CTB), and 21,110 psi (subgrade layer), respectively for 1998 data. These values were calculated after one iteration only with an RMSE of 11.3 percent. Therefore, this research suggests that the backcalculated modulus values for the year 1998 using the BAKFAA 2.0 software and the UMPED software deflection data in 1998 are reasonable and recommended to be used for the 3D-FE numerical analysis if desired.

#### 4.2.4. FWD Dynamic Analysis for Backcalculation of Asphalt Pavement Layer Modulus Values and Comparison with Layered Elastic Static Analysis Results

The FWD is a testing device used to evaluate the physical properties of the pavement. It provides the structural capacity evaluation of the pavement system, which is important for load-carrying capacity analysis. Figure 60 shows an illustration of the FWD test setup and the locations of geophone sensors. Once a specific magnitude of FWD load is dropped on top of a circular steel plate, a load pulse is transmitted on the pavement surface. This action creates a deflection that simulates wheel load caused by a moving vehicle, for example, a heavy truck. The geophone sensor automatically determines the vibration amplitude, depending on the magnitude of the FWD loads. Subsequently, a complex formulation of the computer program will calculate the deflections under each sensor. The line indicates the deflection basin usually obtained from the FWD test. The deflection values under each sensor are used for the backcalculation process to determine the modulus of asphalt, base, subbase, and subgrade layers.

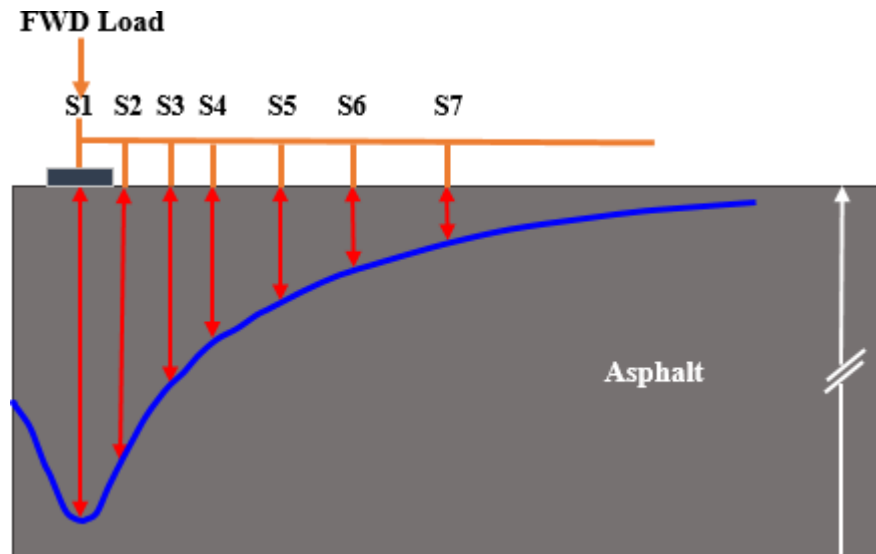


Figure 60. Illustration of FWD load point and the locations of geophone sensors (not to scale)

The previous sub-chapter highlighted the estimation of modulus values using a static backcalculation approach based on the layered elastic analysis. Unfortunately, the computer programs developed for backcalculation of modulus value did not consider the dynamic load of the FWD test. It is noted that the structural response of asphalt pavement is time-dependent and affected by load-time history (Boriboonsin and Momm. 2002; Uddin and Garza 2010; Uddin and Ricalde 2000). For that reason, a more advanced approach to study the effects of the FWD load on pavement structural responses using the 3D-FE modeling was introduced by a few researchers (Boriboonsin and Momm. 2002; Uddin and Garza 2010). Garza (2003) has developed a 3D-FE model using LS-DYNA software to further evaluate the effect of dynamic loading based on the load-time history curve. The sizes of the elements are set in a way that the location of the nodes in the 3D-FE matched with actual distances from the loading point of the geophone sensors used in the FWD testing device. Figure 61 shows the 3D-FE model of uncracked asphalt that consists of asphalt, base, subbase, and subgrade layers used in the previous study (Garza 2003).

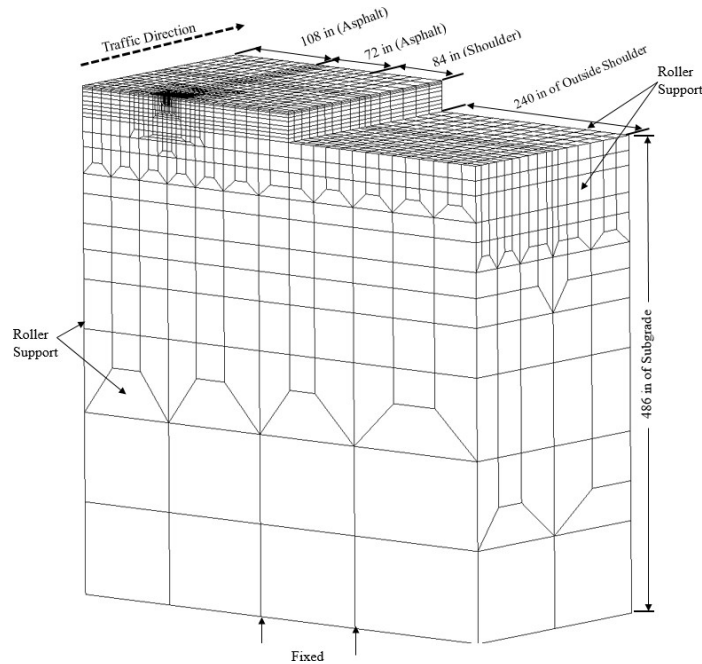


Figure 61. Garza’s 3D-FE model was used to evaluate responses under the FWD load (Garza 2003)

Garza ran multiple 3D-FE simulations under the FWD load and observed the responses at specific nodes of the elements. Subsequently, the responses from the 3D-FE analysis based on factorial design were used to develop the multiple regression equations to predict modulus value for asphalt, base, subbase, and subgrade layers, respectively.

From the previous discussion, it was observed that the UMPED (Boriboonsin and Momm. 2002) static modulus backcalculation program developed at the University of Mississippi showed among the most reasonable predictions of modulus for the section 28-2807 in Mississippi. Based on this statement, this research intends to further evaluate the reasonableness of the predicted modulus values using UMPED static analysis, with Garza’s multiple regression equations to predict modulus values for all four layers. Table 32 summarized the backcalculated modulus values for the asphalt layer, Lime-Filled Asphalt (LFA) base layer, Lime-Treated Subbase (LTS) layer, and subgrade layer (Garza 2003).

Table 32 shows the backcalculated modulus values for all layers using UMPED for drop number two. The outputs for seven sensors are selected for comparison with the modulus values calculated using multiple regression based on the 3D-FE analysis.

Table 32. Summary of modulus values from UMPED for US45N North Project, Section 1, Station 461+05 (After (Garza 2003))

Cycle	Method		Modulus Values: MPa (psi)				
			Asphalt	LFA	LTS	Subgrade	
3	Backcalculation UMPED Drop 2	Thickness mm (inch)	152.4 (6)	152.4 (6)	152.4 (6)	Semi- infinite	Nonlinear Modulus
		Sensor 1-7	4,624 (670,600)	1,040 (150,800)	110 (15,900)	160 (23,240)	118 (17,180)
		Sensor 1-6	4,619 (670,000)	612 (88,700)	176 (25,500)	163 (23,680)	116 (16,870)

#### 4.2.5. Evaluation of Asphalt Pavement Modulus using Predictive Equations Developed from the 3D Numerical Analysis

The multiple regression equations were developed based on the area under deflection- time history method which was described in detail by Garza (2003). The following parameter required to calculate the modulus values based on the regression constant and coefficient values:

- The area from measured deflection-time history (AW) for US 45N as shown in Table 33 (Garza 2003).
- The area under the FWD load/peak load-time history curve (LA = 24.4 msec)
- Radial distances of each sensor (R<sub>1</sub> = 0 in., R<sub>2</sub> = 12 in., R<sub>3</sub> = 24 in., R<sub>4</sub> = 36 in., R<sub>5</sub> = 48 in., R<sub>6</sub> = 60 in., R<sub>7</sub> = 72 in.) (FHWA 2017)
- The plate is a 4-segmented plate with a radius of 5.91 inches
- Layer thicknesses for asphalt, base, and subgrade layers as shown in Table 33 (Garza 2003).

Table 33. Areas from measured deflection-time history for US45N, Cycle 3, Drop 2 (Garza 2003)

AW <sub>1</sub>	246.79 mils-msec	LA	24.40 msec
AW <sub>2</sub>	183.73 mils-msec	T <sub>1</sub>	6 inches
AW <sub>3</sub>	122.38 mils-msec		
AW <sub>4</sub>	83.94 mils-msec	T <sub>2</sub>	6 inches
AW <sub>5</sub>	61.13 mils-msec		
AW <sub>6</sub>	47.32 mils-msec	T <sub>3</sub>	6 inches
AW <sub>7</sub>	36.79 mils-msec		

To obtain the modulus values for all layers, the subgrade modulus must be calculated first, since the subgrade modulus value is required to predict the modulus values for other layers. Equations 4.18 to 3.21 are used to predict modulus values for subgrade layer (E<sub>4</sub>), subbase layer (E<sub>3</sub>), base layer (E<sub>2</sub>), and asphalt layer (E<sub>1</sub>), respectively.

$$\begin{aligned} \log_{10}(E_4) = & 10.005 - 0.0289 \times \log_{10}(1 + T_2) - 0.05 \times \log_{10}(1 + T_3) + 0.2940 \times \\ & \log_{10}(AW_1) + 1.418 \times \log_{10}(AW_3 \times R_3) - 3.0270 \times \log_{10}(AW_4 \times R_4) + 5.679 \times \log_{10}(AW_5 \times \\ & R_5) - 4.382 \times \log_{10}(AW_6 \times R_6) - 1.109 \times \log_{10}(LA \times AW_2 \times R_2) - 0.025 \times \log_{10}[(1 + T_1) \times \\ & (1 + T_2) \times (1 + T_3)] \end{aligned} \quad \text{Eq. 4.18}$$

$$\begin{aligned} \log_{10}[E_3 \times (1 + T^3)] = & 13.76 - 0.373 \times \log_{10}(1 + T_1) - 0.4850 \times \log_{10}(1 + T_2) + 3.103 \times \\ & \log_{10}(1 + T_3) + 0.0616 \times \log_{10}(AW_1) - 5.26 \times \log_{10}(AW_3 \times R_3) + 1.503 \times \log_{10}(AW_4 \times \\ & R_4) - 3.3620 \times \log_{10}(AW_5 \times R_5) - 3.219 \times \log_{10}(AW_6 \times R_6) + 3.09 \times \log_{10}(LA \times AW_2 \times \\ & R_2) - 1.321 \times \log_{10}(AW_6 \times R_6 \times E_4) \end{aligned} \quad \text{Eq. 4.19}$$

$$\begin{aligned} \log_{10}[E_2 \times (1 + T^3)] = & 21.84 - 0.753 \times \log_{10}(1 + T_1) - 0.2230 \times \log_{10}(1 + T_3) + 1.01 \times \\ & \log_{10}(AW_1) + 8.116 \times \log_{10}(AW_3 \times R_3) - 6.022 \times \log_{10}(AW_4 \times R_4) + 7.872 \times \log_{10}(AW_5 \times \end{aligned}$$

$$R_5) - 8.654 \times \text{Log}_{10}(LA \times AW_2 \times R_2) + 3.379 \times \text{Log}_{10}(E_4) - 4.245 \times (AW_6 \times R_6 \times E_4) + 2.903 \times \text{Log}_{10}(LA \times \text{Radius} \times (1 + T_2)) \quad \text{Eq. 4.20}$$

$$\text{Log}_{10} [E_1 \times (1 + T^3)] = -21.182 - 0.0169 \times \text{Log}_{10} (1 + T_2) - 0.0232 \times \text{Log}_{10}(1 + T_3) - 4.197 \times \text{Log}_{10}(AW_1) - 9.705 \times \text{Log}_{10}(AW_3 \times R_3) + 3.774 \times \text{Log}_{10}(AW_4 \times R_4) - 3.966 \times \text{Log}_{10}(AW_5 \times R_5) + 11.478 \times \text{Log}_{10}(LA \times AW_2 \times R_2) - 2.17 \times \text{Log}_{10}(E_4) + 2.416 \times (AW_6 \times R_6 \times E_4) + 3.301 \times \text{Log}_{10}(LA \times \text{Radius} \times (1 + T_1)) \quad \text{Eq. 4.21}$$

The use of logarithms to base 10 was noted in the equations. This implies that data transformation using logarithms to base 10 gives a better correlation coefficient, R values of 0.978, 0.851, 0.889, 0.959 for equations 4.18 to 4.21, respectively (Garza 2003). Based on the previous study by Uddin (Uddin 1984), it was discovered that the radial distance of the sensors helped to improve the R-value. Therefore, Garza (2003) has incorporated the interaction between the area under the deflection-time history curve, radial distance, and modulus value as part of the independent variables in the developed equations. Table 34 summarizes the comparison between the UMPED outputs as compared to the predictions from multiple regression models developed based on the 3D-FE responses.

Table 34. Comparison between UMPED and regression model using areas under deflection-time history data

Highway US45N, North Project, Section 1, Cycle 3, Drop 2			
Layers \ Methods	Regression Model using Areas under Deflection-TimeHistory Curves, psi (Priddy 2014)	Backcalculated Modulus, psi (UMPED)	% Difference UMPED vs Regression Model
Asphalt, E <sub>1</sub>	613,584.4	670,700.0	9.3%
LFA Base, E <sub>2</sub>	95,894.7	150,800.0	57.3%
LTS Subbase, E <sub>3</sub>	12,351.0	15,900.0	28.7%
Subgrade, E <sub>4</sub>	19,692.1	17,180.0	-12.8%

As shown in Table 34, reasonably good results were backcalculated for the asphalt and subgrade layers within ± 15%. The UMPED predicted 9.3% higher asphalt modulus compared to multiple regression prediction models. Additionally, the UMPED calculated 12.8% less subgrademodulus value compared to another method, which is also acceptable for a high variability soil condition. Percent difference in the subgrade modulus could be higher, however, the UMPED has incorporated a certain algorithm to correct for the nonlinear behavior of subgrade soil. On the other hand, the base and subbase layers showed much higher discrepancies in backcalculated modulus values using the two approaches. As demonstrated by Uddin (Uddin 1984), the surface deflection values are relatively insensitive to modulus values of two intermediate layers.



### 4.3. 3D-FE Modeling of Uncracked Asphalt Pavements

#### 4.3.1. Comparison of 3D-FE Half Pavement Simulation Results with Layered Elastic Static Analysis Results

To assess the reliability of the developed 3D-FE model of uncracked pavement, the deflection values at the center of the loading area were extracted and compared with the following data sets:

- Measured asphalt surface deflection value subjected to FWD load (Figure 62), and
- Calculated asphalt surface deflection values using GAMES linear elastic static analysis software (Maina et al. 2012) subjected to truck axle loading.

Table 35 shows in situ linear elastic material properties for Highway US45N, North Project, where the FWD data was measured and used for comparison purposes. Table 36 describes the thickness values, degree of freedom, number of nodes, and elements for asphalt, base, subbase, subgrade layers and include outside shoulder as well. Other important information for the 3D-FE analysis subjected to the FWD load is shown in Table 37.

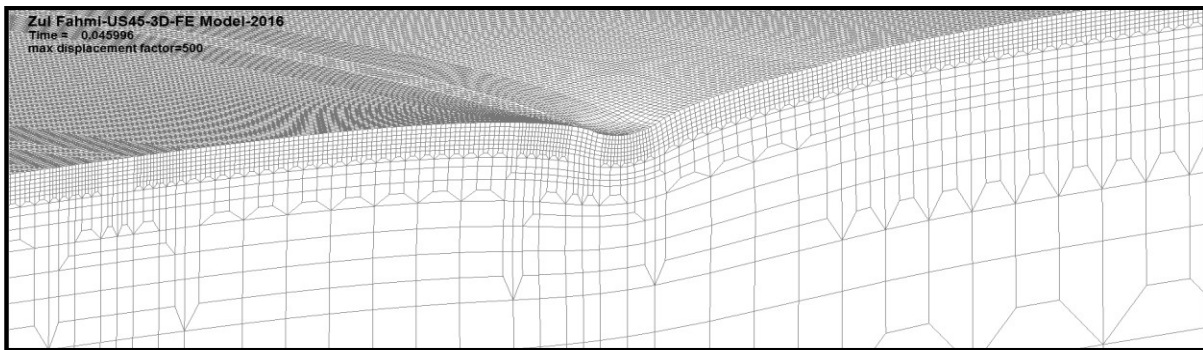


Figure 62. Deformed 3D-FE model subjected to FWD load

The LS-DYNA peak deflections for this analysis were calculated using a pressure value of 579.2 kPa (84 psi) over an area of 344.8 cm<sup>2</sup> (53.45 in<sup>2</sup>), therefore the applied peak load was 39.94 kN (8,979.6 lbf). The LS-DYNA calculated peak deflections were normalized to 40kN (9,000 lbf), multiplying the calculated peak deflections by the factor 1.002 (9,000 / 8,979.6) (Nanagiri 2001).

Table 35. Linear elastic material properties for Highway US45N, North Project, Section 1, Station 461+05, Cycle 2, Drop 2

Layer	Material	Thickness mm (inches)	Young's Modulus MPa (psi)	Poisson's Ratio	Mass Density (lb-sec <sup>2</sup> /in <sup>4</sup> )
1	Asphalt	76.2 (3)	2,290 (332,200)	0.35	0.000230
2	LFA	152.4 (6)	914 (132,500)	0.30	0.000210
3	LTS	152.4 (6)	281 (40,800)	0.30	0.000187
4	Subgrade	1,219.2 (480)	122 (17,740)	0.45	0.000173
Outside Shoulder	Compacted Layer	381 (15)	69 (10,000)	0.45	0.000165

Table 36. Degree of freedom, number of nodes, and elements for the US45N 3D-FE model

Layer	Material	Thickness mm (inches)	Degree of Freedom	No. of Nodes	No. of Elements
1	Asphalt	76.2 (3)	3,036,894	1,016,232	502,686
2	LFA	152.4 (6)	845,192	283,646	180,821
3	LTS	152.4 (6)	59,394	20,196	10,272
4	Subgrade	1,219.2 (480)	174,273	60,049	48,700
Outside Shoulder	Compacted Layer	381 (15)	877,597	296,295	321,268

The GAMES linear elastic static analysis software allows simulation of point loads at four different locations (Figure 63) like the loading configurations embedded in the 3D-FE models of uncracked asphalt pavement (Figure 64). The GAMES linear elastic static analysis software assumes no discontinuity on asphalt pavement surfaces. Table 38 shows the parameters related to the dynamic analysis using the 3D-FE half model subjected to 4,500 lbs truck wheel loads.

Table 37. Parameters for the 3D-FE half model with FWD load

No.	Model Parameters	Total
1	Type of Element: Eight-node solid element (C3D8R)	
2	Number of Elements	1,039,413
3	Number of Nodes	1,113,195
4	Degree of Freedom	3,313,429
5	CPU Time, sec – Window 7 Computer (Xi@MTower™-S/N: 039617; 16 GB RAM, 64-bit Operating System)	2,280
6	Peak Deflection (Load Center)	13.8 mils
7	Initial model preparation time, days	14
8	Load set up time, minutes	5

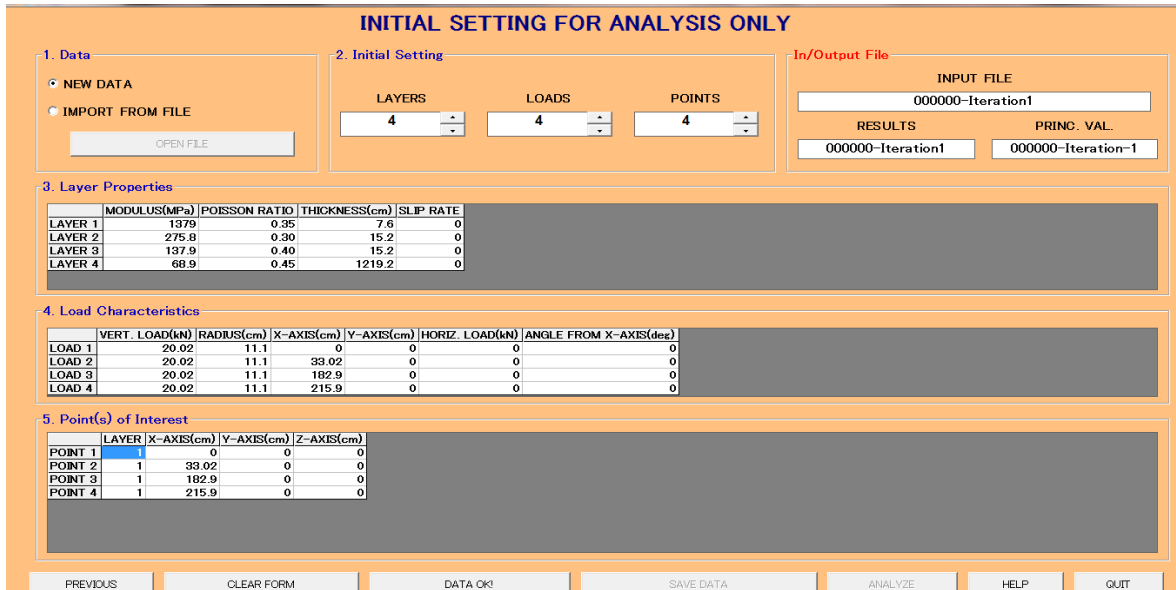


Figure 63. Example of GAMES software interface for initial set up before the structural analysis

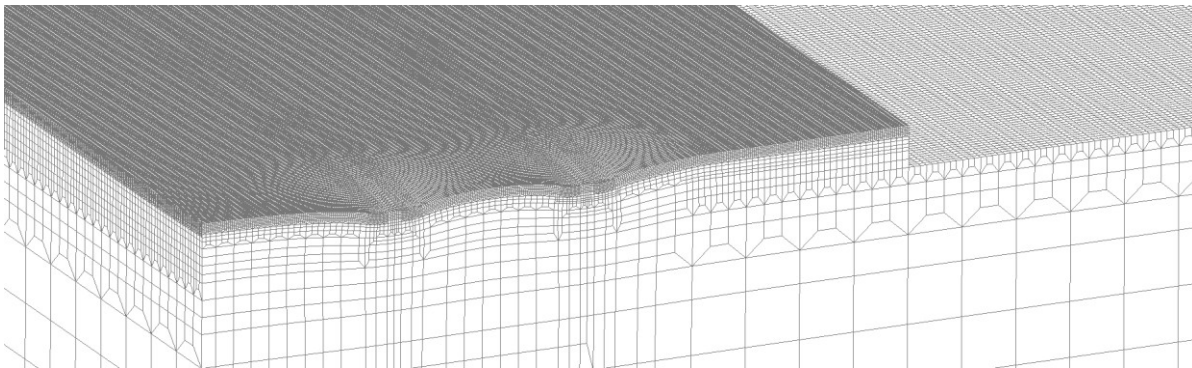


Figure 64. Deformed 3D-FE model subjected to a single axle dual tire load

Table 38. Parameters for the 3D-FE half model with 4,500 lbs truck wheel loads

No.	Model Parameters	Total
1	Type of Element: Eight-node solid element (C3D8R)	
2	Number of Elements	1,039,413
3	Number of Nodes	1,113,195
4	Degree of Freedom	3,313,429
5	CPU Time, sec - Window 7 Computer (Xi@MTower™-S/N: 039617; 16 GB RAM, 64-bit Operating System)	8,880
6	Peak Deflection (Load Center)	13.5 mils
7	Initial model preparation time, days	14
8	Load set up time, minutes	8

Table 39 shows the measured FWD peak deflection value, peak surface deflection value (13.9 mils) extracted from the 3D-FE half model developed in a previous study by Garza (2003), and surface

deflection value (13.8 mils) extracted from the 3D-FE model developed in this research. The calculated deflection value (14.3 mils) using the GAMES software was also shown in Table 39. A low error of -1.7% was calculated based on the 3D-FE model developed in this research.

Table 39. Measured and calculated peak surface deflections subjected to FWD load (normalized to 9,000 lbf)

Sensor Distance mm (in)	FWD Measured	Garza 2003 (3D-FE half model using LS-DYNA)		GAMES (Layered elastic analysis)		Fahmi's 3D-FE half model using LS-DYNA	
	Peak Deflection* $\mu\text{m}$ (mils)	Peak Deflection* $\mu\text{m}$ (mils)	% Error †	Peak Deflection* $\mu\text{m}$ (mils)	% Error †	Peak Deflection* $\mu\text{m}$ (mils)	% Error †
0 (0)	357 (14.04)	354 (13.93)	-0.8	362.6 (14.27)	1.64	350.5 (13.8)	-1.71

\* Deflections normalized to 40kN (9,000 lbf)

† Percentage error compared to the measured peak deflections

Further analysis was conducted to compare peak surface deflection values calculated using the 3D-FE model and GAMES software subjected to truck wheel loads (4,500 lbf) and the results are shown in Table 40. A low error of -4.4% was calculated for the 3D-FE model prepared with in situ modulus values. For the 3D-FE model of uncracked asphalt with various combinations of factorial design (Table 41), a maximum error of -6.5% was recorded. These low error values indicate that the 3D-FE model of uncracked asphalt pavement developed in this research is reliable, practical for asphalt pavement structural response analysis, and recommended for future studies.

Table 40. Comparison of the peak surface deflections calculated using 3D-FE and GAMES software subjected to truck wheel loads (4,500 lbf)

Center of Outside Truck Wheel Contact Area	3D-FE half model developed in this research		GAMES (Layered elastic analysis)	
Distance mm(in)	Peak Deflection* $\mu\text{m}$ (mils)	% Error**	Peak Deflection* $\mu\text{m}$ (mils)	% Error
0 (0)	342.9 (13.50)	-4.40%	358.6 (14.12)	-

\* Deflections normalized to 20kN (4,500 lbf)

\*\* Percentage error compared to the layered elastic analysis (GAMES)

Table 41. Comparison of measured and calculated peak deflections from LS-DYNA finite element software and GAMES layered elastic static analysis software (FWD load)

	Factorial Design	Thickness, in (cm)		Young's Modulus, psi (MPa)				Deflection at the center of loading area, (cm)		
		Asphalt Layer (T <sub>1</sub> )	Subbase Layer (T <sub>2</sub> )	Subgrade (E <sub>4</sub> )	Base (E <sub>2</sub> )	Subbase (E <sub>3</sub> )	Asphalt (E <sub>1</sub> )	Uncracked Pavements (3D-FE)	GAMES	% Diff.
1	000000	3 (7.6)	6 (15.2)	10,000 (68.9)	40,000 (275.8)	20,000 (137.9)	200,000 (1,379)	0.070	0.071	-1.5
2	000011	3 (7.6)	6 (15.2)	10,000 (68.9)	40,000 (275.8)	100,000 (689.5)	1,000,000 (6,894.8)	0.049	0.050	-2.9
3	000111	3 (7.6)	6 (15.2)	10,000 (68.9)	200,000 (1,379)	100,000 (689.5)	1,000,000 (6,894.8)	0.039	0.041	-4.3
4	001000	3 (7.6)	6 (15.2)	50,000 (334.7)	40,000 (275.8)	20,000 (137.9)	200,000 (1,379)	0.035	0.034	3.7
5	001011	3 (7.6)	6 (15.2)	50,000 (334.7)	40,000 (275.8)	100,000 (689.5)	1,000,000 (6,894.8)	0.021	0.021	0.4
6	001111	3 (7.6)	6 (15.2)	50,000 (334.7)	200,000 (1,379)	100,000 (689.5)	1,000,000 (6,894.8)	0.014	0.014	-3.1
7	111111	9 (22.9)	12 (30.5)	50,000 (334.7)	200,000 (1,379)	100,000 (689.5)	1,000,000 (6,894.8)	0.009	0.010	-6.5

**4.3.2. 3D-FE Modeling and Simulations using Factorial Design for Uncracked Asphalt Pavements**

The dynamic analysis is conducted for a broad range of asphalt sections representing normal and strong pavement structures. The 3D-FE half model simulated highway pavement sections that consist of four different layers namely asphalt surface, base, subbase, and soil subgrade layer. The developed 3D-FE model also considers an outside shoulder that has the combined thicknesses of asphalt, base, and subbase layers, respectively.

Six factors are considered in this full factorial experiment design for 3D-FE simulations. Each factor has two levels: medium and high, which contributes to full factorial experiment design with a total of 64 possible treatment combinations (2<sup>6</sup>). All 64 treatment combinations are used in the analysis to understand the effects of different asphalt and subbase layer thicknesses, and Young’s modulus values for all four layers on pavement responses at critical locations. The thickness of the base layer is fixed to six inches throughout the analysis since it is a requirement by MDOT for highway construction procedures. The thickness of the subgrade layer is fixed to 480 based on the successful applications in previous studies.

The treatment combinations were assigned in the following form: the first two numbers represent asphalt thickness (T<sub>1</sub>) and subbase thickness (T<sub>2</sub>) layers; the last four numbers represent the levels for Young’s modulus for subgrade (E<sub>4</sub>), base (E<sub>2</sub>), subbase (E<sub>3</sub>), and asphalt (E<sub>1</sub>) layers as shown in Figure 65. Table 42 shows the arrangement and treatment combinations used in this research. Treatment combinations 1 and 64 describe the weakest and the strongest asphalt pavements, respectively. Figure 66 to Figure 69 show the front views of model 000000, model 010000, model 100000, and model 110000, respectively. Layer thicknesses and modulus values for all 64 treatment combinations are shown in Appendix C.

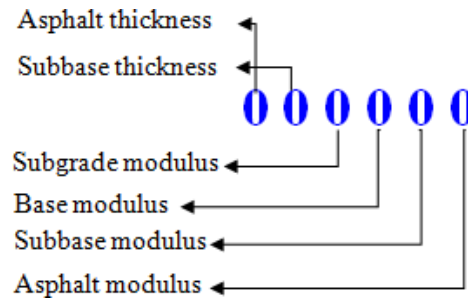


Figure 65. Treatment combination of the factorial design used for 3D-FE simulations

Table 42. Treatment combinations for full factorial experiment design (six factors and two levels) (Connor and Zelen 1959; Uddin 1984)

Levels of the factors				Layer Thickness - mm (in)				
				0 Asphalt - 76.2 (3)		1 Asphalt - 228.6 (9)		
Young's Modulus, E - MPa (ksi)				0	1	0	1	
Subgrade (SG)	Base (B)	Subbase (SB)	Asphalt (A)	Subbase - 152.4 (6)	Subbase - 304.8 (12)	Subbase - 152.4 (6)	Subbase - 304.8 (12)	
0 ESG1 - 68.9 (10)	0 EB1 - 275.8 (40)	0 ESB1 - 137.9 (20)	0 EA1 - 1,379 (200)	0 000000	1 010000	0 100000	1 110000	
			1 EA2 - 6,894.8 (1,000)	1 000001	2 010001	3 100001	4 110001	
		1 ESB2 - 689.5 (100)	0 EA1 - 1,379 (200)	9 000010	10 010010	11 100010	12 110010	
			1 EA2 - 6,894.8 (1,000)	13 000011	14 010011	15 100011	16 110011	
	1 EB2 - 1,379 (200)	0 ESB1 - 137.9 (20)	0 EA1 - 1,379 (200)	17 000100	18 010100	19 100100	20 110100	
			1 EA2 - 6,894.8 (1,000)	21 000101	22 010101	23 100101	24 110101	
		1 ESB2 - 689.5 (100)	0 EA1 - 1,379 (200)	25 000110	26 010110	27 100110	28 110110	
			1 EA2 - 6,894.8 (1,000)	29 000111	30 010111	31 100111	32 110111	
	1 ESG2 - 344.7 (50)	0 EB1 - 275.8 (40)	0 ESB1 - 137.9 (20)	0 EA1 - 1,379 (200)	33 001000	34 011000	35 101000	36 111000
				1 EA2 - 6,894.8 (1,000)	37 001001	38 011001	39 101001	40 111001
			1 ESB2 - 689.5 (100)	0 EA1 - 1,379 (200)	41 001010	42 011010	43 101010	44 111010
				1 EA2 - 6,894.8 (1,000)	45 001011	46 011011	47 101011	48 111011
1 EB2 - 1,379 (200)		0 ESB1 - 137.9 (20)	0 EA1 - 1,379 (200)	49 001100	50 011100	51 101100	52 111100	
			1 EA2 - 6,894.8 (1,000)	53 001101	54 011101	55 101101	56 111101	
		1 ESB2 - 689.5 (100)	0 EA1 - 1,379 (200)	57 001110	58 011110	59 101110	60 111110	
			1 EA2 - 6,894.8 (1,000)	61 001111	62 011111	63 101111	64 111111	

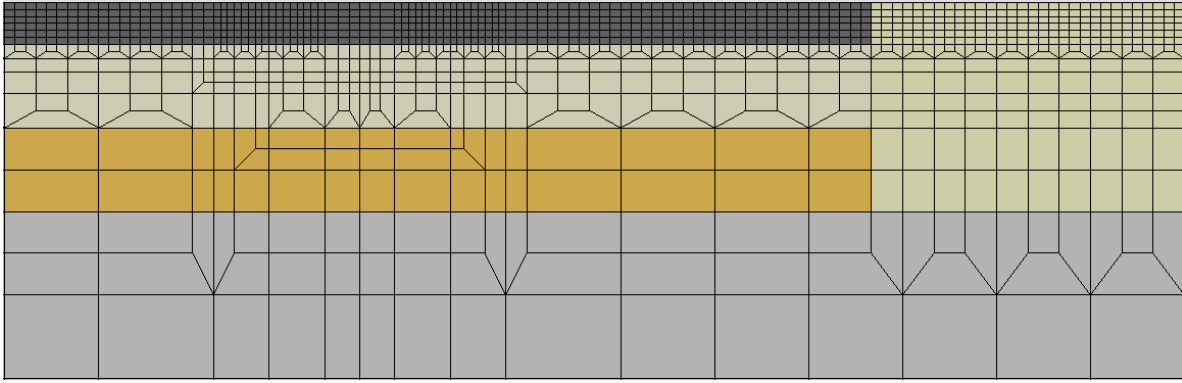


Figure 66. Front view of Model 000000 (Asphalt = 3 in, Base = 6 in, Subbase = 6 in, and Subgrade = 480 in)

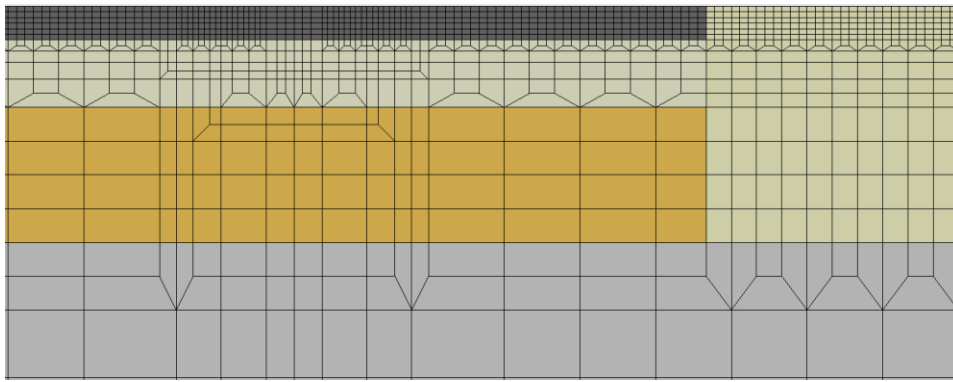


Figure 67. Front view of Model 010000 (Asphalt = 3 in, Base = 6 in, Subbase = 12 in, and Subgrade = 480 in)

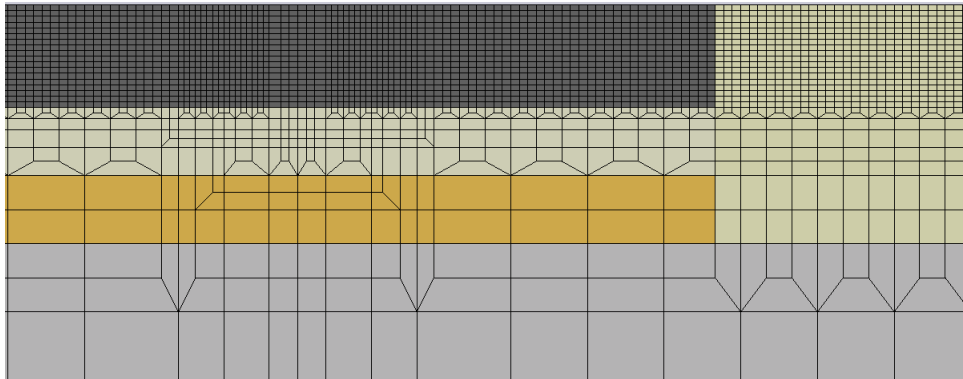


Figure 68. Front view of Model 100000 (Asphalt = 9 in, Base = 6 in, Subbase = 6 in, and Subgrade = 480 in)

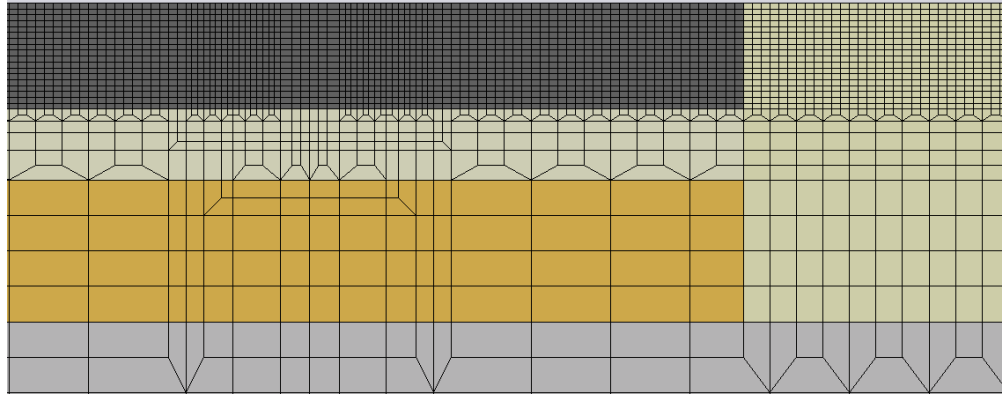


Figure 69. Front view of Model 100000 (Asphalt = 9 in, Base = 6 in, Subbase = 12 in, and Subgrade = 480 in)

### 4.3.3. Structural Response Database using 3D-FE Simulations of Uncracked Pavements Subjected to Axle Truck Loading

In this research, the analysis requires a large number of 3D-FE dynamic analyses using the LS-DYNA software to generate a comprehensive asphalt pavement structural responses database for asphalt pavement thickness design. Those structural responses are surface deflections, stresses, and strains at a few critical pavement response locations as follows and illustrated in Figure 70.

- Asphalt pavement surface deflection under loading area
- Compressive vertical stress in the middle of the asphalt layer
- Tensile horizontal strain at the bottom of the asphalt layer
- Compressive vertical strain in the middle of the base layer
- Tensile horizontal strain at the bottom of the base layer
- Compressive vertical stress in the middle of the subbase layer
- Compressive vertical strain on top of the subgrade

## Critical Pavement Response Locations

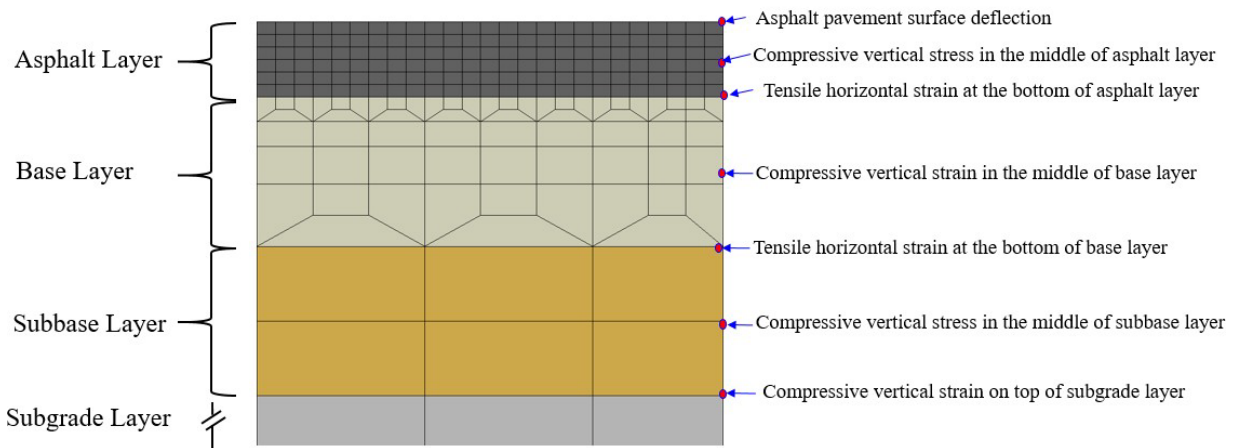


Figure 70. Critical asphalt pavement response locations



These structural responses are required for the following purposes:

- Asphalt pavement surface deflection under loading area is important for backcalculation of asphalt pavement modulus value.
- Compressive vertical stress in the middle of the asphalt layer, compressive vertical strain in the middle of the base layer, compressive vertical stress in the middle of the subbase layer, and compressive vertical strain on top of subgrade are important for rutting distress evaluation in the mechanistic-empirical pavement design method.
- Tensile horizontal strain at the bottom of the asphalt layer and tensile horizontal strain at the bottom of the base layer is important for the assessment of load-related cracking such as alligator crack and longitudinal crack.

The full factorial simulations were conducted for low and high levels and the surface deflections, stresses, and strains for all treatment combinations of uncracked asphalt are summarized in Table 43. Cells highlighted in yellow color indicate maximum values, while cells highlighted in blue color describe the minimum values for all pavement responses extracted from the 3D-FE analysis.

However, for future research, it is recommended to create a full factorial design of uncracked pavements by including a medium level of thickness and a medium level of modulus values for asphalt, base, subbase, and subgrade layers too. Once more data sets are compiled, the structural response prediction equations using the 3D-FE response database will be developed and these equations will provide an easier approach to predict structural responses in asphalt pavement layers.

Further analysis was conducted to assess the effects of thickness and modulus values on asphalt pavement surface deflection response. The selected treatment combinations, asphalt and base layer thicknesses, and modulus values for asphalt, base, subbase, and subgrade layers are shown in Table 44. Similar datasets were used to develop asphalt surface deflection plots at a low and high level of modulus values for all four layers (Figure 71).

Table 43. Surface deflections, stresses, and strains for all treatment combinations of uncracked asphalt

Uncracked Asphalt Pavement Responses Full Factorial Design (2 <sup>6</sup> )		1		2	3	4	5	6	7
		Surface Deflection at the center of loading area		Compressive vertical stress in the middle of asphalt layer (psi)	Tensile horizontal strain at the bottom of asphalt layer (=1000)	Compressive vertical stress in the middle of base layer (psi)	Tensile horizontal strain at the bottom of base layer (=1000)	Compressive vertical stress in the middle of subbase layer (psi)	Compressive vertical strain on top of subgrade layer (=1000)
		No.	Treatment Combinations	mils	inches				
1	000000	27.6	0.028	80.5	0.26750	23.7	0.19791	8.4	0.53100
2	010000	26.1	0.026	80.5	0.26600	24.3	0.18291	7.2	0.35950
3	100000	18.8	0.019	22.9	0.17200	7.0	0.09522	3.7	0.26450
4	110000	18.2	0.018	49.2	0.09375	7.4	0.08814	3.4	0.20050
5	000001	22.8	0.023	66.0	0.12900	14.6	0.14872	6.5	0.43700
6	010001	21.6	0.022	66.2	0.12550	15.2	0.13593	5.7	0.30950
7	100001	13.5	0.014	44.8	0.21695	3.3	0.04394	2.1	0.15100
8	110001	13.1	0.013	45.1	0.03830	3.5	0.04114	2.0	0.12700
9	000010	23.2	0.023	81.4	0.24900	28.0	0.07378	8.3	0.37150
10	010010	20.2	0.020	81.5	0.25400	29.8	0.06548	7.9	0.22600
11	100010	16.8	0.017	50.0	0.07980	8.8	0.03809	3.7	0.20250
12	110010	15.2	0.015	50.4	0.07445	10.2	0.02845	3.8	0.14300
13	000011	19.1	0.019	67.1	0.11300	17.8	0.05219	6.3	0.31550
14	010011	16.5	0.017	67.4	0.10850	19.6	0.04090	6.3	0.20100
15	100011	12.5	0.013	45.6	0.03450	4.2	0.02120	2.2	0.12750
16	110011	11.5	0.012	45.9	0.03155	5.1	0.01517	2.3	0.10130
17	000100	21.0	0.021	93.3	0.04800	25.5	0.10550	5.9	0.37500
18	010100	20.1	0.020	93.3	0.51000	26.1	0.09797	5.2	0.28100
19	100100	16.3	0.016	53.4	0.03440	8.5	0.05833	2.9	0.19900
20	110100	15.9	0.016	53.5	0.03375	7.9	0.05511	2.7	0.16000
21	000101	17.8	0.018	79.4	0.00035	16.8	0.09415	4.4	0.29550
22	010101	17.1	0.017	79.3	0.05620	17.2	0.08810	4.0	0.22550
23	100101	12.3	0.012	48.0	0.02560	4.0	0.03644	1.9	0.12850
24	110101	12.1	0.012	48.0	0.02500	4.2	0.03497	1.8	0.10950
25	000110	18.0	0.018	93.9	0.05345	31.1	0.05210	6.3	0.28550
26	010110	15.6	0.016	94.0	0.06310	32.9	0.04036	6.2	0.18450
27	100110	14.9	0.015	54.1	0.02815	10.1	0.03337	3.1	0.16750
28	110110	13.6	0.014	54.4	0.02725	11.6	0.02547	3.3	0.12150
29	000111	15.3	0.015	80.1	0.05130	21.5	0.05109	4.8	0.23300
30	010111	13.4	0.013	80.4	0.05125	23.4	0.03925	4.9	0.15600
31	100111	11.5	0.012	48.7	0.02165	5.5	0.02445	2.0	0.11550
32	110111	10.6	0.011	49.0	0.01965	6.6	0.01951	2.1	0.09010
33	001000	13.6	0.014	80.9	0.27800	26.1	0.16683	12.7	0.16250
34	011000	14.8	0.015	80.8	0.27900	25.4	0.17824	9.8	0.11200
35	101000	8.7	0.009	26.6	0.48128	9.1	0.07570	6.2	0.08475
36	111000	9.2	0.009	49.6	0.09085	8.6	0.00380	5.0	0.34180
37	001001	10.0	0.010	66.7	0.12100	17.1	0.11511	10.3	0.07689
38	011001	11.0	0.011	66.5	0.12388	16.4	0.12558	8.1	0.09720
39	101001	4.9	0.005	24.7	0.03456	4.8	0.03533	3.7	0.04915
40	111001	5.3	0.005	45.5	0.03574	4.5	0.03809	3.2	0.03931
41	001010	11.2	0.011	81.7	0.26701	30.1	0.07766	12.9	0.15136
42	011010	10.7	0.011	81.7	0.26782	30.6	0.07639	10.6	0.09809
43	101010	7.6	0.008	50.5	0.07590	10.9	0.03261	6.4	0.08456
44	111010	7.4	0.007	52.1	0.07490	11.3	0.03079	5.7	0.06180
45	001011	8.1	0.008	67.6	0.11029	20.1	0.04729	10.5	0.13028
46	011011	7.7	0.008	67.7	0.10927	20.6	0.04529	8.9	0.08889
47	101011	4.4	0.004	46.2	0.03065	5.8	0.01664	4.0	0.05285
48	111011	4.5	0.005	48.4	0.02360	5.1	0.03118	2.8	0.03495
49	001100	8.7	0.009	93.6	0.06871	2.8	0.08202	9.7	0.12075
50	011100	9.5	0.009	93.5	0.06576	27.2	0.08882	7.6	0.08855
51	101100	7.0	0.007	53.8	0.03411	9.5	0.04596	5.2	0.06836
52	111100	7.5	0.007	53.7	0.03487	9.0	0.04942	4.2	0.05165
53	001101	6.8	0.007	79.8	0.05766	19.2	0.07122	7.7	0.09913
54	011101	7.5	0.007	79.7	0.05810	18.5	0.07719	6.1	0.07257
55	101101	4.3	0.004	48.5	0.02283	5.4	0.12339	3.4	0.04458
56	111101	4.5	0.005	48.4	0.02360	5.1	0.03118	2.8	0.03495
57	001110	7.0	0.007	94.15	0.07269	33.1	0.04433	10.4	0.12429
58	011110	6.7	0.007	94.20	0.07523	33.7	0.04189	8.7	0.08288
59	101110	6.2	0.006	54.5	0.02959	12.0	0.02602	5.6	0.07567
60	111110	6.1	0.006	54.5	0.02977	12.5	0.02422	5.0	0.05426
61	001111	5.5	0.005	80.6	0.05373	23.7	0.03969	8.4	0.10624
62	011111	5.2	0.005	80.7	0.05392	0.7	0.03690	7.2	0.07198
63	101111	3.7	0.00374	49.2	0.01944	7.1	0.01890	3.7	0.05258
64	111111	3.6	0.00364	49.3	0.01896	7.5	0.01736	3.4	0.03995
Average		12.2	0.0122	63.9	0.10040	14.8	0.06313	5.6	0.15704
SD		5.9	0.0	18.7	0.1	9.4	0.0	2.8	0.1
COV (%)		48.5	48.5	29.2	105.0	63.4	69.9	49.4	68.9
Tension (+), Compression (-)		+	+	-	+	-	+	-	-
Minimum		3.6	0.004	22.9	0.00035	0.7	0.00380	1.8	0.03495
Maximum		27.6	0.028	94.2	0.51000	33.7	0.19791	12.9	0.53100

Table 44. Surface deflection values for various treatment combinations

<b>Low and high ASPHALT modulus and constant modulus values for base, subbase, subgrade layers</b>									
Sequence no. (database)	Treatment combination	Uncracked pavement Low Level Factorial Design (0)							
		Asphalt (T1)	Subbase (T2)	Subgrade (E4)	Base (E2)	Subbase (E3)	Asphalt (E1)	mils	inches
1	000000	3	6	10,000	40,000	20,000	200,000	27.6	0.0280
5	000001	3	6	10,000	40,000	20,000	1,000,000	22.8	0.0228
3	100000	9	6	10,000	40,000	20,000	200,000	18.8	0.0190
7	100001	9	6	10,000	40,000	20,000	1,000,000	13.5	0.0135
Sequence no. (database)	Treatment combination	Uncracked pavement High Level Factorial Design (1)							
		Asphalt (T1)	Subbase (T2)	Subgrade (E4)	Base (E2)	Subbase (E3)	Asphalt (E1)	mils	inches
57	001110	3	6	50,000	200,000	100,000	200,000	7.0	0.007
61	001111	3	6	50,000	200,000	100,000	1,000,000	5.5	0.005
59	101110	9	6	50,000	200,000	100,000	200,000	6.2	0.006
63	101111	9	6	50,000	200,000	100,000	1,000,000	3.7	0.004

<b>Low and high SUBBASE modulus and constant modulus values for asphalt, base, subgrade layers</b>									
Sequence no. (database)	Treatment combination	Uncracked pavement Low Level Factorial Design (0)							
		Asphalt (T1)	Subbase (T2)	Subgrade (E4)	Base (E2)	Subbase (E3)	Asphalt (E1)	mils	inches
1	000000	3	6	10,000	40,000	20,000	200,000	27.6	0.0280
9	000010	3	6	10,000	40,000	100,000	200,000	23.2	0.0230
2	010000	3	12	10,000	40,000	20,000	200,000	26.1	0.0260
10	010010	3	12	10,000	40,000	100,000	200,000	20.2	0.0200
Sequence no. (database)	Treatment combination	Uncracked pavement High Level Factorial Design (1)							
		Asphalt (T1)	Subbase (T2)	Subgrade (E4)	Base (E2)	Subbase (E3)	Asphalt (E1)	mils	inches
53	001101	3	6	50,000	200,000	20,000	1,000,000	6.8	0.007
61	001111	3	6	50,000	200,000	100,000	1,000,000	5.5	0.005
54	011101	3	12	50,000	200,000	20,000	1,000,000	7.5	0.007
62	011111	3	12	50,000	200,000	100,000	1,000,000	5.2	0.005

<b>Low and high BASE modulus and constant modulus values for asphalt, subbase, subgrade layers</b>									
Sequence no. (database)	Treatment combination	Uncracked pavement with low modulus values for asphalt, subbase, subgrade layers							
		Asphalt (T1)	Subbase (T2)	Subgrade (E4)	Base (E2)	Subbase (E3)	Asphalt (E1)	mils	inches
1	000000	3	6	10,000	40,000	20,000	200,000	27.6	0.0280
17	000100	3	6	10,000	200,000	20,000	200,000	21.0	0.0210
45	001011	3	6	50,000	40,000	100,000	1,000,000	8.1	0.0080
61	001111	3	6	50,000	200,000	100,000	1,000,000	5.5	0.0050

<b>Low and high SUBGRADE modulus and constant modulus values for asphalt, base, subbase layers</b>									
Sequence no. (database)	Treatment combination	Uncracked pavement with low modulus values for asphalt, subbase, subgrade layers							
		Asphalt (T1)	Subbase (T2)	Subgrade (E4)	Base (E2)	Subbase (E3)	Asphalt (E1)	mils	inches
1	000000	3	6	10,000	40,000	20,000	200,000	27.6	0.0280
33	000100	3	6	50,000	40,000	20,000	200,000	13.6	0.0140
29	000111	3	6	10,000	200,000	100,000	1,000,000	15.3	0.0150
64	001111	3	6	50,000	200,000	100,000	1,000,000	3.6	0.0036

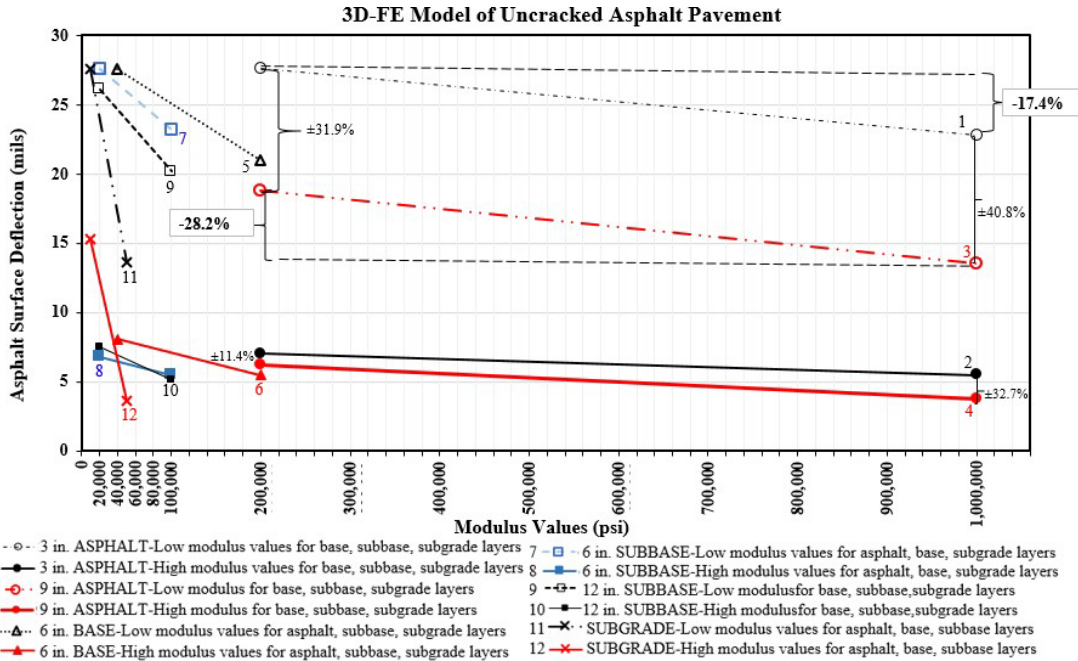


Figure 71. Asphalt surface deflections based on low and high modulus and thickness levels

Key findings from the analysis follow:

- The effect of layer thickness on surface deflection is greater as compared to the effect of asphalt modulus value, for asphalt layers with a weak base, subbase, and subgrade layers. The surface deflection values differ by 36.4% (average) due to asphalt layer thickness changes, as compared to 21.1% (average) change of surface deflection value due to low and high levels of asphalt modulus values.
- However, the effect of modulus value is greater as compared to the effect of asphalt layer thickness for the asphalt layer with a strong base, subbase, and subgrade layers. The surface deflection values differ by 30.9% (average) due to low and high levels of asphalt modulus values, as compared to only 22.1% (average) change in surface deflection value due to different asphalt layer thicknesses.

#### 4.4. 3D-FE Modeling of Longitudinal Crack in Asphalt Pavements

##### 4.4.1. Modeling of Cracked Element Using LS-DYNA Software

The modeling of the cracked element in the asphalt layer is another important contribution of this research. The following approaches are evaluated in this research to simulate the cracked area:

- 1) Initial or trial approach to developing cracked conditions using the existing spring element in the LS-DYNA software.
- 2) Final or selected approach to simulate cracked area in the LS-DYNA software.

#### 4.4.2. Initial or Trial Approach using Spring Element

In this trial run, the 3D-FE model with an uncracked asphalt surface layer was used to test the capability of the spring element to simulate discontinuity in the asphalt layer. Two spring elements were introduced at the symmetry area of the left and right sides asphalt layer. Those two spring elements were placed at the top of the first asphalt layer and at the bottom of the sixth asphalt layer to simulate full depth, as shown in Figure 72. The parameters used in the model and the deflection value from the trial runs are shown in Table 45 and Table 46. The thickness and modulus values for the in situ, low-level model and high-level model are shown in Table 47. The major findings from the trial run are following:

- Table 45 shows that the low-level model (Model 000000) has the highest deflection value of 27.6 mils compared to the high-level model (Model 111111) and in situ condition.
- The high-level model (Model 111111) shows approximately 87% less deflection compared to the low-level model (Model 000000)
- This trial run was conducted to evaluate if the use of spring elements is an appropriate approach to simulate the discontinuity of the asphalt layer.
- An additional run was conducted for uncracked asphalt layer using elastic spring constant,  $k$  calculated using the deflection value of model 000000 (Table 46).
- The analysis shows that the observed deflection values for models with the spring element are the same as the deflection value obtained from uncracked pavement without the spring element.

Therefore, the proposal of using the spring element in the LS-DYNA to simulate a cracked asphalt layer was not accepted and replaced with another cracked simulation approach.

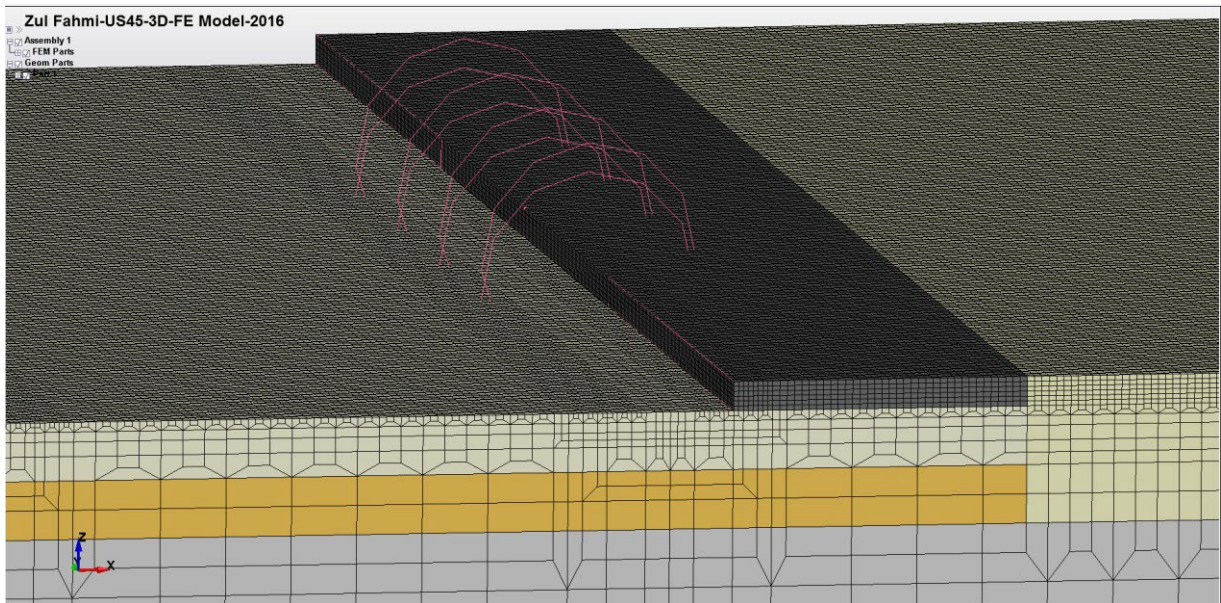


Figure 72. Trial run with two spring elements on top and bottom of asphalt layer to simulate full depth cracked condition

Table 45. Uncracked asphalt layer subjected to dynamic wheel load for models 000000 and 11111 without the spring element on top and bottom of the asphalt layer

No.	Model Parameters for <b>Uncracked</b> Asphalt Layer	Model 000000	Model 111111
1	Type of element	Eight-node solid element (C3D8R)	
2	Number of elements	1,039,413	2,488,835
3	Number of nodes	1,113,195	2,571,316
4	Degree of freedom	3,313,429	7,677,534
5	CPU Time, (Xi@MTower <sup>TM</sup> -S/N:039617; 16 GB RAM, 64-bit Operating System)	1 hour 49 minutes	4 hours 5 minutes
6	Initial model preparation time, days	14	
7	Load set up time, minutes	8	
8	Asphalt pavement surface deflection (Load center), mils	27.6	3.60

Table 46. Uncracked asphalt layer subjected to dynamic wheel load for In Situ Condition and Model 000000 with spring element on top and bottom of the asphalt layer

No.	Model Parameters for <b>Uncracked</b> Asphalt Layer	In situ	Model 000000
1	Type of element	Eight-node solid element (C3D8R)	
2	Number of elements	1,039,413	
3	Number of nodes	1,113,195	
4	Degree of freedom	3,313,429	
5	CPU Time, (Xi@MTower <sup>TM</sup> -S/N: 039617; 16 GB RAM, 64-bit Operating System)	2 hours 46 minutes	1 hour 49 minutes
6	Elastic spring constant, k (psi/in)	7,299.3	4,739.3
7	Elastic spring constant, k used in LS-DYNA (force/deformation), lb-f/in	164,233.6	106,635.1
8	Asphalt pavement surface deflection (load center), mils	13.7	27.6

Table 47. Pavement structures for in situ, low-level Model 000000, and high-level Model 111111

Layers	In situ value	Model 000000	Model 111111
Asphalt Layer	$T_1 = 3$ in	$T_1 = 3$ in	$T_1 = 9$ in
	$E_1 = 332.2$ ksi	$E_1 = 200$ ksi	$E_1 = 1,000$ ksi
	6 in. (fixed)		
Base Layer	$E_2 = 132.5$ ksi	$E_2 = 40$ ksi	$E_2 = 200$ ksi
	$T_2 = 6$ in	$T_2 = 6$ in	$T_2 = 12$ in
Subbase Layer	$E_3 = 40.8$ ksi	$E_3 = 20$ ksi	$E_3 = 100$ ksi
Subgrade Layer	480 in (fixed)		
	$E_4 = 17.74$ ksi	$E_4 = 10$ ksi	$E_4 = 50$ ksi

#### 4.4.3. Development of Cracked Layer using Solid Element

The cracked layer in the 3D-FE cracked asphalt model was developed using the eight-node solid element. The crack layer simulates longitudinal crack with a gap of 0.5-inch in width. It was assumed that the opening of the crack has a constant gap from top to bottom. This research proposes the modeling of longitudinal cracks at different depth level, which is top one-third, middle one-third, bottom one-third, and full depth cracks in the asphalt pavement layer. Figure 73 to Figure 76 show the cracked element for different depth levels. Both pre and postprocessing conditions are shown next.

It is important to know that the deflections are extracted from the NODOUT file under z-displacement, which means the deflection in vertical directions. On the other hand, the stress, and strain values are extracted from the ELOUT file. For example, if the compressive stress values at a certain element are required, the stress values are then extracted from the “sig-zz” column. The “sig-zz” explains the sigma, which is the symbol of stress, and “zz” describes the measurement at the z-direction. Additionally, the strain values are extracted from the “eps-zz” column. The “eps” explains the epsilon, which is the symbol for strain.

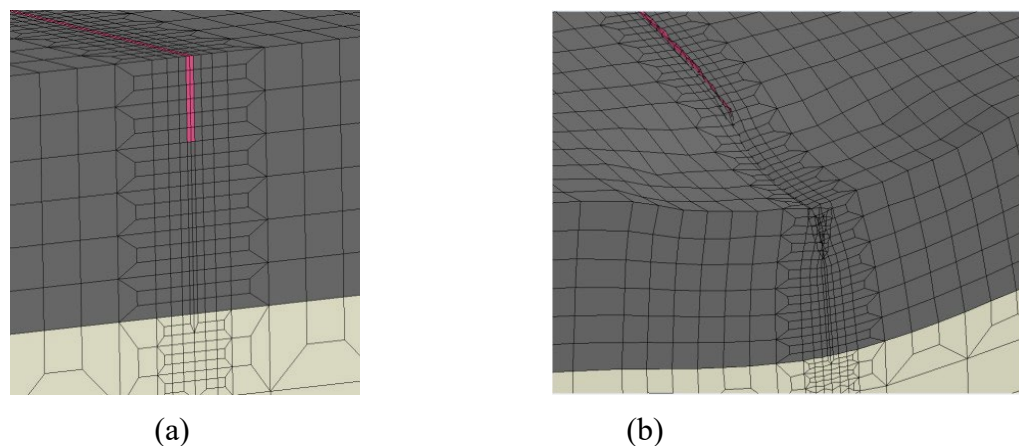


Figure 73. Undeformed (a) and deformed (b) models for the top one-third cracked from overall asphalt thickness

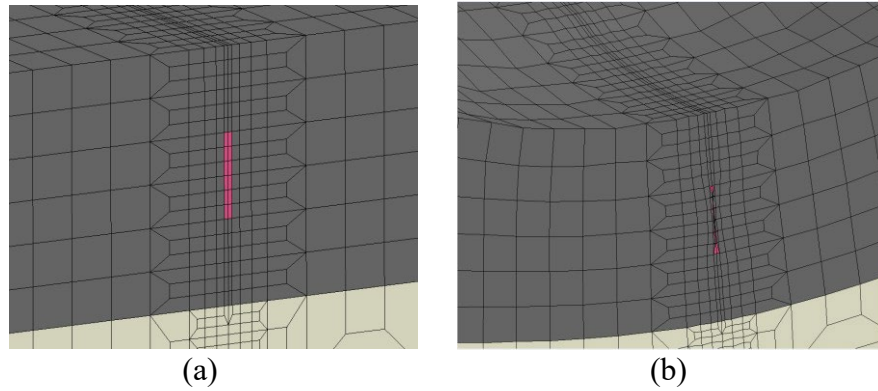


Figure 74. Undeformed (a) and deformed (b) models for the middle one-third cracked from overall asphalt thickness

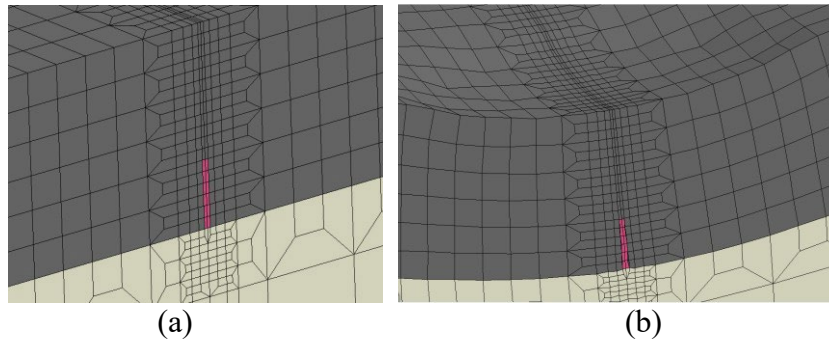


Figure 75. Undeformed (a) and deformed (b) models for the bottom one-third cracked from overall asphalt thickness

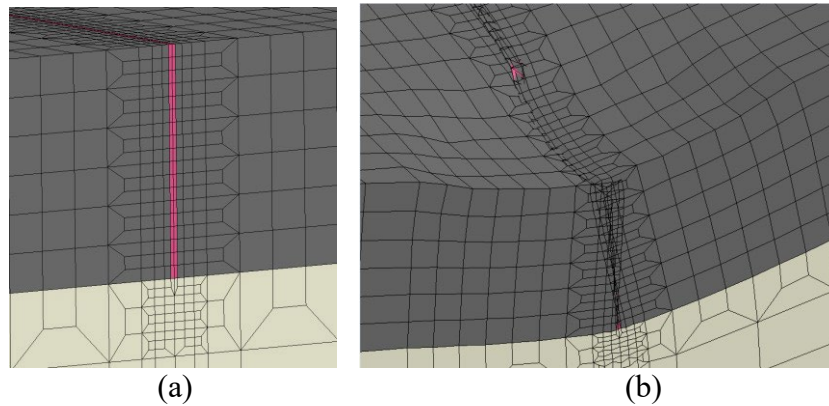


Figure 76. Undeformed (a) and deformed (b) models for the full cracked asphalt layer

In the LS-DYNA software, the stress and strain values are measured at the centroid of the solid element (Livermore 2022). Therefore, the stress and strain values reported in this research are the average of two elements on the left and right sides of the centerline (dash-dash line in Figure 77).



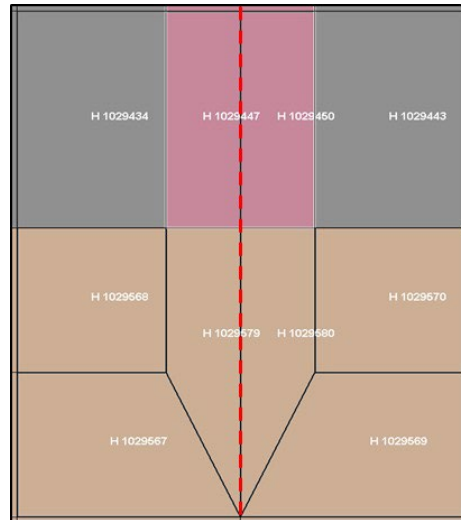


Figure 77. Close up view of the elements close to the centerline of the loading area

The required stress and strain values, for example at the asphalt surface layer, are measured slightly below the surface of the asphalt layer. This implies that the stress and strain depend on the configurations of the elements, which include the ratio between the height and width of a solid element. Thus, it is important to ensure that the element has a reasonable height and width ratio of one over two (1:2) for a more accurate response value. The responses under the wheel load at the cracked areas are also influenced by the responses intrigued by the nearby wheel load as seen in Figure 78. The model developed in this research simulates the actual loading configuration of a single axle truck with two tires on each side.

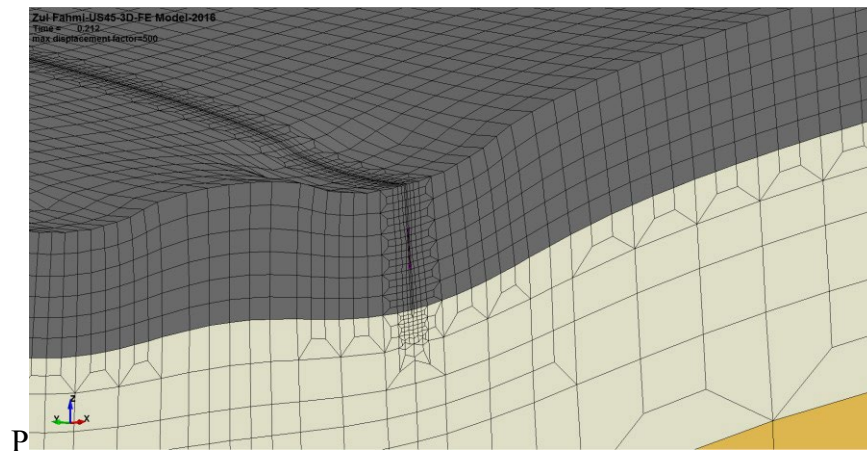


Figure 78. Example of the deformed cracked model with dual tires on each side

#### 4.4.4. Parametric Study Conducted to Determine Modulus Value for the Cracked Layer

Earlier in this research, parametric studies were conducted to determine the modulus value for cracked elements in the 3D-FE cracked model. The modulus value for the cracked layer must be lower than the surrounding asphalt modulus. Key steps to determine the modulus value for the cracked layer follows:

- 1) This research proposed to provide the modulus value for the cracked layer in the 3D-FE, based on the deflection ratios of uncracked and cracked asphalt layers. Therefore, the FWD data was extracted from the LTPP database and the deflection values for test section 28-3085 were evaluated. Table 48 shows FWD data from 1995 and Figure 79 shows an example of a distress map from the LTPP database only for the first 15-meter lengths of the surveyed test section. Multiple block cracks, longitudinal cracks, and transverse cracks were observed on the road surfaces. Based on the best visual assessments, the uncracked and cracked surface conditions were noted and recorded for further analysis. A similar approach was implemented for uncracked and cracked conditions in 2003 as shown in Table 49 and Figure 80.

Table 48. Summary of FWD data for the LTPP section 28-3085 and asphalt surface conditions in 1995

State: Mississippi (28-3085), Test date: 11/9/1995, Deflection Unit ID: 8002-132, CN:1, Drop Number: 2										
No	Point Location	Pavement Surface Temperature (°C)	Drop Load				Pead Deflection (Sensor 1)			Asphalt Surface Condition
			kPa	psi	lbs	Factor (9,000 lbs / measured loads)	Micron	Mils	Normalized to 9,000 lbs (mils)	
1	0	9	570.5	82.7	9081	0.99	470	18.5	18.3	Cracked
2	8.2	9	555	80.5	8834	1.02	669	26.3	26.8	Cracked
3	15.2	10	561	81.4	8930	1.01	578	22.8	22.9	Cracked
4	22.9	11	567.8	82.3	9037	0.99	673	26.5	26.4	Cracked
5	31.1	11	565.8	82.1	9005	0.99	587	23.1	23.1	Cracked
6	38.7	12	561.3	81.4	8934	1.01	589	23.2	23.3	<b>Uncracked</b>
7	45.7	13	555.5	80.6	8842	1.02	921	36.2	36.9	Cracked
8	53.9	12	545.5	79.1	8683	1.04	825	32.5	33.7	Cracked
9	61.6	13	552.8	80.2	8798	1.02	492	19.4	19.8	Cracked
10	69.2	13	549	79.6	8739	1.03	572	22.5	23.2	Cracked
11	76.8	14	550	79.8	8754	1.03	496	19.5	20.1	Cracked
12	83.8	15	552.8	80.2	8798	1.03	513	20.2	20.7	Cracked
13	92	15	558.5	81	8890	1.02	588	23.1	23.4	Cracked
14	99.1	15	564.5	81.9	8985	1.01	436	17.2	17.2	Cracked
15	106.7	15	562.3	81.5	8949	1.01	408	16.1	16.1	Cracked
16	114.3	11	564.3	81.8	8981	1	370	14.5	14.6	Cracked
17	122.5	13	568.5	82.5	9049	0.99	262	10.3	10.3	<b>Uncracked</b>
18	129.5	13	576	83.5	9168	0.98	200	7.9	7.7	Cracked
19	137.2	8	563.3	81.7	8965	1	323	12.7	12.8	Cracked
20	145.4	10	535.8	77.7	8528	1.06	746	29.4	31	Cracked
21	152.4	11	546	79.2	8691	1.04	613	24.1	25	Cracked

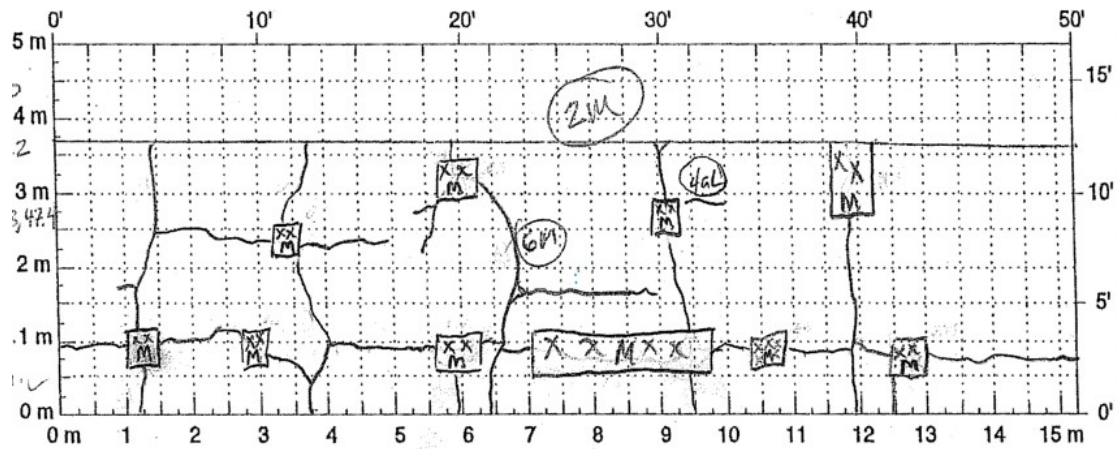


Figure 79. Example of the LTPP manual distress survey manual sketch (Test date: 11/9/1995)

Table 49. FWD data for the LTPP test section 28-3085 and asphalt surface conditions in 2003

State: Mississippi (28-3085), Test date: 3/7/2003, Deflection Unit ID: 8002-132, CN:3, Drop Number: 2										
No	Point Location	Pavement Surface Temperature (°C)	Drop Load				Pead Deflection (Sensor 1)			Asphalt Surface Condition
			kPa	psi	lbs	Factor (9,000 lbs / measured loads)	Micron	Mils	Normalized to 9,000 lbs (mils)	
1	0	7.3	571	82.8	9085	0.99	395	15.5	15.4	Uncracked
2	7.6	8	550	79.7	8746	1.03	538	21.2	21.8	Uncracked
3	15.2	7.8	559	81.1	8898	1.01	465	18.3	18.5	Uncracked
4	22.9	7.8	546	79.2	8691	1.04	578	22.7	23.6	Uncracked
5	30.5	9.6	537	77.9	8568	1.05	746	29.4	30.9	Uncracked
6	38.1	9.6	548	79.5	8723	1.03	692	27.2	28.1	Uncracked
7	45.7	9.8	540	78.4	8599	1.05	863	34	35.6	Cracked
8	53.3	11.3	545	79	8675	1.04	732	28.8	29.9	Cracked
9	61	10.5	540	78.3	8591	1.05	605	23.8	25	Cracked
10	68.6	11.4	538	78.1	8567	1.05	747	29.4	30.9	Cracked
11	76.2	11.5	540	78.3	8591	1.05	564	22.2	23.3	Cracked
12	83.8	10.9	534	77.5	8500	1.06	608	23.9	25.3	Cracked
13	91.4	11.7	552	80	8782	1.02	598	23.5	24.1	Cracked
14	99.1	13.3	543	78.7	8635	1.04	557	21.9	22.8	Cracked
15	106.7	13.2	543	78.8	8647	1.04	473	18.6	19.4	Cracked
16	114.3	5.7	541	78.4	8603	1.04	421	16.6	17.3	Uncracked
17	121.9	13.7	552	80.1	8786	1.02	293	11.5	11.8	Uncracked
18	129.5	9.2	560	81.2	8914	1.01	394	15.5	15.7	Uncracked
19	137.2	7.2	559	81.1	8902	1.01	231	9.1	9.2	Cracked
20	144.8	9.4	556	80.6	8842	1.02	444	17.5	17.8	Uncracked
21	152.4	12.2	539	78.2	8583	1.05	698	28.8	28.8	Uncracked

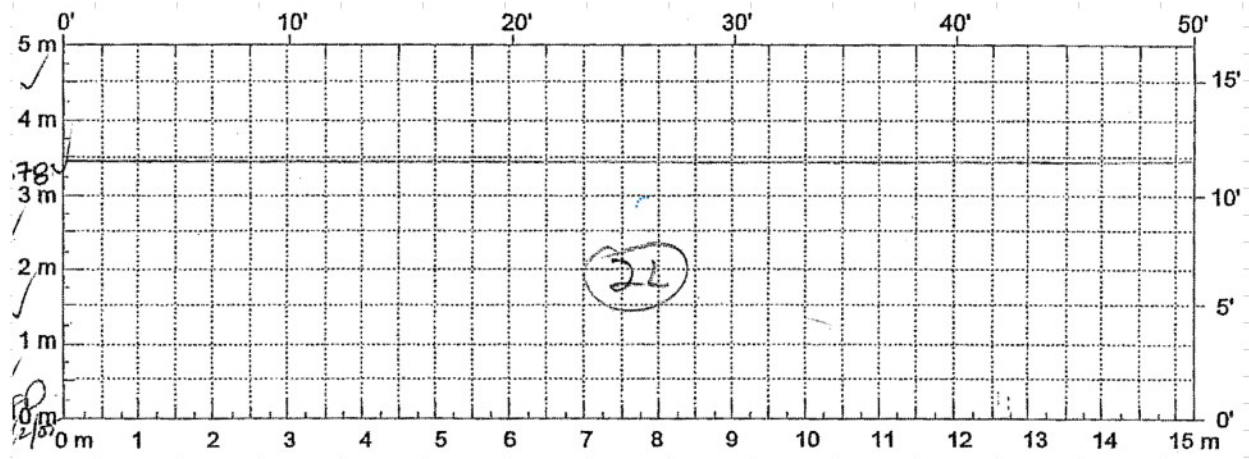


Figure 80. Example of manual distress survey manual sketch (Test date: 03/07/2003)

2) Table 50 shows sensor one peak deflection ratios between uncracked and cracked conditions.

Table 50. Peak deflection ratios between uncracked and cracked pavement for the LTPP test section 28-3085 (deflections normalized to 9,000 lbs.)

No.	SHRP ID	Test Date: 11/9/1995		Test Date: 3/7/2003		Peak deflection ratio between cracked and uncracked pavements	
		Deflections normalized to 9,000 lbs. (mils)	Asphalt Surface Condition	Deflections normalized to 9,000 lbs. (mils)	Asphalt Surface Condition		
1	28-3085	18.3	Cracked	15.4	Uncracked	1.19	
2	28-3085	26.8	Cracked	21.8	Uncracked	1.23	
3	28-3085	22.9	Cracked	18.5	Uncracked	1.24	
4	28-3085	26.4	Cracked	23.6	Uncracked	1.12	
5	28-3085	23.1	Cracked	30.9	Uncracked	0.75	
16	28-3085	14.6	Cracked	17.3	Uncracked	0.84	
18	28-3085	7.7	Cracked	15.7	Uncracked	0.49	
20	28-3085	31	Cracked	17.8	Uncracked	1.74	
21	28-3085	25	Cracked	28.8	Uncracked	0.87	
Test Section 28-3085 in Mississippi						Mean	1.1
						SD	0.4
						COV (%)	34.4

The first 15-meter length of the surveyed test section in 2003 (Figure 80) shows no crack due to maintenance intervention. Figure 81 plot shows peak deflection ratios between uncracked and cracked asphalt pavements for nine selected data points in the LTPP test section. The calculated peak deflection ratio means is 1.1 with a standard deviation of 0.4 and a COV of 34.4%.

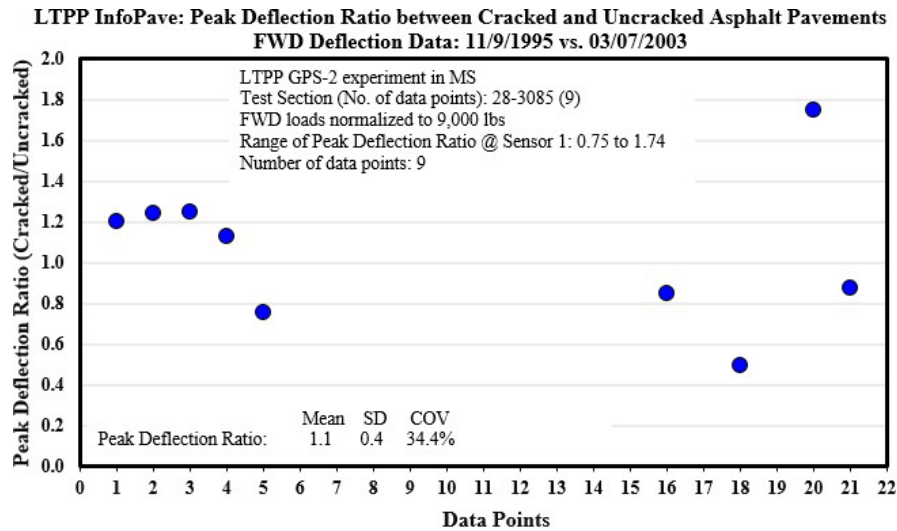


Figure 81. Peak deflection ratios plot of uncracked and cracked pavement for the LTPP test section 28-3085 (deflections normalized to 9,000 lbs.)

- 3) Several values of low modulus of cracked asphalt layer (1,000 to 5,000 psi) and high modulus values of cracked asphalt layer (100,000 to 500,000 psi) were used to calculate the surface deflections. Figure 82 plots the calculated surface deflections for selected cracked layer modulus values.

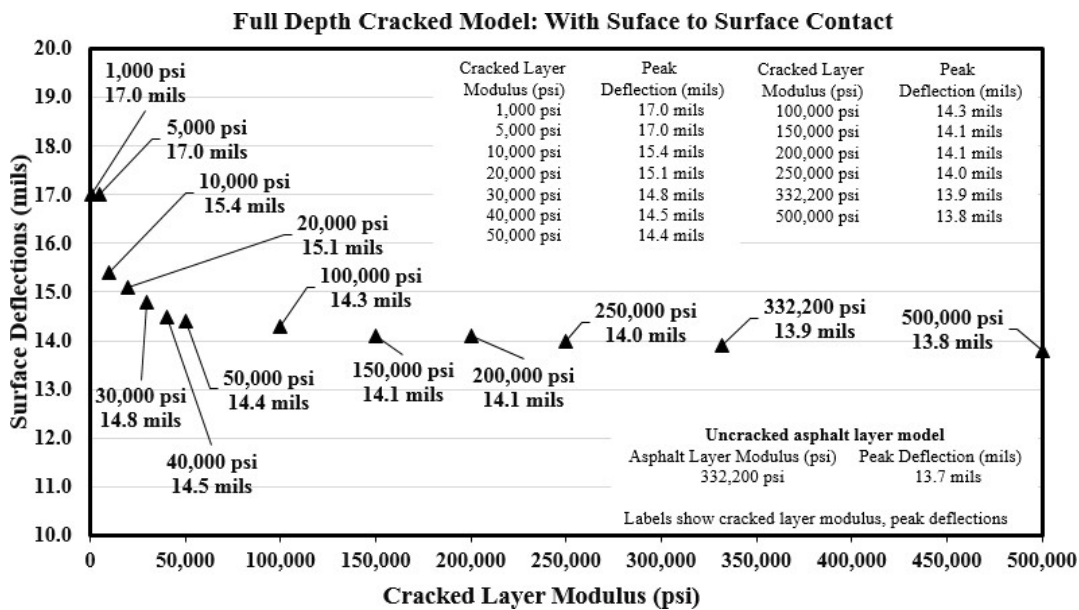


Figure 82. Surface deflections correspond to various cracked layer modulus

- 4) The peak deflection values for cracked models were divided by the peak deflection of the uncracked model of 13.7 mils for in situ conditions with a 332,200-psi modulus value. The resulting peak deflection ratios of cracked and uncracked pavements were summarized in Table 51 and plotted in Figure 83. The mean for the peak deflection ratio is 1.1 and the standard deviation is 0.08.

Table 51. 3D-FE Cracked model: Surface deflections at the center of loading area with plus and minus 1 SD corresponding to various cracked asphalt layer modulus values

Full Depth Cracked Model: With Surface-to-Surface Contact					
Cracked Layer Modulus (psi)	Peak Deflection (mils)	Peak Deflection Ratio (Cracked/Uncracked Model)	Peak Deflection Ratio - SD	Peak Deflection Ratio plus 1SD	Peak Deflection Ratio minus 1SD
1,000	17.0	1.24	0.09	1.33	1.15
5,000	17.0	1.24	0.09	1.33	1.15
10,000	15.4	1.12	0.09	1.21	1.03
20,000	15.1	1.10	0.09	1.19	1.01
30,000	14.8	1.08	0.09	1.17	0.99
40,000	14.5	1.06	0.09	1.15	0.97
50,000	14.4	1.05	0.09	1.14	0.96
100,000	14.3	1.04	0.09	1.13	0.95
150,000	14.1	1.03	0.09	1.12	0.94
200,000	14.1	1.03	0.09	1.12	0.94
250,000	14.0	1.02	0.09	1.11	0.93
332,200	13.9	1.01	0.09	1.10	0.92
500,000	13.8	1.01	0.09	1.10	0.92
Mean (mils)	14.8	1.1	Uncracked model peak deflection insitu condition: 13.7 mils (Asphalt layer modulus = 332,200 psi)		
SD (mils)	1.08	0.08			
COV (%)	7.31	7.31			

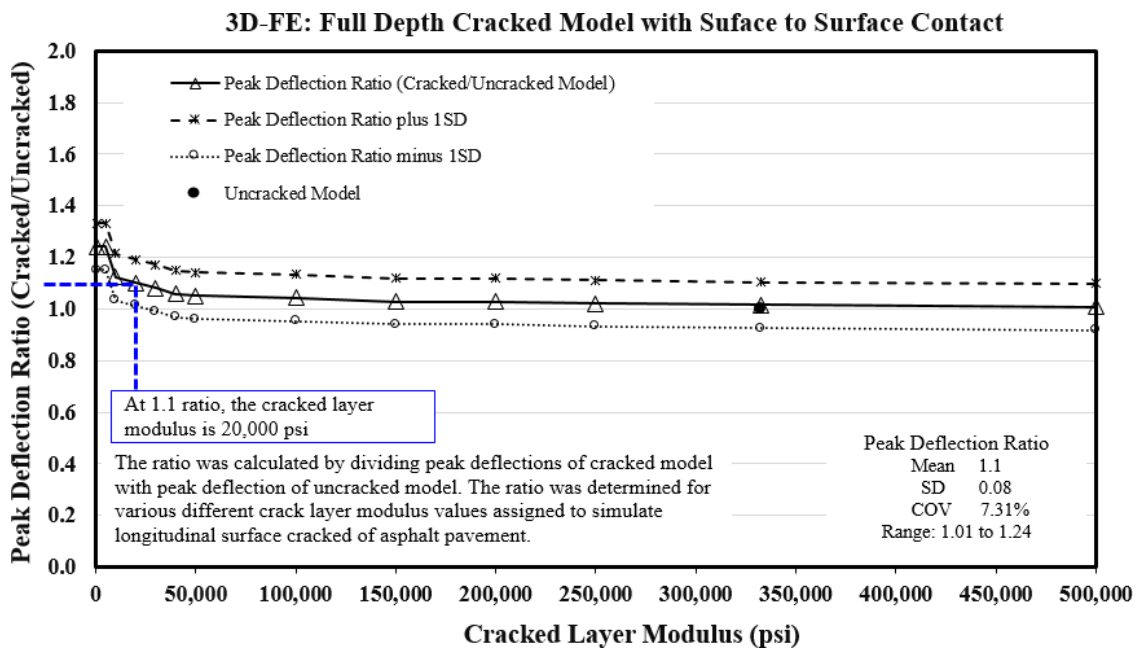


Figure 83. Peak deflection ratio for uncracked and cracked pavements: Surface deflections at the center of the loading area corresponding to various cracked layer modulus values

- 5) As shown in Figure 83, the plot was used to interpolate the modulus value at a 1.1 peak deflection ratio, and it was determined that the corresponding cracked layer modulus value is 20,000 psi. Therefore, the modulus value of 20,000 psi was assigned to the cracked layer at multiple depths.

#### 4.4.5. 3D-FE Modeling and Simulations using Factorial Design for Cracked Asphalt Pavement Subjected to Truck Axle Loading

The full factorial design for the 3D-FE cracked asphalt pavement model was like those implemented for the uncracked asphalt pavement model. Six factors are considered in this factorial experiment design for 3D-FE simulations. Each factor has two levels: low and high, which contributes to the complete factorial experiment design with a total of 64 possible treatment combinations ( $2^6$ ). However, the full factorial design is repeated four times depending on the crack locations (top one-third, middle one-third, bottom one-third, and full-depth cracked).

Once the simulations are completed, further research is recommended to analyze the structural response of the asphalt highway pavement subjected to truckloads on the simulated longitudinal crack. This will help to investigate the effects of the crack depths on surface deflections and other structural responses of stresses and strains at various layer depths and the top of the subgrade. However, only selected combinations of the factorial were analyzed in this research. It is recommended to complete the unfinished simulations of the cracked model to develop a more comprehensive structural response database at multi-depth crack levels. Table 52 shows 64 combinations of the full factorial design proposed for the cracked 3D-FE asphalt pavement models. The thickness and modulus values for asphalt, base, subbase, and subgrade layers at low level (zero) and high level (one) are included as well.

Table 52. Full factorial design for the 3D-FE cracked asphalt pavement model

Levels of the factors				Layer Thickness - mm (in)				
				0 Asphalt - 76.2 (3)		1 Asphalt - 228.6 (9)		
Young's Modulus, E - MPa (ksi)				0	1	0	1	
Subgrade (SG)	Base (B)	Subbase (SB)	Asphalt (A)	Subbase -152.4 (6)	Subbase - 304.8 (12)	Subbase -152.4 (6)	Subbase - 304.8 (12)	
0 E <sub>SG1</sub> - 68.9 (10)	0 E <sub>B1</sub> - 275.8 (40)	0 E <sub>SB1</sub> - 137.9 (20)	0 E <sub>A1</sub> - 1,379 (200)	1 000000	2 010000	3 100000	4 110000	
			1 E <sub>A2</sub> - 6,894.8 (1,000)	5 000001	6 010001	7 100001	8 110001	
		1 E <sub>SB2</sub> - 689.5 (100)	0 E <sub>A1</sub> - 1,379 (200)	9 000010	10 010010	11 100010	12 110010	
			1 E <sub>A2</sub> - 6,894.8 (1,000)	13 000011	14 010011	15 100011	16 110011	
		1 E <sub>B2</sub> - 1,379 (200)	0 E <sub>SB1</sub> - 137.9 (20)	0 E <sub>A1</sub> - 1,379 (200)	17 000100	18 010100	19 100100	20 110100
				1 E <sub>A2</sub> - 6,894.8 (1,000)	21 000101	22 010101	23 100101	24 110101
	1 E <sub>SB2</sub> - 689.5 (100)		0 E <sub>A1</sub> - 1,379 (200)	25 000110	26 010110	27 100110	28 110110	
			1 E <sub>A2</sub> - 6,894.8 (1,000)	29 000111	30 010111	31 100111	32 110111	
	0 E <sub>B1</sub> -	0 E <sub>SB1</sub> - 137.9 (20)	0 E <sub>A1</sub> - 1,379 (200)	33 001000	34 011000	35 101000	36 111000	
			1 E <sub>A2</sub> - 6,894.8 (1,000)	37 001001	38 011001	39 101001	40 111001	
		1 E <sub>A1</sub> - 1,379 (200)	0 E <sub>A1</sub> - 1,379 (200)	41 001010	42 011010	43 101010	44 111010	

1 E <sub>SG2</sub> - 344.7 (50)	275.8 (40)	E <sub>SB2</sub> - 689.5 (100)	1	45	46	47	48	
			E <sub>A2</sub> - 6,894.8 (1,000)	001011	011011	101011	111011	
	1 E <sub>B2</sub> - 1,379 (200)	0 E <sub>SB1</sub> - 137.9 (20)	0	E <sub>A1</sub> - 1,379 (200)	49	50	51	52
				1	001100	011100	101100	111100
			0	E <sub>A2</sub> - 6,894.8 (1,000)	53	54	55	56
				1	001101	011101	101101	111101
			1	E <sub>A1</sub> - 1,379 (200)	57	58	59	60
				1	001110	011110	101110	111110
1 E <sub>SB2</sub> - 689.5 (100)	1	E <sub>A2</sub> - 6,894.8 (1,000)	61	62	63	64		
		1	001111	011111	101111	111111		

#### 4.4.6. Evaluation and Comparison of Structural Response Analysis Results for Uncracked and Cracked Pavements

The structural response analysis of low-level modulus of weak pavements (model 000000) for all depth levels was analyzed. Similar layer thickness and modulus values were used for multi-depth crack layer analysis as shown in Table 53. Table 54 shows the deflection, stress, and strain values for the cracked asphalt layer at various crack depth levels.

Table 53. Layer thicknesses and modulus values for the 3D-FE analysis to study responses at different crack depth levels: Low-Level Modulus (Model 000000)

Cracked Asphalt Pavement			Thickness (in)		Young's Modulus (psi)			
No.	Combination Treatments	Crack Location	Asphalt Layer	Subbase Layer	Subgrade (E4)	Base (E2)	Subbase (E3)	Asphalt (E1)
1	000000	<b>Uncracked</b>	3	6	10,000	40,000	20,000	200,000
2	000000	Top 1/3	3	6	10,000	40,000	20,000	200,000
3	000000	Middle 1/3	3	6	10,000	40,000	20,000	200,000
4	000000	Bottom 1/3	3	6	10,000	40,000	20,000	200,000
5	000000	Full Depth	3	6	10,000	40,000	20,000	200,000

Table 54. Deflection, stress, and strain responses for cracked asphalt layer at various crack depth levels: Low-Level Modulus (Model 000000)

Cracked Asphalt Pavement			Deflection at the center of loading area (mils)	Compressive vertical stress in the middle of the asphalt layer (psi)	Tensile horizontal strain at the bottom of the asphalt layer (÷1000)	Compressive vertical stress in the middle of base layer (psi)	Tensile horizontal strain at the bottom of base layer (÷1000)	Compressive vertical stress in the middle of subbase layer (psi)	Compressive vertical strain on top of subgrade layer (÷1000)
No.	Combination Treatments	Crack Location							
1	000000	<b>Uncracked</b>	27.6	-80.5	<b>0.268</b>	<b>-23.7</b>	0.198	<b>-8.40</b>	-0.531
2	000000	Top 1/3	28.5	-126.6	0.359	-27.1	0.205	-8.56	-0.538
3	000000	Middle 1/3	<b>27.5</b>	<b>-14.1</b>	0.293	-25.7	<b>0.197</b>	-8.41	-0.531
4	000000	Bottom 1/3	27.6	-67.9	0.679	-25.7	0.200	-8.39	<b>-0.530</b>
5	000000	Full Depth	28.6	-33.2	0.641	-29.8	0.206	-8.70	-0.543

The key findings for asphalt pavement with low-level thickness and modulus values follow:

- The highest surface deflection was observed for the asphalt layer with a full-depth crack layer (28.6 mils).
- The highest compressive vertical stress in the middle of asphalt layer was observed for the pavement with the top one-third crack layer (126.6 psi).



- Tensile horizontal stains at the bottom of the asphalt layer were higher for the bottom one-third and full-depth crack layers as compared to other crack locations (more than 0.00064 in./in.)
- The compressive vertical stress in the middle of the base layer was the highest for asphalt pavement with a full-depth crack layer (29.8 psi).
- The tensile horizontal strain at the bottom of the base layer was the highest for asphalt pavement with a full-depth crack layer (0.000206 in./in.).
- The compressive vertical stress in the middle of the subbase layer was the highest for asphalt pavement with a full-depth crack layer (8.7 psi).
- The compressive vertical strain on top of the subgrade layer (0.000543 in./in.)

Further analysis was conducted to compare structural responses between low-level modulus and thin pavements (model 000000) high-level modulus and thick pavements (model 111111). Various combinations of factorial design were also evaluated in this research. Datasets in Table 55 were assigned to these models for the analysis.

Table 56 summarizes the surface deflection, stress, and strain values measured at critical locations for both uncracked and full depth cracked asphalt layers.

Table 55. Layer thicknesses and modulus values for uncracked and full depth cracked asphalt layer at various treatment combinations

No.	Cracked Asphalt Pavement		Thickness (in)		Young's Modulus (psi)			
	Combination Treatments	Crack Location	Asphalt Layer	Subbase Layer	Subgrade (E4)	Base (E2)	Subbase (E3)	Asphalt (E1)
1	000000	<b>Uncracked</b>	3	6	10,000	40,000	20,000	200,000
2	111111	<b>Uncracked</b>	9	12	50,000	200,000	100,000	1,000,000
3	000000	Full Depth	3	6	10,000	40,000	20,000	200,000
4	000011	Full Depth	3	6	10,000	40,000	100,000	1,000,000
5	000111	Full Depth	3	6	10,000	200,000	100,000	1,000,000
6	001000	Full Depth	3	6	50,000	40,000	20,000	200,000
7	001011	Full Depth	3	6	50,000	40,000	100,000	1,000,000
8	001111	Full Depth	3	6	50,000	200,000	100,000	1,000,000
9	111111	Full Depth	9	12	50,000	200,000	100,000	1,000,000

Table 56. Deflection, stress, and strain responses for uncracked and full depth cracked asphalt layer at various treatment combinations

No.	Cracked Asphalt Pavement		Deflection at the center of loading area (mils)	Compressive vertical stress in the middle of the asphalt layer (psi)	Tensile horizontal strain at the bottom of asphalt layer ( $\div 1000$ )	Compressive vertical stress in the middle of base layer (psi)	Tensile horizontal strain at the bottom of base layer ( $\div 1000$ )	Compressive vertical stress in the middle of subbase layer (psi)	Compressive vertical strain on top of subgrade layer ( $\div 1000$ )
	Combination Treatments	Crack Location							
1	000000	<b>Uncracked</b>	27.6	-80.5	0.268	-23.7	0.198	-8.4	0.531
2	111111	<b>Uncracked</b>	<b>3.6</b>	-49.3	<b>0.019</b>	<b>-7.5</b>	<b>0.017</b>	<b>-3.4</b>	<b>-0.040</b>
3	000000	Full Depth	28.6	-33.2	0.641	-29.8	0.206	-8.7	-0.543
4	000011	Full Depth	20.5	-18.8	0.507	-22.9	0.064	-7.1	-0.336
5	000111	Full Depth	16.2	-22.3	-0.231	-31.9	0.054	-5.5	-0.251
6	001000	Full Depth	14.6	-27.8	0.676	-29.8	0.175	-13.0	-0.166
7	001011	Full Depth	9.4	<b>-13.2</b>	1.021	-24.3	0.062	-11.4	-0.138
8	001111	Full Depth	6.5	-16.2	0.048	-32.0	0.042	-9.3	-0.114
9	111111	Full Depth	7.0	-13.4	0.078	-9.6	0.022	-3.8	-0.043

The key finding for uncracked asphalt pavements follows:

- Low-level modulus and thin pavement show higher surface deflection, stress, and strain values at those critical locations as compared to high-level modulus and thick pavement layers.

The key finding for full-depth cracked asphalt pavements follows:

- Low-level modulus and thin pavement show higher surface deflection, stress, and strain values at those critical locations as compared to high-level modulus and thick pavement layers.

Comparison between the uncracked and full-depth cracked asphalt layer indicates that asphalt pavements with full-depth crack show higher surface deflection, stresses, and strains except for compressive vertical stress in the middle of the asphalt layer, as compared to uncracked asphalt pavements. This finding applies to both model 000000 and model 111111, respectively.

#### 4.4.7. Impacts of Longitudinal Crack on Backcalculation of Effective Asphalt Layer Modulus

This research also analyzed the impacts of the longitudinal cracks on the backcalculation of the asphalt layer modulus values. In general, the modulus values for the uncracked pavement are higher as compared to the cracked pavements. The effective modulus values will decrease because of full depth cracks. Table 57 describes the layer thicknesses and the modulus values for different combination treatments of the 3D-FE models that simulated full-depth longitudinal cracks.

Table 57. Layer thicknesses and modulus values for various treatments for the 3D-FE models that simulate full-depth longitudinal cracks

Combination Treatments	Crack Location	Thickness, Inches			Modulus Values, psi			
		Asphalt Layer	Base Layer	Subbase Layer	Asphalt Layer	Base Layer	Subbase Layer	Subgrade Layer
000000	Full Depth	3	6	6	200,000	40,000	20,000	10,000
000011	Full Depth	3	6	6	1,000,000	40,000	100,000	10,000
000111	Full Depth	3	6	6	1,000,000	200,000	100,000	10,000
001000	Full Depth	3	6	6	200,000	40,000	20,000	50,000
001011	Full Depth	3	6	6	1,000,000	40,000	100,000	50,000
001111	Full Depth	3	6	6	1,000,000	200,000	100,000	50,000
111111	Full Depth	9	6	12	1,000,000	200,000	100,000	50,000

Further iterations were conducted to study the effective asphalt modulus values of full-depth longitudinal cracks as compared to the modulus values of the uncracked asphalt pavements. The key steps to execute the iterations follow:

- 1) The deflection values at the center of the loading area ( $W_1$ ) were extracted for the uncracked and cracked asphalt pavement models. Higher-level models show smaller deflection values as compared to the low-level models.
- 2) The GAMES linear elastic software was used to iterate the effective asphalt modulus values of

full-depth cracked models with different combination treatments. This software allows the simulation of point loads at four different locations like the loading configurations in the 3D-FE models.

- 3) Initially, the deflection values for the uncracked models were compared with the deflection values obtained from the GAMES analysis, which assumes no discontinuity on the asphalt pavement surfaces. A less than 6.5% difference in the deflection values was noted, which suggests that the deflection values from the 3D-FE analysis were reliable and acceptable.
- 4) Similar modulus values used in the 3D-FE analysis were used in the GAMES analysis for different combination treatments. Multiple iterations were conducted by changing only asphalt modulus values until the deflection values matched with the deflection values of full-depth cracked models.
- 5) The iterated modulus values were not the final effective modulus values for cracked models.

The iterated modulus values show the required reductions in the asphalt modulus to match the deflection values of the cracked asphalt pavements within  $\pm 1\%$  tolerance criteria.

Therefore, the final effective modulus values were obtained by subtracting the iterates modulus values from the default modulus of uncracked pavements.

- 6) The effective asphalt modulus values for cracked models with full-depth longitudinal cracks were calculated and compared with the uncracked asphalt modulus values.

Table 58 shows the effective modulus values for seven different combination treatments. The combination treatments represent the low and high levels of asphalt and subbase layer thicknesses and low and high levels of modulus values for all layers.

Table 58. Comparisons of the effective asphalt pavement modulus values with uncracked pavements for seven different combination treatments

No.	Combination Treatments	Uncracked Asphalt Modulus (psi)	Effective Asphalt Modulus (Full Depth Cracked), psi	% Reduction in Asphalt Modulus
1	000000	200,000	38,000	81.0
2	000011	1,000,000	250,000	75.0
3	000111	1,000,000	100,000	90.0
4	001000	200,000	91,000	54.5
5	001011	1,000,000	541,000	45.9
6	001111	1,000,000	690,000	31.0
7	111111	1,000,000	865,000	13.5

Based on full-depth cracked 3D-FE model results low-level modulus of weak pavements showed a higher reduction of 81.0% in the asphalt modulus compared to the uncracked 3D-FE model, while the high-level modulus and thick pavement showed a reduction of 13.5% in the asphalt modulus of the uncracked pavement model.

## 5. SUMMARY AND CONCLUSIONS

### 5.1. Summary

A nation's economy and prosperity depend on efficient and safe transportation networks for public mobility and freight transportation. A country's road network is recognized as one of the largest public infrastructure assets. Adverse pavement longitudinal roughness, rutting, cracking, potholes, and surface deterioration of road surface conditions require major maintenance and rehabilitation at significantly high costs. If timely maintenance and rehabilitation are not performed, the pavement damages inflicted by heavy truck traffic repetitions and environmental impacts may lead to life-threatening conditions for road users.

The importance of considering maintenance and rehabilitation intervention factor in the condition deterioration prediction equations was never considered. This research considered the LTPP climatic regions and maintenance and rehabilitation intervention in the development and implementation of enhanced pavement condition deterioration prediction equations. The IRI prediction equation considered the IRI measurement location factor (outside and inside wheel path). The rutting prediction equation included additional factors of in situ modulus of pavement layers and base layer type. Additionally, variance stabilizing transformations were also considered in the development of the rutting and cracking prediction model equations. These considerations are vital for the improved mechanistic-empirical structural design of the asphalt pavement and asset management practices. The regression equations are more objective, incorporate reasonably important independent variables, are easy to implement, and are easy to calibrate for future implementation in other geographical and climatic regions.

The enhanced asphalt highway pavement IRI, rutting, and cracking deterioration prediction equations were developed and evaluated in this research for LTPP data sets of 2,588 for IRI, 214 for rutting, and 2,240 for cracking. Comparatively, the AASHTO MEPDG performance equations were developed using a smaller number of test sections.

The development of a new cracking model using the Unified Cracking Index combines all crack types (alligator, block, longitudinal, and transverse). Block cracking and the combined cracking models are not available in the MEPDG. The concept of the Unified Cracking Index is practical and applicable for a decision support system for the maintenance and rehabilitation programs. This approach together with intervention criteria of maintenance and rehabilitation is a significant enhancement for life-cycle asset management of asphalt highway pavements.

The 3D-FE models of uncracked and cracked pavement layers were also introduced in this research. A new approach to assess asphalt pavement structural responses under single axle dual tires loads was developed and simulated using the 3D-FE dynamic analysis of the cracked and uncracked models. Reasonably good results of the model's verification as compared to the linear elastic program and the previous 3D-FE simulations proved the reliability of the models used in the numerical analysis. These 3D-FE models of asphalt pavements are beneficial for structural response analysis as well as pavement structural design. The analysis considers real-world pavement subgrade model size, truck load-time history, and a rational approach to simulate longitudinal crack in asphalt pavements at partial depths and full depth of the asphalt layers.

## 5.2. Conclusions

The main conclusions for each research topic are listed in the following sections:

### 5.2.1. Evaluation and Enhancement of Condition Deterioration Progression Models

- For the model database, the IRI multiple regression of longitudinal roughness data shows R of 0.633, while the ANN IRI model shows R of 0.717. The verifications using 18 data sets that were not in the model database show a better R of 0.664 for the IRI multiple regression equation as compared to the ANN's R of 0.483. Both IRI multiple regression equation and ANN model show a small RMSE less than 1.1, while the MARE values are 37.7% and 41.3% for the IRI multiple regression and ANN model, respectively.
- The prediction equations from multiple regression modeling and ANN modeling of rutting distress show high R values above 0.93 and 0.94, respectively, for the model database. For rutting verification data sets, both the multiple regression equation and ANN model show similar R values of 0.99. Both rutting multiple regression equation and ANN model show the RMSE less than 1.0, while the MARE is 16.6% and 2.3% for the rutting multiple regression equation and ANN model, respectively.
- The combined UCI cracking equation for the model database shows a correlation, R, of 0.551 for the log model with the RMSE of 19.5% of crack densities in predictions compared to the measured LTPP data. The sigmoid transformed regression equation shows an R of 0.511 with a 4.1% error. In comparison, the ANN model for UCI showed significant improvement in R-value (0.707) with a 14.6% error. It is also showed a high R-value (0.861) and low error for the verification data sets.
- Individual ANN models of cracking (alligator, block, longitudinal, transverse) also showed reasonably accurate results.
- The developed asphalt pavement condition deterioration progression models apply to high-quality pavements only.

### 5.2.2. Material Characterization of Asphalt Pavement Using Nondestructive Deflection Data

- Several modulus backcalculation software, based on the layered linear elastic static analysis were evaluated in this research. The comparison of the backcalculated modulus for the FWD deflection data used indicated that the backcalculated modulus values in the LTPP database were generally unreasonable using the EVERCALC 5.0 software. Overall, BAKFAA 2.0 and PEDD/UMPEDD backcalculated modulus values that were generally reasonable for all pavement layers.
- The results of a climate impact study revealed that the thickness design of longer-lasting pavement performance depends on seasonal layer modulus values considering extreme weather and climate attributes.

### 5.2.3. 3D-FE Modeling of Uncracked Asphalt Pavements

- The 3D-FE model of uncracked asphalt pavement layer was developed using the LS-DYNA finite element software and verified based on the measured peak surface deflection at the center of the loading area under FWD load (9,000 lbf). The verification showed that the 3D-FE models predicted only -1.7% less surface deflection (13.8 mils) as compared to the measured surface deflection of 14.04 mils. Additional 3D-FE simulations subjected to 4,500 lbf of truck wheel load on each tire were conducted. The calculated surface deflection was compared with the surface deflection value calculated using the GAMES linear elastic static analysis program. The calculated % difference was -4.4% which suggested a reliable 3D-FE model developed in this research. A full factorial experiment for six independent variables at two levels was designed, and the simulations for all 64 treatment combinations were executed for the uncracked model.

### 5.2.4. 3D-FE Modeling of Asphalt Pavements with Longitudinal Crack

- The 3D-FE models of the longitudinal crack in the asphalt layer at multiple depths and full depths were also developed in this research. The cracked layer was simulated and subjected to truck wheel loads. The full depth crack, top one-third crack, middle one-third crack, and bottom one-third crack were simulated. However, only selected combinations of the factorial were analyzed due to the LS-DYNA software license expiry. The full depth cracked model shows higher surface deflections as compared to the uncracked model. The top one-third cracked models indicate the highest compressive vertical stress in the middle in the middle of the asphalt layer. Tensile horizontal strain at the bottom of the asphalt layer is the most critical for the bottom one-third cracked model ( $\epsilon = 0.000679$ ), which indicated 139% higher as compared to the uncracked pavements.
- Further analysis was conducted using the cracked model to study the effect of full-depth crack on effective asphalt modulus values. Based on full-depth cracked 3D-FE model results at low-level modulus values of weak pavements showed a significant reduction of 81.0 % in the asphalt modulus compared to the modulus of the uncracked 3D-FE model, while the high-level combination of modulus and thick layer values showed a small reduction of 13.5% in the asphalt modulus of the uncracked pavement model. This analysis of reduction in the effective asphalt modulus due to cracked asphalt layer is not possible by using the traditional layered elastic static analysis that assumes no discontinuity in the pavement layer.

## 5.3. Recommendation for Future Research

- a) Development of pavement performance prediction models for
  - Develop pavement performance prediction models for other types of pavements such as concrete and composite.
  - Utilize Artificial Neural Network (ANN) to develop new models since it was observed to be the best modeling methodology for pavement performance predictions.
- b) Implementation of condition deterioration progression models

- Implement the reasonable condition deterioration progression models asphalt highway pavement, and calibrate, if necessary, for other geographical and climate regions, such as a tropical country.
- Develop models for top-down cracking in asphalt pavements when the pavements relevant condition data is collected and made available.
- Use the LTPP database to develop enhanced condition equations for concrete pavements.

c) Extended database of the 3D-FE modeling of uncracked asphalt pavements

- Create a full factorial design of uncracked pavements by including the medium level of thickness and modulus values for asphalt, base, subbase, and subgrade layers. Conduct additional 3D- FE simulations for extending the 3D-FE structural response database.
- Develop structural response prediction equations using the 3D-FE response database

d) Improvement of the 3D-FE modeling of cracked asphalt pavements

- Conduct 3D-FE simulations for the unfinished combinations of the full factorial design as conducted for the uncracked pavement models. However, the full factorial design is repeated four times depending on the crack locations (top one-third, middle one-third, bottom one-third, and full-depth cracked). Once the simulations are completed, further research is recommended to analyze the structural response of the asphalt highway pavement subjected to truckloads on the simulated longitudinal crack. This will help to investigate the effects of the crack depths on surface deflections and other structural responses of stresses and strains at various layer depths and the top of the subgrade.

## REFERENCES

- AASHTO. 1962. *AASHTO Road Test Report 5 Pavement Research*. Washington, D.C.
- AASHTO. 1993. "AASHTO Guide for Design of Pavements Structures." 624. American Association of State Highway and Transportation Officials.
- AASHTO. 2008. *Mechanistic Empirical Pavement Design Guide: A Manual Practice*. American Association of State Highway and Transportation Officials.
- AASHTO. 2020. "AASHTOWare - AASHTOWare Pavement Overview." Accessed January 30, 2022. <https://www.aashtoware.org/products/pavement/pavement-overview/>.
- AASHTO. 2022. "AASHTOWare Pavement Overview." Accessed February 4, 2022. <https://www.aashtoware.org/products/pavement/pavement-overview/>.
- Ahammed, M. A., S. Kass, and S. Hilderman. 2013. "Implementing the AASHTOWare Pavement ME Design guide: Manitoba issues and proposed approaches." *2013 TAC Conference and Exhibition - Transportation: Better - Faster - Safer, TAC/ATC 2013*.
- Ali GA, Krizek RJ, and Osterberg JO. 1970. "Influence of Poisson's ratio on the surface deflection of layered systems." *Highw Res Rec*, (33): 1–10.
- Ameri, M., N. Yavari, and T. Scullion. 2009. "Comparison of Static and Dynamic Backcalculation of Flexible Pavement Layers Moduli, Using Four Software Programs." *Asian Journal of Applied Sciences*, 2 (3): 197–210. Science Alert. <https://doi.org/10.3923/AJAPS.2009.197.210>.
- Attoh-Okine, N. O. 1994. "Predicting Roughness Progression in Flexible Pavements Using Artificial Neural Networks." *3rd International Conference on Managing Pavements*, 1 (1): 55–62.
- Boriboonsin, K., and H. G. Momm. 2002. "Evaluation of Asphalt Pavement Damage Models Using LTPP Data in Northern Mississippi." *International Contest on LTPP Data Analysis 3rd Year*.
- Burnett, S., M. Gilbert, T. Molyneaux, G. Beattie, and B. Hobbs. 2007. "The performance of unreinforced

- masonry walls subjected to low-velocity impacts: Finite element analysis.” *International Journal of Impact Engineering*, 34 (8): 1433–1450. Pergamon. <https://doi.org/10.1016/j.ijimpeng.2006.08.004>.
- Cardoso, S. H., and A. Fortunato Marcon. 1998. “Pavement Performance Models for the State of Santa Catarina (Brazil).” *4th International Conference on Managing Pavements*.
- Carol, I., A. Idiart, C. M. Lopez, and A. Caballero. 2007. “Advances in meso-mechanical analysis of concrete specimens using zero-thickness interface elements.” *Proceedings of the 6th International Conference on Fracture Mechanics of Concrete and Concrete Structures - Fracture Mechanics of Concrete and Concrete Structures*, 1: 163–174.
- Choi, J. H., T. M. Adams, and H. U. Bahia. 2004. “Pavement roughness modeling using back-propagation neural networks.” *Computer-Aided Civil and Infrastructure Engineering*, 19 (4): 295–303. <https://doi.org/10.1111/j.1467-8667.2004.00356.x>.
- Connor, W. S., and M. Zelen. 1959. *Fractional Factorial Experiment Designs for Factors at Three Levels -*. (National Bureau of Standards Applied Mathematics Series, ed.). U.S. Department of Commerce.
- Dias-Da-Costa, D., J. Alfaiate, L. J. Sluys, and E. Júlio. 2010. “A comparative study on the modelling of discontinuous fracture by means of enriched nodal and element techniques and interface elements.” *International Journal of Fracture*, 161 (1): 97–119. <https://doi.org/10.1007/s10704-009-9432-6>.
- ENR. 2006. “About Industry’s Largest R&D Effort Founded Interstate Construction, AASHTO Road Test.”
- FAA. 2011. “Use of Nondestructive Testing in the Evaluation of Airport Pavements.” *Advisory Circular*, 86.
- FHWA. 1993. “Layer Moduli Backcalculation Procedure: Software Selection.” *Sciences-New York*.
- FHWA. 2006. “Long-Term Pavement Performance (LTPP) Data Analysis Support : National Pooled Fund Study TPF-5 ( 013 ).” *Federal Highway Administration*, 5 (November).
- FHWA. 2016. “Daily Travel by Measured Pavement Roughness - Table HM-47A.” Accessed February 4, 2022. <https://www.fhwa.dot.gov/policyinformation/statistics/2016/hm47a.cfm>.
- FHWA. 2017. *Using Falling Weight Deflectometer Data with Mechanistic-Empirical Design and Analysis, Volume I: Final Report*.
- FHWA, F. H. A. 2019. *LONG-TERM PAVEMENT PERFORMANCE Information Management System User Guide. Information Management System User Guide*.
- Garza, S. G. 2003. “Integration of Pavement Nondestructive Evaluation, Finite Element Simulation, and Air Quality Modeling For Enhanced Transportation Corridor Assessment and Design.” (May).
- GASB. 2000. “Guide to implementation of GASB statement 34 on basic financial statements--and management’s discussion and analysis--for state and local governments : questions and answers.” 261. Governmental Accounting Standards Board of the Financial Accounting Foundation.
- George, K. P., and W. Uddin. 2000. *Subgrade Characterization for Highway Pavement Design. Final Report - Sponsored Research Study SS 131*.
- Haas, R., W. R. Hudson, and J. P. Zaniewski. 1994. “Modern Pavement Management.” *Krieger Publishing Company*, 102 (7): 583.
- Hajj, E., P. Thushanthan, P. Sebaaly, and R. Siddharthan. 2012. “Influence of tire-pavement stress distribution, shape, and braking on performance predictions for asphalt pavement.” *Transportation Research Record*, (2306): 73–85. <https://doi.org/10.3141/2306-09>.
- Huang, Y. H. 2004. “Pavement Analysis and Design.” *Pearson Education*, Second Edi: 775. Pearson/Prentice Hall.
- IBM. 2022. “IBM SPSS Statistics .” Accessed February 8, 2022. <https://www.ibm.com/products/spss-statistics>.
- Jaafar, Z., M. Ahlan, and W. Uddin. 2015. “Modeling of pavement roughness performance using the LTPP database for southern region in the U.S.” *Bituminous Mixtures and Pavements VI*, 713–722. CRC Press.
- Jaafar, Z. F. M., and W. Uddin. 2016. “Modeling of asphalt pavement rutting for ltpv southern region using multiple linear regression method.” *8th International Conference on Maintenance and Rehabilitation of Pavements, MAIREPAV 2016*, (February 2019): 910–919. <https://doi.org/10.3850/978-981-11-0449-7-178-cd>.
- Johannek, L., and L. Khazanovich. 2010. “Comprehensive evaluation of effect of climate in Mechanistic-Empirical Pavement Design Guide predictions.” *Transportation Research Record*, (2170): 45–55. <https://doi.org/10.3141/2170-06>.
- Kargah-Ostadi, N., S. M. Stoffels, and N. Tabatabaee. 2010. “Network-level pavement roughness prediction



- model for rehabilitation recommendations.” *Transportation Research Record*, (2155): 124–133. <https://doi.org/10.3141/2155-14>.
- Livermore, S. T. C. 2022. “Strain measures of solid elements — Welcome to the LS-DYNA support site.” Accessed February 8, 2022. <https://www.dynasupport.com/howtos/element/strain-measures-of-solid-elements>.
- Madanat, A., S. M. Nakat, and Z. el Sathaye. 2005. *Development of Empirical-Mechanistic Pavement Performance Models using Data from the Washington State PMS Database*.
- Mahoney, J. P., B. C. Winters, N. C. Jackson, and L. M. Pierce. 1993. “Some observations about backcalculation and use of a stiff layer condition.” *Transportation Research Record*, (1384): 8–14.
- Maina, J. W., Y. Ozawa, and K. Matsui. 2012. “Linear elastic analysis of pavement structure under non-circular loading.” *Road Materials and Pavement Design*, 13 (3): 403–421. <https://doi.org/10.1080/14680629.2012.705419>.
- MDOT. 2015. “Michigan DOT User Guide For Pavement Design.” *Interim Edition*, (March).
- MDOT. 2019. “County Pavement Condition Rating (PCR) History by Year.” Accessed March 1, 2019. [https://path.mdot.ms.gov/pavement\\_condition](https://path.mdot.ms.gov/pavement_condition).
- Meegoda, J. N., and S. Gao. 2014. “Roughness progression model for asphalt pavements using long-term pavement performance data.” *Journal of Transportation Engineering*, 140 (8): 1–7. [https://doi.org/10.1061/\(ASCE\)TE.1943-5436.0000682](https://doi.org/10.1061/(ASCE)TE.1943-5436.0000682).
- Meyer, M. D., S. McLeod, T. Fidell, H. Gajjar, D. Sood, M. Kamali, R. Wingate, D. O. Willauer, and F. Southworth. 2019. *Freight Transportation Resilience in Response to Supply Chain Disruptions*. National Academies of Sciences, Engineering, and Medicine. Washington, D.C.: Transportation Research Board.
- Mohamed Jaafar, Z. F. bin, W. Uddin, and Y. Najjar. 2016. “Asphalt Pavement Roughness Modeling Using the Artificial Neural Network and Linear Regression Approaches for LTPP Southern Region.” *Transportation Research Board*.
- Muflahi, S. A., G. Mohamed, and S. R. Hallett. 2014. “Investigation of Delamination Modeling Capabilities for Thin Composite Structures in LS-DYNA®.” *13th International LS-DYNA Users Conference*, (G. Balint, B. Antala, C. Carty, J.-M. A. Mabieme, I. B. Amar, and A. Kaplanova, eds.), 1–13. Uniwersytet Śląski. Wydział Matematyki, Fizyki i Chemii. <https://doi.org/10.2/JQUERY.MIN.JS>.
- Najjar, Y. 1999. *Quick Manual for the Use of ANN program TRSEQ1*. Manhattan, Kansas.
- Nanagiri, Y. 2001. “Pavement-Subgrade Material Characterization and Advanced Computer Simulations. Master Thesis.”
- NCHRP. 2004a. “Design Guide: Design of New and Rehabilitated Pavement Structures.” (February): 2–92.
- NCHRP. 2004b. *Guide for Mechanistic-Empirical Design of New and Rehabilitated Pavement Structures - Appendix II-1: Calibration of Fatigue Cracking Models for Flexible Pavements*.
- NCHRP. 2004c. *Guide for Mechanistic-Empirical Design of New and Rehabilitated Pavement Structures - Part 3. Design Analysis - Chapter 3. Design of New and Reconstructed Flexible Pavements*.
- Nguyen, V. P. 2014. “An open source program to generate zero-thickness cohesive interface elements.” *Advances in Engineering Software*, 74: 27–39. Elsevier Ltd. <https://doi.org/10.1016/j.advengsoft.2014.04.002>.
- Paterson, W. 1987. “Road Deterioration and Maintenance Effects: Models for Planning and Management.” *International Study of Highway Development and Management Tools*, 351.
- Paterson, W. 1994a. “Proposal of Universal Cracking Indicator for Pavements.” *Transportation Research Record*, 69–75.
- Paterson, W. D. 1994b. “Proposal of Universal Cracking Indicator for Pavements.” *Transportation Research Record*, (1455): 69–75.
- Paterson, W. D. O. 1989. “Transferable causal model for predicting roughness progression in flexible pavements.” *Transportation Research Record*, (1215): 70–84.
- Plati, C. 2011. “Development of a Method to Establish Criteria for Pavement Roughness Evaluation.” *International Journal of Pavements*, 10 (1-2–3).
- Plumeau, P., M. Berndt, P. Bingham, R. Weisbrod, S. S. Rhodes, J. Bryan, and T. J. Cherrett. 2012. *Guidebook for Understanding Urban Goods Movement. Guidebook for Understanding Urban Goods Movement*. Washington, D.C.: National Academies Press.
- Priddy, L. P. 2014. “Evaluation of Precast Portland Cement Concrete Panels for Airfield Pavement Repairs.”

- Priddy, L. P., A. Bianchini, C. R. Gonzalez, C. S. Dossett, and United States Air Force Academy. 2015. "Evaluation of procedures for backcalculation of airfield pavement moduli." *This Digital Resource was created in Microsoft Word and Adobe Acrobat*. Geotechnical and Structures Laboratory (U.S.).
- Queiroz, C. A. V. 1981. "Performance prediction models for pavement management in Brazil."
- Rahim, A. M., G. Fiegel, K. Ghuzlan, and D. Khumann. 2009. "Evaluation of international roughness index for asphalt overlays placed over cracked and seated concrete pavements." <http://dx.doi.org/10.1080/10298430802342773>, 10 (3): 201–207. Taylor & Francis Group .  
<https://doi.org/10.1080/10298430802342773>.
- Sayers, M. W., T. D. Gillespie, and C. A. V. Queiroz. 1986. "International Road Roughness Experiment: a Basis for Establishing a Standard Scale for Road Roughness Measurements." *Transportation Research Record*, 76–85.
- Schmalzer, P. N. 2006. *Long-Term Pavement Performance Program Manual for Falling Weight Deflectometer Measurements*. Long-Term Pavement Performance Program Manual for Falling Weight Deflectometer Measurements.
- Soncim, S. P., and J. L. Fernandes Jr. 2013. "Roughness Performance Model for Double Surface Treatment Highways." *Transportation Research Board 92nd Annual Meeting*.
- Stubstad, R., Y. Jiang, and E. Lukanen. 2006. "Guidelines for review and evaluation of backcalculation results." (February).
- Uddin, W. 1984. "A Structural Evaluation Methodology for Pavements Based on Dynamic Deflections. Ph.D. Dissertation."
- Uddin, W. 2008. "3D-FE dynamic analysis of pavements subjected to nondestructive impact testing." *NED University Journal of Research*, 5 (1): 1–16. NED University of Engineering and Technology.
- Uddin, W. 2013. *A Synthesis Study of Noncontact Nondestructive Evaluation of Top-down Cracking in Asphalt Pavements*. Final Report FHWA/MS-DOT-RD-13-255, Sponsored Research Study SS 255.
- Uddin, W. 2014. "An overview of GPR applications for evaluation of pavement thickness and cracking." *Proceedings of the 15th International Conference on Ground Penetrating Radar, GPR 2014*, 925–930. IEEE. <https://doi.org/10.1109/ICGPR.2014.6970561>.
- Uddin, W. 2015a. "Appraisal of Mechanistic-Empirical Pavement Design Guide for Highways Being Implemented in the United States and Complementary Needs for Pavement Asset Management." *6th International Conference Bituminous Mixtures and Pavements*.
- Uddin, W. 2015b. *CE585-Highway Pavements*. Course Lecture Notebook. Oxford, Mississippi.
- Uddin, W. 2015c. "Appraisal of Mechanistic-Empirical Pavement Design Guide for Highways being Implemented in the United States and Complementary Needs for Pavement Asset Management." *Proceedings of the 6th ICONF BMP, International Conference Bituminous Mixtures and Pavements*, 195–202. Thessaloniki, Greece: Taylor & Francis.
- Uddin, W., and S. Garza. 2010. "3D-FE Simulation Study of Structural Response Analysis for Pavement-Subgrade Systems Subjected to Dynamic Loads." *Pavements and Materials: Testing and Modeling in Multiple Length Scales*, 170–181. American Society of Civil Engineers. [https://doi.org/10.1061/41129\(385\)15](https://doi.org/10.1061/41129(385)15).
- Uddin, W., S. Garza, and K. Boriboonsomsin. 2003. "A 3D-FE Simulation Study of the Effects of Nonlinear Material Properties on Pavement Structural Response Analysis and Design." *Proceedings of MAIREPAV03 - Third International Symposium on Maintenance and Rehabilitation of Pavements and Technological Control*, 173–180. Guimarães, Portugal.
- Uddin, W., and S. G. Garza. 2003. "3D-FE Simulation and Dynamic Response Analysis of FWD Impact Test on Asphalt Pavements." *International Conference on Highway Pavement Data, Analysis and Mechanistic Design Applications*.
- Uddin, W., R. M. Hackett, A. Joseph, Z. Pan, and A. B. Crawley. 1995. "Three-dimensional finite-element analysis of jointed concrete pavement with discontinuities." *Transportation Research Record*, (1482): 26–32.
- Uddin, W., W. R. Hudson, and R. Haas. 2013. *Public Infrastructure Asset Management*.
- Uddin, W., A. H. Meyer, and W. R. Hudson. 1986. "Rigid Bottom Considerations for Nondestructive Evaluation of Pavements." *Transportation Research Record*, 21–29.

- Uddin, W., P. Noppakunwijai, and T. Chung. 1997. "Performance Evaluation of Jointed Concrete Pavement Using Three-Dimensional Finite-Element Dynamic Analysis." *Transportation Research Board*.
- Uddin, W., and Z. Pan. 1995. "Finite-Element Analysis of Flexible Pavements with Discontinuities." *Proceedings of ASCE Transportation Congress*, 410–423. San Diego: ASCE.
- Uddin, W., and L. Ricalde. 2000. "Implementation of a User Material Routine in 3D-FE Codes for Viscoelastic Modeling and Simulation of Highway and Airport Pavements." *LS-DYNA User Conference*.
- Uddin, W., D. Zhang, and F. Fernandez. 1994. "Finite element simulation of pavement discontinuities and dynamic load response." *Transportation Research Record*, (1448): 100–106.
- Ullidtz, P. 1987. "Pavement Analysis. Developments in Civil Engineering, Volume 19." 318. Elsevier.
- U.S. Army Corps of Engineers. 2021. "Pavement-Transportation Computer Assisted Structural Engineering (PCASE) ." Accessed February 8, 2022. <https://transportation.erd.c.dren.mil/pcase/software.aspx>.
- U.S. Department of Transportation. 2016. "Transportation Statistics Annual Report 2015." *U.S. Department of Transportation, Bureau of Transportation Statistics*, 1–217.
- Wang, P., X. M. Huang, Q. F. Li, and Z. T. Yang. 2008. "Finite Element Analysis of Top- Down Cracking in Semi-Rigid Pavement Structure." *Proceedings in 6th RILEM International Conference on Cracking in Pavements*.
- WSDOT, W. S. D. of T. 2005. "Washington State EVERSERIES © User's Guide Pavement Analysis Computer Software and Case Studies."

# APPENDICES

## Appendix A: Modeling of 3D-FE Cracked Asphalt Pavement Model

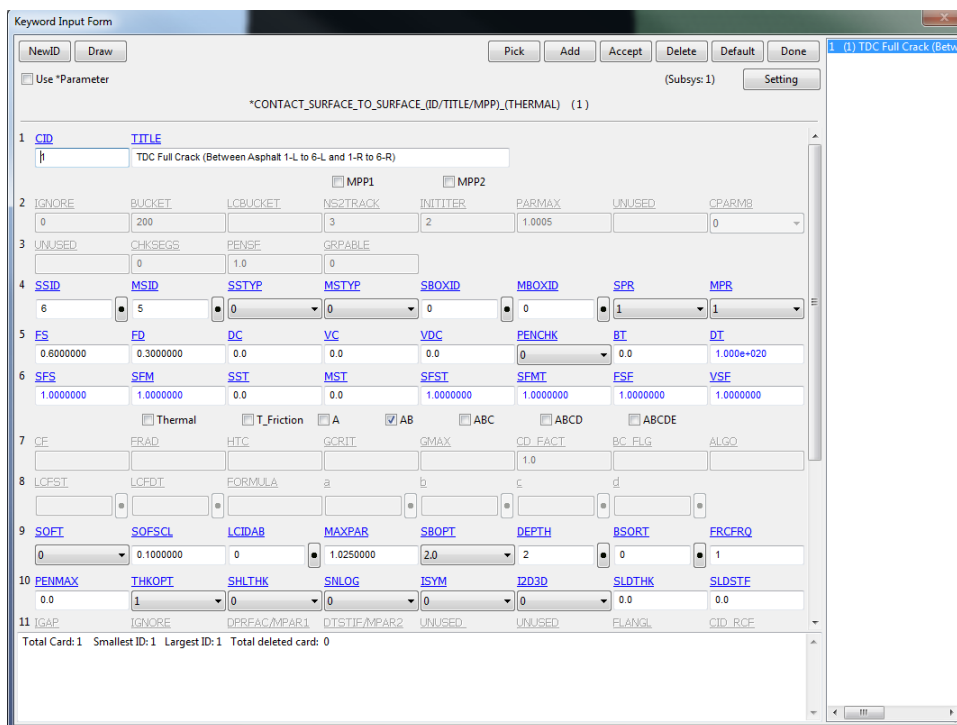


Figure A1. LS-DYNA CONTACT SURFACE TO SURFACE set up in the LS-DYNA software with Static Friction Coefficient (FS = 0.6) and Dynamic Friction of Coefficient (FD=0.3)

### Parameters

**SOFSCL:** Scale factor for constraint forces of soft constraint option (default=1.0). Values greater than 0.5 for single surface contact and 1.0 for a one-way treatment are inadmissible.

**MAXPAR:** Maximum parametric coordinate in segment search (values 1.025 and 1.20 recommended). Larger values can increase the cost. If zero, the default is set to 1.025. This factor allows an increase in the size of the segments. May be useful at sharp corners.

**SBOPT:** Segment-based contact options (SOFT=2).EQ.0: Defaults to 2.

EQ.1: Pinball edge-edge contact (not recommended).EQ.2: Assume planer segments (default).

EQ.3: Warped segment checking.EQ.4: Sliding option

**DEPTH:** Search depth in automatic contact. The value of 1 is sufficiently accurate for most crash applications and is much less expensive. LS-DYNA for improved accuracy sets this value to 2. If zero, the default is set to 2.

LT.0: |DEPTH| is the load curve ID defining searching depth versus time.

**FRCFRQ:** Number of cycles between contact force updates for penalty contact formulations. This option can provide a significant speed-up of the contact treatment. If used, values exceeding 3 or 4 are dangerous. Considerable care must be exercised when using this option, as this option assumes that contact does not change FRCFRG cycles.

EQ.0: FRCFRG is set to 1 and force calculations are performed each cycle-strongly recommended.

**PENMAX:=**Maximum penetration distance for old type 3, 5, 8, 9, and 10 contact or the segment thickness multiplied by PENMAX defines the maximum penetration allowed (as a multiple of the segment thickness) for contact types a 3, a 5, a10, 13, 15, and 26.

EQ.0.0 for old type contacts 3, 5, and 10: Use small penetration search and value calculated from thickness and XPENE, see \*CONTROL\_CONTACT.

EQ.0.0 for contact types a 3, a 5, a10, 13, and 15: Default is 0.4, or 40 percent of the segment thickness

EQ.0.0 for contact type26: Default is 200.0 times the segment thickness

**THKOPT:** Thickness option for contact types 3, 5, and 10:

EQ.0: default is taken from control card, \*CONTROL\_CONTACT, EQ.1: thickness offsets are included,

EQ.2: thickness offsets are not included (old way).

**SNLOG:** Disable shooting node logic in thickness offset contact. With the shooting node logic enabled, the first cycle that a slave node penetrates a master segment, that node is moved back to the master surface without applying any contact force.

EQ.0: logic is enabled (default),

EQ.1: logic is skipped (sometimes recommended for metal forming calculations).

**SLDTHK:** Optional solid element thickness. A nonzero positive value will activate the contact thickness offsets in the contact algorithms where offsets apply. The contact treatment will then be equivalent to the case where null shell elements are used to cover the brick elements. The contact stiffness parameter below, SLDSTF, may also be used to override the default value.

**SLDSTF:** Optional solid element stiffness. A nonzero positive value overrides the bulk modulus taken from the material model referenced by the solid element.

**FS:** Static coefficient of friction if  $FS > 0$  and not equal to 2.

EQ.-1.0: If the frictional coefficients defined in the \*PART section are to be used, set FS to a negative number.

EQ. 2: For contact types SURFACE\_TO\_SURFACE and ONE\_WAY\_SURFACE\_TO\_SURFACE, the dynamic coefficient of friction points to the table, see DEFINE\_TABLE (The table ID is given by FD below.), giving the coefficient of friction as a function

of the relative velocity and pressure. This option must be used in combination with the thickness offset option.

**FD:** Dynamic coefficient of friction. The frictional coefficient is assumed to be dependent on the relative velocity  $v\text{-rel}$  of the surfaces in contact. Give table ID if FS=2 (default=0.0).

**SSID:** Slave Segment Set Up

**MSID:** Master Segment Set Up.

Table A1. Parametric studies were conducted to determine Static Friction Coefficient (FS) and Dynamic Friction of Coefficient (FD) values by comparing the deflection values for the nodes at the center of loading area

Layer Type	Measurement point depth mm (in) from surface layer	Nodes (center of wheel load contact area)	Crack Condition at vertical surface	Static Coefficient of Friction (FS)	Dynamic Coefficient of Friction (FD)	Time (Sec)	Deflection, mm (inch)
Asphalt	0 (0)	584853	TDC - From top to bottom of the first asphalt layer	0.7	0.1	0.212	0.3454 (0.0136)
				0.7	0.2	0.212	0.3454 (0.0136)
				0.7	0.3	0.212	0.3454 (0.0136)
				0.7	0.4	0.212	0.3454 (0.0136)
				0.7	0.5	0.212	0.3454 (0.0136)
				0.7	0.6	0.212	0.3454 (0.0136)
				0.7	0.7	0.212	0.3454 (0.0136)
				0.1	0.3	0.212	0.3454 (0.0136)
				0.2	0.3	0.212	0.3454 (0.0136)
				0.3	0.3	0.212	0.3454 (0.0136)
				0.4	0.3	0.212	0.3454 (0.0136)
				0.5	0.3	0.212	0.3454 (0.0136)
				0.6	0.3	0.212	0.3454 (0.0136)
	38.1 (1.5)	629949	TDC - From top to bottom of the first asphalt layer	0.7	0.1	0.212	0.3429 (0.0135)
				0.7	0.2	0.212	0.3429 (0.0135)
				0.7	0.3	0.212	0.3429 (0.0135)
				0.7	0.4	0.212	0.3429 (0.0135)
				0.7	0.5	0.212	0.3429 (0.0135)
				0.7	0.6	0.212	0.3429 (0.0135)
				0.7	0.7	0.212	0.3429 (0.0135)
				0.1	0.3	0.212	0.3429 (0.0135)
				0.2	0.3	0.212	0.3429 (0.0135)
				0.3	0.3	0.212	0.3429 (0.0135)
				0.4	0.3	0.212	0.3429 (0.0135)
				0.5	0.3	0.212	0.3429 (0.0135)
				0.6	0.3	0.212	0.3429 (0.0135)
	76.2 (3)	681147	TDC - From top to bottom of the first asphalt layer	0.7	0.1	0.212	0.3353 (0.0132)
				0.7	0.2	0.212	0.3353 (0.0132)
				0.7	0.3	0.212	0.3353 (0.0132)
				0.7	0.4	0.212	0.3353 (0.0132)
				0.7	0.5	0.212	0.3353 (0.0132)
				0.7	0.6	0.212	0.3353 (0.0132)
				0.7	0.7	0.212	0.3353 (0.0132)
				0.1	0.3	0.212	0.3353 (0.0132)
				0.2	0.3	0.212	0.3353 (0.0132)
				0.3	0.3	0.212	0.3353 (0.0132)
0.4				0.3	0.212	0.3353 (0.0132)	
0.5				0.3	0.212	0.3353 (0.0132)	
0.6				0.3	0.212	0.3353 (0.0132)	

- BOUNDARY SPC SET used in the LS-DYNA to set boundary conditions for the 3D-FE model of the cracked asphalt layer

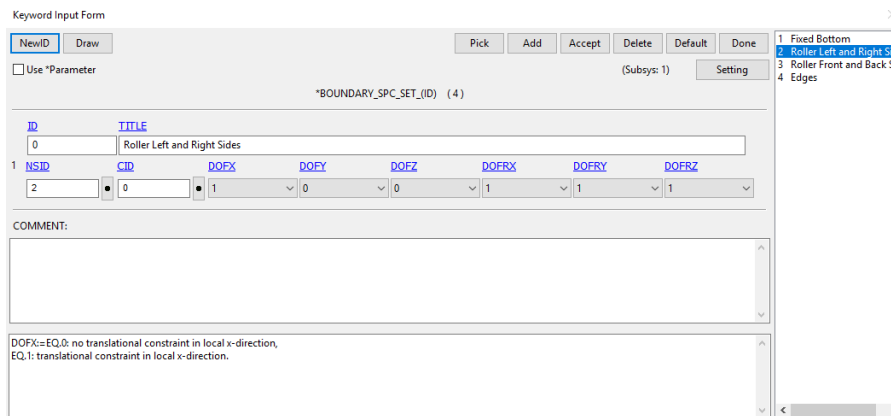


Figure A2. Boundary condition set up for the left and right sides of the 3D-FE model

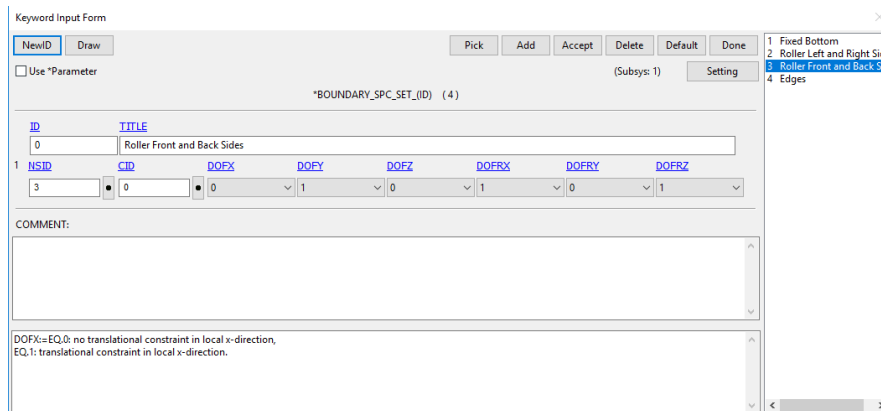


Figure A3. Boundary condition set up for the front and back sides of the 3D-FE model

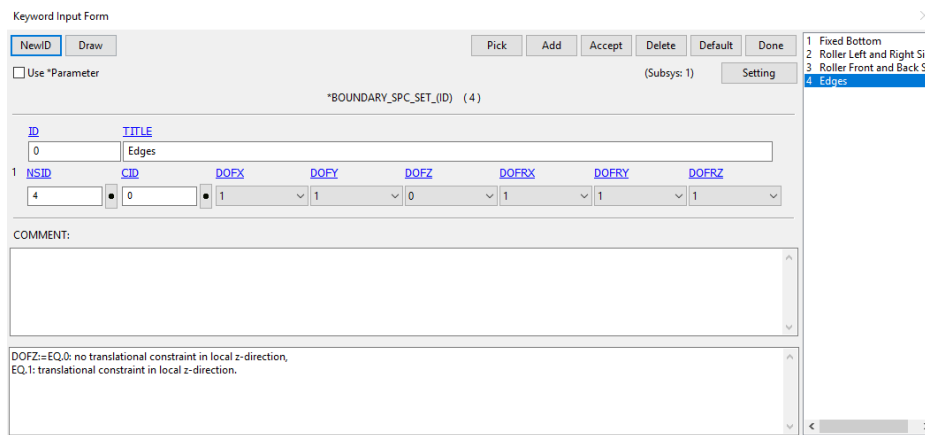


Figure A4. Boundary condition set up for the edges of the 3D-FE model



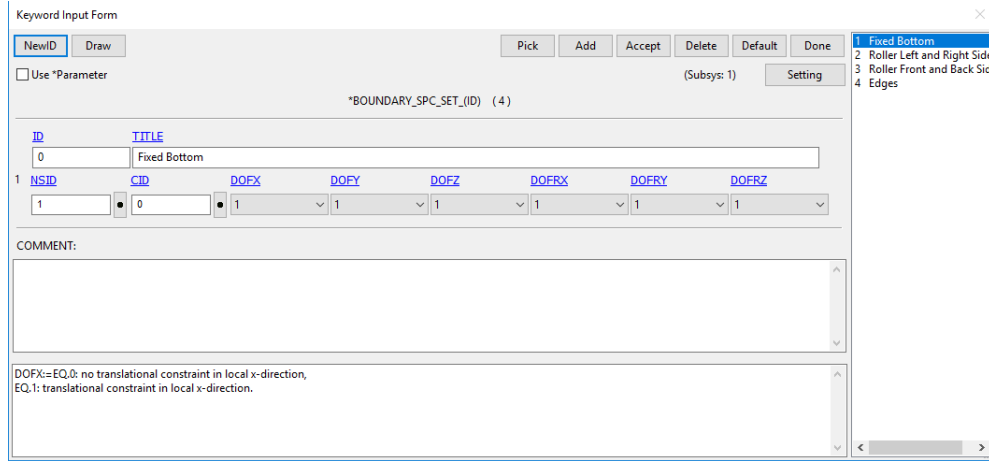


Figure A5. Boundary condition set up for the bottom of the 3D-FE model

Location	Boundary Condition	No. of Nodes	Axis with rotational constraint	Axis with translational constraint	DOF per node (based on: translational constraint)	No. of nodes x DOF
Top	Free					
Bottom	Fixed	50	x, y, and z	x, y, and z	0	0
Left and Right	Roller	4,323	x, y, and z	x	2	8,646
Front and Back	Roller	8,807	x and z	y	2	17,614
Edges	Roller	88	x, y, and z	x and y	1	88
<b>Degree of freedom = (# nodes x # DOF per node) - prescribed DOF</b>					Prescribed DOF	26,348
The number of DOF per node for solid element is three (translation in x,y, and z)						
# of nodes = 1,113,195 (3D-FE model)						
# of elements = 1,039,413 (3D-FE model)						
<b>Degree of freedom = (1,113,195 x 3) - 26,348 = 3,313,237</b>						

Figure A6. Calculation of degree of freedom (DOF) for **uncracked** asphalt model

Location	Boundary Condition	No. of Nodes	Axis with rotational constraint	Axis with translational constraint	DOF per node (based on: translational constraint)	No. of nodes x DOF
Top	Free					
Bottom	Fixed	50	x, y, and z	x, y, and z	0	0
Left and Right	Roller		x, y, and z	x	2	0
Front and Back	Roller	18,149	x and z	y	2	36,298
Edges	Roller	116	x, y, and z	x and y	1	116
<b>Degree of freedom = (# nodes x # DOF per node) - prescribed DOF</b>					Prescribed DOF	36,414
The number of DOF per node for solid element is three (translation in x,y, and z)						
# of nodes = 2,571,316 (3D-FE model)						
# of elements = 2,488,835 (3D-FE model)						
<b>Degree of freedom = (2,571,316 x 3) - 36,414 = 7,677,534</b>						

Figure A7. Calculation of degree of freedom (DOF) for **cracked** asphalt model

## Appendix B: Prediction Model Equation for Condition Deterioration Progression

### Model Summary<sup>b</sup>

Model	R	R Square	Adjusted R Square	Std. Error of the Estimate
1	.633 <sup>a</sup>	.401	.399	.48694

a. Predictors: (Constant), IRI\_D, CND, Air\_Temperature, Total\_Monthly\_Precipitation, Initial\_IRI\_Per\_Measurement\_Year, Cumulative\_Traffic, SN, Reg\_D, Age

b. Dependent Variable: IRI\_Per\_Measurement\_Year\_Yi

Figure B1. IRI Roughness: Model summary

### Coefficients<sup>a</sup>

Model		Unstandardized Coefficients		Standardized Coefficients	t	Sig.
		B	Std. Error	Beta		
1	(Constant)	.642	.053		12.207	.000
	Initial_IRI_Per_Measurement_Year	.726	.020	.581	36.331	.000
	Age	.006	.001	.086	4.552	.000
	SN	-.045	.007	-.114	-6.937	.000
	Cumulative_Traffic	-1.542E-8	.000	-.102	-5.970	.000
	Air_Temperature	.002	.001	.025	1.559	.119
	Total_Monthly_Precipitation	.000	.000	-.042	-2.668	.008
	Reg_D	.080	.022	.063	3.733	.000
	CND	-.105	.023	-.083	-4.582	.000
	IRI_D	-.061	.019	-.049	-3.212	.001

a. Dependent Variable: IRI\_Per\_Measurement\_Year\_Yi

Figure B2. IRI Roughness: Model coefficients

### Model Summary<sup>b</sup>

Model	R	R Square	Adjusted R Square	Std. Error of the Estimate
1	.920 <sup>a</sup>	.847	.836	.11315

a. Predictors: (Constant), Asphalt\_Thickness\_T1, Age, Subbase\_Modulus\_E3, Log10\_Initial\_Rut\_Depth\_Plus\_0.5, CND, Air\_Temperature, Subgrade\_Modulus\_E4, Cumu\_ESALs, Base\_D, Reg\_D, Total\_Thickness\_Tt, Asphalt\_Modulus\_E1, SN, Base\_Modulus\_E2

b. Dependent Variable: Log10\_Avg\_Rut\_Depth\_Plus\_0.5

Figure B3. Rutting: Model summary

**Coefficients<sup>a</sup>**

Model		Unstandardized Coefficients		Standardized Coefficients	t	Sig.
		B	Std. Error	Beta		
1	(Constant)	.058	.075		.775	.439
	Age	.000	.001	-.011	-.362	.718
	Cumu_ESALs	2.962E-9	.000	.010	.304	.761
	SN	.021	.011	.116	1.966	.051
	Asphalt_Modulus_E1	2.562E-8	.000	.037	.666	.506
	Base_Modulus_E2	-1.356E-7	.000	-.106	-1.569	.118
	Subbase_Modulus_E3	-1.171E-7	.000	-.011	-.296	.767
	Subgrade_Modulus_E4	2.348E-7	.000	.008	.219	.827
	Air_Temperature	.000	.001	-.004	-.118	.906
	Reg_D	.010	.025	.013	.380	.705
	CND	.006	.020	.010	.318	.751
	Base_D	-.041	.036	-.071	-1.121	.264
	Total_Thickness_Tt	.000	.002	.006	.134	.893
	Log10_Initial_Rut_Depth_Plus_0.5	.954	.033	.897	28.876	.000
	Asphalt_Thickness_T1	-.011	.005	-.127	-2.036	.043

a. Dependent Variable: Log10\_Avg\_Rut\_Depth\_Plus\_0.5

Figure B4. Rutting: Model coefficients

**Model Summary<sup>b</sup>**

Model	R	R Square	Adjusted R Square	Std. Error of the Estimate
1	.577 <sup>a</sup>	.333	.327	.54826

a. Predictors: (Constant), CND, Log10\_Initial\_UCI\_Combined\_All\_Plus\_0.5, Air\_Temperature, Subbase\_Modulus\_E3, Precipitation, T1\_X\_E1, Asphalt\_Thicknesses, Reg\_D, Cumulative\_ESALs, Total\_Thicknesses, Age\_Survey\_Date, Base\_Modulus\_E2, Subgrade\_Modulus\_E4, Traffic\_X\_Log10\_Initial\_Yc\_Plus\_0.5, SN, Temperature\_X\_E1, Temperature\_X\_Precipitation, Age\_X\_Log10\_Initial\_Yc\_Plus\_0.5, TT\_X\_CND, Asphalt\_Modulus\_E1, SN\_X\_Cumulative\_ESAL

b. Dependent Variable: Log10\_UCI\_Combined\_All\_Plus\_0.5

Figure B5. UCI: Model summary for combined all crack types

**Coefficients<sup>a</sup>**

Model		Unstandardized Coefficients		Standardized Coefficients	t	Sig.
		B	Std. Error	Beta		
1	(Constant)	-.107	.101		-1.054	.292
	Log10_Initial_UCI_Combined_All_Plus_0.5	.781	.048	.763	16.182	.000
	Asphalt_Modulus_E1	1.413E-7	.000	.079	1.447	.148
	Base_Modulus_E2	5.277E-8	.000	.019	.864	.388
	Subbase_Modulus_E3	-7.136E-7	.000	-.026	-1.280	.201
	Subgrade_Modulus_E4	-3.742E-6	.000	-.048	-2.177	.030
	Asphalt_Thicknesses	-.002	.006	-.009	-.277	.782
	Total_Thicknesses	-.002	.002	-.025	-.901	.368
	Age_Survey_Date	.024	.002	.287	12.631	.000
	SN	.014	.013	.034	1.102	.271
	Cumulative_ESALs	3.500E-8	.000	.241	2.827	.005
	Air_Temperature	.001	.002	.022	.628	.530
	Precipitation	.001	.000	.140	3.283	.001
	T1_X_E1	9.234E-9	.000	.029	.832	.406
	Temperature_X_E1	2.083E-9	.000	.038	.805	.421
	SN_X_Cumulative_ESAL	-3.277E-9	.000	-.135	-1.569	.117
	TT_X_CND	-.002	.003	-.041	-.776	.438
	Temperature_X_Precipitation	-2.038E-5	.000	-.059	-1.252	.211
	Age_X_Log10_Initial_Yc_Plus_0.5	-.016	.002	-.343	-6.707	.000
	Traffic_X_Log10_Initial_Yc_Plus_0.5	-2.371E-8	.000	-.119	-4.950	.000
	Reg_D	-.090	.027	-.067	-3.383	.001
	CND	-.323	.066	-.238	-4.864	.000

a. Dependent Variable: Log10\_UCI\_Combined\_All\_Plus\_0.5

Figure B6. UCI: Model coefficients for combined all crack types

**Model Summary<sup>b</sup>**

Model	R	R Square	Adjusted R Square	Std. Error of the Estimate
1	.569 <sup>a</sup>	.324	.318	.55066

a. Predictors: (Constant), CND, Subbase\_Modulus\_E3, Air\_Temperature, Cumu\_ESAL\_X\_Log10\_Initial\_Yac\_Plus\_0.5, Precipitation, T1\_X\_E1, Reg\_D, Asphalt\_Thicknesses, Age\_Survey\_Date, Log10\_Initial\_UCI\_Alligator\_Crack\_Plus\_0.5, Total\_Thicknesses, Base\_Modulus\_E2, Cumulative\_ESALs, Subgrade\_Modulus\_E4, SN, Temperature\_X\_E1, Temperature\_X\_Precipitation, TT\_X\_CND, Age\_X\_Log10\_Initial\_Yac\_Plus\_0.5, Asphalt\_Modulus\_E1, SN\_X\_Cumulative\_ESAL

b. Dependent Variable: Log10\_UCI\_Alligator\_Crack\_Plus\_0.5

Figure B7. UCI: Model summary for alligator crack

**Coefficients<sup>a</sup>**

Model		Unstandardized Coefficients		Standardized Coefficients	t	Sig.
		B	Std. Error	Beta		
1	(Constant)	-.099	.100		-.995	.320
	Log10_Initial_UCI_Alligator_Crack_Plus_0.5	1.041	.055	.945	19.034	.000
	Asphalt_Modulus_E1	1.613E-7	.000	.090	1.650	.099
	Base_Modulus_E2	1.174E-8	.000	.004	.193	.847
	Subbase_Modulus_E3	-1.436E-6	.000	-.052	-2.563	.010
	Subgrade_Modulus_E4	-5.603E-6	.000	-.072	-3.247	.001
	Asphalt_Thicknesses	-.001	.006	-.004	-.108	.914
	Total_Thicknesses	-.003	.002	-.032	-1.139	.255
	Age_Survey_Date	.018	.002	.218	10.797	.000
	SN	.021	.013	.051	1.641	.101
	Cumulative_ESALs	3.454E-8	.000	.239	2.797	.005
	Air_Temperature	.000	.002	-.006	-.180	.857
	Precipitation	.001	.000	.122	2.839	.005
	T1_X_E1	-1.260E-8	.000	-.040	-1.131	.258
	Temperature_X_E1	4.467E-9	.000	.081	1.719	.086
	SN_X_Cumulative_ESAL	-5.167E-9	.000	-.213	-2.456	.014
	TT_X_CND	-.001	.003	-.017	-.320	.749
	Temperature_X_Precipitation	-1.318E-5	.000	-.038	-.805	.421
	Age_X_Log10_Initial_Yac_Plus_0.5	-.028	.003	-.533	-10.207	.000
	Cumu_ESAL_X_Log10_Initial_Yac_Plus_0.5	-2.452E-8	.000	-.118	-5.292	.000
	Reg_D	-.123	.026	-.091	-4.653	.000
	CND	-.228	.066	-.169	-3.433	.001

a. Dependent Variable: Log10\_UCI\_Alligator\_Crack\_Plus\_0.5

**Figure B8. UCI: Model coefficients for alligator crack**

**Model Summary<sup>b</sup>**

Model	R	R Square	Adjusted R Square	Std. Error of the Estimate
1	.493 <sup>a</sup>	.243	.236	.38165

a. Predictors: (Constant), CND, Subbase\_Modulus\_E3, Log10\_Initial\_UCI\_Block\_Crack\_Plus\_0.5, Air\_Temperature, Precipitation, T1\_X\_E1, Reg\_D, Cumulative\_ESALs, Asphalt\_Thicknesses, Age\_Survey\_Date, Total\_Thicknesses, Base\_Modulus\_E2, Subgrade\_Modulus\_E4, SN, Temperature\_X\_E1, Cumu\_ESAL\_X\_Log10\_Initial\_Ybc\_Plus\_0.5, Temperature\_X\_Precipitation, TT\_X\_CND, Asphalt\_Modulus\_E1, Age\_X\_Log10\_Initial\_Ybc\_Plus\_0.5, SN\_X\_Cumulative\_ESAL

b. Dependent Variable: Log10\_UCI\_Block\_Crack\_Plus\_0.5

**Figure B9. UCI: Model summary for block crack**

**Coefficients<sup>a</sup>**

Model		Unstandardized Coefficients		Standardized Coefficients	t	Sig.
		B	Std. Error	Beta		
1	(Constant)	-.363	.070		-5.189	.000
	Log10_Initial_UCI_Block_Crack_Plus_0.5	.621	.051	.645	12.188	.000
	Asphalt_Modulus_E1	2.742E-8	.000	.023	.404	.686
	Base_Modulus_E2	5.835E-8	.000	.033	1.382	.167
	Subbase_Modulus_E3	3.063E-7	.000	.017	.791	.429
	Subgrade_Modulus_E4	2.952E-6	.000	.058	2.468	.014
	Asphalt_Thicknesses	-.001	.004	-.010	-.295	.768
	Total_Thicknesses	-.001	.002	-.013	-.419	.676
	Age_Survey_Date	.003	.001	.055	2.377	.018
	SN	.024	.009	.089	2.737	.006
	Cumulative_ESALs	-1.308E-8	.000	-.138	-1.525	.127
	Air_Temperature	.002	.001	.042	1.129	.259
	Precipitation	.001	.000	.082	1.807	.071
	T1_X_E1	9.487E-9	.000	.045	1.227	.220
	Temperature_X_E1	2.333E-9	.000	.064	1.297	.195
	SN_X_Cumulative_ESAL	4.190E-10	.000	.026	.279	.780
	TT_X_CND	-.003	.002	-.082	-1.466	.143
	Temperature_X_Precipitation	-2.994E-5	.000	-.132	-2.643	.008
	Age_X_Log10_Initial_Ybc_Plus_0.5	-.008	.003	-.188	-3.274	.001
	Cumu_ESAL_X_Log10_Initial_Ybc_Plus_0.5	-2.755E-8	.000	-.095	-2.094	.036
	Reg_D	.019	.018	.022	1.056	.291
	CND	-.062	.046	-.070	-1.342	.180

a. Dependent Variable: Log10\_UCI\_Block\_Crack\_Plus\_0.5

**Figure B10. UCI: Model coefficients for block crack**

**Model Summary<sup>b</sup>**

Model	R	R Square	Adjusted R Square	Std. Error of the Estimate
1	.502 <sup>a</sup>	.252	.245	.30117

a. Predictors: (Constant), CND, Log10\_Initial\_UCI\_Longitudinal\_Crack\_Plus\_0.5, Subbase\_Modulus\_E3, Air\_Temperature, Age\_X\_Log10\_Initial\_Ybc\_Plus\_0.5, Precipitation, T1\_X\_E1, Asphalt\_Thicknesses, Cumulative\_ESALs, Reg\_D, Total\_Thicknesses, Age\_Survey\_Date, Base\_Modulus\_E2, Subgrade\_Modulus\_E4, SN, Temperature\_X\_E1, Cumu\_ESAL\_X\_Log10\_Initial\_Ybc\_Plus\_0.5, Temperature\_X\_Precipitation, TT\_X\_CND, Asphalt\_Modulus\_E1, SN\_X\_Cumulative\_ESAL

b. Dependent Variable: Log10\_UCI\_Longitudinal\_Crack\_Plus\_0.5

**Figure B11. UCI: Model summary for longitudinal crack**

**Coefficients<sup>a</sup>**

Model		Unstandardized Coefficients		Standardized Coefficients	t	Sig.
		B	Std. Error	Beta		
1	(Constant)	-.006	.055		-.109	.913
	Log10_Initial_UCI_Longitudinal_Crack_Plus_0.5	.462	.022	.426	21.101	.000
	Asphalt_Modulus_E1	-4.206E-8	.000	-.045	-.785	.432
	Base_Modulus_E2	5.789E-8	.000	.041	1.733	.083
	Subbase_Modulus_E3	1.207E-7	.000	.008	.395	.693
	Subgrade_Modulus_E4	-8.331E-7	.000	-.021	-.880	.379
	Asphalt_Thicknesses	.004	.003	.037	1.044	.297
	Total_Thicknesses	-.003	.001	-.068	-2.297	.022
	Age_Survey_Date	.004	.001	.096	4.399	.000
	SN	-.002	.007	-.011	-.332	.740
	Cumulative_ESALs	2.068E-8	.000	.275	3.061	.002
	Air_Temperature	.001	.001	.021	.572	.568
	Precipitation	-2.772E-5	.000	-.005	-.111	.911
	T1_X_E1	1.430E-8	.000	.086	2.340	.019
	Temperature_X_E1	-1.389E-9	.000	-.048	-.979	.328
	SN_X_Cumulative_ESAL	-1.942E-9	.000	-.154	-1.638	.102
	TT_X_CND	.003	.002	.118	2.128	.033
	Temperature_X_Precipitation	1.514E-5	.000	.084	1.694	.090
	Age_X_Log10_Initial_Ybc_Plus_0.5	-.001	.001	-.039	-1.583	.113
	Cumu_ESAL_X_Log10_Initial_Ybc_Plus_0.5	-9.902E-9	.000	-.043	-.960	.337
	Reg_D	-.003	.015	-.004	-.175	.861
	CND	-.165	.036	-.234	-4.549	.000

a. Dependent Variable: Log10\_UCI\_Longitudinal\_Crack\_Plus\_0.5

Figure B12. UCI: Model coefficients for longitudinal crack

**Model Summary<sup>b</sup>**

Model	R	R Square	Adjusted R Square	Std. Error of the Estimate
1	.682 <sup>a</sup>	.465	.460	.15750

a. Predictors: (Constant), CND, Log10\_Initial\_UCI\_Transverse\_Crack\_Plus\_0.5, Subbase\_Modulus\_E3, Air\_Temperature, Precipitation, T1\_X\_E1, Asphalt\_Thicknesses, Cumulative\_ESALs, Reg\_D, Total\_Thicknesses, Age\_Survey\_Date, Base\_Modulus\_E2, Subgrade\_Modulus\_E4, Cumu\_ESAL\_X\_Log10\_Initial\_Ytc\_Plus\_0.5, SN, Temperature\_X\_E1, Temperature\_X\_Precipitation, Age\_X\_Log10\_Initial\_Ytc\_Plus\_0.5, TT\_X\_CND, Asphalt\_Modulus\_E1, SN\_X\_Cumulative\_ESAL

b. Dependent Variable: Log10\_UCI\_Transverse\_Crack\_Plus\_0.5

Figure B13. UCI: Model summary for transverse crack

**Coefficients<sup>a</sup>**

Model	Unstandardized Coefficients		Standardized Coefficients	t	Sig.	
	B	Std. Error	Beta			
1	(Constant)	.123	.029		4.233	.000
	Log10_Initial_UCI_Transverse_Crack_Plus_0.5	1.014	.044	1.000	23.064	.000
	Asphalt_Modulus_E1	-5.435E-8	.000	-.095	-1.943	.052
	Base_Modulus_E2	3.391E-8	.000	.039	1.914	.056
	Subbase_Modulus_E3	-2.367E-7	.000	-.027	-1.475	.140
	Subgrade_Modulus_E4	-2.394E-6	.000	-.095	-4.819	.000
	Asphalt_Thicknesses	-.001	.002	-.018	-.612	.540
	Total_Thicknesses	-.002	.001	-.060	-2.383	.017
	Age_Survey_Date	9.592E-5	.001	.004	.178	.858
	SN	-.008	.004	-.059	-2.147	.032
	Cumulative_ESALs	-3.404E-9	.000	-.073	-.872	.383
	Air_Temperature	.000	.001	-.021	-.658	.511
	Precipitation	-1.705E-5	.000	-.005	-.131	.896
	T1_X_E1	1.057E-8	.000	.103	3.306	.001
	Temperature_X_E1	1.479E-10	.000	.008	.199	.842
	SN_X_Cumulative_ESAL	-3.883E-10	.000	-.050	-.617	.538
	TT_X_CND	-.001	.001	-.069	-1.470	.142
	Temperature_X_Precipitation	4.908E-6	.000	.044	1.048	.295
	Age_X_Log10_Initial_Ytc_Plus_0.5	-.019	.002	-.412	-9.554	.000
	Cumu_ESAL_X_Log10_Initial_Ytc_Plus_0.5	-2.632E-8	.000	-.145	-6.262	.000
	Reg_D	-.016	.008	-.036	-1.963	.050
	CND	-.048	.019	-.111	-2.542	.011

a. Dependent Variable: Log10\_UCI\_Transverse\_Crack\_Plus\_0.5

**Figure B14. UCI: Model coefficients for transverse crack**



## Appendix C: Full Factorial Design for Uncracked Asphalt Pavements

No.	Treatment Combinations	Layer thickness, in (T <sub>1</sub> : Asphalt and T <sub>2</sub> : Subbase) and Young's modulus, ksi (E <sub>1</sub> :Asphalt, E <sub>2</sub> : Base, E <sub>3</sub> : Subbase, and E <sub>4</sub> : Subgrade)					
		T <sub>1</sub>	T <sub>2</sub>	E <sub>4</sub>	E <sub>2</sub>	E <sub>3</sub>	E <sub>1</sub>
1	000000	3 in	6 in	10 ksi	40 ksi	20 ksi	200 ksi
2	010000	3 in	12 in	10 ksi	40 ksi	20 ksi	200 ksi
3	100000	9 in	6 in	10 ksi	40 ksi	20 ksi	200 ksi
4	110000	9 in	12 in	10 ksi	40 ksi	20 ksi	200 ksi
5	000001	3 in	6 in	10 ksi	40 ksi	20 ksi	1,000 ksi
6	010001	3 in	12 in	10 ksi	40 ksi	20 ksi	1,000 ksi
7	100001	9 in	6 in	10 ksi	40 ksi	20 ksi	1,000 ksi
8	110001	9 in	12 in	10 ksi	40 ksi	20 ksi	1,000 ksi
9	000010	3 in	6 in	10 ksi	40 ksi	100 ksi	200 ksi
10	010010	3 in	12 in	10 ksi	40 ksi	100 ksi	200 ksi
11	100010	9 in	6 in	10 ksi	40 ksi	100 ksi	200 ksi
12	110010	9 in	12 in	10 ksi	40 ksi	100 ksi	200 ksi
13	000011	3 in	6 in	10 ksi	40 ksi	100 ksi	1,000 ksi
14	010011	3 in	12 in	10 ksi	40 ksi	100 ksi	1,000 ksi
15	100011	9 in	6 in	10 ksi	40 ksi	100 ksi	1,000 ksi
16	110011	9 in	12 in	10 ksi	40 ksi	100 ksi	1,000 ksi
17	000100	3 in	6 in	10 ksi	200 ksi	20 ksi	200 ksi
18	010100	3 in	12 in	10 ksi	200 ksi	20 ksi	200 ksi
19	100100	9 in	6 in	10 ksi	200 ksi	20 ksi	200 ksi
20	110100	9 in	12 in	10 ksi	200 ksi	20 ksi	200 ksi
21	000101	3 in	6 in	10 ksi	200 ksi	20 ksi	1,000 ksi
22	010101	3 in	12 in	10 ksi	200 ksi	20 ksi	1,000 ksi
23	100101	9 in	6 in	10 ksi	200 ksi	20 ksi	1,000 ksi
24	110101	9 in	12 in	10 ksi	200 ksi	20 ksi	1,000 ksi
25	000110	3 in	6 in	10 ksi	200 ksi	100 ksi	200 ksi
26	010110	3 in	12 in	10 ksi	200 ksi	100 ksi	200 ksi
27	100110	9 in	6 in	10 ksi	200 ksi	100 ksi	200 ksi
28	110110	9 in	12 in	10 ksi	200 ksi	100 ksi	200 ksi
29	000111	3 in	6 in	10 ksi	200 ksi	100 ksi	1,000 ksi
30	010111	3 in	12 in	10 ksi	200 ksi	100 ksi	1,000 ksi

Full factorial design considering six factors at two levels (Total 64 cells)							
No.	Treatment Combinations	Layer thickness, in (T <sub>1</sub> : Asphalt and T <sub>2</sub> : Subbase) and Young's modulus, ksi (E <sub>1</sub> :Asphalt, E <sub>2</sub> : Base, E <sub>3</sub> : Subbase, and E <sub>4</sub> : Subgrade)					
		T <sub>1</sub>	T <sub>2</sub>	E <sub>4</sub>	E <sub>2</sub>	E <sub>3</sub>	E <sub>1</sub>
31	100111	9 in	6 in	10 ksi	200 ksi	100 ksi	1,000 ksi
32	110111	9 in	12 in	10 ksi	200 ksi	100 ksi	1,000 ksi
33	001000	3 in	6 in	50 ksi	40 ksi	20 ksi	200 ksi
34	011000	3 in	12 in	50 ksi	40 ksi	20 ksi	200 ksi
35	101000	9 in	6 in	50 ksi	40 ksi	20 ksi	200 ksi
36	111000	9 in	12 in	50 ksi	40 ksi	20 ksi	200 ksi
37	001001	3 in	6 in	50 ksi	40 ksi	20 ksi	1,000 ksi
38	011001	3 in	12 in	50 ksi	40 ksi	20 ksi	1,000 ksi
39	101001	9 in	6 in	50 ksi	40 ksi	20 ksi	1,000 ksi
40	111001	9 in	12 in	50 ksi	40 ksi	20 ksi	1,000 ksi
41	001010	3 in	6 in	50 ksi	40 ksi	100 ksi	200 ksi
42	011010	3 in	12 in	50 ksi	40 ksi	100 ksi	200 ksi
43	101010	9 in	6 in	50 ksi	40 ksi	100 ksi	200 ksi
44	111010	9 in	12 in	50 ksi	40 ksi	100 ksi	200 ksi
45	001011	3 in	6 in	50 ksi	40 ksi	100 ksi	1,000 ksi
46	011011	3 in	12 in	50 ksi	40 ksi	100 ksi	1,000 ksi
47	101011	9 in	6 in	50 ksi	40 ksi	100 ksi	1,000 ksi
48	111011	9 in	12 in	50 ksi	40 ksi	100 ksi	1,000 ksi
49	001100	3 in	6 in	50 ksi	200 ksi	20 ksi	200 ksi
50	011100	3 in	12 in	50 ksi	200 ksi	20 ksi	200 ksi
51	101100	9 in	6 in	50 ksi	200 ksi	20 ksi	200 ksi
52	111100	9 in	12 in	50 ksi	200 ksi	20 ksi	200 ksi
53	001101	3 in	6 in	50 ksi	200 ksi	20 ksi	1,000 ksi
54	011101	3 in	12 in	50 ksi	200 ksi	20 ksi	1,000 ksi
55	101101	9 in	6 in	50 ksi	200 ksi	20 ksi	1,000 ksi
56	111101	9 in	12 in	50 ksi	200 ksi	20 ksi	1,000 ksi
57	001110	3 in	6 in	50 ksi	200 ksi	100 ksi	200 ksi
58	011110	3 in	12 in	50 ksi	200 ksi	100 ksi	200 ksi
59	101110	9 in	6 in	50 ksi	200 ksi	100 ksi	200 ksi
60	111110	9 in	12 in	50 ksi	200 ksi	100 ksi	200 ksi
61	001111	3 in	6 in	50 ksi	200 ksi	100 ksi	1,000 ksi
62	011111	3 in	12 in	50 ksi	200 ksi	100 ksi	1,000 ksi
63	101111	9 in	6 in	50 ksi	200 ksi	100 ksi	1,000 ksi
64	111111	9 in	12 in	50 ksi	200 ksi	100 ksi	1,000 ksi